Neocortical circuits contributing to distinct timescales of plasticity

Chaloner, Fran

Awarding institution:
King's College London

Neocortical circuits contributing to distinct timescales of plasticity

Francesca Chaloner

Thesis submitted for the degree of Doctor of Philosophy

June 2023

Institute of Psychiatry, Psychology and Neuroscience

King's College London

United Kingdom

Supervisors:

Samuel Cooke

Juan Burrone

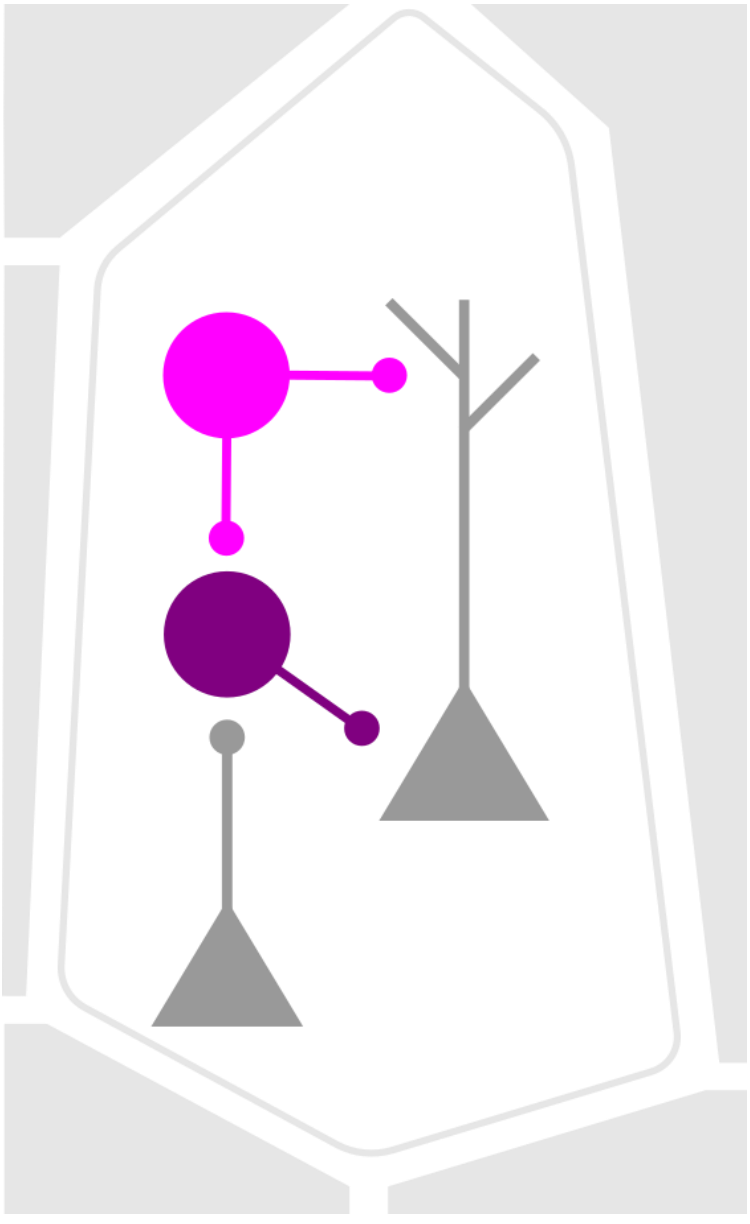

Abstract

Observing the effects of sensory experience in shaping neural activity and intervening in the activity of those neurons provides mechanistic insight into the processes that underlie learning, memory, and perception. Mouse primary visual cortex (V1) provides a model system to interrogate this experience-dependent plasticity and is a popular focus of research due to the ability to tightly control sensory input while directly recording cellular activity in these easily accessible structures. Genetic manipulations of specific cell types in mice can inform us about the relative contribution of different cell types to experience-dependent modifications of activity. How cortical activity alters over seconds, minutes, and days in response to passive viewing of visual stimuli has been relatively well studied. However, the contribution of specific subtypes of cells is unknown. In this thesis I use *in vivo* and *ex vivo* electrophysiology to investigate the changes in neuronal activity across different timescales and probe the contribution to this altered activity of three major neuronal subtypes in primary visual cortex: parvalbumin- and somatostatin-expressing inhibitory GABAergic neurons and layer 6 cortico-thalamic (CT) excitatory cells.

First, I describe three timescales of altered activity in V1 of mice. These include short-term adaptation occurring across seconds and minutes, which feature diminished cortical responses, the latter of which also accompanies behavioural habituation. In contrast, across days visual cortical responses potentiate through a process of stimulus selective response potentiation (SRP), which also accompanies habituation of behavioural responses from day to day. Furthermore, short-term adaptation and SRP interact. As the stimulus becomes familiar across SRP, short-term adaptation of the visual evoked potential (VEP) magnitude disappears. However, short-term adaptation remains intact for novel

stimuli. All timescales of altered activity require expression of NMDA receptors in V1. Furthermore, inactivation of parvalbumin (PV+) neurons prevents expression of SRP and unveils pronounced short-term adaptation even for highly familiar stimuli. To investigate the role of inhibition in more detail, the activity of both parvalbumin and somatostatin (SOM+) inhibitory neurons was manipulated. Reduced activity in PV+ neurons during visual experience is important for the expression of SRP. Interestingly, SOM+ neurons are responsible for the VEP dynamics during presentation of a familiar stimulus. Therefore, SOM+ neurons are progressively engaged by long-term familiarity showing the opposite activity profile to PV+ neurons. There is some evidence that the primary role of SOM+ neurons after SRP is to directly inhibit PV+ neurons. In addition, as a result of SRP there is a reduction of inhibitory input magnitude onto excitatory cells in layer 4, likely reflecting a loss of PV+ neuronal inhibition.

Finally, knock-out of NMDA receptors in layer 6 CT neurons increases VEP magnitude and masks SRP, indicating an additional influence over inhibitory neurons. Interestingly, knock-out of NMDA receptors in layer 6 CT neurons impairs short-term habituation within a session but does not affect long-term habituation. However, further attempts to manipulate these cell types using chemogenetics failed. Nonetheless, activation of layer 6 cells with optogenetics causes inhibition of VEP responses, suggesting that layer 6 excitatory CT neurons target PV+ neurons to mediate inhibition of layer 4 cells. Furthermore, there is no change in excitatory inputs into layer 4 after SRP. Thus, opposing influences on PV+ neuronal activity, layer 6 CT excitatory input and SOM+ inhibition, contribute to differential cortical activity and habituation at multiple timescales.

Acknowledgements

A PhD is a monumental effort, and I would not be here without the support of the following people (and lots of others), I hope you all know how grateful I am but here it is in writing just in case.

Thank you to my supervisor Sam. Your guidance, support and enthusiasm has made me the scientist I am. We have endured many challenges together and I am grateful for all that you have taught me.

To the rest of the lab, Pete, Lucy, Amy, and Antonia. Thank you for the copious favours. It has been a pleasure to do science with you, I wouldn't want it any other way.

Thank you to my second supervisor Juan Burrone for supporting my crazy idea to learn *ex vivo* electrophysiology 5 months before the end of my PhD and Vincenzo Mastrolia for patiently and enthusiastically teaching me.

To all my friends, especially Liz, Katherine, Sass, and Josh (I told you you'd get a shout out), thank you for bringing me so much joy outside of the dominating presence that is a PhD.

Thank you to my family, Dad, Mum, Josh, and Grandma. Mum, you inspire me endlessly, I am a scientist because of you. Dad, thank you for following the 'Dad's terms & conditions' whenever I needed help. Grandad, thank you for instilling a love of learning in me, I wish you could be here to see the end of the PhD.

To Tim, thank you for steadying me through the greatest storms. I am forever thankful for your love and support.

Declaration of contributions

The work presented in this thesis is my own.

Contributions of other members of the lab are as follows:

Genotyping of animals was assisted by Antonia Massmann and Amy Lawson.

Imaging of slides was performed by Lucy Menage.

Data in chapter 2 and layer 6 NMDAR knock-out data in chapter 4 was collected by Samuel Cooke in the Bear lab (MIT)

Peter Sully and Amy Lawson acquired several days of *in vivo* head fixed electrophysiological recordings from 4-6 animals in Chapter 3.

Table of contents

Table of Figures

Table of Tables

Abbreviations

AMPA(R)	α-amino-3-hydroxy-5-methyl-4-isoxazolepropionic acid (receptor)
AR	Adaptation ratio
CNO	Clozapine-N-oxide
dLGN	Dorsal lateral geniculate nucleus
DREADDs	Designer Receptors Exclusively Activated by Designer Drugs
EPSCs	Excitatory post-synaptic currents
GABAergic	(Gamma-Aminobutyric Acid)ergic
IPSCs	Inhibitory post-synaptic currents
LFP	Local-field potential
LTD	Long-term depression
LTP	Long-term potentiation
MD	Monocular deprivation
MMN	Mismatch negativity
NMDA(R)	N-methyl-D-aspartate (receptor)
OD	Ocular dominance
PV	Parvalbumin
SOM	Somatostatin
SRP	Stimulus-selective response potentiation
SSA	Stimulus-selective adaptation

TRN	Thalamic reticular nucleus
V1	Primary visual cortex
VEP	Visual evoked potential

Chapter 1 Introduction

The modulation of brain activity in response to experience is a key function of the mammalian brain. This alteration in activity, over the course of a “learning” period, often manifests as a memory, which directs subsequent sensory processing and behaviour (McGaugh, 2000). Specific environmental elements may acquire a positive, negative (if connected to rewards or penalties, respectively) or neutral valence (if innocuous). In response to such innocuous stimuli there is a reduction in behavioural response, termed habituation (Rankin *et al.*, 2009; Schmid *et al.*, 2014). The appearance of behavioural habituation can result from a memory being formed in response to innocuous stimuli (Sokolov, 1963). Learning, memory, adaptation, and habituation are universal phenomena which are measurable across species.

Copious research has focused on the visual system, due to its comparability across species, to investigate learning, memory, adaptation, and habituation. Investigation of altered visual cortical activity can be done non-invasively in humans (Teyler *et al.*, 2005) and invasively in mice (Frenkel *et al.*, 2006). The mouse is a good system for dissecting out the roles of the cells and circuits that are altered during sensory processing and learning due to recent advances in direct recording of neuronal activity and cell specific manipulation methodologies (Cossart *et al.*, 2005; Magnus *et al.*, 2019; Lee *et al.*, 2020; Steinmetz *et al.*, 2021). Therefore, invasive recordings and cell specific manipulations in mice can provide a wealth of information to probe the cells and circuits that underly these complex phenomena.

1.1 Plasticity and adaptation

1.1.1 Sensory adaptation

Reduction of neural activity in response to repetitive input is an essential process in the brain to dedicate resources to salient stimuli. Adaptation can occur at the synaptic and cellular level and allows the network to adjust to ongoing activity (Whitmire & Stanley, 2016). Early studies of synaptic adaptation made use of simple systems such as *Aplysia* and *Drosophila* (Ramaswami, 2014). However, this phenomenon is observable in mammalian brains. Within the cortex of rodents, synaptic responses adapt to artificial stimulation of terminals (Li *et al.*, 2003), repetitive sensory stimulation (Chung *et al.*, 2002) and continual stimuli presentation (Heintz *et al.*, 2022).

Multiple mechanisms may underlie adaptation of neural responses. The simplest explanation suggests that short-term synaptic depression results from depletion of neurotransmitter pools in the pre-synaptic terminal (Foster & Regehr, 2004). This reduction in neurotransmitter release produces fewer synaptic responses in the post-synaptic terminal i.e., adapted post-synaptic responses. Additionally, post-synaptic receptors may become desensitised and therefore become inactive (Wong *et al.*, 2003). These inactive receptors do not open in response to transmitter release resulting in reduced post-synaptic responses. An additional mechanism contributing to neural adaptation may be recruitment of inhibitory neurons. This recruitment of inhibition may reduce synaptic responses through shunting inhibition, which alters somatic input resistance and thus causes inhibition of action potential generation (Silver, 2010). The contribution of inhibitory neurons to adaptation is discussed in greater depth in 1.3.4.3.

Repetitive passive presentation of a sensory stimulus is a common way to explore sensory adaptation. Importantly, this adaptation is specific to the

features of the stimuli shown, manifesting in response solely to particular orientations and spatial frequencies presented (Bonds, 1984). Thus, the term stimulus-selective adaptation (SSA) defines this phenomenon. SSA occurs at multiple levels of the sensory processing stream, as it is observed in the thalamus and cortex (Chung *et al.*, 2002) and across different sensory cortices (Latimer *et al.*, 2019). Adaptation can occur at both excitatory and inhibitory synapses in a matched manner (Higley & Contreras, 2006; Li & Glickfeld, 2023). Despite inhibitory inputs undergoing adaptation, the overall effect across sensory presentation manifests as a reduction in action potentials in response to stimuli presentation.

Layer 4 action potentials undergo SSA (Natan *et al.*, 2017; Jin & Glickfeld, 2020). As layer 4 is the main thalamo-recipient layer in the cortex, the depression of thalamocortical synapses into layer 4 is most likely the driver of SSA in layer 4. However, thalamic adaptation is less substantial than cortical adaptation (Wang *et al.*, 2010). Furthermore, cortical contrast adaptation typically differs from thalamic contrast adaptation. However, silencing cortical neurons during the adaptation period results in cortical contrast adaptation which mimics thalamic adaptation (King *et al.*, 2016). Therefore, intracortical mechanisms likely contribute to adaptation in layer 4 that occur in addition to adaptation inherited from the thalamus.

Throughout the cortex cells in all layers show adaptation. However, SSA is more pronounced in layers 2/3 and 5/6 compared to layer 4 (Natan *et al.*, 2017; Jin & Glickfeld, 2020). Furthermore, activation of layer 4 occludes SSA in layer 2/3 (Li & Glickfeld, 2023). This suggests that there is propagation of adaptation through the canonical cortical processing stream (L4-L2/3-L5).

The previously discussed studies investigate response adaptation to 4-5 individual stimuli with the adaptation lasting less than 2 seconds. However, adaptation of responses to stimuli can occur over the course of hundreds of seconds. Repetitive stimulation over ~400 seconds shows an exponential reduction of spikes with a time constant of 50 seconds (Ulanovsky *et al.*, 2004).

One theory of adaptation posits that the brain is trying to enhance discriminability of stimuli, as after adaptation the probability of spiking rates overlapping is reduced (von der Behrens *et al.*, 2009). In support of this theory, an ideal observer model was asked to discriminate between sensory stimuli, and after adaptation it was significantly better at discrimination compared to the non-adapted state (Wang *et al.*, 2010). An alternative theory is that adaptation serves a role in conservation of energy, acting as a homeostatic mechanism. At the population level, responses to biased presentation of a stimulus would be expected to change as those cells with preference fire more frequently. However, adaptation-induced changes in orientation tuning curves allow the average population response to remain constant across all orientations even in the face of biased presentation (Benucci *et al.*, 2013). This implies that homeostatic changes to cell responses can help to equalise responses across all cells.

1.1.2 Experience-dependent plasticity

1.1.2.1 Long-term plasticity

One form of long-term plasticity is long-term potentiation (LTP). The term LTP was first coined to describe an experimental finding that high frequency activation of synaptic terminals caused a long-lasting (>3 hours) increase in synaptic field responses (Bliss & Lomo, 1973). A likely mechanism explaining experimental LTP is Hebbian plasticity, which is defined as long-lasting activity-dependent changes in the connections between cells (Hebb, 1949). The NMDA receptor

(NMDAR) was discovered to be a perfect biophysical mechanism to detect the necessary conditions for Hebbian LTP (Collingridge *et al.*, 1983): activity-dependent pre-synaptic release of transmitter and post-synaptic depolarisation. Hebbian LTP consists of long-lasting changes in the AMPA receptor composition of the post-synaptic terminal (Muller *et al.*, 1988) to mediate the increased synaptic field responses (Bliss & Lomo, 1973). However, there is also evidence for changes in the pre-synaptic terminal after LTP induction (Bliss & Collingridge, 1993).

Another type of plasticity is long-term depression (LTD), which can occur at synapses following low frequency stimulation (1 Hz) and is also NMDAR dependent (Dudek & Bear, 1992). Expression of Hebbian LTD is in part dependent on removal of AMPA receptors from the synapse (Beattie *et al.*, 2000). In addition, LTD may involve a reduction of glutamate release from the pre-synaptic terminal (Collingridge *et al.*, 2010).

1.1.2.2 How do we measure the result of long-term plasticity in the brain?

Many mechanisms, including Hebbian-LTP and -LTD, may contribute to the long-term plasticity that is observed as alterations in synaptic strength in response to experience. Experience-dependent long-term plasticity alters the activity of synapses, and thus cellular and network activity, for hours, days (Montgomery *et al.*, 2021) and months (Pérez-Ortega *et al.*, 2021). Therefore, stable longitudinal recordings are required to investigate experience-dependent long-term plasticity. These recordings can be done with chronic implantation of tungsten electrodes to record an extracellular signal, the local field potential (LFP). In response to presentation of visual stimuli, visual evoked potentials (VEPs) are recorded from averaged LFP traces. Importantly, VEPs can be used to investigate experience-

dependent plasticity (Cooke & Bear, 2014) as they reflect stable population synaptic responses (Mitzdorf, 1987; Buzsáki *et al.*, 2012).

1.1.2.3 Sensory deprivation experiments

A common way to study experience-dependent plasticity is through sensory deprivation. Monocular deprivation (MD) is an experimental technique where one eye is closed to deprive sensory input. After MD, there is a reduction of responses to the deprived eye followed by potentiated responses to the un-deprived eye (Wiesel & Hubel, 1963; Shatz & Stryker, 1978). Depression of responses in the deprived eye (Heynen *et al.*, 2003) and potentiation of non-deprived eye responses (Sawtell *et al.*, 2003) require NMDARs. In addition, reduced responses in the deprived eye may occur via depression of synaptic strength (Rittenhouse *et al.*, 1999) or recruitment of inhibition (Maffei *et al.*, 2006). Both synaptic depression and recruitment of inhibition can be NMDAR dependent. Overall, multiple lines of evidence suggest that Hebbian plasticity is a key mechanism that occurs in response to monocular deprivation.

1.1.2.4 Stimulus-selective response potentiation (SRP)

In addition to sensory deprivation experiments, experience-dependent plasticity occurs in response to passive exposure to sensory stimuli. A well-established form of experience-dependent long-term plasticity is stimulus-selective response plasticity (SRP), which occurs over days in response to passive viewing of phase-reversing gratings (Frenkel *et al.*, 2006; Cooke & Bear, 2010; Aton *et al.*, 2014; Cooke *et al.*, 2015). Over days, the magnitude of the visual evoked potential (VEP) recorded from layer 4 potentiates. This potentiation of the VEP is orientation specific as presentation of a novel stimulus produces VEP responses equivalent to baseline (Frenkel *et al.*, 2006; Cooke & Bear, 2010). Investigation into the firing rate of cells in V1 shows an increased peak firing 50ms after familiar

stimulus onset (Cooke *et al.*, 2015) which coincides with the negative peak of the VEP and likely reflects thalamo-cortical synaptic activity. The differential VEP responses to familiar and novel stimuli holds true across cortical layers (Hayden *et al.*, 2023) and is present in the firing of deep layers (Aton *et al.*, 2014; Clawson *et al.*, 2018). Furthermore, changes in the oscillatory state of the visual cortex occurs over learning. Over presentation of a stimulus, there is an orientation specific increase in lower frequency bands, namely alpha (8-12 Hz) and beta (13-30 Hz) which is accompanied by a decrease in gamma frequency (65-80 Hz) (Hayden *et al.*, 2021).

Molecular requirements of SRP induction are the NMDA receptor and AMPA receptor insertion (Frenkel *et al.*, 2006; Cooke & Bear, 2010; Cooke *et al.*, 2015; Hayden *et al.*, 2023) suggesting that Hebbian LTP underlies this phenomenon. Given that the VEP is recorded in layer 4 and potentiates over days, it was hypothesised that Hebbian LTP was occurring at synapses from the thalamus into layer 4. However, Hebbian plasticity does not seem to be the likely mechanism driving change at thalamocortical synapses in layer 4, as evidenced by normal SRP upon knock-out of NMDARs in layer 4 (Fong *et al.*, 2020). A key requirement for this plasticity is sleep, recruiting offline consolidation processes, as potentiation only emerges the following day. Disruption of sleep impairs visual cortical potentiation (Aton *et al.*, 2014; Clawson *et al.*, 2018) and sleep dependent consolidation requires recruitment of a layer 6-thalamic circuit (Durkin *et al.*, 2017).

In addition to excitatory synaptic alterations, there is a key role of inhibition in SRP. In the brain, the two main subtypes of inhibitory GABAergic neurons are parvalbumin (PV+) and somatostatin (SOM+) cells. Synaptic alterations may be occurring at inputs onto PV+ neurons as knock-out of

NMDARs in PV+ neurons impairs plasticity (Kaplan *et al.*, 2016). Loss of NMDARs in PV+ neurons will alter activity in layer 4 as PV+ cells directly inhibit layer 4 excitatory neurons. This observation suggests that during passive experience, encoding of the familiar stimulus is reliant on changes of synaptic inputs to PV+ neurons. In addition, engagement of PV+ neurons during stimulus discrimination is critical as PV+ neuron inactivation with DREADDs blocks differential responses to familiar and novelty stimuli after SRP (Kaplan *et al.*, 2016). In addition, ketamine treatment, which predominantly antagonises NMDARs on PV+ neurons (Moghaddam & Krystal, 2012), disrupts expression of SRP. Therefore, recruitment of PV+ GABAergic neurons is critical for expression of SRP.

Across passive exposure PV+ neuronal activity decreases, and is eventually suppressed below baseline, while the activity of SOM+ neurons increases over learning (Hayden *et al.*, 2021). During presentation of familiar and novel stimuli, PV+ neuronal activity is inhibited during familiar stimulus presentation and is increased for novelty, whereas SOM+ activity is increased during presentation of the familiar stimulus and decreased for novelty (Hayden *et al.*, 2021).

Alternatively, the synaptic alteration may occur in a different layer of the cortex. Knock-out of NMDA receptors in layer 6 excitatory cells impairs plasticity across days (Hayden *et al.*, 2023). However, this mechanism of action may still involve alteration of PV+ neuron activity, as layer 6 targets those PV+ neurons that feed-forward onto layer 4 (Bortone *et al.*, 2014; Kim *et al.*, 2014). Overall, PV+ neurons are in a prime position for gating this form of experience-dependent plasticity (SRP) either through changes of inputs from layer 6, the thalamus, or

SOM+ cells. Throughout learning, there is a potential transition in the activation PV+ cells, shifting from predominantly bottom-up to top-down.

The VEP reflects ongoing synaptic activity and potentiation of the VEP would be expected to result from increased synaptic activity. Increased synaptic activity should result in increased firing of layer 4 cells. However, average firing of layer 4 cells to familiar stimuli is lower than average firing to novel stimuli following SRP (Cooke *et al.*, 2015; Hayden *et al.*, 2023). Investigation into the calcium responses of cells in layer four shows a decrease in activity over SRP and increased calcium transients for novelty (Kim *et al.*, 2020). The reduced calcium transients during familiarity likely reflects redistribution of firing. Despite averaged activity being lower during familiarity than during novelty, there is increased peak-firing (50 ms post stimulus onset) during familiarity (Cooke *et al.*, 2015; Hayden *et al.*, 2023). In addition to layer 4, novelty evoked increases in calcium responses can also been seen in other layers (Homann *et al.*, 2022). The potentiation of the VEP likely occurs due to loss of shunting inhibition, mediated by a reduction of PV+ cell activity (Hayden *et al.*, 2021). This loss of shunting inhibition results in increased excitatory input from the thalamus and can be observed as increased calcium transients seen in the neuropil in layer 4 (Kim *et al.*, 2020).

1.1.3 Behavioural habituation

A reduced behavioural response to innocuous stimuli, termed habituation, is a fundamental feature of sensory processing. Habituation is experimentally observable and ubiquitous across species (George & Peckham, 1887). Early theories of the mechanisms of habituation suggested that stimulus response depression occurred due to synaptic weakening (Groves & Thompson, 1970; Farel & Thompson, 1976). However, an alternative theory suggests that reduced

behavioural output results from increased local inhibitory drive which matches the excitatory output (Ramaswami, 2014; Barron *et al.*, 2017). This matched inhibitory drive, a negative image, may result from potentiation of inhibition onto excitatory cells (Cooke & Ramaswami, 2020). This change in inhibitory drive may be a result of alterations of SOM+ mediated inhibition rather than other inhibitory cells, as habituation selectively recruits SOM+ neurons (Kato *et al.*, 2015). Another theory which implicates inhibition in habituation is the comparator model theory (Sokolov, 1963). The comparator model theory explains that across experience memories are formed for specific stimuli, forming a remote bank of stored memories. Consequently, when exposed to that stimulus again, the net output of the memory circuit is inhibition. Therefore, when encountering a familiar stimulus, inhibition and excitation are matched and no behaviour occurs. In response to a novel stimulus, there is no inhibition and therefore allows behavioural responses (Sokolov, 1963; Cooke & Ramaswami, 2020). In response to visual stimuli, groups of cells respond (Carrillo-Reid *et al.*, 2015) and are stable over many presentations (Pérez-Ortega *et al.*, 2021) suggesting these cells encode for that specific stimulus. These groups that encode for familiar stimuli may recruit inhibition to alter downstream behavioural responses (Kaplan *et al.*, 2016).

However, in opposition to habituation manifesting because of reduced activity, increased cortical responses have been observed alongside habituation. A reduction in behaviour has been associated with cortical stimulus-selective response potentiation (SRP), termed orientation-selective habituation (Cooke *et al.*, 2015). This manifests as a reduced behavioural response to a familiar stimuli and increased response to novel stimuli, and, requires NMDA receptors in visual cortex (Cooke *et al.*, 2015; Fong *et al.*, 2020). Furthermore, a recent observation

indicates that behavioural habituation results from an increase in spontaneous activity (Miller *et al.*, 2022). This increased activity blunts the sharp shifts between pre- and post- stimulus activity. A common computation in the cortex is change detection. The reduced difference between the activity profiles between pre- and post- stimulus activity precludes change detection and results in reduced behavioural output (Miller *et al.*, 2022). Overall, it is likely that both synaptic weakening and long-term memory formation happens to mediate short-term and long-term habituation (Sanderson & Bannerman, 2011).

1.2 Connectivity of the Visual System

1.2.1 Thalamic input to V1

The dorsal lateral geniculate nucleus (dLGN) of the thalamus was originally considered a relay nucleus passing information from retina to layer 4 in the visual cortex, but is now understood to have complex computational roles that modulate or gate information flow (Sillito & Jones, 2002). This is in part due to modulatory inputs from the cortex and the thalamic reticular nucleus (TRN) (Guillery & Sherman, 2002). The TRN is a thalamic inhibitory nucleus which directly inhibits the dLGN relay cells which project to the cortex (Kim *et al.*, 1997). The thalamus directly targets layer 4 cells in the neocortex and afferents into layer 4 comprise of ~6% of synaptic inputs in this layer in cat visual cortex (Ahmed *et al.*, 1994). From the thalamus, 85% of synapses terminate in layer 4 (Binzegger *et al.*, 2004) and provide direct excitatory input (Sermet *et al.*, 2019).

Repetitive stimulation of synaptic inputs can cause depression or facilitation of synaptic potentials recorded from the target cells. In layer 4, synaptic inputs from the thalamus are depressing (Lee & Sherman, 2008; Cruikshank *et al.*, 2010). This synaptic depression of thalamocortical inputs to layer 4 cells may

contribute adaptation of spiking responses in layer 4 neurons during stimulus presentation (King *et al.*, 2016; Jin & Glickfeld, 2020).

Within the cortex, layer 4 excitatory cells show orientation selectivity (Niell & Stryker, 2008). Orientation selectivity in layer 4 cortex can be explained by feedforward input from multiple orientation insensitive dLGN cells whose circular receptive fields align with the orientation preference of the neuron (Hubel & Wiesel, 1962; Priebe, 2016). However, ~50% of the boutons of thalamic terminals into layer 4 show orientation selectivity (Sun *et al.*, 2016). This orientation selectivity of dLGN cells may be a result of cortical feedback. In support of this, orientation selectively was present in the F1 modulation of thalamic excitation; F1 modulation is the extent to which the amplitude of the response fluctuates in magnitude at the same temporal frequency as the stimulus. The absolute firing rate of thalamic neurons is not orientation selective (Lien & Scanziani, 2013), suggesting that orientation selectivity of thalamic afferents may be modulated by feedback from the cortex. However, cells in the dLGN have been shown to be orientation selective after inactivation of the cortex (Scholl *et al.*, 2013), which dismisses the idea that orientation selectivity of dLGN is inherited from cortical feedback. Overall, there may be partial inheritance of orientation selectivity in layer 4 from orientation tuned cells in the thalamus (Priebe, 2016).

Thalamic afferents in layer 4 make significant connections to PV+ neurons to provide feed-forward inhibition. Inputs from the thalamus provide stronger excitatory input onto PV+ neurons than onto layer 4 excitatory cells (Cruikshank *et al.*, 2007, 2010). Furthermore, thalamic activation evokes action potentials in ~60% of inhibitory compared to ~5% of excitatory cells (Porter *et al.*, 2001). Despite robust recruitment of PV+ neurons by the thalamus, these inputs

are strongly depressing (Gabernet *et al.*, 2005; Kloc & Maffei, 2014). This suggests that initially the thalamus mediates strong feed-forward inhibition, but this wanes after longer bouts of activity. The temporal dynamics which control feedforward inhibition mediated by the thalamus limits the window in which sensory information can pass to the cortex to ~10 ms (Wilent & Contreras, 2004; Gabernet *et al.*, 2005).

In response to synaptic inputs, cells produce action potentials which may occur consistently at regular intervals (tonic firing) or in bursts (burst firing). Different output modes, tonic or burst firing, of the thalamus may alter the onward transmission of information due to the temporal integration window. Output from the thalamus can be either tonic or bursting (Sherman & Guillery, 2002). Bursting output from the thalamus triggers greater action potential generation in cortical cells than tonic firing (Swadlow & Gusev, 2001). This greater action potential generation following thalamic bursting may result in more reliable information flow. In line with this, thalamic bursting tightens the sensory-evoked responses in layer 4 excitatory cells (Borden *et al.*, 2022). Thus, bursting may be able to convey information prior to the feed-forward inhibition recruitment.

1.2.2 Layer 6 parallel processing and feedback

In addition to layer 4, the thalamus targets cells in deep layers, particularly layer 6 (Constantinople & Bruno, 2013), resulting in a parallel processing stream within the cortex. Thalamic inputs into layer 6 show synaptic depression (Beierlein & Connors, 2002), are sharply tuned for orientation, have sparse firing (Vélez-Fort *et al.*, 2014) and alter their firing to reflect stimulus intensity (Voigts *et al.*, 2020).

Within layer 6, there are two main subtypes of excitatory cells, cortico-cortical (CC) which project within or to other cortical areas and corticothalamic (CT) which provide feedback to the LGN (Zhang & Deschênes, 1997; Binzegger

et al., 2004; Feldmeyer, 2012). These CT neurons also provide a striking additional intracortical connection to layer 4. Therefore, CT cell in layer 6 can modulate both thalamic and cortical activity.

The number of synaptic inputs from layer 6 to layer 4 is ~7 times larger than that from the thalamus to layer 4 (Ahmed *et al.*, 1994), Furthermore, inputs to layer 4 from layer 6 show short-term facilitation (Lee & Sherman, 2008). Therefore, the intracortical input onto layer 4 is larger than that from the thalamus and becomes more pronounced during extended periods of activity allowing for stronger modulation of bottom-up sensory input. Furthermore, it is important to understand the mechanisms by which layer 6 modulates information through layer 4. Stimulation of layer 6 cells only elicits weak excitatory responses in layer 4 neurons, but triggers strong inhibitory responses (Olsen *et al.*, 2012; Kim *et al.*, 2014). Layer 6 may target PV+ neurons in layer 4, which locally target layer 4 excitatory cells (Kim *et al.*, 2014; Yetman *et al.*, 2019) or target layer 6 PV+ neurons, which project up to layer 4 to evoke inhibition (Bortone *et al.*, 2014). Therefore, intracortical modulation of thalamic drive is predominantly inhibitory and likely gates sensory information flow.

In addition, inputs from layer 6 targets both relays cells in the first-order sensory thalamic nucleus and inhibitory neurons in the thalamic reticular nucleus (TRN) (Jurgens *et al.*, 2012). These inputs from layer 6 are facilitating and activation of CT cells results in predominantly inhibitory responses in thalamic excitatory relay cells due to the recruitment of the TRN (Cruikshank *et al.*, 2010; Jurgens *et al.*, 2012; Olsen *et al.*, 2012). Layer 6 inputs into the thalamus comprise of ~30% of the synaptic input whereas retinal input is ~ 10% (Sillito *et al.*, 2006). This is a striking demonstration of why the thalamus is not simply a

relay nucleus for sensory information as modulatory connections from the cortex outweigh the direct sensory input.

1.3 Cortical Inhibition

Inhibitory GABAergic neurons comprise 10-20% of the cells in rodent visual cortex (Meyer *et al.*, 2011), which is similar across species (Hendry *et al.*, 1989; Gabbott & Bacon, 1994). These inhibitory neurons are composed of 3 main subtypes: parvalbumin positive (PV+), somatostatin positive (SOM+) and 5Ht3aR neurons (Xu *et al.*, 2010; Rudy *et al.*, 2011). These sub-types have diverse morphology, electrophysiological properties, and connectivity. Of all neurons, PV+ and SOM+ neurons comprise 40% and 30% respectively (Rudy *et al.*, 2011). Inhibitory GABAergic neurons exert strong control over cortical activity as in the awake animal, inhibition is dominant over excitation (Haider *et al.*, 2013).

1.3.1 PV+ inhibitory neurons

PV+ inhibitory neurons are distinguished by their fast firing-rates (Kawaguchi & Kubota, 1997; Hasenstaub *et al.*, 2005; Cruikshank *et al.*, 2007). There are two main subsets of PV+ neurons, basket cells and chandelier cells (Tremblay *et al.*, 2016). Basket cells encompass the cell body of their targets and exert shunting inhibition; shunting inhibition is the result of open GABAergic channels increasing membrane conductance causing the amplitude of any excitatory inputs to be reduced (Silver, 2010). During visual input, shunting inhibition is the prevailing form of inhibition (Borg-Graham *et al.*, 1998). The other subtype of PV+ neurons are chandelier cells, which synapse onto the axon initial segment of target cells, blocking AP generation (Harris & Mrsic-Flogel, 2013; Tremblay *et al.*, 2016; Hooks & Chen, 2020). PV+ cells receive both local excitatory inputs within the cortex (Reyes *et al.*, 1998) and inputs from the thalamus (Cruikshank *et al.*,

2007). Notably, excitatory inputs to PV+ neurons are strongly depressing (Beierlein *et al.*, 2003).

1.3.2 SOM+ inhibitory neurons

Another subtype of inhibitory neurons are SOM+ cells, which were originally described as Martinotti cells (MCs) (Kawaguchi & Kubota, 1997; Wang *et al.*, 2004). Additional subgroups of SOM+ neurons have been observed. These include MCs, which reside and project across cortical layers, and other groups with more localised morphology restricted to the thalamo-recipient layers (Ma *et al.*, 2006; McGarry *et al.*, 2010). SOM+ neurons synapse onto the dendrites of their targets (Rudy *et al.*, 2011; Urban-Ciecko & Barth, 2016), contributing to more local dendritic computations between excitatory and inhibitory inputs. Both local excitatory inputs (Reyes *et al.*, 1998; Kapfer *et al.*, 2007; Silberberg & Markram, 2007) and thalamic excitatory inputs (Beierlein *et al.*, 2003) to SOM+ neurons are strongly facilitating. This suggests a more substantial recruitment after sustained excitatory activity. Consistent with this idea, burst stimulation of local excitatory neurons reliably activates ~30% of SOM+ neurons (Kwan & Dan, 2012).

1.3.3 Connectivity of PV+ neurons and SOM+ inhibitory neurons

Strong feed-forward inhibition onto excitatory cells is mediated by PV+ neurons (Xue *et al.*, 2014). Feedforward inhibition may dominate over feed-forward excitation (Cruikshank *et al.*, 2007, 2010), resulting in an inhibition dominated regime in the awake cortex (Haider *et al.*, 2013). Furthermore, PV+ cells show reciprocal connectivity, as photostimulation of PV+ neurons evoked inhibitory post-synaptic currents (IPSCs) in other PV+ neurons comparable to that observed in excitatory neurons (Pfeffer *et al.*, 2013). Reciprocal connection probability between PV+ cells is greater than the connection probability of PV+ to

excitatory cells (Jiang *et al.*, 2015; Campagnola *et al.*, 2022). Overall, PV+ cells uniquely show reciprocal and excitatory connectivity as there is a lack of connectivity from PV+ neurons onto SOM+ neurons (Pfeffer *et al.*, 2013). Furthermore, PV+ neuronal output is depressing (Beierlein *et al.*, 2003; Ma *et al.*, 2012). Functional assessment of PV+ inhibition via optogenetic translaminar activation of PV+ neurons evokes a cortex wide reduction in activity (Li *et al.*, 2019), suggesting a dominant inhibitory motif across all layers of the cortex.

Thalamic drive onto SOM+ neurons is much lower than that to PV+ neurons (Sermet *et al.*, 2019). SOM+ neurons receive predominantly local cortical inputs from both excitatory and inhibitory cells (Adesnik *et al.*, 2012; Jiang *et al.*, 2015; Campagnola *et al.*, 2022). Layer specific motifs in connectivity exist for the different sub-types of SOM+ cells. In layer 4, non-Martinotti SOM+ cells directly target PV+ neurons, causing disinhibitory responses in layer 4 excitatory cells (Li *et al.*, 2019). This motif exists in the hippocampus, where SOM+ activation blocks firing in PV+ neurons (Chamberland *et al.*, 2023) and in layer 4 in the cortex (Ma *et al.*, 2012; Xu *et al.*, 2013). While SOM+ cells do also target excitatory cells in layer 4 (Ma *et al.*, 2012), they heavily bias towards targeting of PV+ neurons. This is revealed by SOM+ activation evoking stronger IPSCs in PV+ neurons than in excitatory cells in layer 4 (Xu *et al.*, 2013). This inhibition leads to a reduction in firing in PV+ neurons and, critically, an increase in spiking output from layer 4 excitatory cells when SOM+ cells are activated (Xu *et al.*, 2013). However, Martinotti cells in layers 2/3 and 5 exert an predominantly inhibitory influence over excitatory cells (Kapfer *et al.*, 2007; Silberberg & Markram, 2007; Xu *et al.*, 2013). This local output from SOM+ neurons to excitatory cell is dense, with connections observed ~50% of the time within 400 microns (Fino & Yuste, 2011). Regardless of the target of SOM+ neurons, IPSCs

show facilitation (Ma *et al.*, 2012; Xu *et al.*, 2013). Despite this anatomical bias of disinhibition in layer 4 and inhibition elsewhere, layer 2/3 and 5 have been found to have some SOM to PV+ connections (Pfeffer *et al.*, 2013).

1.3.4 Divergent and convergent roles of PV+ and SOM+ inhibitory neurons in sensory stimuli processing, learning, and memory

1.3.4.1 Arithmetic operations of PV+ and SOM+ inhibitory neurons

A fundamental way in which neurons alter their activity in response to environmental demands is gain modulation. Gain modulation alters the input/output (I/O) curve of a neuron (Ferguson & Cardin, 2020), therefore altering the sensitivity of neurons to a given input. Additive and subtractive effects maintain the slope of the I/O curve but shift the firing lower or higher. Divisive and multiplicative effects change the slope of the I/O curve but have no effect on the baseline (Wilson *et al.*, 2012). The former often sharpens stimulus selectivity, whereas the latter allows changes in sensitivity to inputs, but maintains selectivity. Both excitation and inhibition can cause changes in neuronal gain (Murphy & Miller, 2003). Inhibitory inputs have subtractive effects on synaptic responses (Chance *et al.*, 2002) and action potential firing (Holt & Koch, 1997). However, shunting inhibition has a divisive effect on the I/O curve (Mitchell & Silver, 2003). How do we explain inhibition mediating both subtractive and divisive changes? The localisation of inhibitory inputs can push the system towards different computations. Inhibition at the level of the soma exerts divisive effects (changing the slope of the I/O curve), whereas inhibition at the level of the dendrite produces subtractive effects (Vu & Krasne, 1992). Due to the anatomical biases of PV+ and SOM+ inhibition onto the cell body and dendrites respectively, it has been proposed that these cell types contribute to different computations. Activation of PV+ neurons causes a primarily divisive effect on the I/O curve, whereas SOM+

activation causes subtractive effects (Atallah *et al.*, 2012; Wilson *et al.*, 2012; El-Boustani & Sur, 2014; Phillips & Hasenstaub, 2016). However, this may be dependent on the strength of the stimuli, as manipulation of SOM+ neurons with large stimuli shows divisive inhibition (El-Boustani & Sur, 2014). In addition, this may be dependent on intact local network connectivity as *ex vivo* recordings show SOM+ mediated division and PV+ mediated subtraction (Dorsett *et al.*, 2021).

1.3.4.2 Response profiles to visual stimuli

Regardless of inhibitory neurons having a subtractive or divisive effect over the cortex, inhibitory control over cortical activity is essential for sensory processing. Inhibition can allow for greater stimulus selectivity or allow for adaptation of activity over time. PV+ neurons lack orientation selectivity and exhibit broad tuning. Whereas excitatory cells are often highly orientation selective (Kerlin *et al.*, 2010). A contributing factor to this lack of orientation selectivity is that PV+ neurons receive broad input from many differently-tuned excitatory cells (Hofer *et al.*, 2011). PV+ neurons are correlated with the local network during artificial stimulation (Kwan & Dan, 2012) and exhibit stimulus-dependent and independent activity (Hofer *et al.*, 2011). This finding suggests PV+ neuronal activity is driven by local connections to one another and less so by sensory input. Activation of PV+ neurons has been found to sharpen V1 orientation tuning, allowing greater behavioural discrimination of orientations (Lee *et al.*, 2012), which may be mediated via an 'iceberg effect': a relative sharpening of tuning curves due to the suppression of non-preferred inputs below AP threshold (Shapiro *et al.*, 2022). SOM+ neurons have comparable moderately selective orientation tuning to excitatory cells in layer 2/3 and 4 (Ma *et al.*, 2010) and are activated strongly in response to full field visual stimuli (Keller *et al.*, 2020).

1.3.4.3 Contribution to stimulus response adaptation

In response to sensory input neural activity diminishes (Whitmire & Stanley, 2016) which is in part mediated by recruitment of inhibition (Ramaswami, 2014). A commonly observed phenomenon is adaptation of responses to stimuli over several minutes, which can be observed at multiple levels of the sensory processing stream (Kohn, 2007). This stimulus induced adaptation is observable in excitatory spiking responses (Natan *et al.*, 2015), calcium transients, evoked potentials (Hamm & Yuste, 2016) and intracellular voltage fluctuations (Chen *et al.*, 2015). Often, short-term adaptation is investigated within the confines of an oddball paradigm. This paradigm involves a frequent stimulus being presented and interrupted by an unexpected 'oddball' stimulus. These two stimuli are presented a total of ~88% and ~12% of the time, respectively. In this paradigm, stimulus specific adaptation (SSA) is defined as weakening of responses to the frequent stimulus, whereas an increased response to the oddball is defined as deviance detection (Ross & Hamm, 2020). Both SOM+ and PV+ neurons show reduced firing and membrane voltage response during repetitive stimuli presentation and exhibit increased responses to deviant stimuli (Chen *et al.*, 2015; Natan *et al.*, 2015). PV+ and SOM+ cells have distinct responses to frequent and oddball stimuli, suggesting that they may be involved in modulating the subsequent effects observed in excitatory cells. Inactivation of PV+ and SOM+ neurons reduces the difference between responses of excitatory cells to standard and oddball stimuli (Natan *et al.*, 2015). Interestingly, this difference is mediated via different mechanisms for each neuron subtype. When PV+ neurons are inactive, responses to both standard and oddball are increased, whereas when SOM+ neurons are inactive, responses to only the standard increases (Natan *et al.*, 2015). This suggests that SOM+ are only engaged to modify

responses to the standard and not the deviant, whereas PV+ neurons are engaged independent of stimulus type. During ‘frequent’ presentation, excitatory responses decrease, however, when SOM+ neurons are inactive this response decrement does not occur (Natan *et al.*, 2015) suggesting SOM+ inhibitory drive is needed for this response decrement. The SOM+ mediated effect was true for layer 4 but did not hold true in layer 2/3 (Natan *et al.*, 2015), which may reflect the different circuit motifs exhibited by these cells. In contrast, Hamm and Yuste (2016) did not see any impact of SOM+ neuron inactivation on the response decrement to frequent stimuli, but observed a significant impairment in deviance detection (Hamm & Yuste, 2016). However, these differences may come from the former study using inhibiting optogenetics, which are presented randomly across all standard and deviant stimuli, and the latter using inhibiting chemogenetics, which affects the system for the entire duration of the standard/ deviant trails.

Responses of cells also varies over shorter timescales. Over 10 seconds of stimuli presentation, there is facilitation and depression of excitatory cell activity (Heintz *et al.*, 2022). Interestingly, PV+ neuron activity increases over 10s, whereas SOM+ neurons show a combination of depression and sensitisation, ~70% and 30% of cells respectively. Furthermore, activation of PV+ neurons drives depression in excitatory cells whereas activation of SOM+ neurons drives sensitisation in excitatory cells (Heintz *et al.*, 2022).

Release of excitatory cells through SOM+-PV+ mediated disinhibition has consequences on stimuli processing, acting as a gating mechanism for forward transmission of information and plasticity. While viewing visual stimuli, SOM+ activation causes decreased firing in PV+ neurons, affecting orientation tuning of PV+ neurons and shifts PV+ activity into synchronicity with pyramidal cells (Cottam *et al.*, 2013). Entrainment of network activity may allow more

coordinated information flow. The idea of coordinated activity is important for information processing and variability of activity over repetitive stimulus presentations can limit information flow. During visual stimuli presentation, SOM+ activation and the resultant inhibition of PV+ neurons increases reliability of excitatory cell firing from trial to trial (Rikhye *et al.*, 2021), lending support to the idea that SOM+ neurons gate information flow by harnessing this disinhibitory motif. Furthermore, excitatory neurons lack responsiveness to visual gratings, however, in a small population of excitatory cells (~12%) SOM+ activation unmasks responses to visual stimuli (Heintz *et al.*, 2022). This unveiling of excitatory cell activity supports the conclusion that SOM+ neurons cause disinhibition, which may allow for greater activity in response to sensory stimuli, thereby resulting in experience-dependent Hebbian plasticity. In addition to SOM+ neurons mediating direct inhibition through GABA receptors onto PV+ neurons, the neuropeptide somatostatin, which can be co-released with GABA from SOM+ neurons, improves visual discrimination through increased orientation selectivity of layer 4/5 excitatory cells. This action occurs through suppression of PV+ visual responses, likely via a suppression of excitatory inputs onto PV+ cells (Song *et al.*, 2020).

1.3.4.4 Changes in activity over learning

Learning has a profound effect on the response properties of GABAergic neurons. Over learning, PV+ neurons become more orientation selective (Khan *et al.*, 2018). However, there are heterogenous changes in SOM+ orientation selectivity across learning. Correlation between SOM+ neurons and excitatory cells predicts changes in excitatory cell responses over learning (Khan *et al.*, 2018), suggesting SOM+ neurons may gate experience-dependent plasticity. Importantly, these tasks involved reward based learning. The introduction of

rewards (Garrett *et al.*, 2023) rapidly increases excitatory responses and suppresses SOM+ neurons (Kato *et al.*, 2015). Furthermore, task-based paradigms can reduce the activity of SOM+ neurons (Makino & Komiyama, 2015).

It important to note how both PV+ neurons and SOM+ neurons alter their activity during passive experience. Over passive exposure to a single orientation, SOM+ neuron activity increases and PV+ neuron decreases and becomes inhibited (Makino & Komiyama, 2015; Hayden *et al.*, 2021). The resultant PV+ neuron activity during novelty is increased and SOM+ activity is decreased (Hayden *et al.*, 2021). Furthermore, repetitive sound exposure causes a reduction in excitation and an increase in inhibition in layer 2/3 as a result of increased SOM+ activity and decreased PV+ activity, whereas in layer 4 there is both reduced excitation and inhibition (Kato *et al.*, 2015). Exposure to sets of images evokes larger in response to novel images compared to familiar images in SOM+ neurons (Garrett *et al.*, 2023). In addition, excitatory cells have increased calcium responses to novel stimuli and decreased calcium responses to familiar stimuli (Kim *et al.*, 2020; Garrett *et al.*, 2023). This supports the idea of SOM+ mediated disinhibition, as under this regime, higher SOM+ activity during familiarity should result in increased excitatory responses. Furthermore, cell spiking (action potentials) in layer 4 in response to novel stimuli is on average greater than in response to familiarity, despite an increase in peak-firing to familiar stimuli (Cooke *et al.*, 2015; Hayden *et al.*, 2023). SOM+ disinhibition may contribute these changes in action potential distribution in response to familiar and novel stimuli as there is a change in PV+ neuronal synchronicity during SOM+ activation (Cottam *et al.*, 2013).

1.3.4.5 Brain state dynamics

Brain activity follows specific timing regimes, and these can be observed as phasic activity recorded in local field potentials and EEG (Buzsáki *et al.*, 2012). Different oscillatory states occur during different processing modes and modulation is influenced by the level of inhibition. Higher-frequency states, like gamma (30-80 Hz) and Beta (13-30 Hz) are associated with active processing, whereas lower-frequency states, like alpha (8-12 Hz) are associated with quiet wakefulness and sleep likely recruiting offline-processing mechanisms (Alitto & Dan, 2010).

General suppression of PV+ cells has been found to have a broadband effect of increased power across the spectrum (Veit *et al.*, 2017) supporting their role in gain of neuronal responses. However, driving PV+ cells with a range of frequencies from 1-200 Hz increases power in the 20-80 Hz frequency band in the anaesthetised (Cardin *et al.*, 2009) and awake animals (Chen *et al.*, 2017). This suggests an important role of rhythmic activity of these cells in the production of the gamma rhythm in the brain, which is important in active processing. This control of gamma may arise from the membrane properties of PV+ neurons as these cells do not attenuate to high-frequency inputs. Furthermore, inputs to PV+ neurons produce spiking output in the 30-80 Hz range (Hasenstaub *et al.*, 2005). In addition, during visual stimuli presentation, beta and gamma (65-80) power normally increases, but PV+ inactivation reduces this visually evoked beta and gamma (Chen *et al.*, 2017). Overall, PV+ neurons mediate gamma band production, but due to their strong influence over the cortex, manipulating these cells also affects the higher end of the beta band (Cardin *et al.*, 2009; Chen *et al.*, 2017; Veit *et al.*, 2017).

SOM+ neurons likely mediate beta frequency as SOM+ inactivation decreases power in the 20-30 Hz range (Veit *et al.*, 2017) and driving SOM+ neurons with frequencies ranging from 1-200 Hz reliably evoked activity in the 5-30Hz range (Chen *et al.*, 2017). Additionally, the visual stimulus evoked beta power increase is blocked by SOM+ inactivation (Chen *et al.*, 2017). During presentation of deviant stimuli in oddball paradigms theta/ alpha power increases, but SOM+ inactivation blocks this effect (Hamm & Yuste, 2016).

High-frequency (gamma) power decreases and low-power (alpha/ beta) increases during stimulus-selective response potentiation (SRP). The change in gamma and beta oscillations tallies with the decrease of PV+ activity and increased SOM+ activity (Hayden *et al.*, 2021), strongly suggesting that the oscillatory changes observed over SRP could be a consequence of the changing GABAergic neuronal activity.

1.3.5 Disrupted inhibition in disease

Inhibitory GABAergic neurons are well-established to be critical during normal cortical processing. Additional evidence for this critical role is that inhibition is commonly disrupted in disease (Barron *et al.*, 2017; Heinze *et al.*, 2021). In humans, inhibitory markers are altered in schizophrenia (Lewis *et al.*, 2005) and autism spectrum disorder (ASD) (Blatt & Fatemi, 2011).

To probe the mechanisms of these diseases, murine models can be used to investigate circuit abnormalities that mimic some elements of disease. Mouse models of genes associated with schizophrenia find disrupted connectivity between PV+ neurons and excitatory cells resulting in impaired cortical processing and behaviour (Fazzari *et al.*, 2010; Del Pino *et al.*, 2013; Mukherjee *et al.*, 2019; Batista-Brito *et al.*, 2023).

1.4 Tools to measure neuronal activity in mouse visual cortex: benefits and drawbacks

1.4.1 Recording cellular activity

Traditionally, investigation into visual cortical plasticity has occurred in cats and non-human primates (Wiesel & Hubel, 1963; Hubel *et al.*, 1977). Recent work has favoured the mouse as a common system to investigate visual changes due to the wide range of experimental genetic tools that can be used to target specific molecular and circuit mechanisms (Montgomery *et al.*, 2021; Niell & Scanziani, 2021). Despite the evident differences in the mouse brain, such as a lissencephalic structure and lack of orientation maps, which results in a “salt and pepper” mapping of orientation (Ohki *et al.*, 2005), the mouse brain shares many morphological and functional characteristics with human brains. These include a retinotopic organisation, a 6-layer visual cortex and similar proportions of excitatory and inhibitory neurons. While vision is not the mouse’s dominant sense, they can differentiate contrasts, spatial frequencies, and directionality. Genetic manipulation is a common technique in mice which allows targeting of specific cell types (Huberman & Niell, 2011). This is achieved by expressing CRE recombinase, or an alternative recombinase, under a genetic promotor unique to that cell type. Consequently, an injection of a recombinase-dependent virus allows expression of specific channels which can inhibit or activate these cells with light or ligands. In the DREADDs (Designer Receptors Exclusively Activated by Designer Drugs) system, a modified muscarinic G-protein coupled receptor that induces inhibition (hM4Di) or activation (hM3Dq) of cells after the application of clozapine-N-oxide (CNO) (Armbruster *et al.*, 2007; Urban & Roth, 2015). The optogenetic system makes use of light gated ion channels to allow activation (Channelrhodopsin: ChR) or inhibition (Halorhodopsin: NpHR) with blue light and

green light respectively (Lee *et al.*, 2020). Overall, the mouse provides a unique set of tools to investigate specific cell types by altering their activity, within a system that is comparable to non-human primates and humans.

The lack of orientation mapping in the mouse brain is beneficial for recording, as recording from a small area will pick up responses to visual stimuli with different feature selectivities. A common technique is the use of blunt tungsten electrodes implanted into the brain, which records an extracellular signal: the local field potential (LFP). The LFP reflects ongoing, synchronous synaptic activity (Haider *et al.*, 2016) from ~250 microns around the electrode (Katzner *et al.*, 2009). Furthermore, these electrodes can be chronically implanted which allows for recordings to take place during long-term and short-term learning and plasticity. The contributing factors to the LFP signal have not been fully dissected and will in some part be contributed to by, to name a few, action potentials, glial electrical activity, and volume conduction from other areas (Buzsáki *et al.*, 2012). Thus, a major drawback of LFP is the inability to distinguish the origins of the signal fully. High-density silicon probes with multiple channels allows for recording of LFP and single units (action potentials) from different cell types. Spike-wave sorting allows allocation of these units to specific cell types, for example PV+ neurons are fast-spiking and have a short AP latency (Kawaguchi *et al.*, 2019). This technique can delineate the origin of the electrophysiological signal more precisely than LFP but will still potentially mis-label cell types. A key benefit of these techniques is the recording of neural activity in the awake behaving animal with high temporal precision.

1.4.2 Recording synaptic currents

A general limitation of extracellular signals is the contribution to the signal from multiple neurons and synapses. Current flow across the membrane of single cells

can be observed with intracellular recording (Hodgkin & Huxley, 1952). Intracellular recordings are commonly achieved by targeting of neurons using a glass pipette in ex-vivo slices (Suter *et al.*, 1999). Ex-vivo electrophysiology is a useful tool for investigating changes in the excitatory and inhibitory synaptic inputs that a cell receives (Reyes *et al.*, 1998). Furthermore, *ex vivo* electrophysiology can be used to probe changes in intrinsic properties of cells, for example AP firing threshold (Tremblay *et al.*, 2016). In addition, using the genetic tools outlined above, specific cell types expressing fluorescent markers can be targeted for intracellular recordings. Targeted intracellular recording from specific cell subtypes allows investigation of changes of synaptic inputs directly onto these cells (Pan-Vazquez *et al.*, 2020). However, the most obvious limitation of this technique is dissociation of the cells in the slice from the intact awake system.

1.4.3 Cell specific manipulations

Despite the key benefits and flexibility of current techniques allowing for cell specific activation and inhibition, both DREADDs and optogenetics have side effects which need to be controlled for. In chemogenetics (DREADDs), the ligand CNO can be metabolised to clozapine, which can have off target behavioural effects (Manvich *et al.*, 2018) in a dose dependent manner (MacLaren *et al.*, 2016).

Optogenetics makes use of inflow and outflow of ions to control cell activity. The optogenetic actuator ChR is a sodium channel and cells in the brain have adequate mechanisms to deal with greater sodium presence. Thus, longer activation of cells should not cause any hang-over effects in the cells. However, extended activation of the actuator NpHR (Halorhodopsin), which is a chloride channel, produces excessive chloride within the cells can trigger light-off evoked

rebound firing (Raimondo *et al.*, 2012) and requires extended periods of recovery to allow cells to return to normal. A further consideration with light is penetration into the brain, shorter wavelengths like blue light show a superficial spatial localisation (~300 µm), whereas longer wavelengths (red/ orange) can penetrate to deeper layers (~700 µm) (Li *et al.*, 2019). Therefore, to target deeper layers with light, optic fibres need to be implanted further into the brain.

Due to the off-target effects, when using chemogenetics and optogenetics, an empty vector control, lacking the active receptor/ channel, must be used and the ligand or light delivered to these animals. Furthermore, while using optogenetics if experimental conditions allow, an internal control (light off/ light on) can be used within a session to dissociate any hang-over effects induced by light inactivation and activation. A common conception is that opposite manipulations will cause opposite effects on the experimental phenomenon being recorded. However, activation and inhibition of the same cell type can have asymmetrical effects on neuronal response properties and these differences are exacerbated by differences in the baseline activity of the network (Phillips & Hasenstaub, 2016). Furthermore, an important consideration is the ability of the brain to compensate for these disruptions, whereby the manipulations can transiently effect activity or behaviour (Hong *et al.*, 2018). Thus, careful interpretation of positive and negative influence on specific cell types must occur.

1.5 Thesis aims and outline

Despite the well-established changes in visual cortical activity due to the plasticity that occurs over days (Clawson *et al.*, 2018; Henschke *et al.*, 2020; Montgomery *et al.*, 2021) changes in activity over shorter timescales, specifically over the course of minutes and seconds, has not been investigated. Inhibitory neurons can mediate direct inhibition onto excitatory cells or disinhibition due to inhibitory-

to-inhibitory connections. There is a nuanced role of inhibition and disinhibition in visual cortical plasticity and adaption over different timescales. Contributions to changes in activity at different timescales by different cell types has not been directly assessed. In this thesis I pursued three main aims:

1. Dissect out different timescales of visual cortical plasticity and adaptation in addition to the previously published long-term plasticity (SRP) and the associated contribution of PV+ neurons and NMDA receptors to these timescales of plasticity (Chapter 2).
2. To further investigate the role of PV+ and SOM+ inhibitory neurons in visual cortical plasticity and adaptation. In addition, to investigate changes in inhibitory synaptic currents in layer 4 (Chapter 3).
3. To probe the role of prenatal deletion of ErBB4, a genetic risk factor in schizophrenia, in visual cortical plasticity and adaptation (Chapter 4)
4. To investigate whether Layer 6 plays a role in visual cortical plasticity and adaptation due to connections to PV+ neurons and the thalamus. In addition to this, pilot experiments were done to probe changes in excitatory synaptic inputs into visual cortex (Chapter 5).

Chapter 2 Multiple Mechanistically Distinct Timescales of Neocortical Plasticity Occur During Habituation

In this chapter I discuss the changes in visual cortical activity that occur over seconds, minutes and days and the involvement of NMDA receptors and PV+ interneurons.

2.1 Statement of work

Paper was submitted and reviewed to Frontiers in Cellular Neuroscience and published 2022. Data was originally collected by Sam Cooke in Mark Bear's lab (MIT). Raw data used in figures 1 and 2 previously published by Kim et al. 2020. Raw data used in figure 3 and 4 previously published by Cooke et al. 2015, and figure 5 published by Kaplan et al. 2016. Extended data analysis was performed on this data, by myself, which elucidated further phenotypes which are discussed below. PDF of published and formatted paper is in Appendix A.

2.2 Introduction

Learning and memory enable organisms to adapt to altered pressures in the environment to produce appropriate responses to stimulus and context over a variety of timescales (McGaugh, 2000). Substantial gaps remain in our understanding of the neural underpinnings of these processes, in part due to difficulties in observing and intervening in underlying plasticity as learning and memory occur (Neves *et al.*, 2008). Habituation is one relatively robust, easy to observe and apparently simple form of learning, in which organisms acquire familiarity with innocuous stimuli and selectively reduce behavioural responses to those stimuli over seconds, minutes, and days (Cooke & Ramaswami, 2020). Habituation forms a foundation for further learning by enabling energy and attention to be devoted to stimuli of already established salience, or novel stimuli

that may have future significance (Rankin *et al.*, 2009; Schmid *et al.*, 2014) and disruptions in this process likely contribute to a range of psychiatric and neurological disorders (Ramaswami, 2014; McDiarmid *et al.*, 2017). This form of learning has commonly been ascribed to a neural process known as adaptation, which reduces feedforward synaptic activity in response to repeated non-associative stimulation (Groves & Thompson, 1970), especially over shorter timescales (Chung *et al.*, 2002). However, a competing theory, known as the comparator model (Sokolov, 1963), suggests the formation of long-lasting memory of familiar stimuli through Hebbian synaptic potentiation, which in turn suppresses behavioural output by recruiting inhibitory systems. It remains possible that both models apply but over different timescales (Cooke & Ramaswami, 2020). In this study, we have assessed plasticity in primary visual cortex (V1) of mice in response to repeated presentations of oriented, phase reversing visual stimuli to assess whether different directions of plasticity can be observed across different timescales.

It is now well established that the magnitude of visual-evoked potentials (VEPs) recorded in layer 4 of mouse binocular V1 increases dramatically over days of repeated stimulation through an orientation-specific form of plasticity known as stimulus-selective response potentiation (SRP) (Frenkel *et al.*, 2006; Cooke & Bear, 2010). This form of plasticity is also manifest as an increase in the peak firing rate of V1 neurons (Aton *et al.*, 2014; Cooke *et al.*, 2015) and many of the known molecular mechanisms are consistent with the involvement of Hebbian synaptic potentiation, notably including a requirement for the NMDA receptor during induction and AMPA receptor insertion during expression (Frenkel *et al.*, 2006; Cooke & Bear, 2010). Importantly, mice produce behavioural responses to the onset of these visual stimuli that exhibit significant orientation-selective

habituation over days (Cooke *et al.*, 2015; Kaplan *et al.*, 2016; Fong *et al.*, 2020; Finnie *et al.*, 2021), and this process also requires the presence of NMDA receptors in V1. In addition, a cortical cell-type that exerts exquisite inhibitory control over excitatory cell activity, the parvalbumin-expressing (PV+) inhibitory interneurons (Atallah *et al.*, 2012), are critical for differential cortical and behavioural responses to familiar and novel stimuli after SRP and accompanying habituation (Kaplan *et al.*, 2016). Thus, SRP comprises a robust and relatively well understood form of plasticity that occurs concomitantly with and shares mechanism with long-term memory.

One fascinating feature of SRP is that it does not manifest within a ~30-minute recording session but starts to emerge the following day (Frenkel *et al.*, 2006) and recent work has demonstrated that SRP is dependent on consolidation processes that occur during sleep (Aton *et al.*, 2014; Durkin *et al.*, 2017). Activity in the primary relay nucleus of the thalamus, the dorsal lateral geniculate nucleus (dLGN), does increase over the course of 30 minutes prior to the emergence of SRP in the cortex (Durkin *et al.*, 2017), but there has so far been no description of what happens over this time-course in V1. Although we have previously described evidence for a faster adaptation that is apparent when comparing the beginning of a 200-phase reversal block with the end (Kim *et al.*, 2020), we have not described the time-course of this adaptation during this 100-second block. In neither case is there any understanding of the underlying mechanism. In the current study, we show that cortical plasticity accompanying behavioural habituation occurs across seconds, minutes, and days of repeated stimulus experience. Notably, these forms of plasticity diverge in direction and mechanism, and there is evidence of an interaction in which long-term familiarity suppresses adaptation. In striking opposition to our observations of SRP during

long-term habituation (Cooke *et al.*, 2015), layer 4 response magnitude decreases over seconds and minutes in V1. Loss of expression of NMDA receptors from neurons in V1 impairs plasticity and adaptation across all timescales. However, inactivation of PV+ neurons has a more nuanced effect, revealing the existence of two separable forms of fast adaptation within a stimulus block. Moreover, we show that the interaction between long-lasting familiarity and adaptation requires the activity of PV+ neurons. Thus, a range of mechanistically separable forms of plasticity can be assayed across different timescales in the same learning mouse.

2.3 Materials and Methods

2.3.1 Animals

All procedures were carried out in accordance with the guidelines of the National Institutes of Health and protocols approved by the Committee on Animal Care at the Massachusetts Institute of Technology. Figure 1 and 2 is composed of data from male C57B6/J mice (Charles River laboratory international, Wilmington, MA). NMDA knock-down experiments (Figure 3, 4) make use of GRIN$^{fl/fl}$ mice (B6.129S4-*Grin1*^{tm2Stl}/J – Jackson laboratory). PV+ interneuron inactivation (Figure 5) uses PV-Cre mice (B6;129P2-*Pvalb*$^{tm1(cre)Arbr}$/J – Jackson laboratory). All animals had food and water available ad libitum and were maintained on a 12-hour light-dark cycle.

2.3.2 Viral transfection

In the NMDAR knock-down and PV+ inactivation experiments viral vectors were administered via stereotaxic injections into the mice. For the NMDA knock-down, GRIN$^{fl/fl}$ mice (B6.129S4-*Grin1*^{tm2Stl}/J – Jackson laboratory) underwent surgery at ~ 1 month. AAV8-hSyn-GFP-Cre (knockdown; UNC viral core) or AAV8-hSyn-GFP (control; UNC viral core; generated by B. Roth's laboratory) were injected in

quantities of 13.5 nl 10 times at depths 600 µm, 450 µm, 300 µm, and 150 µm below surface. Each injection was separated by 15 s and after repositioning 5 minutes was allowed. For the PV+ inactivation experiment, AAV9-hSyn-DIO-HA-hM4D(Gi)-IRES-mCitrine virus (UNC viral core – generated by Dr. Brian Roth's laboratory) was injected into PV-Cre or WT-littermates in quantities of 81 nl at depths 600 µm, 450 µm, 300 µm below surface, including a 5-minute delay after repositioning. Viral transfections were performed in both hemispheres and were immediately followed by V1 electrode implantation, outlined below. Following surgery, mice were allowed 3 weeks for full viral expression.

2.3.3 V1 electrode implantation

Mice were anaesthetized with an intraperitoneal (i.p) injection of 50 mg/kg ketamine and 10 mg/kg xylazine for surgery. 1% lidocaine hydrochloride anaesthetic was injected locally under the scalp and 0.1 mg/kg Buprenex was delivered sub-cutaneously for analgesia. Iodine and 70% ethanol were used to clean the scalp. The skull was cleaned, dried, and scored using a blade. A steel headpost was fixed over the frontal suture using super glue (ethyl cyanoacrylate). Burr holes were drilled 3.1 mm lateral to lambda (to target binocular V1). Tungsten recording electrodes (FHC, Bowdoinham, ME, US) were implanted 450 µm below surface in both hemispheres. Silver wire reference electrodes were placed in prefrontal cortex bi-laterally.

2.3.4 Visual Stimuli

Visual stimuli were generated using software developed by Jeff Gavornik (https://github.com/jeffgavornik/VEPStimulusSuite). The display was 20 cm in front of the mouse, and mean luminance was 27 cd/m2. Sinusoidal phase reversing gratings were presented full field, reversing at 2 Hz. In most experiments, blocks consisted of 200 phase reversals, each block was presented

5 times interleaved with 30 seconds of grey screen. Gamma-correction was performed to maintain constant luminance between gratings and grey screen. The 5 blocks were repeated until day 6. On the final day, day 7, the familiar orientation (X°) was pseudo-randomly interleaved (such that no more than 2 blocks of the same orientation were shown in sequence) with a novel orientation (X+90°). Orientations were never within 25° of horizontal. In the PV+ inactivation experiment (Figure 5) 10 blocks were shown. On day 7 familiar (X°) and novel (X°-60) stimuli were shown. Then CNO was administered at 5mg/kg via intraperitoneal (i.p) injection. After a 15-minute wait, the familiar stimulus (X°) was presented with a new novel stimulus (X°+60).

2.3.5 *In vivo* data acquisition and analysis

Mice recovered from electrode implantation then underwent 2 days of habituation, followed by the 7-day protocol outlined above. All data was acquired using the Plexon data acquisition system (Plexon Inc, Dallas, TX, US). Local field potentials (LFP) were collected from V1 in both hemispheres, and piezoelectrical signal was reduced in amplitude and digitized into a third recording channel. Animals were head fixed at the opening of a metal cylinder tube and positioned on a piezoelectric transducer placed under the front paws but touching the metal cylinder. Piezoelectric signal therefore consists of mainly front paw movement but hind paw/ whole body movements also contribute to the signal due to vibrations via the metal tube. All digital channels were recorded at 1 kHz sampling and run through a 500 Hz low-pass filter. Data was extracted into Matlab using custom software. For the analysis over days, 450 ms traces following stimulus onset were averaged over 1000 phase reversals (5 blocks x 200 phase reversals). For the across block analysis, traces were averaged over 200 phase reversals. For the within-block analysis (1v2, 1v200), each individual phase reversal was averaged

over 5 blocks. VEP magnitude was taken as the minimum microvolt value from 1-100 ms following onset subtracted from the maximum microvolt value taken from 75-250 ms following onset.

2.3.6 Statistics

All data is expressed as mean ± SEM and number of animals is represented by n. All statistical analysis is non-parametric due to small n numbers negating true testing of normality. For comparisons between two groups or time points, a paired Wilcoxon signed rank test is used, for adaptation ratio analysis a one-sample Wilcoxon signed rank test is used with a μ of 1. Repeated measures Friedman test is used for analysis across multiple time points within one group. Where multiple tests have been performed, all p values are adjusted using false discovery rate (FDR) correction.

2.4 Results

2.4.1 Habituation can be observed within and across days in the same animal

Visual stimuli were presented over multiple timescales within a longitudinal experimental design to awake head-fixed mice. This approach allowed for investigation into the change in neocortical activity across these different timescales as visual-evoked behaviour was concomitantly monitored. Awake mice were head-fixed and viewed full field, oriented, 0.05 cycles/degree, 100% contrast, phase-reversing, sinusoidal grating stimuli while concurrently recording layer 4 local fields potentials (LFPs) with chronically implanted tungsten microelectrodes and behaviour using a piezoelectric sensor (Figure 2.1A). After a 5-minute period of grey screen (equivalent luminance to the grating stimuli to follow) to settle the animal into head-fixation, a stimulus of one fixed orientation (X°) was presented at a temporal frequency of 2 Hz for 200 phase reversals,

resulting in ~100 seconds of continuous stimulus presentation (we describe this as a stimulus **block** throughout). This block was repeated 5 times with 30-second-long grey screen intervals separating them. Overall, this session lasted approximately 15 minutes (5 minutes of grey followed by ~10 minutes of stimulus blocks and intervening grey). These sessions, each containing 5 separated blocks, were then repeated once each over 6 days. On the 7th day, 5 blocks of the original orientation (X°) were presented pseudo-randomly interleaved with a novel orientation (X+90°), such that no more than 2 blocks of one orientation were presented in sequence (Figure 2.1B). This experimental design allowed for analysis of habituation and cortical plasticity across days and within a day.

We found that behavioural habituation occurred both within a day and across days. After the onset of a block of visual stimuli, animals produce a pronounced behavioural response, which we measured using a piezoelectric device and previously termed a vidget (Cooke *et al.*, 2015). Using the vidget, we were able to observe behavioural habituation within a single recording session on day 1 (n = 30), when the X° stimulus was novel. The vidget magnitude dropped considerably by the second block and remained low (Figure 2.1C; Friedman test: p = 0.008, Wilcoxon signed-rank on B1-B2: p = 0.02, B1-B3: p = 0.7, B1-B4: p = 0.04, B1-B5: p = 0.5; FDR correction for multiple comparisons), indicating the occurrence of short-term habituation on day 1. When averaged over all 5 blocks, the magnitude of vidgets was greater on day 1 than on the following days (Figure 2.1D; Friedman test: p=0.3; Wilcoxon signed-rank on day 1- day 2: p = 0.05, day 1- day 3: p = 0.05, day 1- day 4: p = 0.2, day 1- day 5: p = 0.09, day 1- day 6: p = 0.05; FDR correction for multiple comparisons), indicating the occurrence of long-term habituation. During presentation of blocks of a novel stimulus (X+90°), interleaved with the familiar X° stimulus on the final day, vidgets were increased

in magnitude for the novel compared to the familiar stimulus (Figure 2.1E; Wilcoxon signed-rank test: $p<0.001$), just as we have described previously (Cooke *et al.*, 2015; Kaplan *et al.*, 2016; Fong *et al.*, 2020).

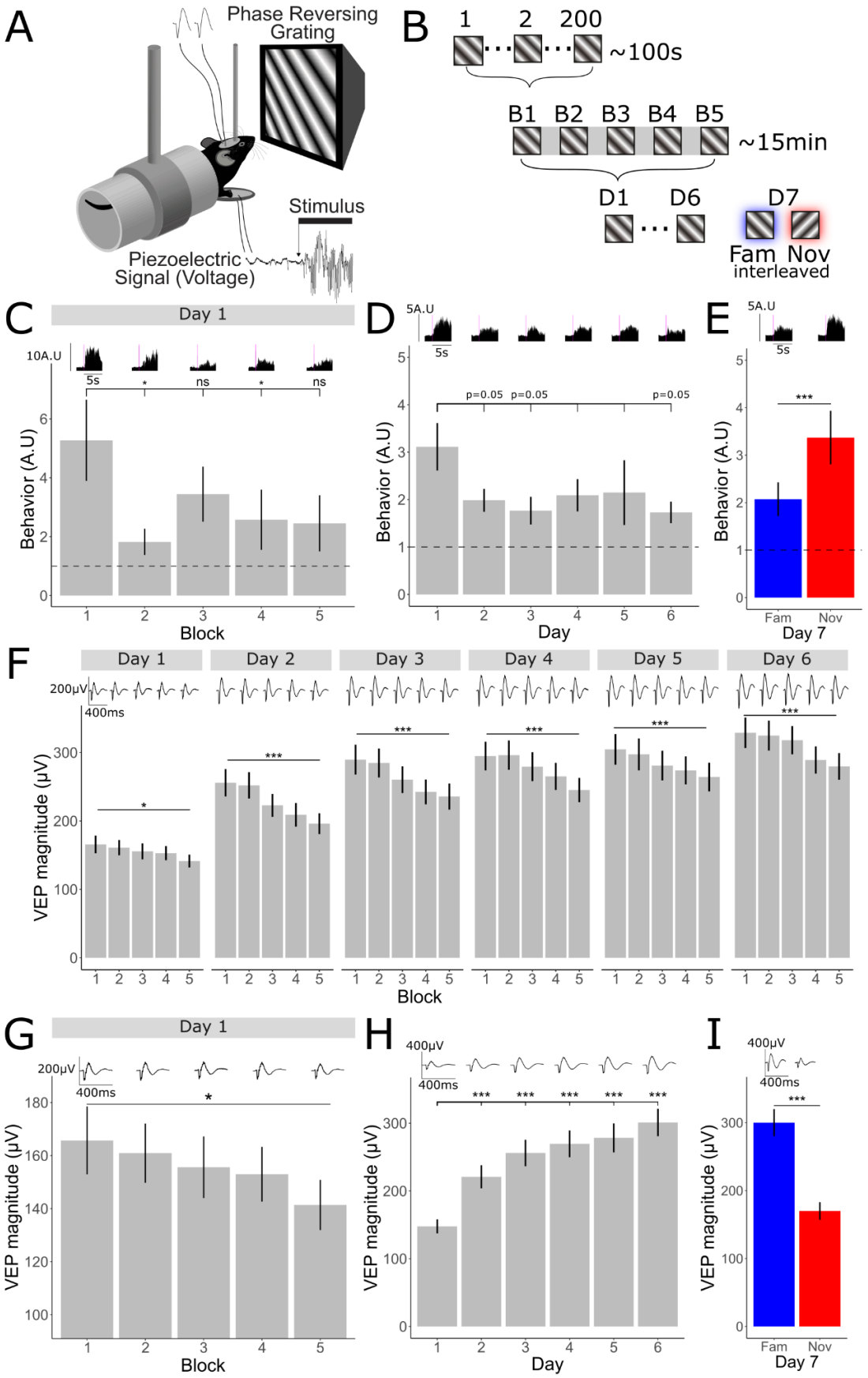

Figure 2.1 V1 plasticity accompanying long- and short-term habituation occurs in opposing directions (A) Schematic of recording set-up. Mice viewed phase reversing gratings while layer 4 local-field potentials were recorded through implanted tungsten electrodes and movement was recorded through a piezo-electrical device. (B) 1 through 200 individual phase reversals were shown lasting approximately 100

seconds (1 block). Five blocks were shown lasting approximately 15 minutes within one session. One session of 5 blocks was shown for 6 days. On the 7th day, the familiar orientation (previously viewed) and a novel orientation were shown pseudo-randomly interleaved. (C) Comparison of behavior across blocks (n = 30). Friedman test $\chi2(4) = 13.8$, $p = 0.008$. Post-hoc analysis of individual comparisons of block 1-block 2: $p = 0.02$, block 1-block 3: $p = 0.7$, block 1-block 4: $p = 0.04$, block 1-block 5: $p= 0.5$. FDR correction for multiple comparisons. (D) Behavioral change over day 1 to day 6 (n = 30). Freidman test $\chi2(5) = 6.55$, $p = 0.3$. Post-hoc analysis of individual comparisons of day 1-day 2: $p = 0.05$, day 1-day 3: $p = 0.05$, day 1-day 4: $p = 0.2$, day 1- day 5: $p = 0.09$, day 1-day 6: $p = 0.05$. FDR correction for multiple comparisons. (E) Behavioral response to familiar and novel (n = 30). Wilcoxon signed-rank test fam vs nov: $p < 0.001$. (F) VEP magnitude from block 1 to 5 over 6 days (n = 33). Comparison across blocks, Friedman test, day 1: $\chi2(4) = 12.8$, $p = 0.01$, day 2: $\chi2(4) = 69.8$, $p < 0.001$, day 3: $\chi2(4) = 55.1$, $p < 0.001$, day 4: $\chi2(4) = 43.8$, $p < 0.001$, day 5: $\chi2(4) = 32.5$, $p < 0.001$, day 6: $\chi2(4) = 38.6$, $p < 0.001$. FDR correction for multiple comparisons. (G) VEP magnitude from block 1 to 5 on day 1 (n = 33). Friedman test across blocks on day 1; $p = 0.01$. (H) VEP magnitude potentiation over day 1 to day 6 (n = 33). Freidman test $\chi2(5) = 95.9$, $p < 0.001$. Post-hoc analysis of individual comparisons of day 1-day 2, day 3, day 4, day 5, day 6: all $p < 0.001$, FDR correction for multiple comparisons. (I) VEP magnitude response to familiar and novel (n = 33). Wilcoxon signed-rank test fam vs nov: $p < 0.001$. Asterisks throughout denote significance (*$p < 0.05$, **$p < 0.01$, ***$p < 0.001$) while ns denotes non-significant. Where $p = 0.05$, this is explicitly stated.

2.4.2 V1 plasticity accompanying long- and short-term habituation occurs in opposing directions

Phase-locked LFP responses from layer 4 were averaged together to assess changes in visual-evoked potential (VEP) magnitude within a day and across days (n = 33). We found that the changes in VEP magnitude occurred in differing directions dependent upon the timescale. A very clear decrement in VEP magnitude was apparent over the course of 5 blocks of stimulus presentation (~10 minutes) within day 1 (Figure 2.1F, G; Friedman test across blocks on day 1; $p=0.01$), following the trend of behavioural habituation. This effect became more pronounced after the first day of stimulus presentation (Figure 2.1F; Friedman test: day 1; $p=0.01$, day–2 - 6 $p<0.001$; FDR multiple comparisons corrected). In contrast, across days there was significant potentiation of VEP magnitude (Figure 2.1H; Friedman test: $p<0.001$) and this potentiation was orientation specific, because VEP magnitude was reduced to baseline in response to the novel orientation (Figure 2.1I; Wilcoxon signed-rank test: p

<0.001). Thus, SRP is also present in these animals, just as described previously (Frenkel *et al.*, 2006; Cooke & Bear, 2010). Importantly, a response decrement accompanies short-term habituation, while response potentiation accompanies long-term habituation in the same animals.

2.4.3 Short-term adaptation occurs within a stimulus block

Next, we wanted to determine whether even shorter timescales of plasticity could be identified within the same experiments, this time focusing on plasticity across a single stimulus block. We averaged VEP magnitude for each of the 200 phase reversals within a block across all 5 blocks on day 1 and across animals (n = 33). Over the course of 200 phase reversals (~100s) we observed a reduction in the VEP magnitude (Figure 2.2A). Most notably, there was an immediate reduction from phase 1 to phase 2 (Figure 2.2A, B; Wilcoxon signed-rank on phase 1 to 2: $p<0.001$), followed by a striking rebound over the next few phase reversals. A steadier reduction in VEP magnitude was observed across all 200 phase reversals, culminating in a significant difference between phase reversal 1 and phase reversal 200 (Figure 2.2A, C; Wilcoxon signed-rank on phase 1 to 200: $p = 0.001$). Thus, clear evidence is apparent of adaptation within a stimulus block, indicating at least one, and perhaps two additional potential timescales of plasticity to be investigated.

2.4.4 Short-term adaptation is modulated by stimulus familiarity

Short-term adaptation occurred from both the first to the second and the first to the last phase reversal in a stimulus block when a stimulus was relatively novel on day 1, but did that plasticity persist for highly familiar stimuli? By assessing averaged within-block adaptation over the course of 6 days of long-term observation, we found that adaptation from the first to the second phase reversal was gradually reduced over days (Figure 2.2D; Wilcoxon signed-rank test on

phase 1 vs 2 on day 1: $p < 0.001$, day 2: $p < 0.001$, day 3: $p = 0.002$, day 4: $p = 0.008$, day 5: $p = 0.05$, day 6: $p = 0.04$; FDR correction for multiple comparisons). Although this adaptation from the first to the second phase reversal lessened as the stimulus became familiar over days, significant adaptation remained and the adaptation ratio (AR) ($1^{st}/2^{nd}$) was always significantly above 1 (Figure 2.2E; one sample Wilcoxon signed-rank test on AR ($\mu=1$) on day 1: $p < 0.001$, day 2: $p < 0.001$, day 3: $p < 0.001$, day 4: $p < 0.001$, day 5: $p < 0.001$, day 6: $p = 0.002$; FDR correction for multiple comparisons). On day 7, there was greater adaptation for the novel stimulus than for the familiar orientation in pseudo-randomly interleaved blocks (Figure 2.2F; Wilcoxon signed-rank test on phase 1 vs 2 on day 7 fam: $p = 0.02$, day 7 nov: $p < 0.001$; FDR correction for multiple comparisons) and the AR ($1^{st}/2^{nd}$) for the familiar stimulus was significantly reduced compared to that in response to the novel stimulus (Figure 2.2G; Wilcoxon signed rank day 7 fam AR vs day 7 nov AR: $p = 0.009$) suggesting modulation of adaptation from the 1^{st} to 2^{nd} phase reversal by long-term familiarity.

A more pronounced modulation of adaptation by long-term familiarity was observed for adaptation from the first to the last phase reversal. Adaptation from phase reversal 1 to 200 was no longer significant by day 4 and thereafter (Figure 2.2H; Wilcoxon signed-rank phase 1 v 200 on day 1: $p = 0.008$, day 2: $p = 0.04$, day 3: $p < 0.001$, day 4: $p = 1$, day 5: $p = 0.4$, day 6: $p = 1$; FDR correction for multiple comparisons). In this case, the adaptation ratio ($1^{st}/200^{th}$) became statistically indistinguishable from 1 by day 4 for the familiar orientation (Figure 2.2I; one sample Wilcoxon signed-rank test on AR ($\mu=1$) on day 1: $p < 0.001$, day 2: $p = 0.001$, day 3: $p < 0.001$, day 4: $p= 0.1$, day 5: $p = 0.006$, day 6: $p = 1$; FDR correction for multiple comparisons). The adaptation from reversal 1 to 200 only returned when a novel orientation was presented on the final day (Figure 2.2J;

Wilcoxon signed-rank phase 1 v 200 on day 7 fam: p = 1, day 7 nov: p < 0.001; FDR correction for multiple comparisons). The AR ($1^{st}/200^{th}$) for the familiar stimulus was significantly different to that in response to the novel stimulus (Figure 2.2K; Wilcoxon signed rank day 7 fam AR vs day 7 nov AR: p < 0.001) showing that adaptation from the 1^{st} to 200^{th} phase reversal is strongly modulated by long-term familiarity.

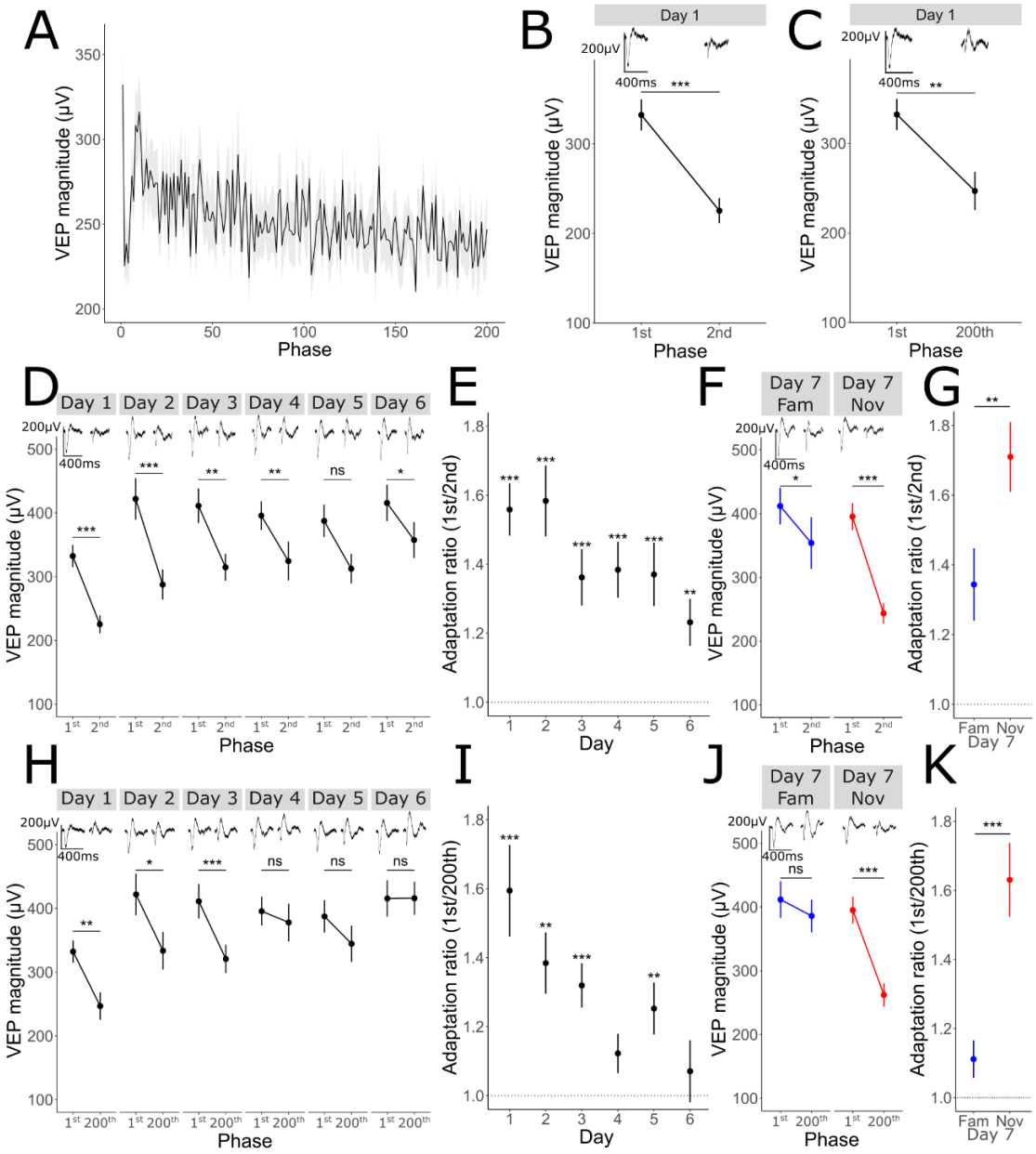

Figure 2.2 Short-term adaptation occurs within a stimulus block and is modulated by familiarity (A) Mean ± SEM VEP magnitude for phase reversal 1 to 200 (n = 33). (B) VEP magnitude in response to the first phase reversal and the 2nd, Wilcoxon signed rank 1st vs 2nd: p < 0.001 (n = 33). (C) VEP magnitude in response to the first phase reversal and the 200th, Wilcoxon signed rank 1st vs 200th: p = 0.001 (n = 33). (D)

VEP potential magnitude in response to the 1st vs 2nd phase reversal over 6 days (n = 33). Wilcoxon signed rank 1st vs 2nd day 1: $p < 0.001$, day 2: $p < 0.001$, day 3: $p = 0.002$, day 4: $p = 0.008$, day 5: $p = 0.05$, day 6: $p = 0.04$. FDR correction for multiple comparisons. (E) Adaptation ratio (1st/2nd) over 6 days. Wilcoxon signed-rank test on AR ($\mu=1$) day 1: $p < 0.001$, day 2: $p < 0.001$, day 3: $p < 0.001$, day 4: $p < 0.001$, day 5: $p < 0.001$, day 6: $p = 0.002$. FDR correction for multiple comparisons. (F) VEP potential magnitude in response to the 1st vs 2nd phase reversal on day 7 (n = 33). Wilcoxon signed rank 1st vs 2nd day 7 fam: $p = 0.02$, day 7 nov: $p < 0.001$. FDR correction for multiple comparisons. (G) Adaptation ratio (1st/2nd) on day 7. Wilcoxon signed-rank test fam vs nov: $p = 0.009$. (H) VEP potential magnitude in response to the 1st vs 200th phase reversal over 6 days (n = 33). Wilcoxon signed rank 1st vs 200th day 1: $p = 0.008$, day 2: $p = 0.04$, day 3: $p < 0.001$, day 4: $p = 1$, day 5: $p = 0.4$, day 6: $p = 1$. (I) Adaptation ratio (1st/200th) over 6 days. Wilcoxon signed-rank test on AR ($\mu=1$) day 1: $p < 0.001$, day 2: $p = 0.001$, day 3: $p < 0.001$, day 4: $p = 0.1$, day 5: $p = 0.006$, day 6: $p = 1$. FDR correction for multiple comparisons. (J) VEP potential magnitude in response to the 1st vs 2nd phase reversal on day 7 (n = 33). Wilcoxon signed rank 1st vs 200th day 7 fam: $p = 1$, day 7 nov: $p < 0.001$. (K) Adaptation ratio (1st/200th) on day 7. Wilcoxon signed-rank test fam vs nov: $p < 0.001$. Asterisks throughout denote significance (*$p < 0.05$, **$p < 0.01$, ***$p < 0.001$) while ns denotes non-significant.

2.4.5 Both short-term and long-term habituation require NMDA receptors in V1

Given the critical role of NMDA receptors (NMDAR) in a wide range of plasticity, and a known requirement in SRP and long-term habituation (Frenkel *et al.*, 2006; Cooke *et al.*, 2015), we sought to investigate habituation and accompanying plasticity over shorter timescales after local NMDAR knock-down in V1. Knock-down of NMDAR was achieved by expressing CRE recombinase via AAV viral vector injection bilaterally into V1 in a GluN1-floxed (GRIN fl/fl) mouse line (Figure 2.3A), thus knocking down expression of this mandatory subunit for NMDAR only within V1 (n = 11 mice). In the control condition, GRIN fl/fl littermates were injected with a comparable vector, sharing serotype, promoter and fluorophore, which lacked CRE recombinase (n = 11). As we have shown (Figure 2.1), behavioural habituation occurs both across days and within a day from block 1 to block 5. We found that loss of NMDARs from V1 affects both timescales. Behavioural activity usually drops from the first block to the second and remains low (Figure 2.1), and we found that to also be true in the WT littermate control mice (Figure 2.3B; Friedman test for block 1 to 5: $p = 0.003$, Wilcoxon signed-

rank test in WT group B1-B2: p = 0.1, B1-B3: p = 0.02, B1-B4: p = 0.02, B1-B5: p = 0.02; FDR correction for multiple comparisons). However, knock-down of NMDARs in V1 prevents the reduction in behaviour across blocks (Figure 2.3B; Friedman test for block 1 to 5: p = 0.3, Wilcoxon signed-rank in KD group B1-B2: p= 0.8, B1-B3: p = 0.5, B1-B4: p = 0.2, B1-B5: p = 0.1; FDR correction for multiple comparisons). As we reported previously (Cooke et al. 2015), behavioural habituation from day 1 to day 6 is absent in the KD group (Figure 2.3C; Friedman test in KD group: p = 0.3, in WT group: p = 0.001; FDR correction for multiple comparisons). On day 7 there was no difference in the behavioural response between the novel and familiar stimulus in the KD group, whereas in the WT group behavioural activity was higher in response to the novel stimulus (Figure 2.3D; Wilcoxon signed-rank fam vs nov in KD: p = 0.2, in WT: p = 0.009).

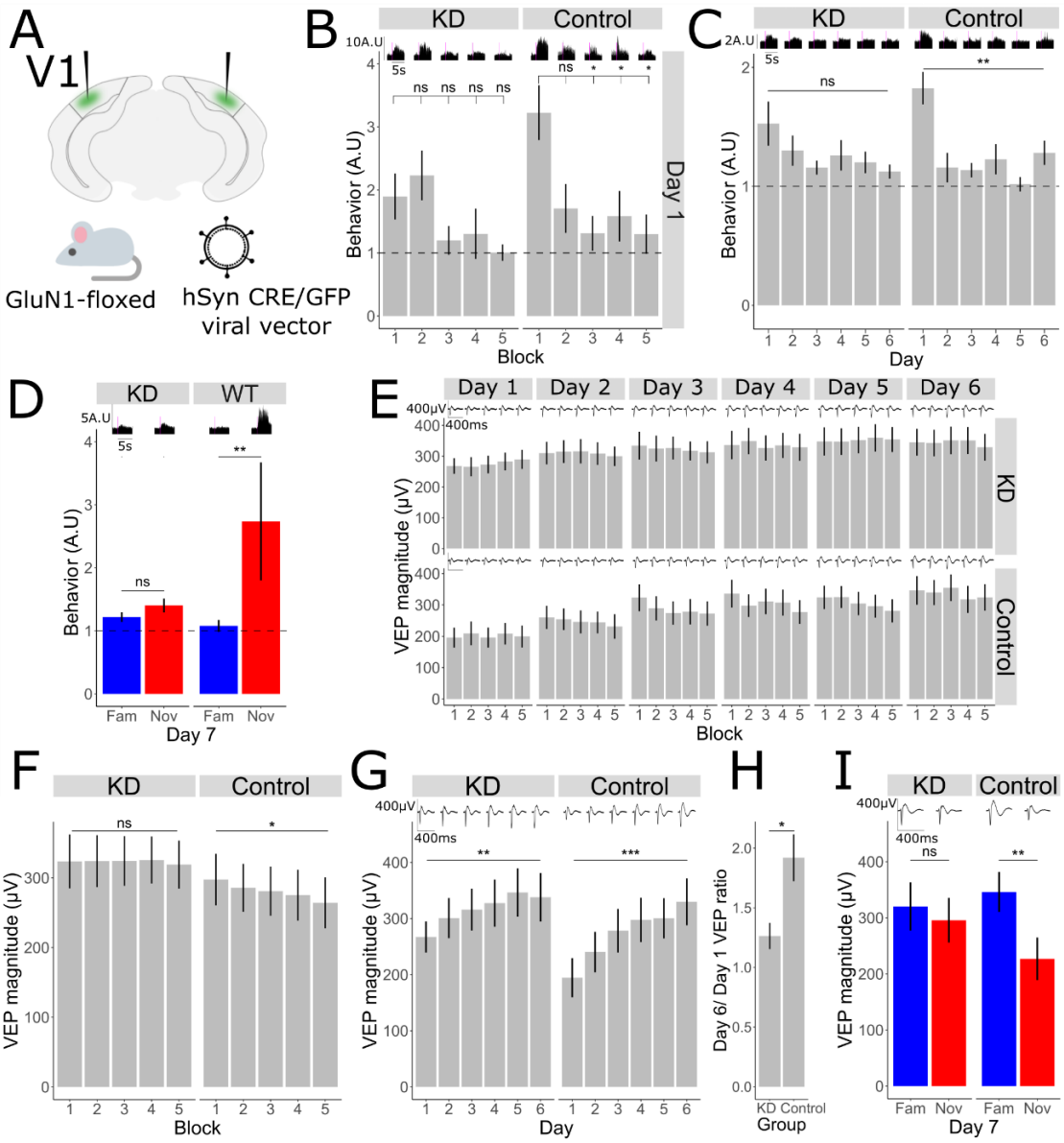

Figure 2.3 Bidirectional plasticity occurring in V1 during short- and long-term habituation require NMDA receptors in V1 (A) Schematic of the experimental set-up in which a Cre recombinase was locally expressed bilaterally in binocular V1 using an AAV viral vector to knockdown the mandatory GluN1 subunit of the NMDA receptor in GluN1-floxed mice. (B) Comparison of behavior across blocks for KD group (n = 11). Friedman test $\chi2(4) = 4.7$, p = 0.3. Post-hoc analysis of individual comparisons of block 1-block 2: p = 0.8, block 1-block 3: p = 0.5, block 1-block 4: p = 0.3, block 1-block 5: p= 0.1. Comparison of behavior across blocks for WT group (n = 11). Friedman test $\chi2(4) = 10.8$, p = 0.03. Post-hoc analysis of individual comparisons of block 1-block 2: p = 0.1, block 1-block 3: p = 0.02, block 1-block 4: p =0.02, block 1-block 5: p= 0.02. FDR correction for multiple comparisons. (C) Behavioral change over day 1 to day 6 in KD group (n = 11), Freidman test $\chi2(5) = 5.9$, p = 0.3. In WT group (n = 11), Freidman test $\chi2(5) = 21.6$, p = 0.001. FDR correction for multiple comparisons. (D) Behavioral response to familiar and novel. Wilcoxon signed-rank test fam vs nov in KD group: p = 0.2, in WT group: p = 0.009. FDR correction for multiple comparisons. (E) VEP magnitude change from block 1 to block 5 for day 1 to day 6 (n = 11 for each group). (F) VEP potential magnitude averaged over day 1 to day 6. Comparison over blocks for KD group, Friedman test $\chi2(4) = 0.7$, p = 0.9 (n = 11). Comparison over blocks for WT group, Friedman test $\chi2(4) = 12.1$, p = 0.03 (n = 11). FDR correction for multiple comparisons. (G) VEP

magnitude across day 1 to 6 in knock-down (KD) and wild-type (WT groups). Friedman test for KD group: $\chi2(5) = 15.4$, $p = 0.008$ ($n = 11$). Friedman test for WT group: $\chi2(5) = 36.5$, $p < 0.001$ ($n = 11$). FDR correction for multiple comparisons. (H) Ratio of day 6 VEP magnitude to day 1 VEP magnitude in KD and control group. Wilcoxon signed rank between groups: $p = 0.04$. (I) VEP magnitude response to familiar and novel, Wilcoxon signed-rank test fam vs nov for KD group: $p = 0.2$, for WT group: $p = 0.003$ ($n = 11$). FDR correction for multiple comparisons. Asterisks throughout denote significance (*$p < 0.05$, **$p < 0.01$, ***$p < 0.001$) while ns denotes non-significant.

2.4.6 Bidirectional plasticity occurring in V1 during short- and long-term habituation require NMDA receptors in V1

Within the same dataset, we now assessed the within-day VEP magnitude reduction that accompanies within-day habituation. The reduction in VEP magnitude across 5 blocks was modest in this dataset and was less apparent in these subjects than in the subjects described in figure 1 (Figure 2.3E). Nevertheless, by averaging the block-to-block VEP magnitudes observed during short-term habituation across days, a significant within-day VEP suppression was observed in the GRIN fl/fl littermate control animals (Figure 2.3F; $n = 11$; Friedman test in control group: $p = 0.03$; FDR correction for multiple comparisons). In contrast, this significant VEP decrement was not observed in the NMDAR KD mice (Figure 2.3F; $n = 11$; Friedman test in KD group: $p = 0.9$, FDR correction for multiple comparisons), indicating that the within-day reduction in VEP magnitude accompanying short-term habituation requires NMDAR, just as with the habituation itself. As previously reported (Cooke *et al.*, 2015), VEP magnitude potentiation from day 1 to 6, or SRP, is reduced in the knock-down (KD) group compared to control (Figure 2.3G; $n = 11$; Friedman test in KD group: $p = 0.008$, WT group: $p < 0.001$; FDR correction for multiple comparisons). Comparing the ratio of day 6 to day 1 in the control and KD group shows a significant reduction in this plasticity over days after NMDAR KD (Figure 2.3H; Wilcoxon signed rank between control and KD day 6/day 1 ratio: $p = 0.04$). On day 7, there was no difference in VEP magnitude between the familiar and novel

orientation in the KD group, whereas the VEP magnitude to the novel stimulus in the control group was significantly different (Figure 2.3I; n = 11; Wilcoxon signed-rank fam vs nov in KD: p = 0.2, control: p = 0.003; FDR correction for multiple comparisons).

2.4.7 V1 adaptation requires NMDA receptors in V1 across short and longer timescales

As we have shown above, short-term adaptation within our paradigm ordinarily occurs from both the 1st to the 2nd phase reversal and the 1st to the 200th phase reversal but disappears as the stimulus becomes familiar (Figure 2.2). Within the GRIN1 fl/fl dataset, this adaptation was similarly present in the GRIN fl/fl controls on day 1 and the subsequent two days, eventually becoming non-significant by day 4 and thereafter for highly familiar stimuli (Figure 2.4A, B; one sample Wilcoxon signed-rank test on AR (1st/2nd) (μ = 1) control group on day 1: p = 0.02, day 2: p = 0.01, day 3: p = 0.02, day 4: p = 0.2, day 5: p = 0.3, day 6: p = 0.03; FDR correction for multiple comparisons). However, after knock-down of NMDAR in V1, adaptation from the 1st to the 2nd phase reversal was absent on day 1 and all subsequent days (Figure 2.4A, B; one sample Wilcoxon signed-rank test on AR (1st/2nd) (μ = 1) KD group on day 1: p = 0.6, day 2: p = 0.9, day 3: p = 0.5, day 4: p = 0.4, day 5: p = 0.4, day 6: p = 0.4). When blocks of stimuli for familiar and novel orientations were presented pseudo-randomly interleaved on day 7, this 1st/2nd reversal adaptation was reduced for familiar but not novel stimuli in the control mice (Figure 2.4A, B; one sample Wilcoxon signed-rank test on AR (1st/2nd) (μ = 1) on day 7 fam: p = 0.03, day 7 nov: p = 0.008; FDR correction for multiple comparisons), but not present for either stimulus in the NMDAR KD mice (Figure 2.4A, B; one sample Wilcoxon signed-rank test on AR (1st/2nd) (μ = 1) KD group on day 7 fam: p = 1, day 7 nov: p = 0.6). The same phenotype was present

when investigating adaptation from the 1st to the 200th phase reversal. Loss of NMDARs prevented any short-term adaptation expression across all days and stimulus type (Figure 2.4C, D; one sample Wilcoxon signed-rank test on AR (1st/200th) (μ=1) KD group on day 1: p = 0.3, day 2: p = 0.3, day 3: p = 0.3, day 4: p = 0.3, day 5: p = 0.5, day 6: p = 0.5, day 7 fam: p = 0.5, day 7 nov: p = 0.4; FDR correction for multiple comparisons), while it remained present in the control mice over the first 5 days of stimulus presentation, and re-emerged to a novel stimulus on day 7 (Figure 2.4C, D; one sample Wilcoxon signed-rank test on AR (1st/200th) (μ=1) control group on day 1: p = 0.02, day 2: p = 0.02, day 3: p = 0.02, day 4: p = 0.02, day 5: p = 0.04, day 6: p = 0.08, day 7 fam: p = 0.8, day 7 nov: p = 0.008; FDR correction for multiple comparisons. Thus, short-term adaptation of VEP magnitude in V1 requires the presence of functional NMDAR.

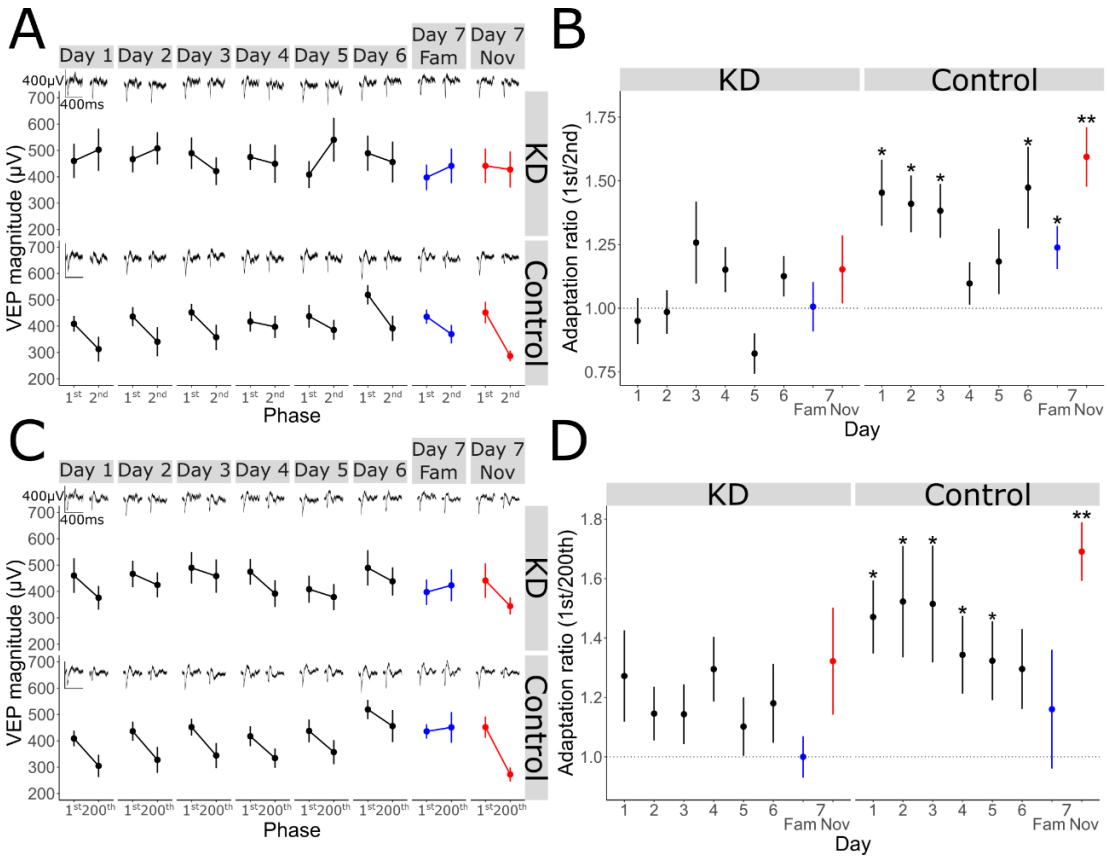

Figure 2.4 V1 adaptation requires NMDA receptors in V1 across short timescales (A) VEP magnitude in response to the 1st and 2nd phase reversal in GluN1 KD and WT group across all days (n = 11) (B) Adaptation ratio (1st/2nd) across days. Wilcoxon signed-rank test on AR (μ=1) in KD group on day 1: p = 0.6, day 2: p = 0.9, day 3: p

= 0.5, day 4: p = 0.4, day 5: p = 0.4, day 6: p = 0.4, day 7 fam: p = 1, day 7 nov: p = 0.6. Wilcoxon signed-rank test on AR (μ=1) in WT group on day 1: p = 0.02, day 2: p = 0.01, day 3: p = 0.02, day 4: p = 0.2, day 5: p = 0.3, day 6: p = 0.03, day 7 fam: p = 0.03, day 7 nov: p = 0.008. FDR correction for multiple comparisons. (C) VEP magnitude in response to the 1st and 200th phase reversal in KD and WT group across all days. (D) Adaptation ratio (1st/200th) across days. Wilcoxon signed-rank test on AR (μ=1) in KD group on day 1: p = 0.3, day 2: p = 0.3, day 3: p = 0.3, day 4: p = 0.3, day 5: p = 0.5, day 6: p = 0.5, day 7 fam: p = 0.5, day 7 nov: p = 0.4. Wilcoxon signed-rank test on AR (μ=1) in WT group on day 1: p = 0.02, day 2: p = 0.02, day 3: p = 0.02, day 4: p = 0.02, day 5: p = 0.05, day 6: p = 0.08, day 7 fam: p = 0.8, day 7 nov: p = 0.008. FDR correction for multiple comparisons. Asterisks throughout denote significance (*p < 0.05, **p < 0.01, ***p < 0.001).

2.4.8 A key role for the activity of Parvalbumin-expressing interneurons in long-term familiarity exposes a mechanistic difference between timescales of adaptation

Previously, we have shown that parvalbumin-expressing (PV+) inhibitory neurons in V1 are critical for the expression of long-term familiarity. We inactivated these neurons using a cell type-specific chemo-genetic approach in which the hM4Di DREADDS receptor was expressed in PV+ neurons of V1, disrupting SRP expression (Kaplan *et al.*, 2016). Therefore, we decided to assess whether these PV+ neurons in V1 are required for the modulation of adaptation by long-term familiarity that we have described in the current study (Figure 2.2). Bilateral injection of an AAV viral vector into V1 of a PV-Cre mouse to express hM4Di in these cells (Figure 2.5A) enabled subsequent inactivation of V1 PV+ interneurons after SRP and long-term habituation had been established over 6 days. Specifically, on day 7, familiar (X°) and novel (X+60°) orientations were pseudo-randomly interleaved in a standard design to test for selective SRP/habituation to the familiar orientation. After this, mice were systemically injected (i.p) with clozapine-n-oxide (CNO), which binds to hM4Di to inactivate expressing neurons, before re-testing response to blocks of the familiar and a new novel stimulus (X-60°) to assess modulation of adaptation by long-term familiarity (Figure 2.5B). Prior to inactivation of PV+ neurons, VEP magnitude was significantly potentiated

in response to the familiar stimulus and therefore significantly greater in magnitude than response to the novel stimulus (Figure 2.5C; Wilcoxon signed-rank day 7 fam vs nov: $p < 0.001$; FDR correction for multiple comparisons). However, as we have reported previously (Kaplan *et al.*, 2016), after inactivation of PV+ interneurons, there was no difference in VEP magnitude in response to familiar and novel stimuli (Figure 2.5C; Wilcoxon signed-rank day 7 fam vs nov w/ CNO: $p = 0.09$; FDR correction for multiple comparisons). It is important to note that after inactivation of PV+ interneurons, the general VEP magnitude was higher due to the loss of inhibition in the cortex. The inactivation of V1 PV+ inhibitory neurons also impaired behaviourally manifest novelty detection as the behavioural response to a novel stimulus was significantly greater than the response to the familiar stimulus before inactivation of PV+ neurons (Figure 2.5D; Wilcoxon signed-rank day 7 fam vs nov: $p = 0.02$; FDR correction for multiple comparisons), but was suppressed after inactivation of these neurons and no longer different during PV+ inactivation (Figure 2.5D; Wilcoxon signed-rank day 7 fam vs nov w/ CNO: $p = 0.2$; FDR correction for multiple comparisons).

As we have shown in the current study, short-term adaptation from the first to the second phase reversal progressively reduces as the stimulus becomes familiar and is selectively suppressed on day 7 to highly familiar stimuli, but not novel stimuli (Figure 2.2). Here we show that, although VEP magnitude generally increases, inactivation of PV+ interneurons had no effect on the modulation of $1^{st}/2^{nd}$ phase reversal short-term adaptation (Figure 2.5E, F, G). Strong adaptation from the first to the second phase reversal was absent when the stimulus was familiar and present when the stimulus was novel, regardless of whether PV+ neurons were inactivated. This observation is most clear when we normalize to the magnitude of the first phase reversal in order to remove the

confound of increased overall response after PV+ inactivation (Figure 2.5F; normalized to the first phase reversal; Wilcoxon signed rank phase 1 vs 2 on day 7 fam: $p = 0.5$, day 7 nov: $p < 0.001$, day 7 fam w/ CNO: $p = 0.9$, day 7 nov w/ CNO: $p = 0.004$ ($n = 14$). The adaptation ratio ($1^{st}/2^{nd}$) was significantly different between the familiar and the novel stimulus both before and after PV+ neuronal inactivation (Figure 2.5G; Wilcoxon signed rank on day 7 fam AR vs day 7 nov AR: $p = 0.007$, Wilcoxon signed rank on day 7 fam w/ CNO AR vs day 7 nov w/ CNO AR: $p = 0.02$($n = 14$). Thus, inactivation of PV+ interneurons does not affect the short-term adaptation from the 1^{st} to the 2^{nd} phase reversal, nor its suppression by long-term familiarity.

Strikingly, the adaptation from the first to the last phase reversal of a stimulus block follows a different pattern. While adaptation is suppressed by familiarity on day 7 but present for the novel stimulus before PV+ neuronal inactivation (Figure 2.5H, I, J), it is strongly apparent for both familiar and novel stimuli during PV+ neuronal inactivation (Figure 2.5I; normalized to the first phase reversal; Wilcoxon signed rank phase 1 vs 200 on day 7 fam: $p = 0.005$, day 7 nov: $p < 0.001$, day 7 fam w/ CNO: $p = 0.005$, day 7 nov w/ CNO: $p = 0.003$ ($n = 14$). The adaptation ratio ($1^{st}/200^{th}$) is significantly different for familiar and novel stimuli before PV+ inactivation (Figure 2.5J; Wilcoxon signed rank on day 7 fam AR vs day 7 nov AR: $p = 0.007$ ($n = 14$). After application of CNO the AR is equivalent for both the familiar and novel stimuli (Figure 2.5J; Wilcoxon signed rank on day 7 fam w/ CNO AR vs day 7 nov w/ CNO AR: $p = 0.8$). Therefore, the modulation of the short-term adaptation from the $1^{st}/200^{th}$ phase reversal by familiarity is not present after inactivation of PV+ interneurons, which differs from the effect on adaptation $1^{st}/2^{nd}$ phase reversal, indicating two mechanistically distinct processes.

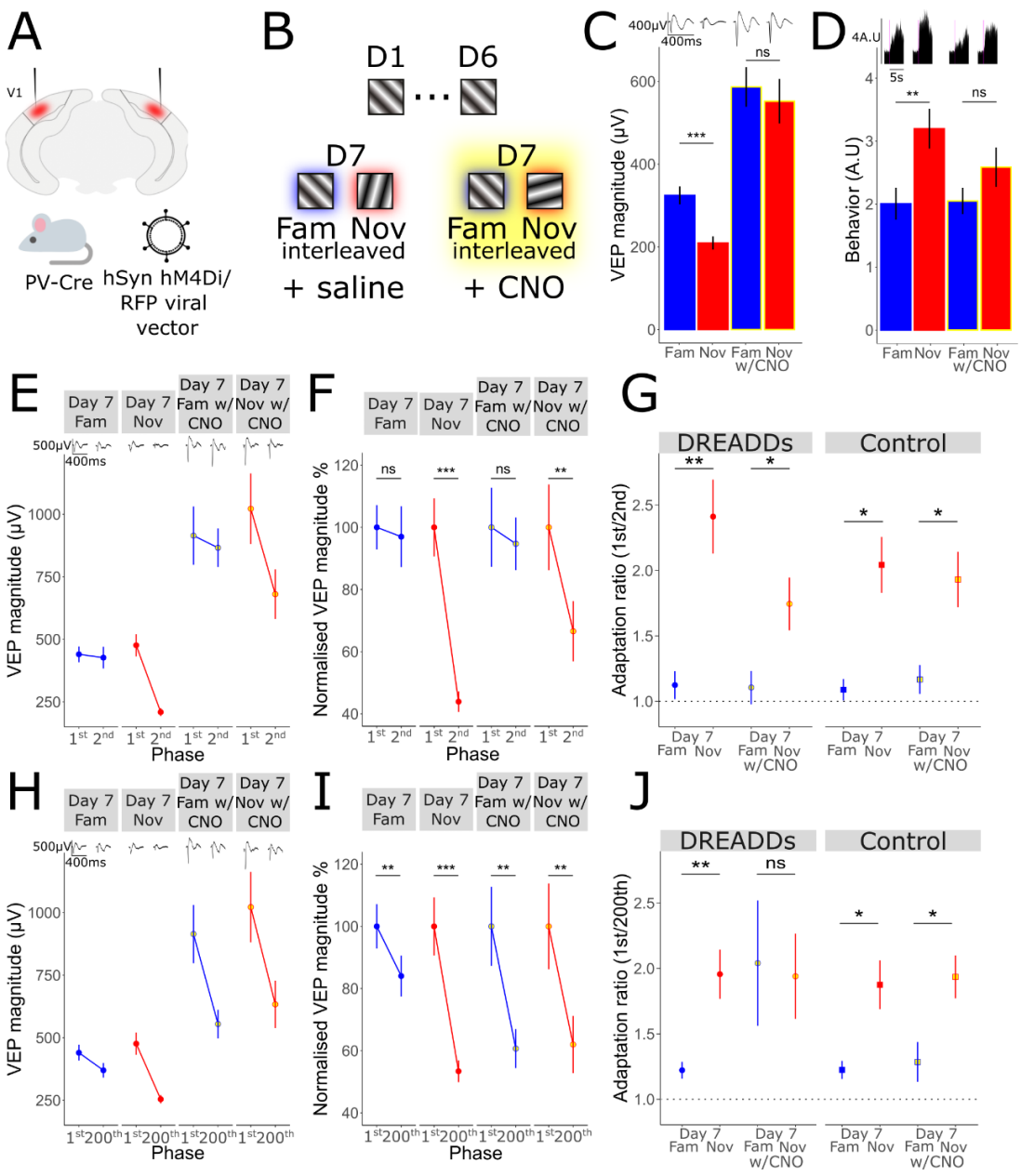

Figure 2.5 A key role for the activity of Parvalbumin-expressing inhibitory interneurons in long-term familiarity exposes a mechanistic difference between timescales of adaptation (A) Schematic of the experimental set-up in which hM4Di was selectively expressed in parvalbumin-expressing (PV) inhibitory neurons of V1 using an AAV viral vector in PV-Cre mice. (B) Schematic of visual presentation protocol in which all mice underwent a standard 6-day SRP protocol before testing response to familiar and novel stimuli during systemic saline injection or CNO application, which were administered prior to presentation to familiar and novel stimulus. (C) VEP magnitude in response to familiar and novel stimuli with and without CNO-induced PV+ neuronal inactivation. Wilcoxon signed rank day 7 fam vs nov: $p < 0.001$. Wilcoxon signed rank day 7 fam vs nov with CNO: $p = 0.09$. (D) Behavioral change in response to familiar and novel stimuli with and without CNO. Wilcoxon signed rank day 7 fam vs nov: $p = 0.02$. Wilcoxon signed rank day 7 fam vs nov with CNO: $p = 0.2$. (E) VEP magnitude is response to the 1st and the 2nd phase reversal in response to familiar and novel stimuli with and without CNO. (F) VEP magnitude to the 1st and the 2nd phase reversal normalized to the 1st phase reversal in response to familiar and novel stimuli with and without CNO. Wilcoxon signed rank phase 1 vs 2 on day 7 fam ($n = 14$): $p = 0.5$, day 7 nov: $p < 0.001$, day 7 fam w/ CNO: $p = 0.9$, day 7 nov w/ CNO: $p = 0.004$. (G) Adaptation ratio (1st/2nd) in

response to familiar and novel stimuli with and without CNO. Wilcoxon signed rank (n = 14): day 7 fam AR vs day 7 nov AR in DREAADs group: p = 0.007; day 7 fam w/ CNO AR vs day 7 nov AR w/ CNO in DREAADs group: p = 0.02. Wilcoxon signed rank (n = 7): day 7 fam AR vs day 7 nov AR in WT group: p = 0.03; day 7 fam w/ CNO AR vs day 7 nov AR w/ CNO in WT group: p = 0.02. FDR correction for multiple comparisons. (H) VEP magnitude in response to the 1st and the 200th phase reversal in response to familiar and novel stimuli with and without CNO. (I) VEP magnitude to the 1st and the 200th phase reversal normalized to the 1st phase reversal in response to familiar and novel stimuli with and without CNO. Wilcoxon signed rank phase 1 vs 200 on day 7 fam: p = 0.005, day 7 nov (n = 14): p < 0.001, day 7 fam w/ CNO: p = 0.005, day 7 nov w/ CNO: p = 0.003. (J) Adaptation ratio (1st/200th) in response to familiar and novel stimuli with and without CNO. Wilcoxon signed rank day 7 fam AR vs day 7 nov AR in DREAADs group (n = 14): p = 0.007; day 7 fam w/ CNO AR vs day 7 nov AR w/ CNO in DREAADs group: p = 0.8. Wilcoxon signed rank (n = 7); day 7 fam AR vs day 7 nov AR in WT group: p = 0.03; day 7 fam w/ CNO AR vs day 7 nov AR w/ CNO in WT group: p = 0.04. FDR correction for multiple comparisons. Asterisks throughout denote significance (*p < 0.05, **p < 0.01, ***p < 0.001) while ns denotes non-significant.

2.5 Discussion

In the current study we have identified multiple timescales of visual response adaptation that occur during habituation in mice. We have expanded on our previous characterization of stimulus-selective response potentiation (SRP), a form of long-term cortical response potentiation that occurs concomitantly with long-term habituation, to reveal that the reverse effect of response decrement coincides with short-term habituation. Moreover, we have identified shorter-term forms of adaptation that occur over seconds. We also reveal that the NMDA receptor serves as a key molecular mechanism shared by all these forms of plasticity (Figure 2.6A). In addition, we show that these various forms of plasticity are not isolated phenomena, because short-term adaptation and SRP over days clearly interact, such that adaptation no longer occurs for highly familiar stimuli. We also demonstrate that this suppression of adaptation across hundreds of stimuli by long-term familiarity is gated by the activity of PV+ inhibitory interneurons in V1 because inactivating these neurons causes short-term adaptation to re-emerge to highly familiar stimuli (Figure 2.6B). Finally, we make the important observation that the fastest form of adaptation that we have

measured, occurring within a second of stimulus presentation, remains suppressed for familiar stimuli even after inactivation of PV+ interneurons, indicating that there may be at least two mechanistically separable timescales of adaptation present within our paradigm. Thus, we have revealed a multitude of forms of cortical plasticity that can be assessed in passively viewing mice to gain a deeper understanding of the processes of habituation.

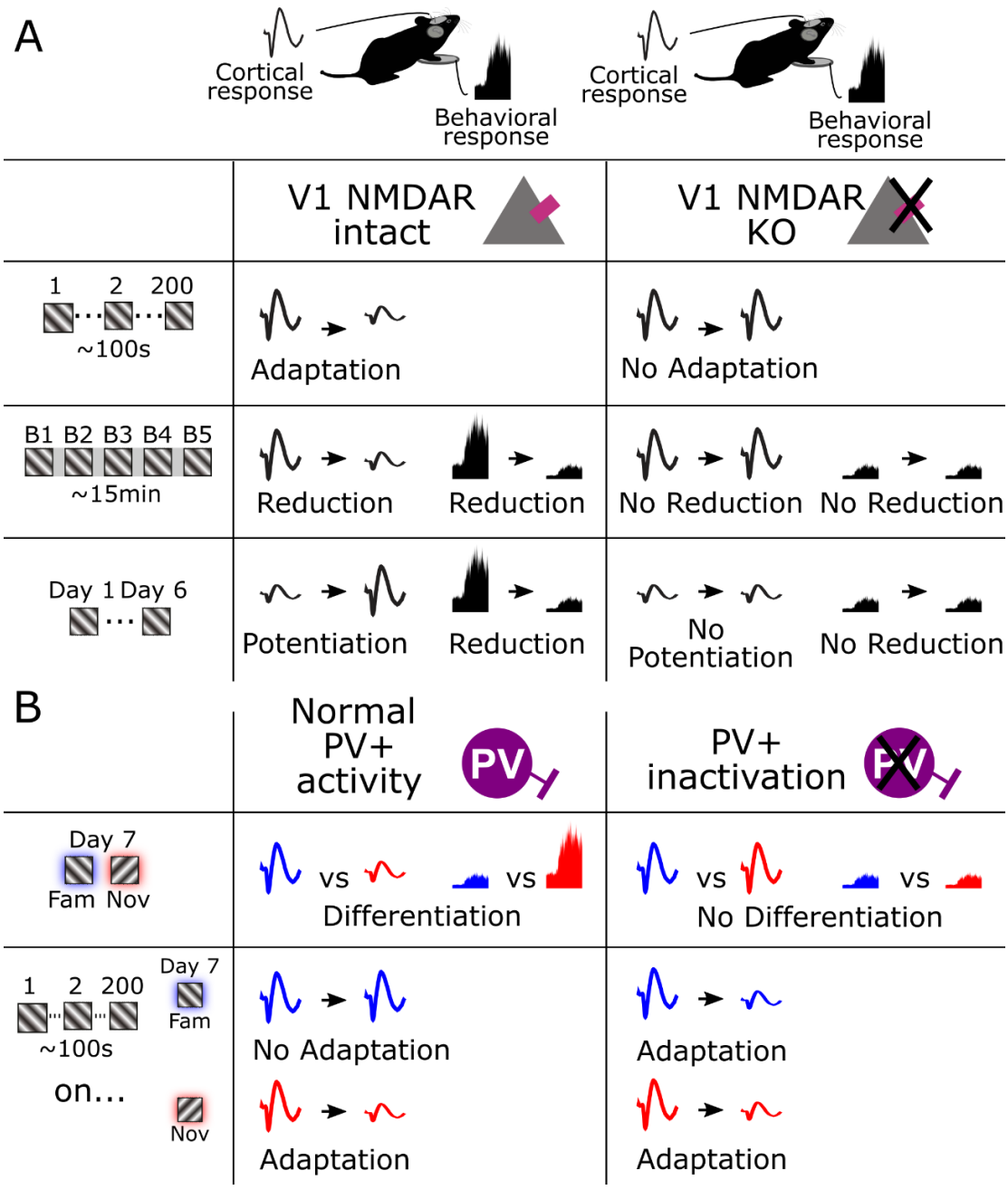

Figure 2.6 Schematic summarizing fundamental cortical and behavioral changes across multiple timescales (A) Cortical and behavioral changes over seconds,

minutes, and days (left), and the result of NMDR KO on these changes. (B) Cortical and behavioral changes in response to a familiar and novel stimulus and the associated adaptation (left), and the result of PV+ interneuron inactivation on these changes.

The longest-term form of plasticity we have described here is already well characterized: potentiation of the VEP in layer 4 over days is described as stimulus-selective response potentiation (SRP) due to its high degree of stimulus-selectivity (Frenkel *et al.*, 2006; Cooke & Bear, 2010) and it occurs concurrently with long-term behavioural habituation (Cooke *et al.*, 2015; Kaplan *et al.*, 2016; Fong *et al.*, 2020; Finnie *et al.*, 2021), just as we further confirm here. Despite the clear reliance of SRP and accompanying habituation on V1 NMDA receptors, selective knock-down of NMDARs in excitatory neurons of layer 4, the locus where SRP is manifest, does not impair SRP or accompanying habituation (Fong *et al.*, 2020). This observation indicates that the potentiation is an echo of plasticity occurring elsewhere in V1, or in a different cell type within layer 4. Therefore, the direct strengthening of synapses at thalamocortical inputs to layer 4 now seems an unlikely explanation for SRP. Although local field potentials are thought to primarily report synaptic activity rather than action potentials (Katzner *et al.*, 2009; Buzsáki *et al.*, 2012), potentiation of VEP magnitude may reflect a loss of shunting inhibition that allows an increased synaptic response to thalamic input, rather than a potentiation of the synaptic input itself. We have previously shown that parvalbumin-expressing (PV+) inhibitory interneurons, which provide this powerful shunting inhibition, show reduced activity over days as the stimulus becomes familiar during SRP (Hayden *et al.*, 2021). In addition, cell-specific interventional approaches reveal that a normal range of activity in PV+ neurons is required for differential response to familiar or novel stimuli after SRP, either cortically or behaviourally (Kaplan *et al.*, 2016). Thus, it seems likely that SRP

reflects a loss of PV+ inhibition. How this contributes to a decrement in behaviour, as is observed in the concomitant long-term habituation, remains unclear (Montgomery *et al.*, 2021). One possible arrangement is that increased cortical output recruits another form of inhibition to suppress behavioural output. This arrangement would accord with the comparator model of habituation, in which long-lasting memory is formed in the cortex through elevated synaptic activity that enables recognition of familiarity and suppresses output through feedforward inhibition, as suggested by Sokolov (Sokolov, 1963) and others (Konorski, 1967; Wagner, 1981). To confirm that SRP conforms to this model will require measurement of V1 output from the deeper layers of neocortex, with the prediction that this activity is suppressed by superficial layers as they exhibit potentiation. It will also be critical to identify the inhibitory intermediary that leads to this cortical output. One strong candidate for this inhibitory suppression has recently emerged (Pluta *et al.*, 2019).

The behavioural response decrement over the course of minutes, reflecting habituation over an intermediate time-scale, has been investigated by others (Sanderson & Bannerman, 2011). The reduction in VEP magnitude that coincides with this within session habituation has not formally been described by us previously. Our observations of a decrement in VEP magnitude are notable because of the striking contrast with SRP, which coincides with a similar reduction in behaviour in the same animals, but in that case over days (Figure 2.1). Visual cortical activity decreases during repetitive presentation of natural movies (Deitch *et al.*, 2021), suggesting that this reduced activity can occur in response to multiple different types of visual stimuli, and the well-documented phenomenon of mis-match negativity, in which novel oddball stimuli evoke increased magnitudes of event-related potentials (ERP) relative to repetitions of

increasingly familiar stimuli, occurs across similar timescales (Näätänen *et al.*, 2007; Garrido *et al.*, 2009). In a similar paradigm to ours, thalamic activity has been observed to increase over ~30 minutes (Durkin & Aton, 2019), and it remains possible that the plasticity they have observed is, through some unidentified inversion, the origin of cortical decrement and behavioural habituation. However, the reliance of both VEP decrement and concomitant habituation on NMDARs within V1 strongly suggests that this is not the case (Figure 2.3). Dual recordings of thalamic and cortical neurons may be required to resolve the origins of these effects, and targeted interventions in the thalamus may also prove informative. Investigation of changes over the course of minutes in response to both a familiar and novel grating (currently not possible due to the interleaving of these stimuli) would elucidate if this reduction of cortical activity is indiscriminate to the type of visual stimulus being shown or is also orientation specific, indicating cortical plasticity that is potentially very similar to the familiarity effect observed leading up to mismatch negativity. Recent work has shown that mismatch negativity depends upon activity of the somatostatin-expressing (SST+) inhibitory interneurons (Hamm & Yuste, 2016), suggesting that modification of SST+ inhibition may account for our observations. This class of interneurons primarily target dendrites of excitatory cells and PV+ interneurons (Cottam *et al.*, 2013; Pfeffer *et al.*, 2013; Xu *et al.*, 2013; Rikhye *et al.*, 2021) and they have been shown to be strongly influenced by stimulus familiarity (Kato *et al.*, 2015; Makino & Komiyama, 2015; Hayden *et al.*, 2021). Inhibition on the dendrites of excitatory neurons, where the majority of synaptic contacts are made, may contribute to reduced synaptic activity during habituation (Natan *et al.*, 2015), or these cells may influence the activity of PV+ neurons to mediate the reduction in V1 response, as they are known to do in layer 4 (Xu *et al.*, 2013). It

would be informative to measure the activity of these inhibitory neurons in layer 4 of V1 across this timescale and more informative still to monitor inhibitory responses in principle excitatory neurons during this within-session habituation. Given the dependency of the phenomenon that we have described on NMDARs, one intriguing hypothesis is that excitatory synapses onto SST+ neurons are potentiated during repeated stimulus presentation. Knocking down the NMDAR expression within these cells would test this hypothesis. It also remains possible that other types of inhibition are increasingly engaged to produce habituation, as has recently been hypothesized (Ramaswami, 2014). In line with the NMDAR dependence of the reduced behavioural responses, again, this process may involve synaptic depression of excitatory synapses within V1. Much further work is required to investigate the underlying mechanisms of this intermediate form of behavioural and cortical response adaptation.

Over even shorter timescales of seconds, the VEP adaptation that we observe here within continuous blocks of stimulation is a commonly reported phenomenon (Chung *et al.*, 2002; Beierlein *et al.*, 2003; von der Behrens *et al.*, 2009; Cruikshank *et al.*, 2010). The most parsimonious explanation for response decrement is that it reflects a depression of excitatory synapses within the canonical excitatory synapses of V1 through a process of adaptive filtration, which is perhaps the dominant theory of habituation (Horn, 1967; Groves & Thompson, 1970). This depression could potentially occur through Hebbian depression mechanisms (Lee *et al.*, 1998) at excitatory synapses within the cortex (Chen *et al.*, 2015), or the thalamus (Li *et al.*, 2003), or through short-term effects on synaptic release (Moulder & Mennerick, 2006). That the origin of response depression is cortical is supported by its reliance V1 NMDARs. Specifically, we show that both the adaptation from the 1st to the 2nd phase

reversal (0.5 s), and the adaptation from the 1st to 200th phase reversal (100 s) is impaired by a loss of NMDAR expression in V1 (Figure 2.3). This somewhat surprising finding implicates the occurrence of a Hebbian form of plasticity that is at least induced post-synaptically at short timescales (Bliss & Collingridge, 1993). Additionally, we have made the intriguing additional observation that a loss of activity in PV+ neurons after chemo-genetic inactivation re-instates short-term adaptation even to highly familiar stimuli (Figure 2.4). The immediate conclusion from this observation is that short-term adaptation does not rely in any way on inhibition mediated by PV+ neuronal activity, in striking contrast to long-term familiarity. The reinstated short-term adaptation may therefore arise from the cortex responding to a familiar stimulus as if it were novel. Alternatively, it remains possible that the loss of adaptation with long-term familiarity arises from a gradual reduction in PV+ mediated inhibition through the course of a stimulus block that perfectly matches excitatory synaptic depression. Inactivation of PV+ neurons would remove this gradual effect and expose the depression occurring at those excitatory inputs. Using calcium imaging, we have previously observed the gradual loss of PV+ neuronal engagement across phase reversals for familiar but not novel stimuli, so this remains a plausible arrangement (Hayden *et al.*, 2021). Interestingly, using a similar method in excitatory neurons we have also previously reported a perplexing mismatch with the electrophysiological measurements of SRP: when measuring VEP magnitude or peak unit firing rate, a pronounced potentiation is observed (Cooke *et al.*, 2015), while a reduction of signal is observed with calcium imaging (Kim *et al.*, 2020). In the current study we have added to that conundrum, as we reveal short-term adaptation across seconds that is limited to novel stimuli (Figure 2.2), while we previously revealed a similar effect with calcium imaging but limited to familiar stimuli (Kim *et al.*,

2020). The only likely explanation for these curiously mismatched observations is that our electrophysiological methods have detected a fast phasic effect which is potentiated by familiarity over days and diminished to novel stimuli over seconds, while the calcium sensors detect a more sustained diminishment of calcium flux as a result of familiarity over either time-course. Further experiments comparing phasic and drifting gratings or using intracellular electrophysiology may be informative in this regard. It will also be interesting to use calcium imaging to assess the intermediate timescale that we have reported here which occurs from block to block over minutes within a session (Figure 2.1), to determine if the mismatch between the two methods persists even across this timescale. Our prior study indicates that for this timescale, at least, findings with electrophysiology and calcium imaging will align (Kim et al. 2020).

The storage and retrieval of familiarity plays a major role in reserving energy and attention for only those stimuli that are most pertinent to a task or context and is therefore critical for survival and wellbeing. Understanding how these apparently relatively simple forms of learning and memory are implemented is a greater challenge than expected and there appear to be multiple solutions to the same problem, some of which engage feedforward plasticity, others which engage inhibitory systems and more complicated circuitry. These various mechanisms may all play out within one structure but across different timescales. In this study, we have revealed the measurement of multiple mechanistically distinct forms of plasticity occurring in the same animals across seconds, minutes and days of repeated stimulus presentation, providing great potential to gain a deep understanding of a foundational set of learning and memory processes. We have monitored these changes using LFP recordings, suggesting that much of the observed phenomenology is likely to translate to non-invasive

electroencephalogram (EEG) recordings, providing future potential for translation into human subjects, where forms of plasticity such as mismatch negativity have already been described (Näätänen et al. 2007).

Chapter 3 Role of inhibitory neurons in cortical plasticity at multiple timescales

In this chapter I describe the critical role of inhibitory neurons in primary visual cortex, namely parvalbumin and somatostatin neurons, during different timescales of plasticity. Somewhat surprisingly, alterations in inhibitory cell activity, connections and synaptic inputs are essential to adaptation of activity across days, minutes and seconds.

3.1 Statement of work

All work was performed and analysed by F.C.

3.2 Introduction

It is a core capacity of the brain to encode sufficient information about the environment to govern future behavioural decisions. Specific features of the environment are encoded within select regions of the brain, and within these regions, select circuits subserve different roles. The activity profile of specific cells and circuits may differ during learning and during memory recall. Across repeated presentations, groups of cells that respond to visual input can be both transient and stable (Pérez-Ortega *et al.*, 2021). Therefore, the differential recruitment of types of cells during learning and during memory recall must be examined.

Experience-dependent formation of connections between cells is critical to sensory processing, encoding and plasticity in the adult (Cooke & Bear, 2014). An important modification that occurs over learning is altered inhibitory input onto excitatory cells (Khan *et al.*, 2018; Poort *et al.*, 2022). Modification of inhibition in the visual cortex over learning changes the response properties of the visual cortex; for example, sharpens orientation tuning (Lee *et al.*, 2012) and causes reduction of trial to trail variability of responses (Rikhye *et al.*, 2021). This altered

inhibitory input onto excitatory cells can be recorded intracellularly as changes in inhibitory synaptic currents (IPSCs) (Mody & Pearce, 2004). Changes in IPSCs may provide insight into changes in inhibitory synaptic connections after experience-dependent plasticity.

A well-established form of experience-dependent plasticity is stimulus-selective response potentiation (SRP), where the magnitude of visual-evoked potentials (VEPs) recorded in layer 4 of mouse binocular V1 increases dramatically over days of repeated stimulation. As the response to a novel stimulus is unaffected, this VEP potentiation is selective to the orientation shown (Frenkel *et al.*, 2006; Cooke & Bear, 2010). In addition to potentiation over days, within-session short-term adaptation of VEP magnitude occurs across tens of seconds (Kim *et al.*, 2020; Chaloner & Cooke, 2022). These robust forms of plasticity and accompanying habituation serve as a foundation for studying how cortical interventions affect these processes. SRP and short-term adaptation both require NMDA receptors in V1 (Frenkel *et al.*, 2006; Cooke & Bear, 2010; Chaloner & Cooke, 2022), which suggests that Hebbian plasticity processes underlie these phenomena. However, NMDA receptors were indiscriminately altered in both excitatory and inhibitory neurons in the above studies. Therefore, it is unknown whether excitatory or inhibitory inputs are altered through Hebbian plasticity.

Since inhibitory neurons are well known to be involved in adaptation and learning (Barron *et al.*, 2017), initial research sought to understand their function across SRP. Inhibiting PV+ cell activity after SRP and knock-out of NMDARs in PV+ neurons prevents the differential response to familiar and novel stimuli (Kaplan *et al.*, 2016; Chaloner & Cooke, 2022). Interestingly when a highly familiar stimulus is presented that has been viewed over multiple previous days,

PV+ neuronal responses are suppressed below baseline levels. However, they are re-engaged when a novel stimulus is presented, even interleaved during the same recording session (Hayden *et al.*, 2021). In parallel to a reduction in PV+ neuronal activity over learning, SOM+ neurons increase their activity across repeated stimulus presentation over days, over the same time-course as suppression of PV+ activity is observed (Hayden *et al.*, 2021). Within layer 4, it is now known that SOM+ inhibitory neurons inhibit PV+ neurons to cause disinhibition of excitatory responses (Xu *et al.*, 2013; Li *et al.*, 2019). Although this mechanism has not yet been proven to underlie SRP, the increased SOM+ neuronal activity occurring across the same time-course as SRP may inhibit PV+ neuronal activity to mediate potentiation of the VEP magnitude.

Alterations in activity over shorter timescales are also influenced by inhibitory neurons. Short-term adaptation over tens of seconds is strongly modulated by long-term familiarity, such that short-term adaptation of the VEP magnitude is lost as the stimulus becomes familiar. Inactivation of PV+ neurons precludes the alteration of adaptation by familiarity (Chaloner & Cooke, 2022). Furthermore, PV+ neuronal activity reduces in response to familiar but not novel stimuli across shorter timescales (Hayden *et al.*, 2021). SOM+ cells also alter their activity over tens of seconds; SOM+ neuronal activity increases when familiar stimuli are presented but not when novel stimuli are presented (Hayden *et al.*, 2021). However, during continual presentation of a visual stimulus PV+ inhibitory neuronal activity facilitates (Heintz *et al.*, 2022). Furthermore, Heintz (2022) observed depression of the activity of SOM+ neurons over several seconds. Therefore, SOM+ depression may result in reduced inhibition onto PV+ neurons, leading to an increase in PV+ cell activity and a decrease in excitatory cell responses (Heintz *et al.*, 2022). Thus, these observations suggests that even

over shorter timescales, the dynamics of excitatory cells are directly affected by SOM+ inhibition of PV+ neurons (Xu *et al.*, 2013). However, it is important to note that presentation of a constant stimulus (Heintz *et al.*, 2022) and a phase reversing stimuli (Hayden *et al.*, 2021) is likely to result in different dynamics of PV+ and SOM+ neurons. Overall, it remains unknown the exact impact of SOM+ neuron recruitment (Hayden *et al.*, 2021) on short-term adaptation of the VEP magnitude during presentation of a familiar phase-reversing stimulus.

In the current chapter I will show that normal PV+ neuronal activity during learning is critical for expression of familiarity. In addition, I will show that recruitment of SOM+ neurons is necessary for the short-term adaptation and disinhibition of VEP responses during familiarity. Furthermore, I will present attempts to probe the mechanism by which SOM+ neurons allow disinhibition of VEP responses during familiarity. Finally, I will reveal that, after SRP, the amplitude of inhibitory synaptic currents recorded from layer 4 excitatory cells decreases.

3.3 Materials and Methods

3.3.1 Animals

All procedures were performed in accordance with the UK Animals (scientific procedures) Act (1986). All animals were maintained in a C57Bl/6J background (Charles River Laboratories). Animals received food and water *ad libitum*. Experiments in which PV+ neurons were inactivated (hM4Di) during learning used the PV-Cre mouse line (B6;129P2-*Pvalb*$^{tm1(cre)Arbr}$/J, Jackson laboratory). SOM+ neuron manipulation (optogenetics) uses SOM-Cre (B6J.Cg-Sst$^{tm2.1(cre)Zjh}$/MwarJ, Jackson laboratory). For SOM+ activation (Channelrhodopsin) combined with PV+ neuron inactivation (hM4Di) the PV-flp mouse line (B6.Cg-*Pvalb*$^{tm4.1(flpo)Hze}$/J, Jackson laboratory) was crossed with the

SOM-Cre mouse line (B6J.Cg-Sst$^{tm2.1(cre)Zjh}$/MwarJ). Male heterozygotes were used.

3.3.2 Viral transfection

All injections were preceded and followed by 3 minutes wait time. Viral injections were performed in both hemispheres at ± 3.1 from lambda and were immediately followed by electrode implantation (outlined below).

For all experiments, mice were allowed at least 2 weeks recovery following surgery before the start of the head fixation, and at least 18 days prior to optogenetics stimulation or CNO injection.

3.3.2.1 PV+ inactivation with hM4Di during learning

In experiments with DREADDs inactivation of PV+ neurons using PV-Cre mice, 100nl of cre-dependent hM4Di or serotype matched control mCherry virus was injected at ± 3.1 from lambda at 2 nl/s at depths 600 µm, 450 µm, 300 µm, and 150 µm below surface (Table 3.1).

3.3.2.2 Activation/ Inactivation of SOM+ cells with ChR/ HaloR

For experiments involving SOM+-Cre 100nl of AAV was injected at 2 nl/s at depths 600 µm, 450 µm, 300 µm, and 150 µm below surface (Table 3.1).

3.3.2.3 Activation of SOM+ cells with ChR and inhibition of PV+ cells with hM4Di

For experiments in the SOM-Cre and PV-flp cross, originally a cocktail of Cre-ChR and flp-DREADDs (2-parts ChR/EYFP, 1-part DREADDs/mCherry) (Table 3.1). However, this caused reduced expression of ChR and did not replicate the previous finding with ChR alone. Therefore, injections were separated, 100 nl of Cre-dependent ChR or EYFP (Table 3.1) virus was injected at 2 nl/s at depths 600 µm, 450 µm, 300 µm, and 150 µm below surface at coordinates ± 3.1 from lambda and skin was resealed with Vetbond tissue adhesive. A week later (6-8

days) either 50 ml or 100 nl of the flp-dependent hM4Di or mCherry (diluted 2:1) (Table 3.1) virus was injected at 2 nl/s at depths 600 µm, 450 µm, 300 µm, and 150 µm below surface.

Table 3.1 Table of viruses used

SOM-Cre	pAAV-EF1a-double floxed-hChR2(H134R)-EYFP-WPRE-HGHpA (AAV5)	Channel Rhodopsin for excitation (blue 465nm)
	pAAV-Ef1a-DIO eNpHR 3.0-EYFP (AAV5)	Halo Rhodopsin for inhibition (green 550nm)
	pAAV-Ef1a-DIO EYFP (AAV5)	Empty vector control
PV-Cre	pAAV-hSyn-DIO-hM4D(Gi)-mCherry (AAV8)	DREADDs inhibition
	pAAV-hSyn-DIO-mCherry (AAV8)	Empty vector control
SOM-Cre x PV-flp	pAAV-hSyn-fDIO-hM4D(Gi)-mCherry-WPREpA (AAV Retrograde) pAAV-EF1a-double floxed-hChR2(H134R)-EYFP-WPRE-HGHpA (AAV5)	DREADDs inhibition Channel Rhodopsin for excitation (blue 465nm)
	pAAV-Ef1a-fDIO mCherry (AAV Retrograde) pAAV-Ef1a-DIO EYFP (AAV5)	Empty vector control

3.3.3 V1 electrode and optic fibre implantation

Mice underwent surgery at ~ 6 weeks of age (~P45). Mice were anaesthetized with isoflurane and 5 mg/kg carprofen was delivered via a sub-cutaneous injection for analgesia. Iodine and saline were used to clean the scalp. The skull was cleaned, dried, and scored using a cross hatch pattern with a scalpel blade. A steel headpost was fixed over the frontal suture and skin adhered to skull surface using super glue (ethyl cyanoacrylate). Burr holes were drilled ± 3.1 mm lateral to lambda (to target binocular V1). Tungsten recording electrodes were implanted 470 µm below surface in both hemispheres. Silver wire reference electrodes were placed bilaterally in prefrontal cortex. For optogenetic experiments, optic cannula (Thorlabs; CFMLC12L02) were bilaterally implanted

lateral to V1 electrodes at a 22-degree angle just below surface. All implants and the headpost were fixed in place with Superbond dental cement to form a fully enclosed headcap.

3.3.4 Visual Stimulus presentation

The display was 20 cm in front of the mouse and mean luminance was 27 cd/m2. Sinusoidal phase reversing gratings are presented at a spatial frequency of 0.05 cycles/degree and were presented full field, reversing at 2 Hz. Gamma-correction was performed to maintain constant luminance between gratings and grey screen. A piezo-electric device was placed under the animals against the tube to pick up paw and body movement. In some experiments a camera was placed to record the face and paws to track movement (Figure 3.1).

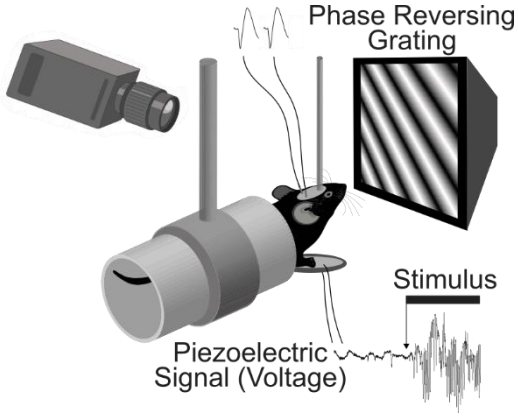

Figure 3.1 Schematic outlining the recording set-up.

3.3.4.1 PV+ inactivation with hM4Di during learning

For inactivation of PV+ neurons, visual stimuli were generated with software from Jeff Gavornik (https://github.com/jeffgavornik/VEPStimulusSuite). Mice underwent 2 days habituation, then were shown 10 blocks of 200 phase reversals with 30 s grey screen on day 1 through day 3 after intraperitoneal injection (IP) of CNO at 5 mg/kg and a delay of 15 minutes. One day was allowed for washout of CNO. Then on day 5, 10 blocks of a familiar (X°) and a novel stimulus (X° + 90°) were presented (Figure 3.2A).

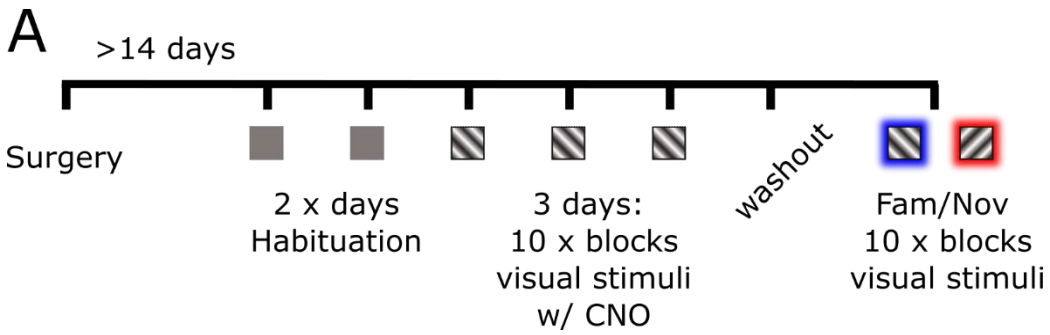

Figure 3.2 Schematic for PV+ inactivation protocol

3.3.4.2 Experiments involving optogenetics

For experiments involving the use of optogenetics(https://www.psychopy.org/) was used to produce sinusoidal phase reversing grating because additional software was needed that included digital control of LED driver (PlexBright® Optogenetic Stimulation System) with a DAQ to control digital channel output (National Instruments (NI), USB-6001). For all experiments, 2 days of habituation to grey screen (10 mins) was followed by visual stimuli presentation. On day 1 through day 6 blocks consisted of 200 phase reversals each block was presented 5 times interleaved with 30 seconds of grey screen with the first block being preceded by 300 s of grey screen (Figure 3.3).

3.3.4.3 Activation of SOM+ cells with ChR

For ChR experiments, 5 blocks of familiar and novel are shown with and without LED. These blocks were interleaved with 30 s of grey screen between blocks (20 blocks total). Blue light (465 nm) was presented at an intensity of 1.5 mW and light was initiated 0.5 s prior to onset of block and stopped 0.5 s after end of block. In addition to day 7 familiar and novel stimuli presentation, PsychoPy was used to generate an oddball paradigm which consisted of 12 blocks of 128 gratings, of which 88% were standard (Y°), 6% an oddball (Y° + 90°) and 6% oddball with LED (Y° + 90°). Stimuli were presented for 500ms and followed by 1000 ms of

grey before the next stimulus. Each block was separated by 20 s of grey screen and light was initiated 0.5 s before onset of visual stimulus and ceased concurrently with the sinusoidal grating. For investigation of across-block plasticity, 10 blocks of one orientation were presented sequentially, separated 30 s of grey screen respectively while LED presented light during every block (Figure 3.3A).

3.3.4.4 SOM+ inhibition with HaloR

For HaloR experiments, 2 blocks of familiar and novel were shown with and without LED interleaved with 210 s of grey screen (8 blocks total). Green light (550 nm) was presented at an intensity of 6-7 mW. Difference in block number and grey-screen interval is due hang-over effects of HaloR stimulation which will be described in the results section. In addition to day 7 familiar and novel stimulus presentation, PsychoPy was used to generate an oddball paradigm which consisted of 12 blocks of 128 gratings, of which 88% were standard (Y°), 6% an oddball (Y° + 90°) and 6% oddball with LED (Y° + 90°). All stimulus statistical properties were the same as outlined in ChR section. For investigation of across-block plasticity, 5 blocks of one orientation were presented sequentially, separated by 210 s of grey screen respectively while LED presented light during every block (Figure 3.3B).

3.3.4.5 Activation of SOM+ cells with ChR and inhibition of PV+ cells with hM4Di

For the PV-flp and SOM-Cre cross, 5 blocks of familiar (X°) and novel (X° + 90°) stimuli were shown on day 7, with and without LED, interleaved with 30 s of grey screen between each block (20 blocks total). Blue light (465 nm) was delivered at an intensity of 1.5 mW. After 1-3 days, CNO was administered via I.P injections at 5 mg/kg, then 15 minutes later, 5 blocks of familiar (X°) and new novel (X° +

115°) are shown with and without LED stimulation interleaved with 30 s of grey screen (20 blocks total) and blue light (465 nm) was presented at an intensity of 1.5 mW (Figure 3.3C).

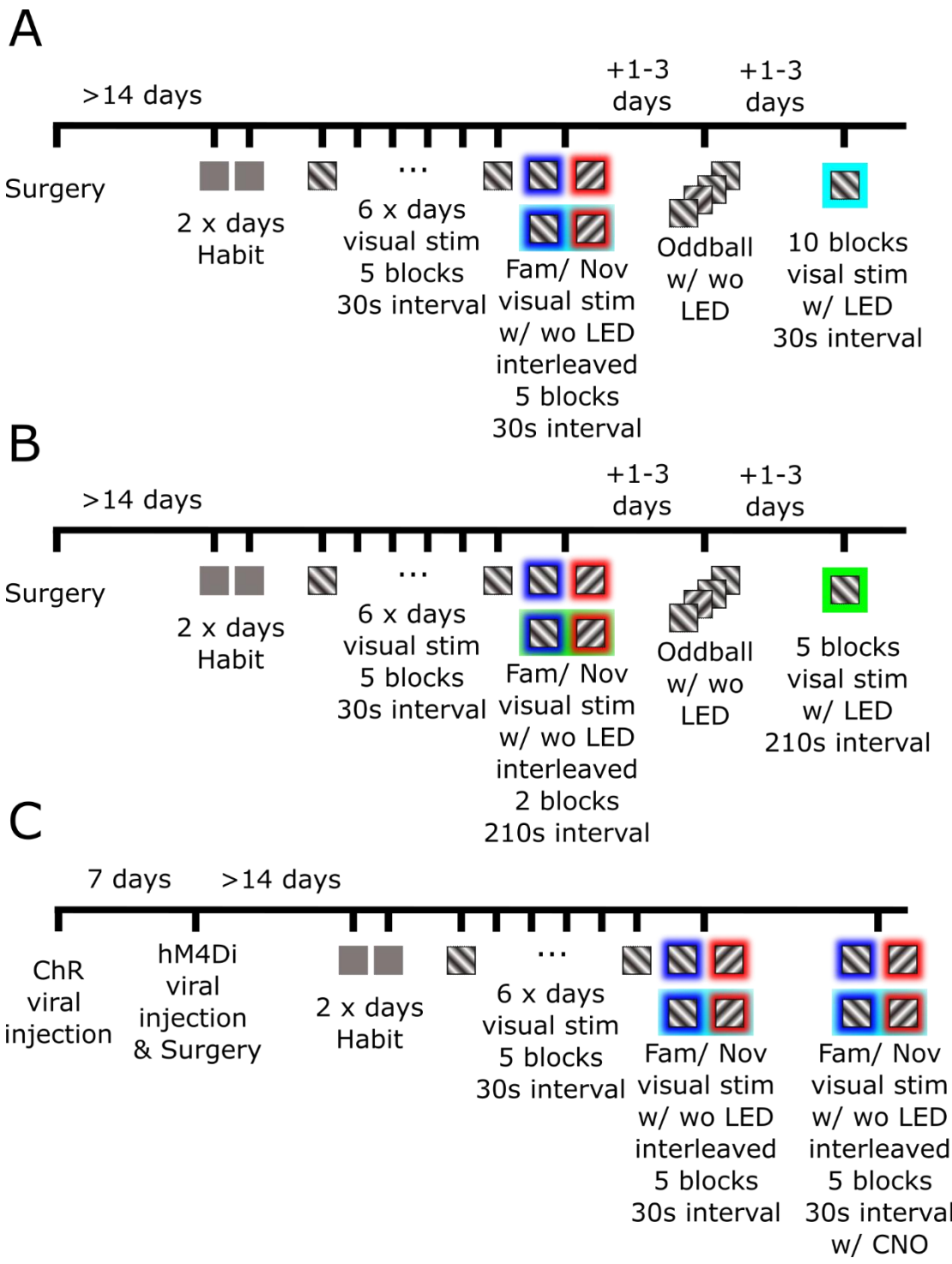

Figure 3.3 Schematic for experiments using optogenetics

3.3.5 Data acquisition

All data were acquired using the Plexon data acquisition system (OmniPlex® Neural Recording Data Acquisition System, Plexon Inc, Dallas, TX, US). Local field potentials (LFP) were collected from V1 in both hemispheres and a 32-channel analogue head-stage was used with Plexon's DigiAmp™ acquisition system. All digital channels were recorded at a 1 kHz sampling rate and run through a 500 Hz low-pass filter and 0.5 Hz high-pass filter. A piezoelectric device was used to pick up a generalized behavioural measure and this signal was acquired into an analogue channel. Video data was acquired by a camera (camera: BFS-U3-13Y3M-C USB 3.1 Blackfly® S, Monochrome Camera, lens: Urth 46mm Infrared (R72) Lens Filter (Plus+), optic: Computar MLH10X Macro lens 13-130mm 1/2" Manual Zoom C-mount) tps://bonsai-rx.org/) was used to integrate with the Plexon acquisition system such that video recording was initiated and terminated simultaneously with recording on the Plexon system.

3.3.6 Analysis and statistics

Data were extracted into Matlab using custom software and the OmniPlex and MAP Otps://plexon.com/software-downloads/#software-downloads-SDKs). For the average VEP for each day, 450 ms traces following stimulus onset were averaged over 1000 phase reversals (5 blocks x 200 phase reversals). For the across-block analysis, traces were averaged over 200 phase reversals for each block (5 or 10). For the within-block analysis (1 v 2, 1 v 200), each individual phase reversal (1 through 200) was averaged over 2, 5, or 10 blocks. For all experiments involving evoked responses, VEP magnitude was taken as the minimum microvolt value from 1-75 ms following onset subtracted from the maximum microvolt value taken from 75-250 ms following onset. The first negativity was the minimum from 1-57 ms, and the maximum was 75-250 ms

following onset. For the oddball paradigm, visual evoked potentials in response to the frequent stimuli were averaged over 1344 presentations and oddballs were averaged over 96 for both LED off and LED on.

All data is expressed as mean ± SEM and number of animals is represented by n. All statistical analyses are non-parametric due to small n numbers negating true testing of normality. For comparisons between two groups or time points, a paired Wilcoxon signed rank test is used. Repeated measures Friedman test is used for analysis across multiple time points within one group. Where multiple tests have been performed, all p values are adjusted using false discovery rate (FDR) correction.

3.3.7 *Ex vivo* data acquisition and analysis

3.3.7.1 Stereotaxic surgeries

Recording from PV+ neurons while activating SOM+ with ChR:

In the left hemisphere ChR was injected at 2 nl/s at depths 600 µm, 450 µm, 300 µm, and 150 µm below surface at coordinates -3.1 from lambda and skin was resealed with Vetbond tissue adhesive. One week later, flp-dependent mCherry was injected at 2 nl/s at depths 600 µm, 450 µm, 300 µm, and 150 µm below surface at coordinates - 3.1 from lambda in the left hemisphere and electrodes were implanted as outlined above only in the right hemisphere. Animals were allowed 5 days recovery prior to head fixation.

Recording from excitatory cells in visual cortex:

Electrodes were implanted as outlined above only in the right hemisphere. Animals were allowed 5 days recovery prior to head fixation.

3.3.7.2 Visual stimuli presentation

For all slice electrophysiology experiments, animals were shown 7 days of 1 block (200 phase reversals) at 20, 40, 60, 80, 100, 120, 140, 160, 180 degrees to

maximise range of visual induced plasticity. Control animals were shown grey screen with the same mean luminance for equivalent time.

3.3.7.3 Slice preparation and data acquisition

Slice solution containing N-methyl-D-glucamine (NMDG) was made following quantities in Table 3.2, pH was adjusted to 7.3-7.4 with concentrated HCl. In a heating bath, half of the NMDG solution was warmed to 32° with mesh containers submerged, the other half is transferred to a beaker and placed in ice. Holding aCSF (Table 3.2) was adjusted to pH 7.3-7.4 with KOH and moved to a mesh lined container and kept at room temperature. All solutions were carbogenated (95% O2/ 5% CO2) for at least 20 minutes before slicing. Using a vibratome, the blade was fixed and aligned to < 0.5 µm. The animal was anaesthetized with a ketamine/ xylazine cocktail at a dose of 25 mg/ml and 4 mg/ml, respectively. The animal was perfused with ice cold NMDG solution for 60 s and brain was dissected out and dropped in ice cold NMDG solution for 10-15 s. Cuts are made coronally to remove the cerebellum and front 1/3rd of the brain with a blade. Then the brain was glued rostral side down onto the vibratome cutting dish and placed into the ice-cold slicing bucket. Ice-cold NMDG solution was poured into the slicing dish to cover the brain. The brain was sliced at 0.05 mm/s speed, with 70 Hz and 1 mm of blade vibration. Slices were cut 300 µm thick and taken from ~-4.5 to ~2.8 AP from bregma. Slices were then moved to the 32° NMDG solution for 20 minutes and then moved to room temperature holding aCSF for 2 hours.

Recording aCSF was made following the quantities in Table 3.2 and was washed over the recording stage and heated to 32°, once the slice was placed in the bath it was held in place with a harp and left for 20 minutes to acclimate. Pipettes were pulled to yield a resistance of between 3-5 MΩ and intracellular solutions used are described in Table 3.2.

For all experiment, cells were patched 430-520 µm from surface of brain to target layer 4 cells. For recordings from excitatory cells, intracellular solution (Table 3.2) contained 5 mM QX-314 to block action potentials. At a voltage of -70 mV, spontaneous excitatory post-synaptic currents (sEPSCs) were recorded for 5 minutes after a delay of 5 minutes for the intracellular solution to equilibrate. Voltage was then increased to 0 mV and a delay of 5 minutes was allowed for the cell to equilibrate, then 5 minutes of recording spontaneous inhibitory post-synaptic currents (sIPSCs) was performed.

For recording from PV+ neurons while manipulating SOM+ with ChR, mCherry was visualised with 585 nm light and whole cell patch clamping was performed in voltage clamp mode. Recording paradigm was performed as described above but every 60 seconds blue light (470 nm) was presented at 20 Hz for 5 pulses for evoked IPSCs.

3.3.7.4 Analysis and statistics

All statistical analysis is non-parametric due to small n numbers negating true testing of normality. For comparisons between two groups or time-points, an unpaired Wilcoxon signed rank test is used. For individual cells, quantiles were calculated based on all IPSC events. Quantile values were then averaged to produce an average quantile curve for each group, and then a Kolmogorov-Smirnov test was performed on averaged curves. Where multiple tests have been performed, all p values are adjusted using false discovery rate (FDR) correction.

Table 3.2 Slice solutions

NMDG Slice solution

Vol (L) 0.1			For	250 mL	300 mL	
	MW	mM	gr			
NMDG	195.22	93	1.815546	4.538865	5.446638	
Glucose	180	20	0.36	0.9	1.08	
Hepes	238.3	20	0.4766	1.1915	1.4298	
KCl	Slice solution 10x Stock	2.5	10	25	30	mL
NaHCO3		30				
NaH2PO4		1.2				
Na+ Ascorbate	198	7	0.1386	0.3465	0.4158	
Thiourea	76.12	2	0.015224	0.03806	0.045672	
Na+ pyruvate	110	4	0.044	0.11	0.132	
CaCl2	CaCl2 1M stock	0.5	0.05	0.125	0.15	mL
MgSO4	MgSO4 1M stock	10	1	2.5	3	mL

Holding aCSF

Vol (L) 0.1			For	300 mL	500 mL	
	MW	mM	gr			
NaCl	58.44	95	0.55518	1.66554	2.7759	
Glucose	180	12	0.216	0.648	1.08	
Hepes	238.3	20	0.4766	1.4298	2.383	
KCl	Slice solution 10x Stock	2.5	10	30	50	mL
NaHCO3		30				
NaH2PO4		1.2				
Na+ Ascorbate	198	7	0.1386	0.4158	0.693	
Thiourea	76.12	2	0.015224	0.045672	0.07612	
Na+ pyruvate	110	4	0.044	0.132	0.22	
CaCl2	CaCl2 1M stock	2	0.2	0.6	1	mL
MgSO4	MgSO4 1M stock	2	0.2	0.6	1	mL

Recording aCSF

Vol (L) 0.1			For	250 mL	500 mL	
	MW	mM	gr			
NaCl	58.44	124	0.724656	1.81164	3.62328	
KCl	74.55	5	0.037275	0.093188	0.186375	
Na2HPO3	138	1.25	0.01725	0.043125	0.08625	
Glucose	180	5	0.09	0.225	0.45	
NaHCO3	84	26	0.2184	0.546	1.092	
Hepes	238.3	5	0.11915	0.297875	0.59575	
CaCl2	CaCl2 1M stock	2	0.2	0.5	1	mL
MgSO4	MgSO4 1M stock	1	0.1	0.25	0.5	mL

Slice solution 10x Stock

Vol (L) 0.5			
	MW	mM	gr

KCl	74.55	25	0.931875
NaH2PO4	138	12	0.828
NaHCO3	84	300	12.6

Intracellular solution

Vol (L) **0.05**	MW	mM	gr
KMeSO4	134.2	135	0.90585
KCl	74.55	5	0.018638
Hepes	238.3	10	0.11915
EGTA	380.35	0.2	0.003804
MgATP	551.14	5	0.137785
NaGTP	523.18	0.3	0.007848
Na_2-Phosphocreatine	255.08	10	0.12754
$MgCl_2 * 6H_2O$	203.3	1	0.010165
QX-314 **(if AP block required)**	343.31	5	0.0858

3.4 Results

3.4.1 PV+ neurons are required during learning to enable encoding of familiarity

3.4.1.1 PV+ inactivation during learning prevents cortical differentiation of familiarity and novelty

Previously, we have shown that PV+ neurons are essential for differential responses of the cortex to familiar and novel stimuli once familiarity has been fully established. However, it is unknown how PV+ neurons are involved during habituation (learning), and whether they participate in forming a memory of a stimulus. Here I aim to answer this question by inactivating PV+ neurons with hM4Di (Figure 3.4A) during early stimulus presentation. Animals were shown visual stimuli for 3 consecutive days with CNO application to inactivate PV+ neurons. This treatment was followed by 24 hours to allow for full washout of the drug, and then on day 4 of visual stimuli presentation, familiar and novel orientations were presented (Figure 3.4B). Previous work relied upon 6

consecutive days of stimulus presentation. However, due to the unknown effect of several days of CNO application on PV+ neuron inactivation and early pandemic restrictions preventing weekend access, a protocol was devised with 3 consecutive days of CNO application prior to visual stimulus presentation, followed by a 4^{th} day for familiar and novel stimulus presentation without CNO. Stimulus-selective response potentiation (SRP) occurred in response to 3 days of stimulus presentation, resulting in a significant differential response to familiar and novel stimuli on day 4 in control animals (Figure 3.4C, Wilcoxon signed-rank test: $p = 0.002$; FDR correction for multiple comparisons, $n = 11$). Inactivation of PV+ neurons during day 1-3 of visual stimuli caused disinhibition of cortical responses. After wash-out of CNO, there was no difference of VEP magnitude in response to familiar and novel stimuli on day 4 (Figure 3.4C ($n = 11$), Wilcoxon signed-rank test: $p = 0.2$; FDR correction for multiple comparisons). In the normal condition, piezo-recorded behavioural responses to novel stimuli were increased compared to familiar stimuli (Figure 3.4D ($n = 11$); Wilcoxon-signed rank test: $p = 0.02$; FDR correction for multiple comparisons). After inactivation of PV+ neurons during learning, behavioural responses were equivalent to familiar and novel stimuli (Figure 3.4D ($n = 11$); Wilcoxon-signed rank test: $p = 0.7$; FDR correction for multiple comparisons). Thus, disruption of normal changes in PV+ neuron activity over learning prevents encoding of stimulus familiarity, as both cortical and behavioural responses to familiar stimuli mimic responses to novel.

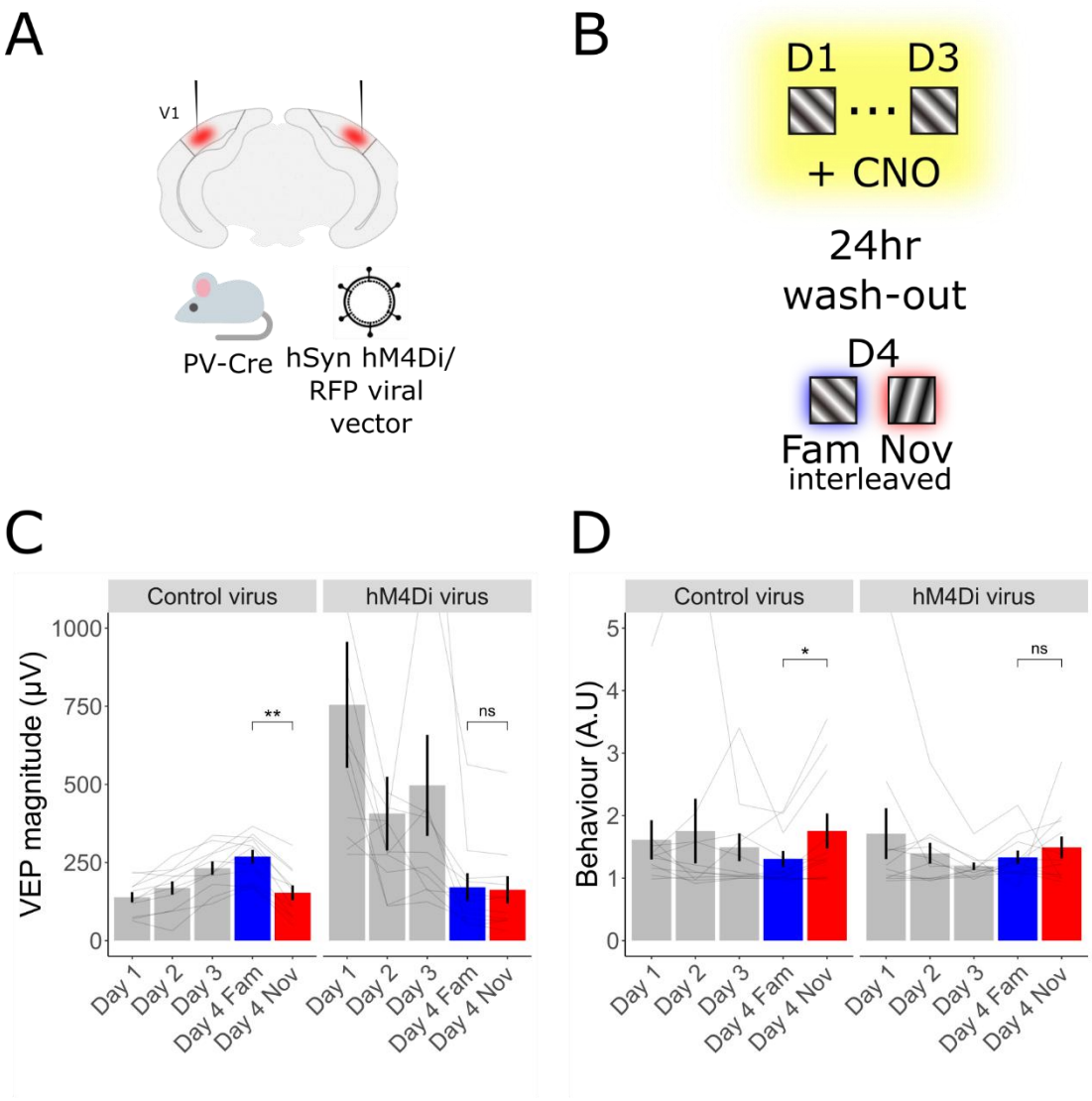

Figure 3.4 Inactivation of PV+ neurons during learning: (A) Schematic to show experimental set-up. (B) Schematic to show visual stimuli presentation protocol. (C) VEP magnitude in response to visual stimuli presentation w/ CNO application (day 1-3) and familiar/novel stimuli presentation after CNO washout (n = 11). (D) Behaviour in response to visual stimuli presentation w/CNO application (day 1-3) and familiar/novel stimuli presentation after CNO washout (n = 11).

3.4.1.2 Short-term adaptation during familiar stimulus presentation mimics novelty after PV+ neuron inactivation

Short-term adaptation of the VEP magnitude across phase reversals occurs only in response to novel stimuli (2.4.4). PV+ neuron inactivation during learning results in the persistence of adaptation from the 1st to 2nd phase reversal for both familiar and novel stimuli (Figure 3.5A (n = 11), Wilcoxon signed-rank FDR correction for multiple comparisons: Control virus: Day 4 Fam 1 v 2: p = 0.3, Day

4 Nov 1 v 2: p = 0.08 (close to significant decrease), hM4Di virus: Day 4 Fam 1 v 2: p = 0.004, Day 4 Nov 1 v 2: p = 0.004). Due to large variability, the adaptation ratio for familiar and novel is not significantly different for control animals (Figure 3.5B (n = 11); Wilcoxon signed-rank FDR correction for multiple comparisons: control virus p = 0.3) as normally expected (2.4.3). Adaptation from the 1st to 2nd phase reversal response to novel stimuli is similar to responses to familiar after PV+ neuron inactivation but does show a similar trend towards greater adaptation in response to novelty (Figure 3.5B (n = 11); Wilcoxon signed-rank FDR correction for multiple comparisons: hM4Di virus p = 0.1).

Short-term adaptation also occurs over 100 seconds from the 1st to 200th phase reversal in response to novel stimuli (Figure 3.5C (n = 11), Wilcoxon signed-rank FDR correction for multiple comparisons: Control virus - Day 4 Fam 1 v 2: p = 0.9, Day 4 Nov 1 v 2: p = 0.008). This results in a significantly greater adaptation ratio in response to novel than to familiar (Figure 3.5D (n = 11); Wilcoxon signed-rank FDR correction for multiple comparisons: Control virus p = 0.004). After inactivation of PV+ neurons during learning, short-term adaptation from the 1st to the 200th phase reversal is maintained (Figure 3.5C (n = 11), Wilcoxon signed-rank FDR correction for multiple comparisons: hM4Di virus: Day 4 Fam 1v2: p = 0.04, Day 4 Nov 1v2: p = 0.008). However, the adaptation ratio in response to novel stimuli is still greater than familiar (Figure 3.5D (n = 11); Wilcoxon signed-rank FDR correction for multiple comparisons: hM4Di virus p = 0.02). This result provides further evidence to support the conclusion that disruption of normal changes in PV+ neuron activity over learning prevents encoding of stimulus familiarity.

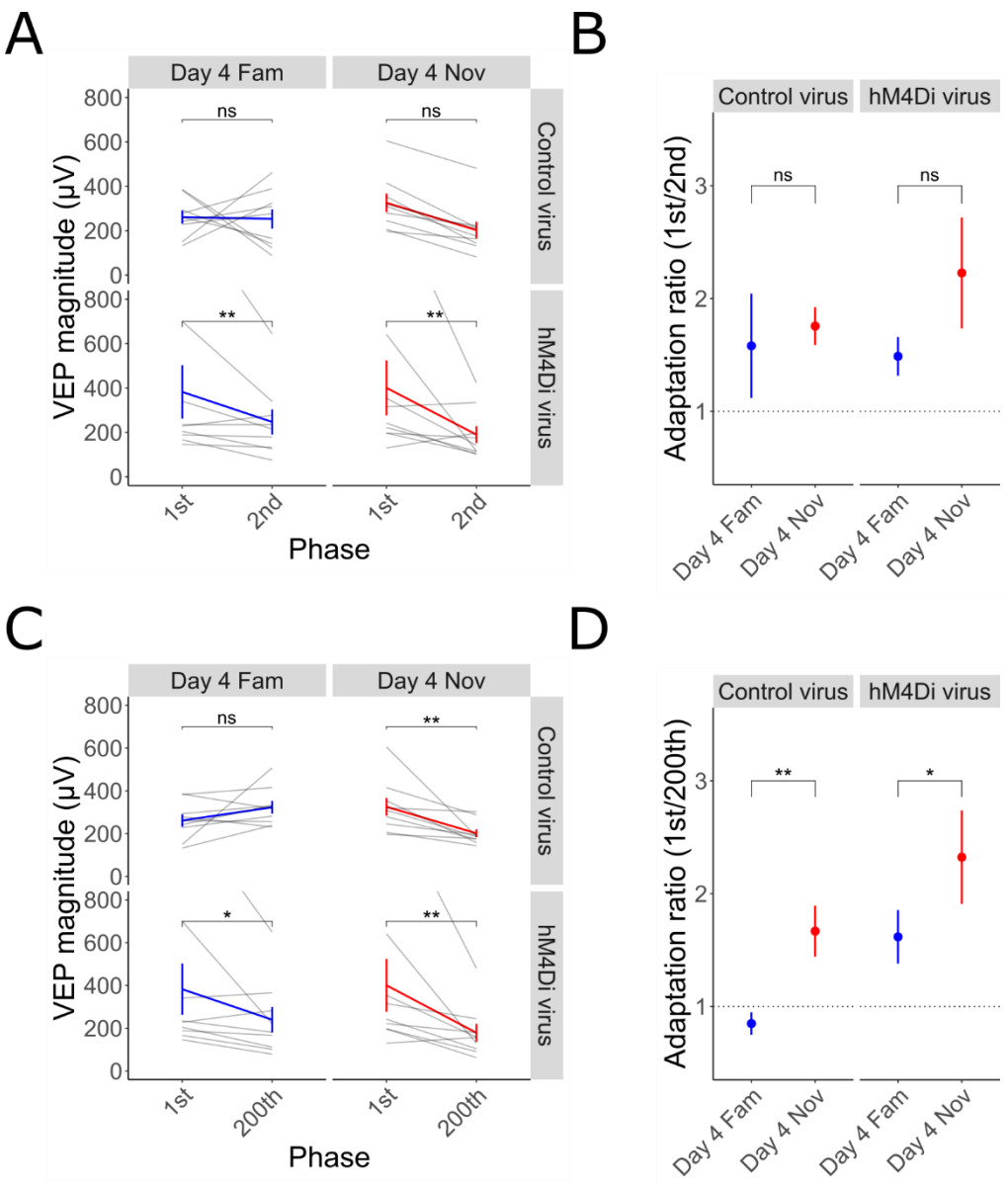

Figure 3.5 Short-term adaptation is maintained after inactivation of PV+ neurons: (A) VEP magnitude in response to 1st and 2nd phase reversal for control and hM4Di groups in response to familiar / novel stimuli (n = 11). (B) Adaptation ration (1st/2nd) for control and hM4Di groups in response to familiar / novel stimuli (n = 11). (C) VEP magnitude in response to 1st and 200th phase reversal for control and hM4Di groups in response to familiar / novel stimuli (n = 11). (D) Adaptation ration (1st/200th) for control and hM4Di groups in response to familiar / novel stimuli (n = 11).

3.4.1.3 Effect of DREADDs wanes over repeated applications but still causes disinhibition of responses compared to baseline

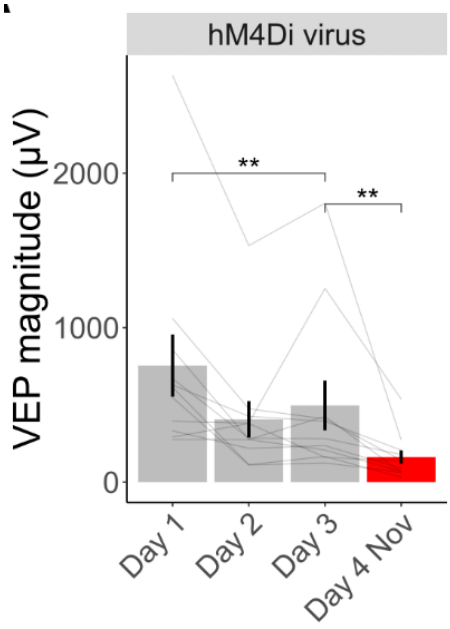

Figure 3.6 Effect of repeated CNO application over days (n = 11).

The DREADDs system relies on hM4Di receptors. These modified Muscarinic receptors are G-protein coupled receptors, which get internalised after ligand binding (Calebiro & Godbole, 2018). Therefore, binding of CNO to hM4Di likely causes internalisation of receptors, which then require replacement for similar efficacy the following session. On day 1 of CNO application, there is pronounced disinhibition in the cortex due to PV+ neuron inactivation. Over progressive CNO application on day 2 and 3, VEP magnitude decreases significantly (Figure 3.6 (n = 11); Friedman test: day 1 – day 3: $p = 0.004$). This indicates that the efficacy of DREADDs decreased over repeated applications. However, despite reducing efficacy, there is still substantial inactivation of PV+ neurons because VEP magnitude on day 3 was significantly greater than the baseline response to a novel stimulus after CNO washout (Figure 3.6 (n = 11); Wilcoxon signed-rank Day 3 – Day 4 Nov: $p = 0.002$).

3.4.2 SOM+ neuron activation alters responses over short and long timescales

3.4.2.1 SOM+ neuron activation disinhibits responses to novelty

During learning, calcium imaging indicates that SOM+ neurons increase their activity and have greater activity in response to familiar stimuli than novel stimuli (Hayden *et al.*, 2021). Therefore, SOM+ neurons may be recruited during familiarity to disinhibit responses to familiar stimuli. Responses to novelty may be of lower magnitude and equivalent to baseline due to lack of SOM+ neuron mediated disinhibition. To test this possibility, I activated SOM+ neurons using ChR during familiar and novel stimuli presentation. Initially, either a conditional ChR AAV virus or a matched control virus was delivered to V1, followed by electrode and optic fibre implantation in SOM+-Cre mice (Figure 3.7A, B, C). Normally, SRP manifests as increased VEP magnitude over days. In response to novel stimuli after SRP, VEP magnitude is reduced back to baseline magnitude. In empty vector control animals, light presentation had no effect on familiar/novel difference or VEP magnitude (Figure 3.7D (n = 9); Wilcoxon signed-rank, FDR correction for multiple comparisons, Control group: Fam LED Off v Nov LED Off $p = 0.008$, Fam LED On v Nov LED On $p = 0.008$, Fam LED Off v Fam LED On $p = 0.7$, Nov LED Off v Nov LED On $p = 1$. Figure 3.7E (n = 9); Wilcoxon signed-rank, FDR correction for multiple comparisons, Control group: LED Off v LED On $p = 1$). In animals expressing ChR in SOM+ neurons, VEP magnitude potentiation occurred, and familiar/novel differences remained intact when no light was present (Figure 3.7D (n = 9); Wilcoxon signed-rank, FDR correction for multiple comparisons; ChR group: Fam LED Off v Nov LED Off $p = 0.008$). Activation of SOM+ neurons with light had no effect on the VEP magnitude in response to familiar stimuli but caused increased VEP magnitude in response to novel stimuli

(Figure 3.7D (n = 9); Wilcoxon signed-rank, FDR correction for multiple comparisons, ChR group: Fam LED Off v Fam LED On p = 0.8, Nov LED Off v Nov LED On p = 0.01). There was still a significant difference between responses to familiar and novel stimuli despite the increased VEP magnitude in response to novel stimuli during SOM+ activation (Figure 3.7D (n = 9); Wilcoxon signed-rank, FDR correction for multiple comparisons, ChR group: Fam LED On v Nov LED On p = 0.008). However, the familiar/novel ratio was significantly reduced following SOM+ activation (Figure 3.7E (n = 9); Wilcoxon signed-rank, FDR correction for multiple comparisons, ChR group: LED Off v LED On p = 0.02). Therefore, recruitment of SOM+ neurons causes an increase in VEP magnitude uniquely to novel stimuli. This supports the hypothesis that engagement of SOM+ inhibitory neurons during familiarity contributes to the increase in VEP magnitude, suggesting a disinhibitory role.

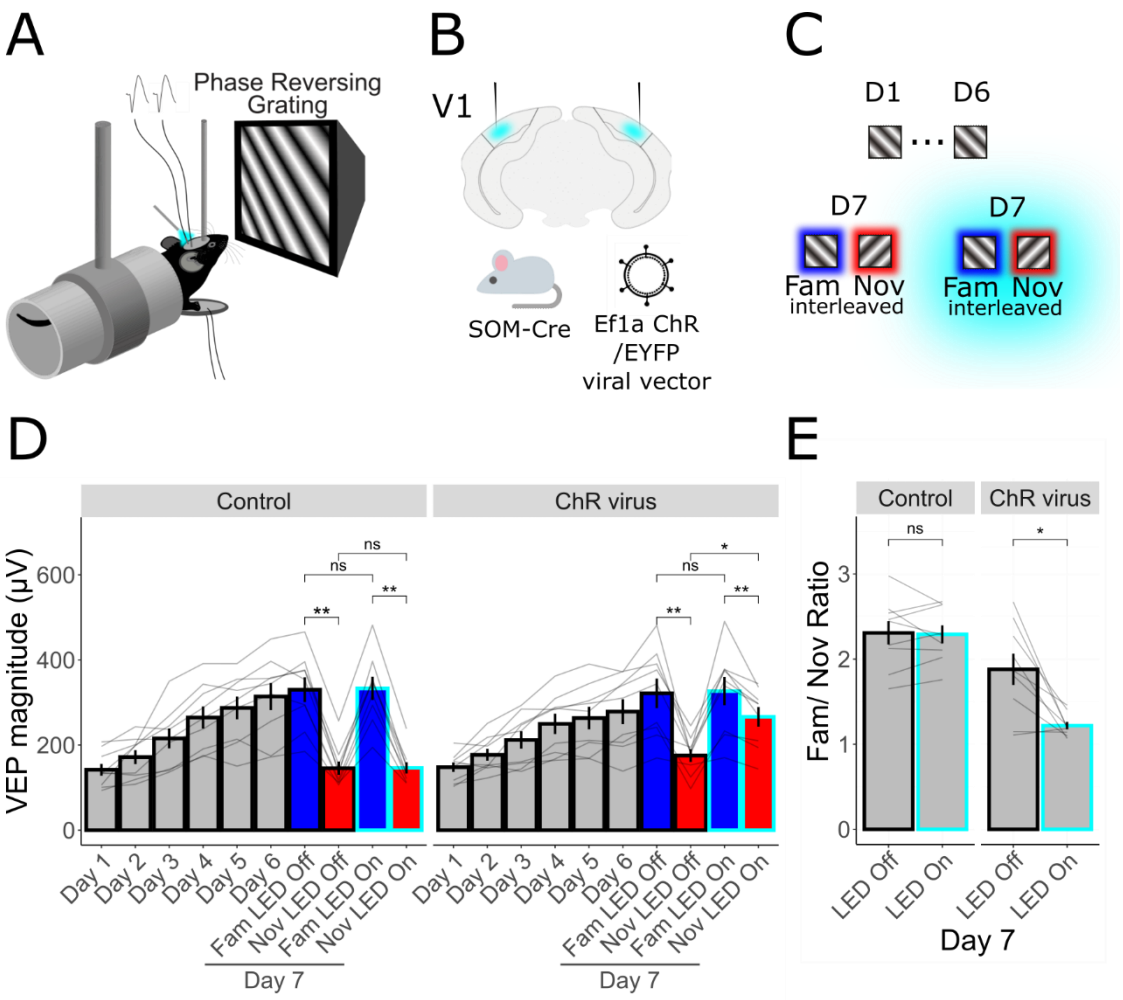

Figure 3.7 SOM+ neuron activation with ChR: (A) Schematic of recording set-up. (B) Schematic of viral expression strategy. (C) Schematic of visual stimuli presentation. (D) VEP magnitude response during visual stimuli presentation across 6 days, and in response to familiar/novel stimuli with and without LED stimulation for control and ChR groups (n = 9). (E) Familiar/novel ratio for control and ChR groups with and without LED stimulation (n = 9).

3.4.2.2 SOM+ neuron activation causes facilitation of responses across blocks

During visual stimuli presentation, stimuli were shown for 5 blocks of 200 phase reversals (~100s per block), interleaved with 30 seconds of grey screen. On day 7, each stimulus condition (Fam/Nov, Fam/Nov w/ LED) is presented pseudorandomly and then the 4x sequence was repeated, such that on day 7 each block for 1 stimulus was separated by ~8 minutes. The within-block adaptation noted in chapter 2 did not occur over these longer block intervals

(Figure 3.8B Fam Off & Nov Off (n = 9)). Interestingly, when activating SOM+ neurons during the first block of stimuli, VEP magnitude was equivalent to baseline novel responses (Figure 3.8B (n = 9)). Subsequently, there was a large jump of the VEP magnitude from block 1 to block 2, which then plateaued for both familiar and novel stimuli (Figure 3.8B (n = 9)). However, the plateau magnitude was reduced for novel compared to familiar stimuli, resulting in the slight familiar/novel difference noted in Figure 3.7D.

Despite the large break between each block with LED on, this plateau effect may be a result of fatigue of cells to optogenetic activation. Evidence against this idea is provided by the observation that responses to familiar/novel are normal when the light is off. Due to the pseudorandom presentation schedule, this 'LED Off' control block may have been shown directly (30s) after an 'LED On' block. To probe this further, a control experiment was performed where 1 block of visual stimuli was shown (~100s per block), then the 2x blocks of grey screen (~100s per block) was shown with the LED On. Then, a further 4 blocks of visual stimuli were shown with LED On followed by 2 blocks of visual stimuli with no LED. After the light induced increase of visual responses with the LED on, responses to visual stimuli following with the LED off returned back to baseline (Figure 3.8D (n = 1)). This finding suggests that 30 seconds of grey screen prior to visual stimulus is sufficient recovery time for any optogenetic hang-over effects (Figure 3.8D (n = 1)). Additionally, the finding suggests that persistent SOM+ activation independent of visual stimuli results in increased VEP magnitude to subsequent visual stimuli (Figure 3.8D (n = 1)). This effect also occurs over 10 blocks of stimuli interleaved with 30 seconds of grey over ~ 30 minutes total, where initial SOM+ activation has little effect on VEP magnitude and progressive activation causes increased VEP magnitude across a block's presentation

(Figure 3.8C (n = 10); Freidman test, ChR group: $p < 0.001$). Overall, these data suggest that SOM+ activation leads to increased VEP magnitude but requires persistent activation of SOM+ neurons over the course of minutes to manifest.

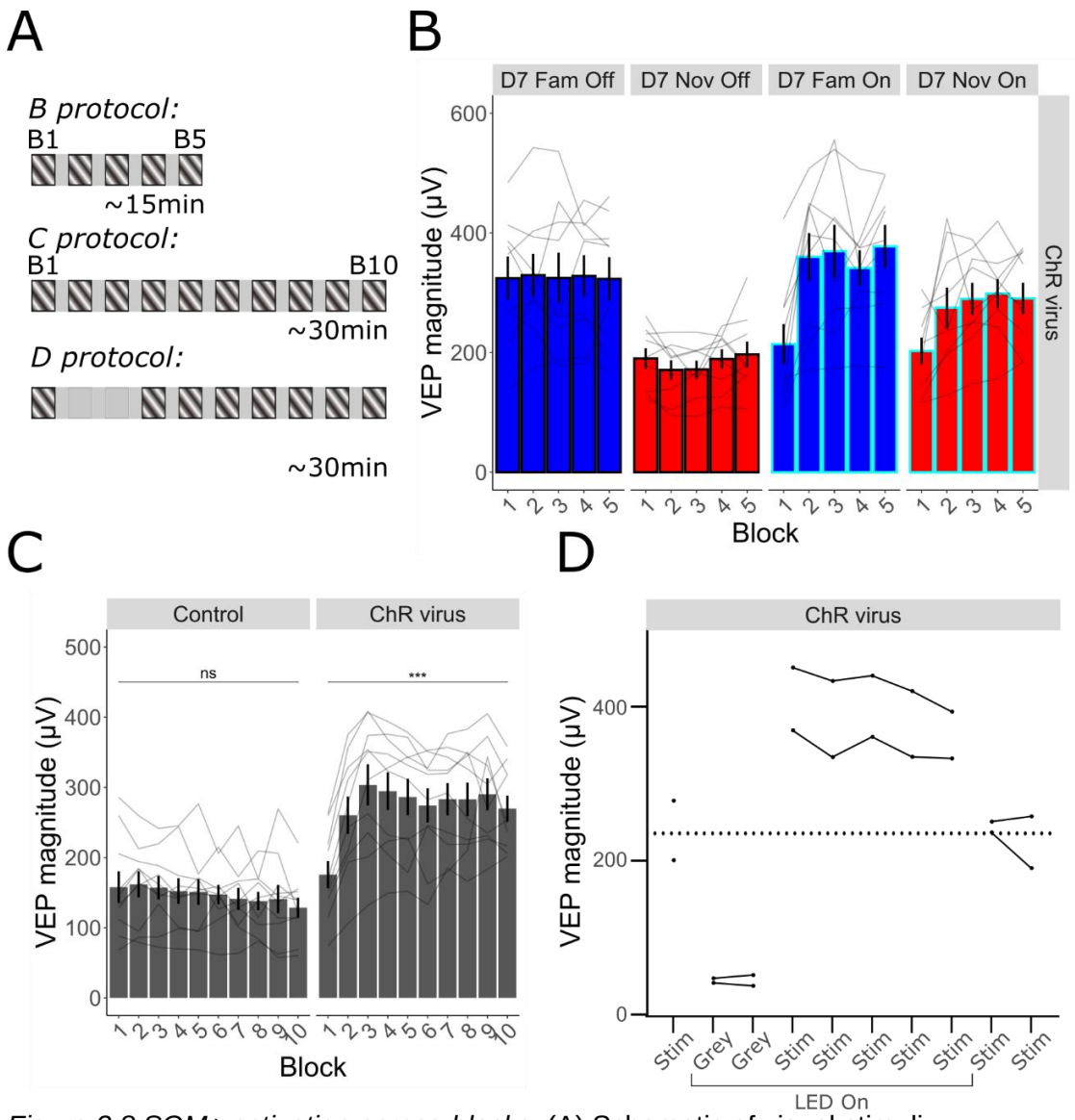

Figure 3.8 SOM+ activation across-blocks: (A) Schematic of visual stimuli presentation for B, C and D. (B) VEP magnitude responses across 5 blocks of familiar/novel stimuli with and without LED stimulation for ChR group (n = 9). (C) VEP magnitude responses across 10 blocks of novel stimuli with LED stimulation for control and ChR groups (n = 10). (D) Control experiment to test responses of cortex immediately following LED stimulation to activate SOM+ neurons (n = 1, two hemispheres).

3.4.2.3 SOM+ neuron activation prevents within-block short-term adaptation

During visual stimulus presentation, short-term adaptation occurs from the 1st to 2nd phase reversal, but only when novel (i.e., never previously experienced) stimuli are presented (2.4.4). Animals expressing an empty vector control virus show no adaptation from the 1st to 2nd phase reversal during familiarity (Figure 3.9A (n = 9); Wilcoxon signed-rank test FDR corrected, Control group 1st v 2nd - D7 Fam Off p = 1, D7 Fam On p = 1) and short-term adaptation during novelty for both LED off and on conditions (Figure 3.9A (n = 9); Wilcoxon signed-rank test FDR corrected, Control group 1st v 2nd - D7 Nov Off p = 0.07 (just short of significance), D7 Nov On p = 0.008). This resulted in an adaptation ratio (AR) close to 1 for familiarity and increased AR for novelty (Figure 3.9B (n = 9); Wilcoxon signed-rank test FDR corrected, Control group - Fam LED Off v Nov LED Off p = 0.1, Fam LED On v Nov LED On p = 0.02). There was no short-term adaptation for both familiar and novel stimuli during activation of SOM+ neurons, but normal VEP magnitude dynamics held true in the absence of light (Figure 3.9A (n = 9); Wilcoxon signed-rank test FDR corrected, ChR group - D7 Fam Off p = 0.7, D7 Nov Off p = 0.008, D7 Fam On p = 1, D7 Nov On p = 0.7). In the absence of light, there was a large increase in the AR for novelty compared to familiarity, but when light was delivered, AR was close to 1 for both stimuli and not significantly different (Figure 3.9B (n = 9); Wilcoxon signed-rank test FDR corrected, ChR group - Fam LED Off v Nov LED Off p = 0.02, Fam LED On v Nov LED On p = 0.2).

Short-term dynamics over a slightly longer timescale of 100 seconds also occur during repeated visual stimuli presentation, manifesting as reduced VEP magnitude from the 1st to 200th phase reversal (2.4.4). This short-term adaptation

occurs in response to novelty but not long-term familiarity in control animals regardless of light condition (Figure 3.9C (n = 9); Wilcoxon signed-rank test FDR corrected, Control group 1^{st} v 200^{th} - D7 Fam Off p = 1, D7 Nov Off p = 0.02, D7 Fam On p = 1, D7 Nov On p = 0.02). This resulted in significantly increased AR to novelty compared to familiarity (Figure 3.9D (n = 9); Wilcoxon signed-rank test FDR corrected, Control group - Fam LED Off v Nov LED Off p = 0.008, Fam LED On v Nov LED On p = 0.02). Activation of SOM+ neurons prevents short-term adaptation of the VEP magnitude from the 1^{st} to the 200^{th} phase reversal, whereas normal dynamics occur when these neurons are not artificially stimulated in the same animals (Figure 3.9C (n = 9); Wilcoxon signed-rank test FDR corrected, ChR group 1^{st} v 200^{th} - D7 Fam Off p = 1, D7 Nov Off p = 0.2, D7 Fam On p = 1, D7 Nov On p = 1). The AR was close to 1 for both stimulus conditions when SOM+ neurons were activated, whereas when the light was off, AR was significantly increased for novelty versus familiarity (Figure 3.9D (n = 9); Wilcoxon signed-rank test FDR corrected, ChR group - Fam LED Off v Nov LED Off p = 0.04, Fam LED On v Nov LED On p = 0.6). These findings support the notion that SOM+ neurons are activated during familiarity but not novelty because activation mimics the short-term VEP magnitude dynamics that occur during familiarity.

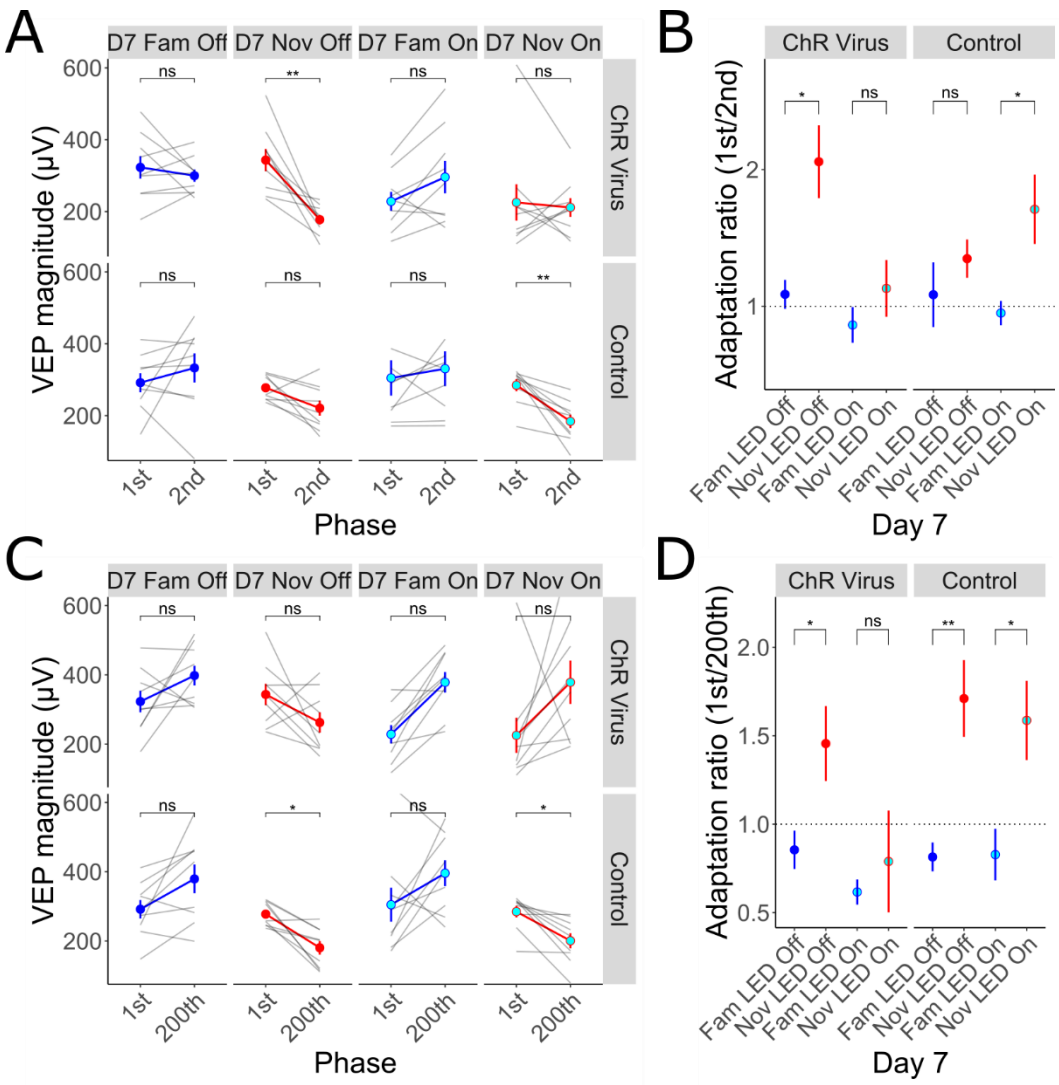

Figure 3.9 Short-term adaptation during SOM+ activation: (A) VEP magnitude in response to 1st and 2nd phase reversal during familiar/novel stimulus presentation with and without LED stimulation for control and ChR groups (n = 9). (B) Adaptation ratio (1st/2nd) during familiar/novel stimulus presentation with and without LED stimulation for control and ChR groups (n = 9). (C) VEP magnitude in response to 1st and 200th phase reversal during familiar/novel stimulus presentation with and without LED stimulation for control and ChR groups (n = 9). (D) Adaptation ratio (1st/200th) during familiar/novel stimulus presentation with and without LED stimulation for control and ChR groups (n = 9).

3.4.3 SOM+ activation with simultaneous PV+ neuronal inactivation

Converging evidence supports the hypothesis that SOM+ neurons increase their activity over learning, and consequently inhibit PV+ neurons to produce disinhibition of layer 4 responses. To directly test this hypothesis, the aim was to inactivate PV+ neurons with DREADDs while activating SOM+ neurons with ChR. This approach required use of SOM-Cre recombinase mice crossed with PV-Flp

recombinase mice. By use of viruses that were Cre-dependent for ChR and Flp-dependent for hM4Di, I aimed to restrict the expression of these actuators in SOM+ or PV+ neurons, respectively. Initially, viruses were injected as a cocktail. Here, the effect of activating SOM+ neuron was weak compared to the previously observed effect (Figure 3.10A (n = 6), Figure 3.7A), but the effect of inactivating PV+ neurons nevertheless replicated the previous observations (Figure 3.10A (n = 6), 2.4.8). The limited expression of ChR may occur either through degradation of the ChR vector in the cocktail, or, as all cells are exposed to both viruses, some form of anti-viral mechanism. Therefore, the ChR vector was injected a week earlier than the hM4Di one, which produced a slightly more substantial effect during SOM+ activation, like that observed previously for the one virus treatment (Figure 3.10B (n = 6), Figure 3.7A). However, now the effect of PV+ inactivation did not mimic results observed previously (Figure 3.10B (n = 6), 2.4.8). This suggests weak expression of hM4Di in PV+ neurons. Furthermore, the effect size for SOM+ activation was still lower than that observed previously. Therefore, further adjustment of both ChR and hM4Di viral titre is needed to replicate the previous findings for each manipulation when combined. However, this was not possible in the current project due to cessation of experimental work. The method shows promise but needs further refinement.

Despite the variability in effect size across different versions of the protocol, to investigate any effect of these manipulations, all animals from all protocol versions were averaged (Figure 3.10C, D (n = 12)). In line with previous findings, familiar/novel ratio decreased both after SOM+ neuronal activation and PV+ neuronal inactivation (Figure 3.10D (n = 12)). Combined SOM+ neuronal activation and PV+ neuronal inactivation caused the largest increase in VEP magnitude, suggesting a summative effect (Figure 3.10C, D (n = 12)). However,

the familiar/novel ratio was similar to SOM+ activation and PV+ inhibition alone (Figure 3.10D (n = 12), close to 1 in 3.4.2.1 and (Kaplan *et al.*, 2016)). This hints at a conclusion that artificial inactivation of PV+ neurons mimics and occludes the effect of SOM+ activation. However, further work is required. Therefore, the mechanism by which SOM+ effects VEP magnitude may be reliant on inhibition of PV+ neurons.

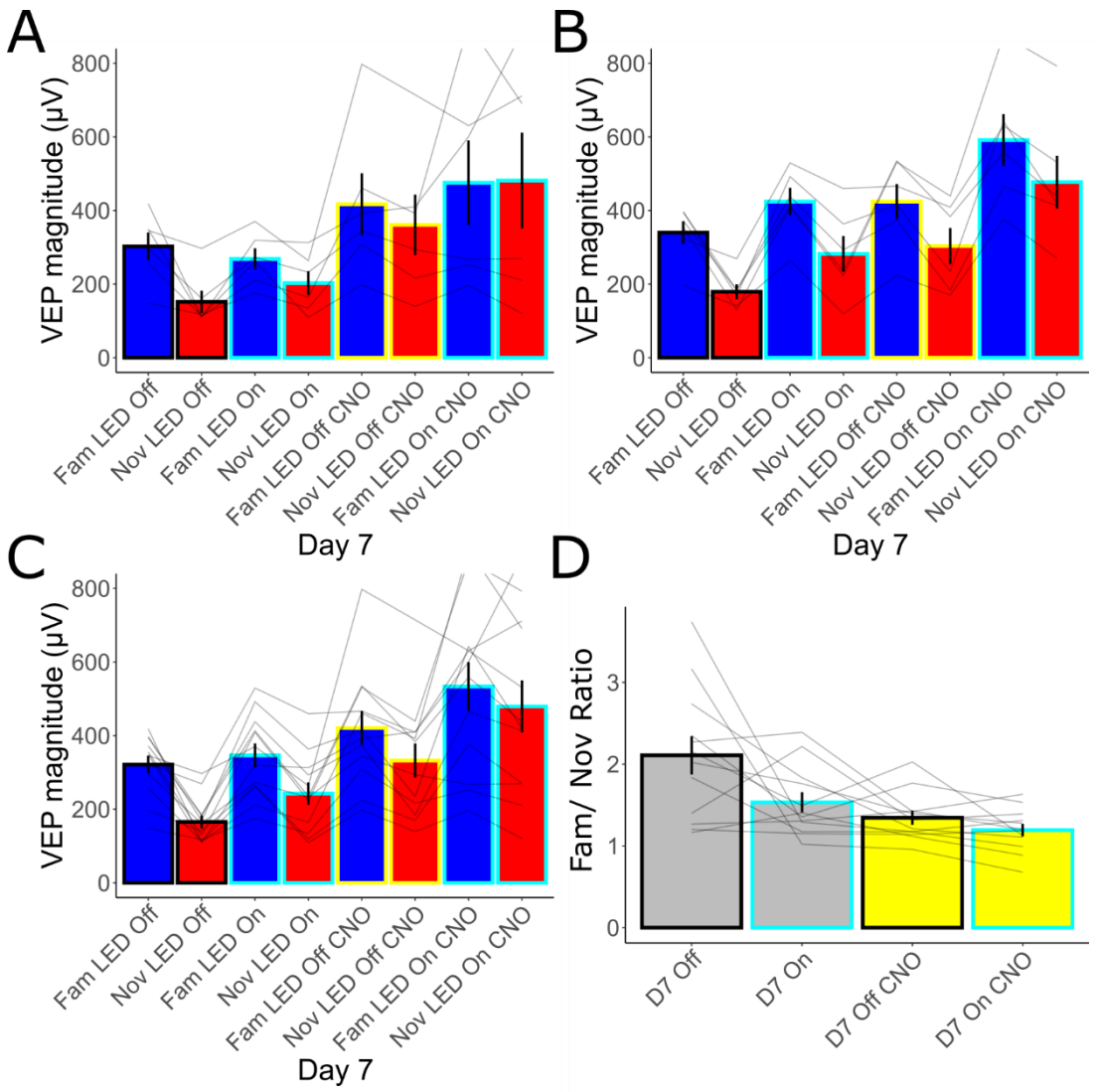

Figure 3.10 Combined SOM+ activation with ChR and PV+ inactivation with hM4Di: VEP magnitude in response to familiar/novel stimuli with and without LED stimulation, and with and without CNO application in (A) combined viral injections (n = 6); (B) Split viral injections (n = 6); (C) all animals from all protocols averaged (n = 12. (D) Familiar/novel ratio from all animals in normal familiar/novel stimulus presentation, familiar/novel stimulus presentation with LED stimulation, familiar/novel stimulus presentation with CNO application, familiar/novel stimulus presentation with LED stimulation and CNO application (n = 12).

3.4.4 SOM+ neuron inactivation alters responses over long timescales

3.4.4.1 SOM+ neuron inactivation causes reduced responses to both familiar and novel stimuli and maintains familiar/novel distinction

There is a growing body of evidence showing that SOM+ neurons are recruited during familiarity, and that activating these cells can mimic responses to familiarity. However, the question remains as to whether inactivating SOM+ neurons mimics responses to novelty? To test this, I inactivated SOM+ neurons using HaloRhodopsin (HaloR) during presentation of familiar and novel visual stimuli (Figure 3.12A, B, C).

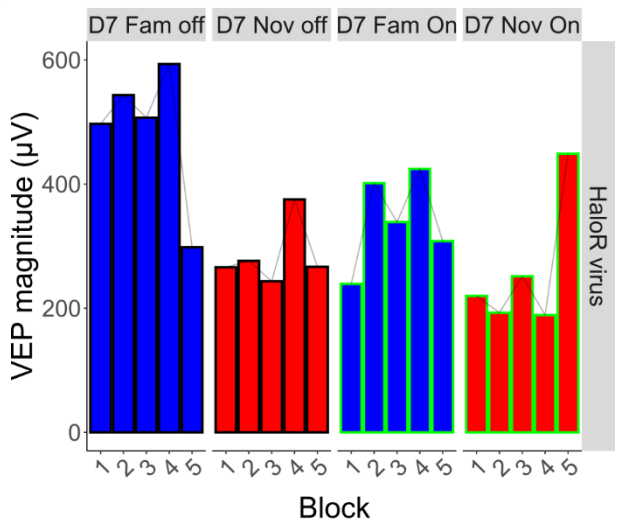

Figure 3.11 SOM+ inactivation with HaloRhodopsin using 5 blocks interleaved with 30s grey screen

Initially, I used the same protocol as all previous experiments had used, where each condition (D7 Fam Off, D7 Nov Off, D7 Fam On, D7 Nov On) was presented pseudo-randomly with an inter-block interval of 30 seconds, repeated 5 times. However, when investigating the VEP magnitude by block, light off conditions showed variability in VEP magnitude, suggesting hang-over effects after inactivation of SOM+ neurons with light (Figure 3.11). To allow full recovery of normal cortical activity, each block was interleaved with 210 s grey screen. This limited total block number to 8 (2 per condition) to ensure the animal was not in the head holder for too long. Furthermore, each condition was presented in the same order for every repeat (D7 Nov On, D7 Nov Off, D7 Fam On, D7 Fam Off) to prevent sequential 'LED

on' blocks. This new protocol has no hang-over effects on VEP responses in light off condition (Figure 3.13A).

Inactivation of SOM+ neurons was achieved using HaloR during presentation of familiar and novel visual stimuli on day 7 (Figure 3.12A, B, C). In animals expressing a control virus, there was normal potentiation of VEP magnitude over days resulting in familiar/ novel differences on day 7 in both light on and light off trials (Figure 3.12D (n = 9); Wilcoxon signed-rank, FDR correction for multiple comparisons, Control group: Fam LED Off v Nov LED Off $p = 0.005$, Fam LED On v Nov LED On $p = 0.005$). No difference should be expected in the magnitude of responses in light on/ off conditions. However, there was significantly decreased VEP magnitude in response to novelty during the light on condition in control animals (Figure 3.12D (n = 9); Wilcoxon signed-rank, FDR correction for multiple comparisons, Control group: Fam LED Off v Fam LED On $p = 1$, Nov LED Off v Nov LED On $p = 0.005$), resulting in increased familiar/novel ratio between groups (Figure 3.12E (n = 9); Wilcoxon signed-rank, FDR correction for multiple comparisons, Control group: LED Off v LED On $p = 0.008$). This may be a result of sequential block presentation promoting within-block adaptation (Figure 2.1).

SOM+ inactivation resulted in reduced VEP responses to both familiar and novel stimuli, maintaining differential responses to familiar and novel stimuli (Figure 3.12D (n = 9); HaloR group: Fam LED Off v Nov LED Off $p = 0.005$, Fam LED On v Nov LED On $p = 0.005$, Fam LED Off v Fam LED On $p = 0.005$, Nov LED Off v Nov LED On $p = 0.009$). Due to comparable effects on responses to novel and familiar stimuli, the familiar/novel ratio was equivalent in both conditions (Figure 3.12E (n = 9); Wilcoxon signed-rank, FDR correction for multiple comparisons, HaloR group: LED Off v LED On $p = 0.3$). Overall, SOM+

inactivation indiscriminately inhibited VEP responses to both familiar and novel stimuli. Despite the broad effect, the observation of reduced responses following SOM+ inactivation supports the notion that SOM+ inhibitory neurons target PV+ inhibitory neurons, with responses decreasing as PV+ neurons are released from inhibitory control mediated by SOM+ neurons.

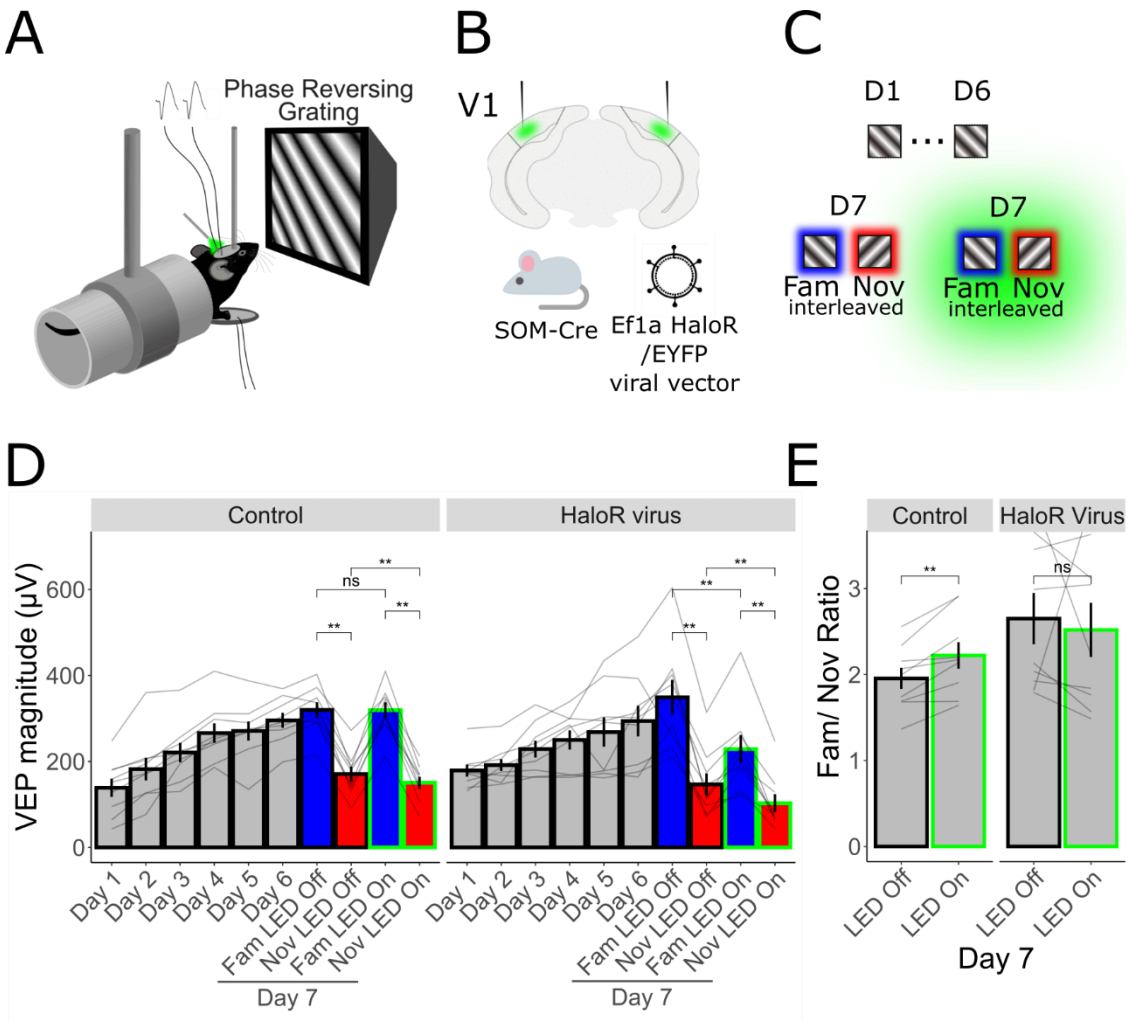

Figure 3.12 SOM+ neuron inactivation with HaloR: (A) Schematic of recording set-up. (B) Schematic of viral expression. (C) Schematic of visual stimuli presentation. (D) VEP magnitude response during visual stimuli presentation across 6 days, and in response to familiar/novel stimuli with and without LED stimulation for control and HaloR groups (n = 9). (E) Familiar/novel ratio for control and HaloR groups with and without LED stimulation (n = 9).

3.4.4.2 Effect of SOM+ neuron inactivation on within-block adaptation is harder to interpret due to long stimulus interval times

Stimulus-selective response potentiation occurring over days, is an opposing effect to the adaptation that occurs over minutes (Figure 2.1). This adaptation is subtle, but manifests as reduced VEP magnitude across 5 stimulus blocks, each interleaved with 30 seconds of grey. Increasing the length of the inter-block interval to 210 seconds was an attempt to combat hang-over effects of optogenetics. However, during familiar/novel presentation, there was no obvious VEP adaptation across blocks or between groups (Figure 3.13A (n = 9)). To probe changes further, 5 blocks were shown interleaved with 210 seconds of grey on a single day (~30 mins) with a novel stimulus. In animals expressing both control virus and HaloR virus, VEP magnitude significantly increased across blocks (Figure 3.13B (n = 9); Friedman test: Control group block 1 – block 5 p = 0.008, HaloR group block 1 – block 5 p = 0.02). Therefore, SOM+ inactivation likely has no effect of VEP dynamics across tens of minutes but extending the interval across blocks appears to switch the direction of observed plasticity, which is an interesting observation that will need further investigation.

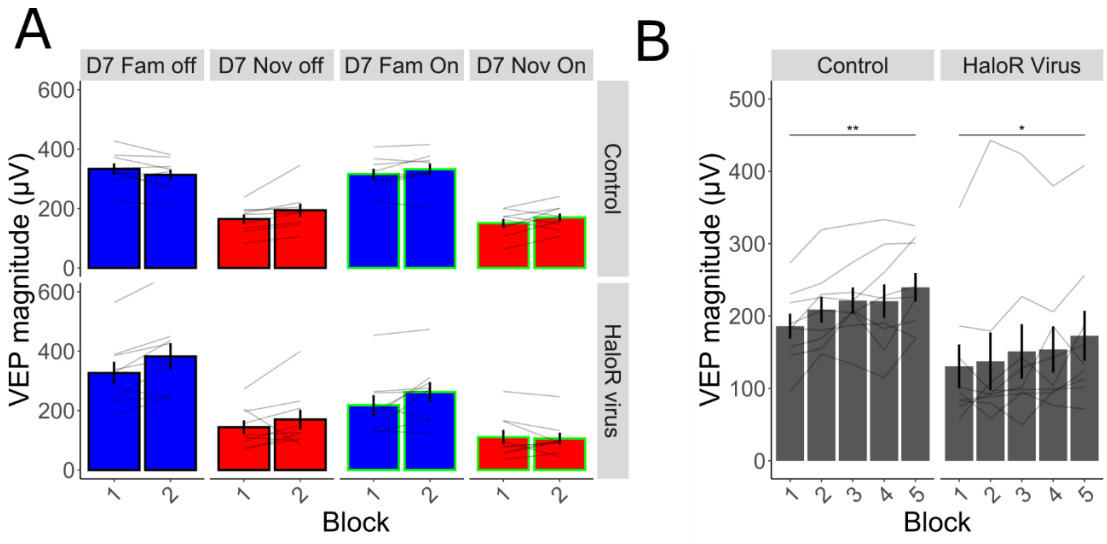

Figure 3.13 Within-block responses during SOM+ inactivation: (A) VEP magnitude responses across 2 blocks of familiar/novel stimuli with and without LED stimulation

for HaloR and control groups (n = 9). (B) VEP magnitude responses across 5 blocks of novel stimuli with LED stimulation for control and ChR and control groups (n = 9).

3.4.4.3 Effect of SOM+ neuron inactivation on within-block short-term adaptation is harder to interpret due to reduced block number resulting in variable data

Local field potential (LFP) responses to each individual stimulus presentation are variable. Therefore, for most studies investigating evoked potentials, many presentations of single stimuli are averaged to gain a metric of the evoked potential. To investigate changes over days, VEPs are averaged from 1000 phase reversals (Figure 3.14A) and to investigate changes over blocks VEPs are averaged from 200 phase reversals (Figure 3.14B). These averaged VEPs are smooth and have clearly defined negative peaks at ~50 ms and positive peaks at ~100ms for calculation of VEP magnitude. However, when investigating changes within-blocks (across 200 phase reversals), only 5 time series can typically be averaged for each phase reversal (1^{st}, 2^{nd}…200^{th}), one for each of the 5 blocks shown. This approach results in a noisy averaged VEP for each phase reversal, but this waveform still has defined negative and positive peaks (Figure 3.14C). For SOM+ neuron inactivation with HaloRhodopsin, the protocol involved presenting 2 blocks separated with 210 s of grey screen due to pronounced hang-over effects of optogenetic inactivation. Two timeseries from two blocks averaged together resulted in a very noisy VEP, which lacks clearly defined positive and negative peaks (Figure 3.14D).

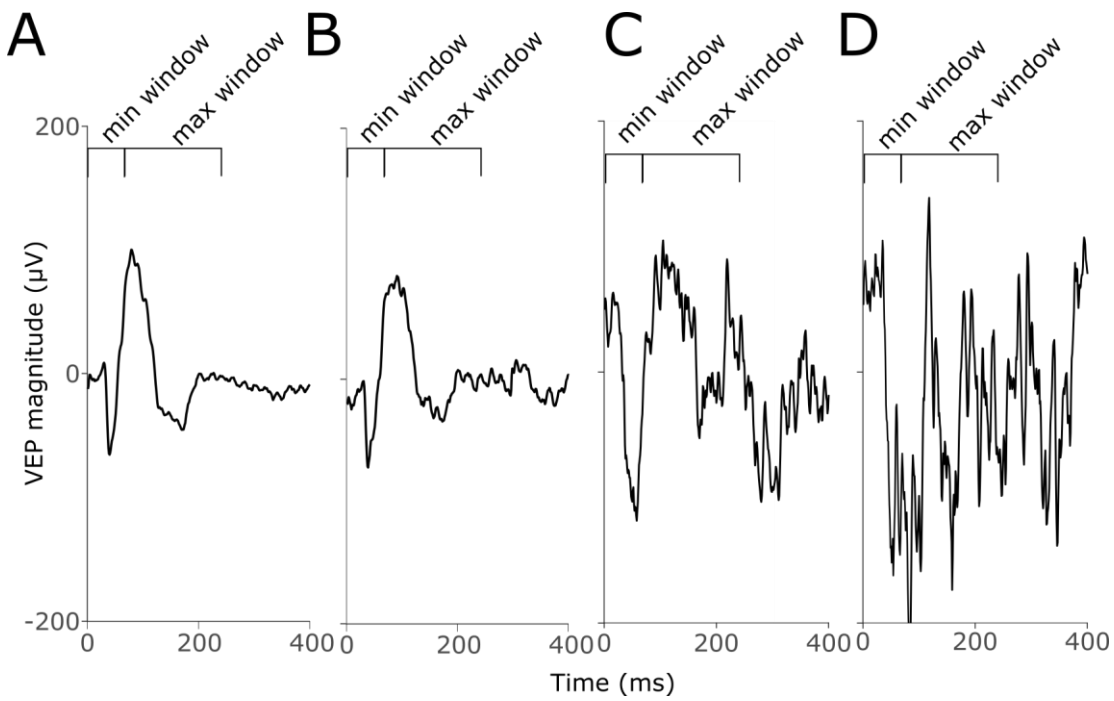

Figure 3.14 Averaged VEP responses: VEPs averaged over (A) 1000 phase reversal blocks; (B) 200 phase reversals; (C) 5 phase reversals; (D) 2 phase reversals

In experiments using HaloRhodopsin to inhibit SOM+ neurons, average traces from 2 blocks produce noisy VEP waveforms. This makes the data highly variable while analysing short-term changes (Figure 3.14D) and the study is perhaps underpowered for this analysis. The well-known short-term adaptation in response to novelty but not familiarity (Figure 2.2) is absent in control groups (Figure 3.15A, B, C, D, Table 3.3, Table 3.4 (n = 9)). In HaloR animals, there was a hint of short-term adaptation from the 1st to 2nd phase reversal in light off and light on conditions (Figure 3.15A (n = 9), Table 3.3), resulting in a significant increase in AR to novelty for both light on and off conditions (Figure 3.15B (n = 9), Table 3.4). When inactivating SOM+ neurons with light, VEP short-term dynamics from the 1st to 200th phase reversal were normal. However, in the light off condition there was no short-term adaptation (Figure 3.15C (n = 9), Table 3.3). This resulted in significantly different AR in response to familiar/novel stimuli during light on but not during light off (Figure 3.15D (n = 9), Table 3.4). Therefore, the interpretation of the SOM+ inactivation on short-term dynamics of VEP

magnitude is challenging, and potentially more subjects will be required. This data is highly variable and both control animals and within-animal control conditions (LED Off) do not replicate our well-established phenomenon.

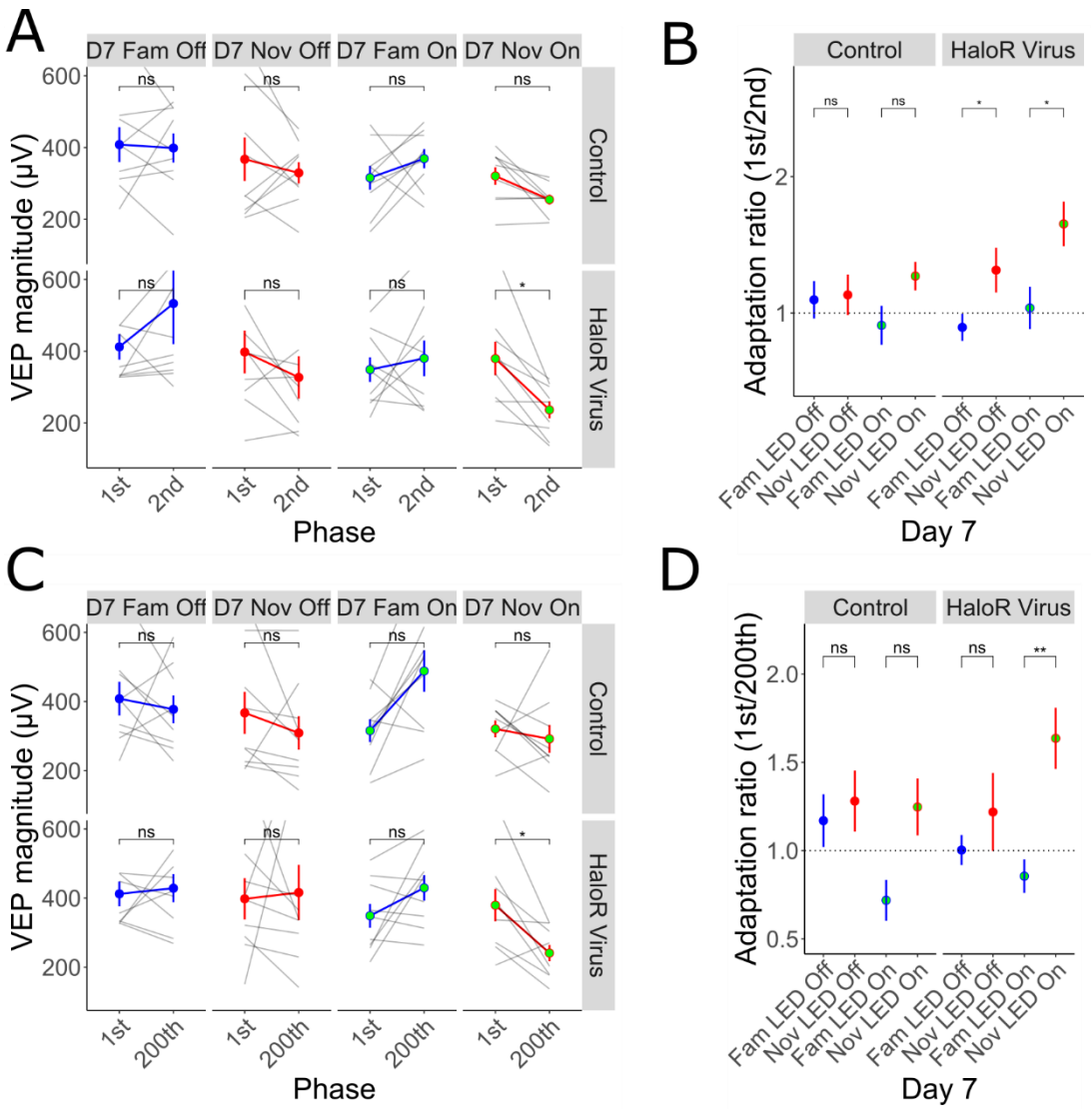

Figure 3.15 Short-term adaptation during SOM+ inactivation: (A) VEP magnitude in response to 1st and 2nd phase reversal during familiar/novel stimulus presentation with and without LED stimulation for control and HaloR groups (n = 9). (B) Adaptation ratio (1st/2nd) during familiar/novel stimuli presentation with and without LED stimulation for control and HaloR groups (n = 9). (C) VEP magnitude in response to 1st and 200th phase reversal during familiar/novel stimulus presentation with and without LED stimulation for control and HaloR groups (n = 9). (D) Adaptation ratio (1st/200th) during familiar/novel stimulus presentation with and without LED stimulation for control and HaloR groups (n = 9).

Table 3.3 Statistics for short-term adaptation in control and HaloR groups

Group	group1	group2	Day	p value
Control	1st	2nd	D7 Fam Off	0.7
Control	1st	2nd	D7 Nov Off	0.7

Control	1st	2nd	D7 Fam On	0.9
Control	1st	2nd	D7 Nov On	0.08
HaloR Virus	1st	2nd	D7 Fam Off	0.9
HaloR Virus	1st	2nd	D7 Nov Off	0.2
HaloR Virus	1st	2nd	D7 Fam On	0.9
HaloR Virus	1st	2nd	D7 Nov On	0.02
Control	1st	200th	D7 Fam Off	0.5
Control	1st	200th	D7 Nov Off	0.2
Control	1st	200th	D7 Fam On	1
Control	1st	200th	D7 Nov On	0.4
HaloR Virus	1st	200th	D7 Fam Off	0.8
HaloR Virus	1st	200th	D7 Nov Off	0.5
HaloR Virus	1st	200th	D7 Fam On	0.9
HaloR Virus	1st	200th	D7 Nov On	0.05

Table 3.4 Statistics for Adaptation Ratio comparisons for HaloR and control animals

Group	**group1**	**group2**	**p value**
Control AR (1st/2nd)	D7 Fam Off	D7 Nov Off	0.2
Control AR (1st/2nd)	D7 Fam On	D7 Nov On	0.1
HaloR Virus AR (1st/2nd)	D7 Fam Off	D7 Nov Off	0.04
HaloR Virus AR (1st/2nd)	D7 Fam On	D7 Nov On	0.04
Control AR (1st/200th)	D7 Fam Off	D7 Nov Off	0.3
Control AR (1st/200th)	D7 Fam On	D7 Nov On	0.07
HaloR Virus AR (1st/200th)	D7 Fam Off	D7 Nov Off	0.3
HaloR Virus AR (1st/200th)	D7 Fam On	D7 Nov On	0.008

3.4.5 Behavioural changes during activation and inactivation of SOM+ neurons are variable and inconclusive

Animal behaviours tend towards higher variability than physiological phenomena due to added complexity. Generally, this necessitates a larger sample size to allow for analyses (>15) (Cooke *et al.*, 2015). Furthermore, different acquisition methods can result in a smoothed signal if digitised, and a sharper signal if acquired via analogue inputs. Previous analysis methods worked on a piezo-electrical behavioural signal that was a smoothed and amplified digital signal and the area under the curve captured the dynamics of the signal well (Figure 2.1). My current behavioural analysis follows the same analysis pipeline. However, the

signal acquired in the current experiments was through non-amplified analogue inputs, resulting in very sharp deflections and low signal-to-noise. Therefore, analysis pipelines that involve calculation of ‘area under the curve’ fail to capture the full dynamics of the data. Therefore, current analysis of behavioural data acquired through a piezo electric device is harder to interpret. Behavioural changes over days do not show the well-established habituation (Cooke *et al.*, 2015) (Figure 2.1), resulting in no significant differences for behavioural responses over days or when comparing familiar and novel stimuli (Figure 3.16 (n = 9), Table 3.5, Table 3.6).

Full validation of behavioural data collection is needed, including both amplification of the piezo signal and alternative analyses, for example moving average to smooth the data and Z-score normalisation. Furthermore, video data was collected in parallel which will likely provide much finer behavioural detail than the crude measure recorded from the piezo electric device. However, video data analysis pipelines will require training neural networks (Mathis *et al.*, 2018) or PCA analysis (Syeda *et al.*, 2022), and this remains a work in progress that will require further validation on these data sets.

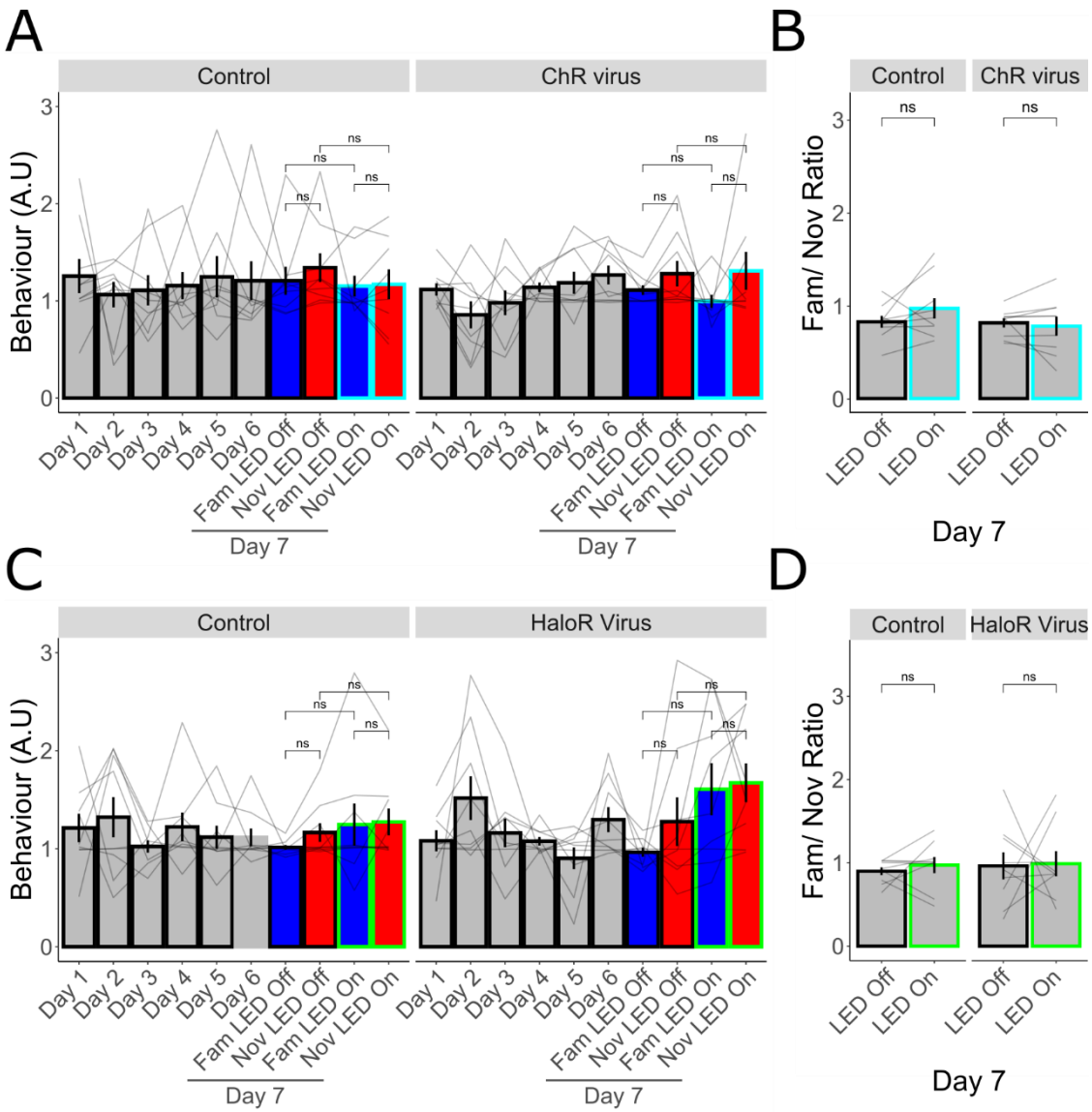

Figure 3.16 Behavioural responses during SOM+ activation and inactivation: (A) Behavioural response during visual stimuli presentation across 6 days, and in response to familiar/novel stimulus with and without LED stimulation for control and ChR groups (n = 9). (B) Familiar/novel ratio for control and ChR groups with and without LED stimulation (n = 9). (C) Behavioural response during visual stimuli presentation across 6 days, and in response to familiar/novel stimulus with and without LED stimulation for control and HaloR groups (n = 9). (D) Familiar/novel ratio for control and HaloR groups with and without LED stimulation (n = 9).

Table 3.5 Statistics for comparisons of behavioural responses to familiar/novel stimuli in SOM+ optogenetics experiments

Group	group1	group2	p value
Control	D7 Fam off	D7 Nov off	0.6
Control	D7 Fam On	D7 Nov On	0.9
Control	D7 Fam off	D7 Fam On	0.7
Control	D7 Nov off	D7 Nov On	0.7
ChR	D7 Fam off	D7 Nov off	0.5
ChR	D7 Fam On	D7 Nov On	0.6

ChR	D7 Fam off	D7 Fam On	0.6
ChR	D7 Nov off	D7 Nov On	0.5
Control	D7 Fam off	D7 Nov off	0.4
Control	D7 Fam On	D7 Nov On	0.9
Control	D7 Fam off	D7 Fam On	0.4
Control	D7 Nov off	D7 Nov On	0.4
HaloR Virus	D7 Fam off	D7 Nov off	0.7
HaloR Virus	D7 Fam On	D7 Nov On	0.7
HaloR Virus	D7 Fam off	D7 Fam On	0.4
HaloR Virus	D7 Nov off	D7 Nov On	0.4

Table 3.6 Statistics for comparisons of adaptation ration to familiar/novel stimuli in SOM+ optogenetics experiments

Group	**group1**	**group2**	**p value**
Control	LED Off	LED On	0.4
ChR	LED Off	LED On	0.8
Control	LED Off	LED On	0.9
HaloR Virus	LED Off	LED On	0.9

3.4.6 SOM+ neurons are required for oddball responses

The short-term adaptation discussed here is a result of repetitive presentation of one stimulus orientation over minutes and seconds. A well-established phenomenon that reveals both responses to repetitive stimuli and responses to 'surprise' stimuli, is the oddball paradigm. The oddball paradigm shows a frequent stimulus interrupted with an unexpected oddball stimulus for an overall presentation frequency of 88% and 12% of the time, respectively (Figure 3.17A). In response to oddball stimuli, VEP responses are increased compared to responses to frequent stimuli (Figure 3.17B, C). In human EEG this effect manifests as an increase in the negative-going component of the VEP. Hence, it is often described as mis-match negativity (MMN).

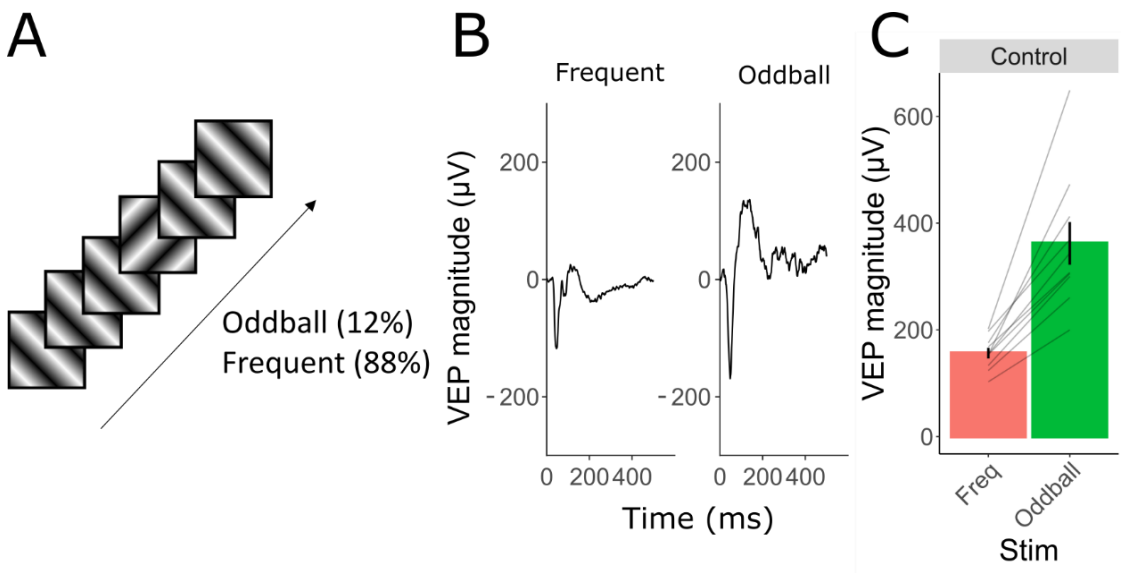

Figure 3.17 Oddball responses: (A) Oddball paradigm. (B) VEP waveform in response to frequent and oddball stimuli. (C) VEP magnitude in response to frequent and oddball stimuli (n = 10).

Evidence suggests that SOM+ neurons play a role in oddball responses, as inactivation with hM4Di DREADDs prevents the differential response (Hamm & Yuste, 2016). However, in the DREADDs experiment there was no temporal control of SOM+ inhibitory neurons. In contrast, temporal precision can be achieved with optogenetics. Therefore, I investigated the role of SOM+ neurons during oddball stimuli using activating and inhibiting optogenetics. Furthermore, as there is existing evidence that SOM+ neurons are involved in oddball responses (Natan *et al.*, 2015). Thus, these experiments act as validation that optogenetics in SOM+ cells works as expected.

Oddball responses are much larger than responses to frequent stimuli in the control conditions with and without light (Controls: Figure 3.18A (n = 10)). Waveforms for VEPs have a negative deflection at ~50 ms and a positive deflection at ~100 ms. During oddball responses, both the negative and positive components of the VEP were significantly increased in response to oddball stimuli (Controls: Figure 3.18B, C (n = 10), Table 3.7).

Activation of SOM+ neurons prevented normal oddball responses (Figure 3.19A, Figure 3.18A (n = 10); Wilcoxon signed-rank FDR corrected: ChR group – Freq v Oddball p = 0.004, Freq v Oddball w/ light p = 0.07, Oddball v Oddball w/ light p = 0.1). During SOM+ activation, there was a substantial reduction of the positive component of the VEP, and for many animals this component remained below 0 mV (Figure 3.19A, Figure 3.18B (n = 10); Wilcoxon signed-rank FDR corrected: ChR group – Freq v Oddball p = 0.003, Freq v Oddball w/ light p = 0.1, Oddball v Oddball w/ light p = 0.003). The negative component of the VEP in response to oddball stimuli was larger when SOM+ inhibitory neurons were activated, but variable across animals, (Figure 3.19A, Figure 3.18C (n = 10); Wilcoxon signed-rank FDR corrected: ChR group – Freq v Oddball p = 0.004, Freq v Oddball w/ light p = 0.04, Oddball v Oddball w/ light p = 0.4).

Oddball responses during inactivation of SOM+ cells was significantly reduced compared to normal oddball responses. However, oddball responses during inactivation were still significantly increased compared to responses to frequent (Figure 3.19B, Figure 3.18D (n = 9); Wilcoxon signed-rank FDR corrected: ChR group – Freq v Oddball p = 0.006, Freq v Oddball w/ light p = 0.009, Oddball v Oddball w/ light p =0.006). Notably, this effect is uniquely mediated though a reduction in the positive going component of the VEP (Figure 3.19B, Figure 3.18E (n = 9); Wilcoxon signed-rank FDR corrected: ChR group – Freq v Oddball p = 0.008, Freq v Oddball w/ light p = 0.07, Oddball v Oddball w/ light p = 0.009) as SOM+ inactivation had no effect on the negative-going component of the VEP (Figure 3.19B, Figure 3.18F (n = 9); Wilcoxon signed-rank FDR corrected: ChR group – Freq v Oddball p = 0.008, Freq v Oddball w/ light p = 0.008, Oddball v Oddball w/ light p = 0.8). In control animals, oddball responses

were normal in both light on and light off conditions (Figure 3.18D, E, F (n = 9), Table 3.7).

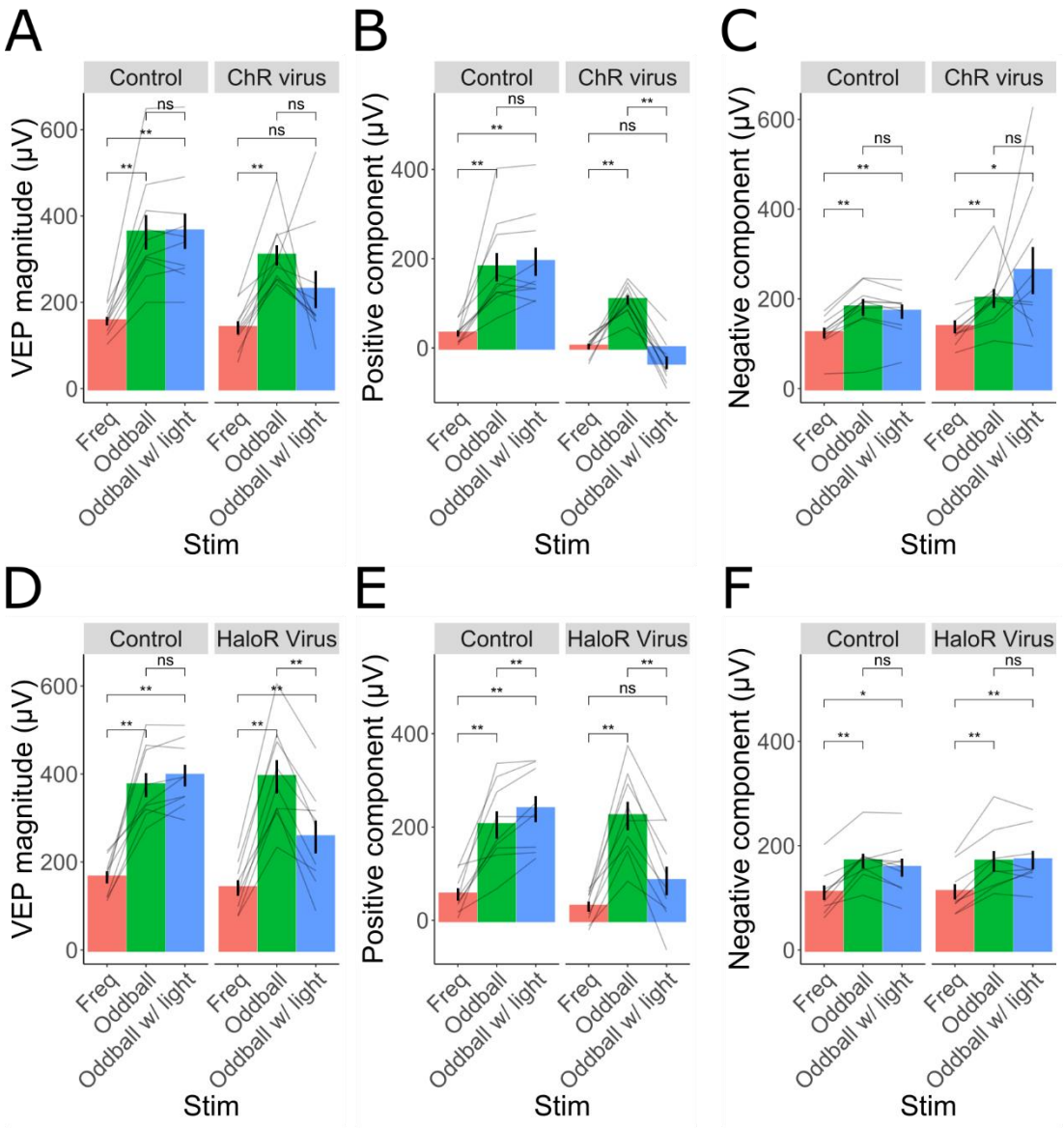

Figure 3.18 Oddball responses during SOM+ neuronal manipulation: (A) VEP magnitude in response to frequent, oddball, and oddball with LED stimulation for control and ChR animals (n = 10). (B) Positive component in response to frequent, oddball, and oddball with LED stimulation for control and ChR animals (n = 10). (C) Negative component in response to frequent, oddball, and oddball with LED stimulation for control and ChR animals (n = 10). (D) VEP magnitude in response to frequent, oddball, and oddball with LED stimulation for control and HaloR animals (n = 9). (E) Positive component in response to frequent, oddball, and oddball with LED stimulation for control and HaloR animals (n = 9). (F) Negative component in response to frequent, oddball, and oddball with LED stimulation for control and HaloR animals (n = 9).

Table 3.7 Statistics for comparisions in oddball experiments

	Group	**group1**	**group2**	**p value**
Mag	ChR control	freq	oddball	0.004

Mag	ChR control	freq	oddball w/ LED	0.004
Mag	ChR control	oddball	oddball w/ LED	0.8
Neg	ChR control	freq	oddball	0.004
Neg	ChR control	freq	oddball w/ LED	0.004
Neg	ChR control	oddball	oddball w/ LED	0.08
Pos	ChR control	freq	oddball	0.003
Pos	ChR control	freq	oddball w/ LED	0.003
Pos	ChR control	oddball	oddball w/ LED	0.2
Mag	HaloR Control	freq	oddball	0.006
Mag	HaloR Control	freq	oddball w/ LED	0.006
Mag	HaloR Control	oddball	oddball w/ LED	0.1
Neg	HaloR Control	freq	oddball	0.008
Neg	HaloR Control	freq	oddball w/ LED	0.01
Neg	HaloR Control	oddball	oddball w/ LED	0.09
Pos	HaloR Control	freq	oddball	0.008
Pos	HaloR Control	freq	oddball w/ LED	0.008
Pos	HaloR Control	oddball	oddball w/ LED	0.009

Even though opposing manipulation of SOM+ neurons generated a similar overall result of diminishing the oddball response, SOM+ activation and inhibition produce a noticeably distinct VEP waveforms (Figure 3.19A, B, C, D). Uncorrected statistical comparison shows a significant difference in the waveforms between groups after ~100 ms (Figure 3.19E; black dots are timepoints that are significantly different). After correction for multiple comparisons, the difference between the waveforms is significant at the positive component (150-200 ms) (Figure 3.19F; black dots are timepoints that are significantly different). Overall, the observation that oddball responses are impaired following activation and inactivation of SOM+ neurons suggests that normal activity of SOM+ neurons is critical for increased responses to oddball stimuli, as disruption in either direction (activation or inhibition) impairs responses.

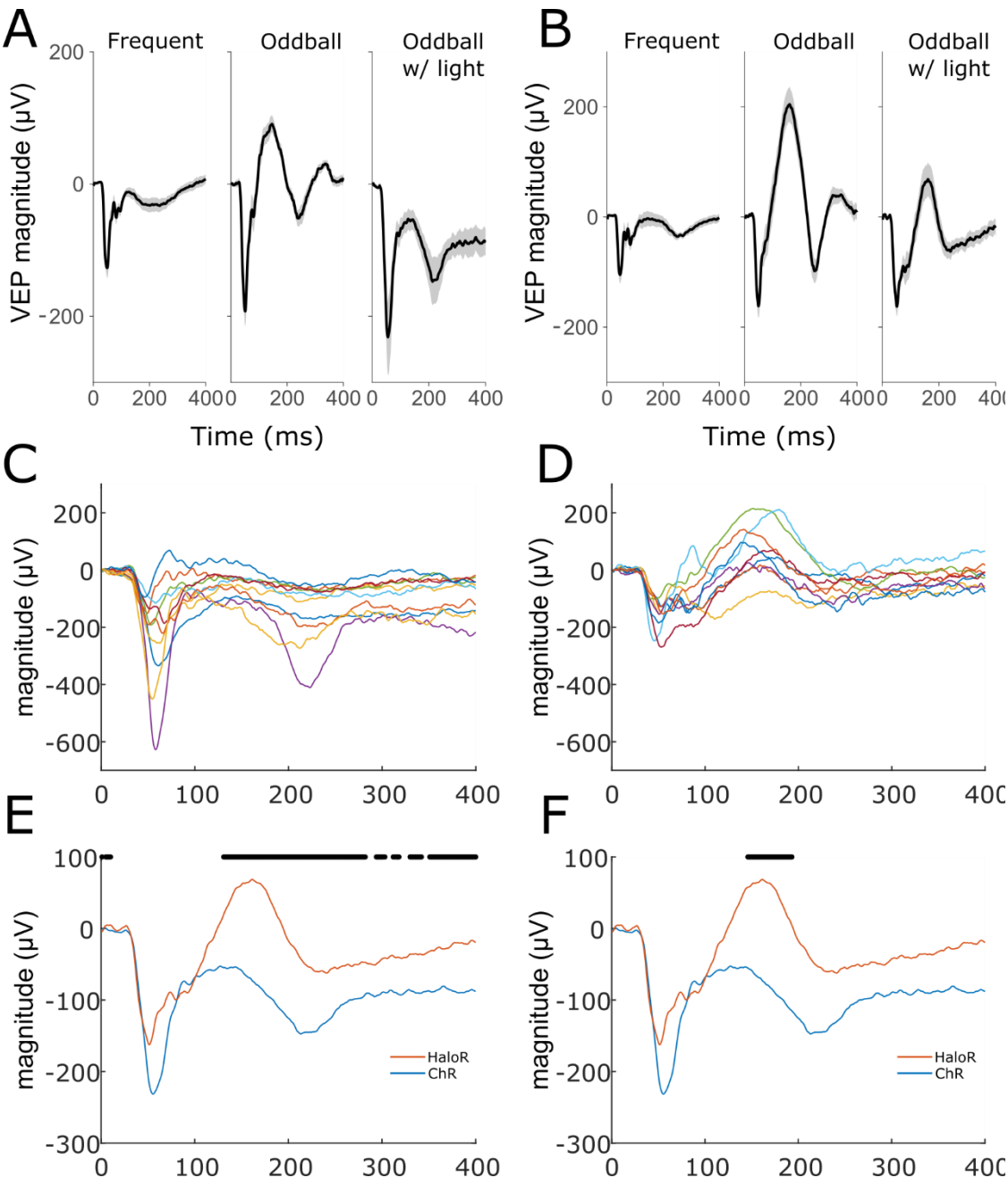

Figure 3.19 Comparison of waveforms for SOM+ activation with ChR and SOM+ inactivation with HaloR: Averaged waveform of all animals for frequent, oddball, and oddball stimuli with LED on for (A) SOM+ activation with ChR and (B) SOM+ inactivation with HaloR. (C) Individual wave forms for n = 9 animals for oddball stimuli with LED on for SOM+ activation with ChR. (D) Individual wave forms for n = 10 animals for oddball stimuli with LED on for SOM+ inactivation with HaloR. (E) Uncorrected statistical comparison. (F) Corrected statistical comparison.

3.4.7 Synaptic alterations after SRP

Current investigations into the circuits and cells which are altered over SRP have occurred via extracellular recordings of synaptic events, spiking activity (Cooke *et al.*, 2015; Durkin *et al.*, 2017), calcium imaging (Hayden *et al.*, 2021) and cell

specific manipulations (Kaplan *et al.*, 2016; Fong *et al.*, 2020; Chaloner & Cooke, 2022). These techniques are limited to only observing changes in population synaptic activity and cell firing. To investigate changes in direct synaptic inputs to cells, intracellular recording must be performed using *ex vivo* slice electrophysiology. Despite the large potentiation of the VEP magnitude in layer 4 *in vivo*, it is unknown if this effect manifests as observable changes at the individual synaptic level.

To test changes at the synaptic level, SRP was saturated in response to multiple orientations. Due to the 'salt-and-pepper' distribution of orientation selective cells in V1, patching of cells in layer 4 would randomly target cells with different orientation selectivity. Therefore, SRP must be saturated to all orientations to produce a distributed synaptic effect that one could realistically hope to observe *ex vivo*.

3.4.7.1 Inhibitory synaptic current (IPSC) peak-amplitude is reduced after SRP

Voltage-clamp recordings were performed on cells in layer 4 of primary visual cortex (Figure 3.20A). Spontaneous inhibitory synaptic currents (IPSCs) were recorded at 0 mV, which prevents flow through sodium and potassium channels and allows isolation of inhibitory currents. IPSC peak-amplitude is decreased after SRP saturation compared to animals presented only grey screen (Figure 3.20B; Wilcoxon signed-rank test: $p = 0.08$, $n = 9$). This falls short of significance likely due to only recording from 9 cells in 3 animals per group, and most studies use >15 cells from ~5 animals. Further data was not collected due to time constraints; however, this experiment is a pilot experiment for future directions. Quantiles of IPSC peak-amplitudes were calculated for each cell, and values were averaged over 9 cells in each group. Average quantile values were plotted

and show a leftward shift in the SRP group (Figure 3.20C; Kolmogorov-Smirnov test: p = 0.001). In addition, there is a leftward shift of the histogram of all IPSCs across all cells (Figure 3.20D). Overall, this suggests reduced amplitude of IPSCs after SRP.

While investigating waveforms during analysis, IPSCs clustered into shorter events (<30 ms) and longer events (>80 ms) (Figure 3.20E, G). Interestingly, only the shorter events showed a trend towards decreased peak-amplitude after SRP saturation, whereas the longer events were comparable across groups (Figure 3.20E, F, G, H). It is likely that the ion channels which contribute to these short and long events are different.

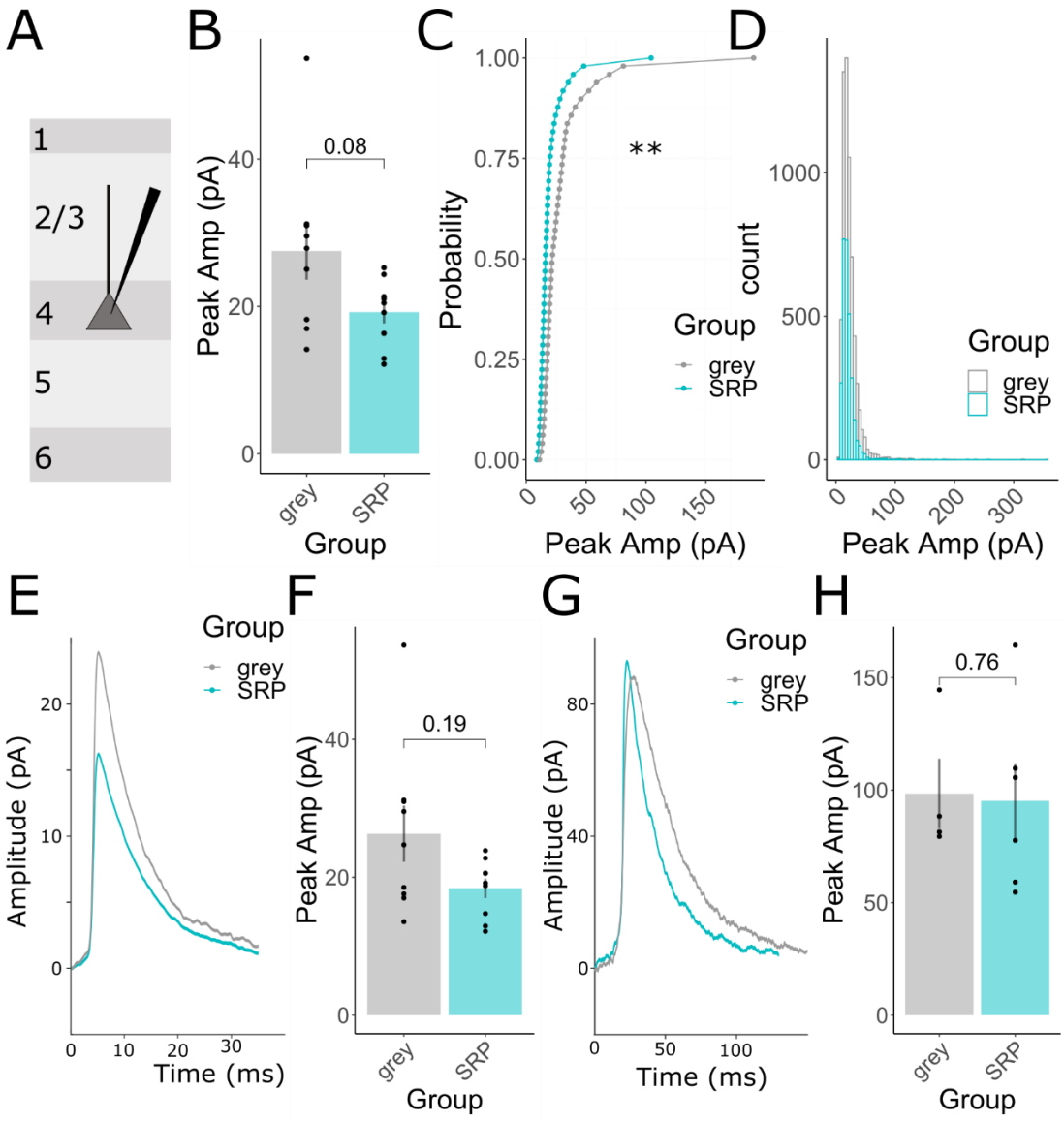

Figure 3.20 IPSCs recorded from layer 4 excitatory cells: (A) Schematic of recording protocol. (B) Peak amplitude averaged from individual cells in grey and SRP group (n = 9). (C) Average quantile curve for grey and SRP groups. (D) histogram of all IPSCs from grey and SRP groups. (E) Averaged traces of short IPSC events. (F) Peak amplitude of short IPSCs averaged from individual cells in grey and SRP group (n = 9). (G) Averaged traces of long IPSC events. (H) Peak amplitude of long IPSCs averaged from individual cells in grey and SRP groups (n = 9).

3.4.7.2 SOM+ directly inhibit PV+ neurons

The goal was to investigate SOM+ evoked IPSCs recorded in PV+ neurons to investigate if there are changes after SRP. However, due to issues with expression of Flp-dependent mCherry in PV+ neurons to allow fluorescence guided patching, only a few PV+ neurons were recorded while stimulating SOM+ neurons with ChR (Figure 3.21A). Proof-of-principle experiments showed that activation of SOM+ neurons with light in brain slices produced evoked IPSCs in layer 4 PV+ neurons (Figure 3.21B; example trace from 1 neuron). All PV+ cells (n = 3) recorded from layer 4 showed evoked IPSCs during SOM+ activation.

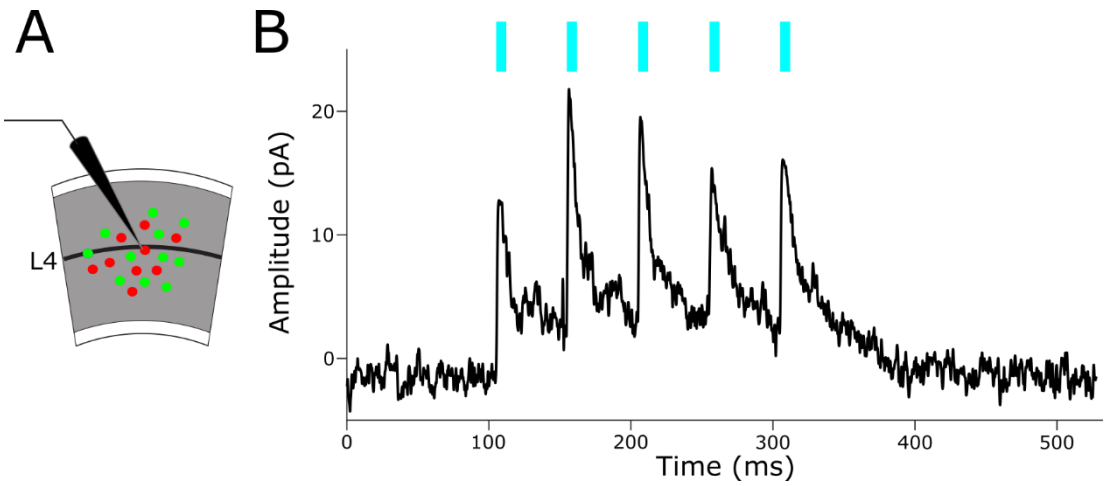

Figure 3.21 Evoked IPSCs recorded from PV+ neurons: (A) schematic of recording protocol. (B) Example trace of optogenetic activation of SOM+ cells and resultant IPSCs recorded from PV+ neurons in layer 4.

3.5 Discussion

In the current chapter I have described the involvement of both PV+ and SOM+ inhibitory neurons across long and short timescales of plasticity and adaptation. Previous findings show that PV+ inhibitory neurons are required for expression

of differential responses to familiar and novel stimuli (Kaplan *et al.*, 2016; Chaloner & Cooke, 2022). In addition, PV+ neurons are required during learning to produce altered responses to familiar stimuli. Furthermore, SOM+ neurons have a disinhibitory effect over the cortex and contribute to the potentiation of the VEP magnitude with increasing familiarity as shown by both activation and inhibition of SOM+ neurons. Notably, activation of SOM+ neurons prevents short-term adaptation, which is normally preserved for novel stimuli. Overall, these findings suggest that SOM+ neurons are, in substantial part, responsible for the dynamics of VEPs during familiarity over short and long timescales. This effect may be mediated through direct inhibition of PV+ neurons. Furthermore, SOM+ inhibitory neurons are required for normal responses to oddball stimuli. Importantly, at the level of individual synapses, inhibitory events on layer 4 excitatory cells decrease in amplitude after visual stimuli presentation.

3.5.1 Are PV+ neurons in layer 4 a gating system for plasticity?

In V1, there is intense feed-forward activation of PV+ neurons in layer 4 from the thalamus (Porter *et al.*, 2001; Cruikshank *et al.*, 2007, 2010). This limits the sensory processing window (Gabernet *et al.*, 2005) and tightly controls the onward transmission of information. The current finding that PV+ neuronal inactivation during learning prevents stimulus-selective response potentiation suggests that PV+ neurons may gate plasticity by controlling sensory information flow to the cortex. Currently, it is unknown if PV+ neurons gate plasticity during visual stimulus presentation or in the following hours, as hM4Di inhibition can last several hours. Therefore, an important follow up experiment will be to target the time window of PV+ neuron inactivation relative to learning. Inactivation could occur, for instance, immediately after visual stimulus presentation, to several

hours later during the animals sleep phase, as it is already known that SRP is reliant on sleep (Aton *et al.*, 2014; Durkin *et al.*, 2017).

Across SRP, PV+ neuronal activity is decreased (Hayden *et al.*, 2021). Furthermore, there is a redistribution of excitatory cell spiking following SRP. During presentation of familiar stimuli, peak firing is greater than that during novelty, but average firing is decreased (Cooke *et al.*, 2015; Hayden *et al.*, 2023). Nuanced differences in PV+ neuron activity in response to familiar and novel stimuli across the presentation window (500 ms) likely mediate the redistribution of firing. It will be important to investigate PV+ neuronal activity across the 500 ms window of stimuli presentation while familiar and novel stimuli are presented to elucidate if they control the redistribution of firing observed.

3.5.2 Contrasting disinhibitory and inhibitory roles of SOM+ neurons

In layer 4, SOM+ neurons directly inhibit PV+ neurons, thereby disinhibiting excitatory cells (Xu *et al.*, 2013; Li *et al.*, 2019). Therefore, opposing top-down inhibition of PV+ neurons by SOM+ neurons and bottom-up activation of PV+ neurons from the thalamus will have a different impact on the gating of plasticity. Evidence presented here supports the idea that in layer 4, SOM+ neurons mediate disinhibition, even if that motif is not consistent across cortical layers. SOM+ activation results in increased VEP magnitude and prevents short-term adaptation during novelty, suggesting that the VEP dynamics observed during familiarity are a direct result of SOM+ neuron recruitment (Kato *et al.*, 2015; Hayden *et al.*, 2021).

Short-term adaptation of VEP magnitude during novelty may be a result of direct SOM+ inhibitory drive onto excitatory cells causing adaptation of responses (Natan *et al.*, 2015). However, SOM+ neurons are weakly activated, and show stagnant dynamics across tens of seconds during novel stimuli

(Hayden *et al.*, 2021). Evidence suggests that SOM+ neurons do not mediate short-term adaptation of VEP magnitude through direct inhibition. Alternatively, short-term adaptation may result from depression of thalamic drive into V1 (Lee & Sherman, 2008), which may occur independently of stimulus type. If there is a matched reduction in PV+ neuronal activity (Hayden *et al.*, 2021) to the reduction in thalamic drive, this may manifest as the VEP magnitude, which is a population-level signal, failing to adapt. This reduction in PV+ neuronal drive may be mediated by an increase in SOM+ inhibition (Hayden *et al.*, 2021). Therefore, we hypothesise that SOM+ neurons are predominantly disinhibitory across shorter timescales, but this is yet to be tested. To provide further understanding of the mechanisms that mediate short-term adaptation of VEP magnitude, recording the output of the thalamus or imaging the terminals originating from thalamus is required. In addition, simultaneous recording of changes in spiking output of PV+ and SOM+ neurons across shorter timescales may identify how changes in inhibitory tone contribute to or mask the adaptation generated at the level of the thalamic input.

It is curious that activation of SOM+ neurons during the first block of stimuli causes VEP magnitude responses to remain close to baseline. By the second stimulus block during SOM+ activation, responses to both familiar and novel are increased. These responses become close to or equal to responses during baseline familiar responses. Control experiments suggest that this is a physiological response of SOM+ cells to repetitive activation, rather than non-specific effects of ChR activation. Inputs to SOM+ neurons are strongly facilitating (Reyes *et al.*, 1998; Beierlein *et al.*, 2003; Kapfer *et al.*, 2007; Silberberg & Markram, 2007) and burst stimulation of excitatory cells recruits SOM+ neurons (Kwan & Dan, 2012). Therefore, activation of SOM+ by optogenetics may cause

facilitation of SOM+ neuronal activity in response to repetitive stimulation. This effect may cause a progressive reduction in PV+ neuronal activity, which manifests as increased VEP magnitude across blocks observed here. An essential experiment to shed light on why this occurs is observation of the activity of SOM+ neurons across multiple blocks of visual stimulus presentation. This will provide information on the changes in these cells over several minutes. Furthermore, recording the activity of SOM+ neurons in response to optogenetic activation across blocks will clarify why progressive SOM+ activation causes potentiation of the VEP magnitude.

It is well established that in layer 4, SOM+ neurons predominantly target PV+ neurons (Xu *et al.*, 2013; Li *et al.*, 2019) whereas in layers 2/3 and 5, SOM+ neurons exert an inhibitory influence over excitatory cells (Kapfer *et al.*, 2007; Silberberg & Markram, 2007; Xu *et al.*, 2013). During oddball presentation there is a large reduction in the positive-going component of the VEP after SOM+ activation. The positive component of the VEP reflects synaptic activity in layer 2/3 (Cooke *et al.*, 2015; Hayden *et al.*, 2023). Therefore, activation of SOM+ neurons may cause direct inhibition of excitatory cells in supragranular layers resulting in a reduction of the positive component on the VEP. Moreover, we find that SOM+ inactivation also impairs oddball responses. In line with our findings, SOM+ neuron inactivation impairs deviance detection (Hamm & Yuste, 2016). Previously, it has been observed that opposing optogenetic manipulation of cells can produce asymmetrical effects (Phillips & Hasenstaub, 2016). Therefore, our finding that both activation and inhibition of SOM+ neurons has similar effects, rather than opposite effects, on oddball responses, at least in terms of magnitude, is not unusual. As both activation and inhibition of SOM+ neurons impair oddball

responses, it is likely that there is an ideal operating range in which SOM+ neurons work within to mediate responses to oddball stimuli.

3.5.3 Changes in inhibitory inputs

After SRP, spontaneous IPSC peak-amplitude is decreased. This suggests that not only do PV+ neurons decrease their activity over learning (Hayden *et al.*, 2021), but inhibitory synapses are altered after visual stimuli presentation. Reduced IPSC amplitude may be due to decreased release of GABA from terminals or fewer GABA receptors on the post-synaptic terminal (Mele *et al.*, 2016). Furthermore, inhibitory events cluster into long events (> 50 ms) and short events (<30 ms). Fast and slow $GABA_A$ mediated currents have been described previously in the hippocampus (Capogna & Pearce, 2011) and layer 4 of visual cortex (Sceniak & Maciver, 2008). It is likely the events observed here are $GABA_{Afast}$ and $GABA_{Aslow}$ events, as they have similar dynamics to those described previously in layer 4 visual cortex (Sceniak & Maciver, 2008). However, it cannot be excluded that these events are mediated by $GABA_B$ receptor signalling (Connors *et al.*, 1988). To elucidate the contribution of $GABA_A$ and $GABA_B$ receptors to these IPSCs, drug application experiments need to be performed in slice to specifically block $GABA_{Afast}$, $GABA_{Aslow}$, and $GABA_B$ mediated currents.

3.5.4 Caveats and Future directions

The use of Halorhodopsin to inactivate SOM+ neurons caused unwanted effects in the responses of the cortex even after cessation of light. This meant extended inter-block intervals had to be used, reducing the total block number. Therefore, short-term changes could not be examined. Additional experiments to inactivate SOM+ neurons with DREADDs would allow investigation of the effect of inhibiting SOM+ neurons on short-term adaptation.

We have evidence suggesting SOM+ neurons mediate disinhibition through PV+ neurons at multiple timescales. However, we have yet to prove this. Combined activation of SOM+ neurons and inhibition of PV+ neurons would fully assess whether SOM+ neurons mediate cortical familiarity via PV+ neuronal intermediaries. In the current experiment, both activation of SOM+ cells and inhibition of PV+ cells didn't reach the effect size observed previously. Validation of viral titre and volume in the combined experiment must be done to reach the observed effect size for each condition individually before the experiment can be completed. Furthermore, the subsequent experiment should make use of laminar probes, which records cell spiking and LFP across layers. This will allow observation of the changes in activity of putative PV+ neurons, putative SOM+ neurons, and excitatory cells. Importantly, laminar probes allow investigation of the changes in activity of these cells across all layers. This approach will provide direct evidence that the SOM+ disinhibitory motif is unique to layer 4 (Xu *et al.*, 2013; Li *et al.*, 2019). Furthermore, *ex-vivo* interrogation of reduced inhibition after SRP is required to localise the synapses which are altered. Dual patching recordings from both excitatory and PV+ cells while recording spontaneous and evoked IPSCs from SOM+ activation with ChR should be performed. If SOM+ inhibition of PV+ neurons increases due to SRP, then we expect to see a significant increase in the magnitude of evoked IPSCs onto PV+ neurons. In addition, recordings from excitatory cells will show if or how SOM+ inhibition onto excitatory neurons is altered.

A large caveat with the current experiments is the lack of behavioural changes in the SOM+ optogenetic experiments. Previous work has observed behavioural habituation concurrently with SRP (Cooke *et al.*, 2015) when recording a crude measure of front paw movement though a piezo-electric device.

The same set-up in the current experiments did not yield these differences, likely due to differences in acquisition of the signal and lower numbers of animals. Recent research used videos to observe changes orofacial movements and paw digit movement (Mathis *et al.*, 2018; Stringer *et al.*, 2019; Birman *et al.*, 2022; Syeda *et al.*, 2022). Video data was collected in parallel and must be analysed using pipelines like DeepLabCut (Mathis *et al.*, 2018) and FaceMap (Syeda *et al.*, 2022) to asses habituation of face and paw movement in the experiments acquired in this chapter.

Chapter 4 Developmental loss of ErbB4 from MGE-derived neurons impairs visual cortical plasticity

In this chapter I discuss the impairment of normal visual cortical dynamics over seconds, days and in an oddball task following prenatal knock-out of ErbB4 from PV+ inhibitory neurons.

4.1 Statement of work

Mice were generously provided by the Rico lab. All other work was performed by F.C.

4.2 Introduction

For the brain to encode certain aspects of the environment, the formation synaptic connections between inhibitory and excitatory cells must occur during development (Kirmse & Zhang, 2022). Developmental formation of these connections sets a framework for consequent experience-dependent plasticity to occur (Hooks & Chen, 2020).

Different subtypes of inhibitory neurons originate from different areas of the embryonic brain during development, PV+ and SOM+ cells originate in the medial ganglionic eminence (MGE) (Wonders & Anderson, 2006). After migration of these neurons from the from the MGE to the cortex, specific synaptic receptors are critical for development of normal synaptic connections within the cortical circuit. One such receptor is Erb-B2 Receptor Tyrosine Kinase 4 (ErbB4), which is predominantly expressed in hippocampal and cortical inhibitory neurons. Expression of ErbB4 is biased towards PV+ neurons and is only expressed in a small number of SOM+ neurons (Fazzari *et al.*, 2010). Furthermore, ErbB4 is found at both GABAergic cell synaptic terminals and on the post-synaptic density of excitatory to inhibitory cell synapses (Yau *et al.*, 2003; Fazzari *et al.*, 2010)

(Figure 4.1). Prenatal deletion of ErbB4 from inhibitory neurons reduces excitatory inputs onto PV+ neurons. In addition to this, inputs from PV+ neurons onto excitatory cells are reduced (Del Pino *et al.*, 2013) (Figure 4.1).

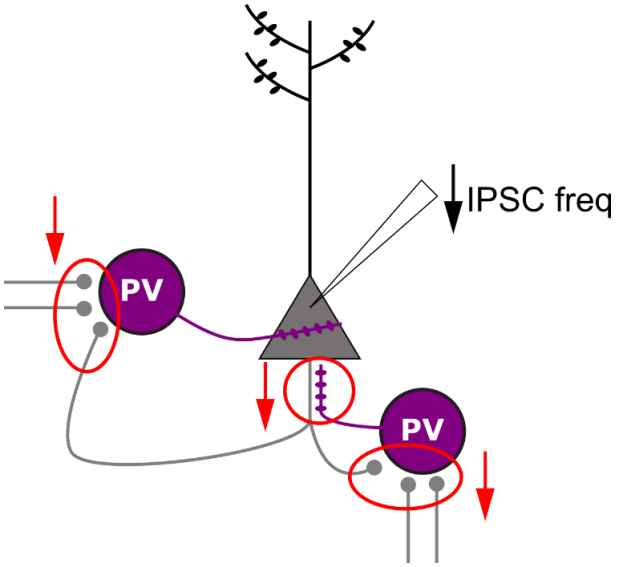

Figure 4.1 Schematic of deficits following ErbB4 knock-out in MGE-derived neurons (Fazzari *et al.*, 2010; Del Pino *et al.*, 2013)

Interestingly, Erbb4 and its signalling partner Neuregulin1 (Nrg1) are susceptibility genes in schizophrenia (Rico & Marín, 2011). Both ErbB4 and Nrg1 meet genome wide association study (GWAS) criteria for this condition (Agim *et al.*, 2013), suggesting a contribution of mutations in this gene to some instances of schizophrenia. In addition, animal models with deficits in ErbB4-Nrg1 signalling may replicate some of the phenotypes of schizophrenia (Karl *et al.*, 2007; Del Pino *et al.*, 2013). Therefore, investigation into the consequence of disrupted ErbB4-Nrg1 signalling may elucidate some of the circuit deficits which contribute to schizophrenia.

There is converging evidence that PV+ neurons are involved in experience-dependent plasticity to passive presentation of visual stimuli. Expression of stimulus-selective response potentiation (SRP) of VEP magnitude (Cooke & Bear, 2010) is reliant on PV+ neurons (Kaplan *et al.*, 2016; Chaloner & Cooke, 2022). In addition, PV+ neuronal activity decreases concomitantly with SRP (Hayden *et al.*, 2021). Therefore, modification of the activity of PV+ neurons likely occurs through synaptic plasticity or modified input onto PV+ neurons.

Thus, prenatal disruption of excitatory and PV+ connectivity through ErbB4 deletion may alter the activity of PV+ neurons and impact SRP.

In this chapter, I will show that prenatal Erbb4 knock-out in PV+ inhibitory neurons impairs long-term experience-dependent plasticity and short-term adaptation. In addition, oddball responses are impaired following prenatal ErbB4 deletion. Thus, normal development of synaptic connectivity of PV+ inhibitory neurons is essential for plasticity processes across multiple timescales.

4.3 Methods

4.3.1 Animals

All procedures were performed in accordance with the UK Animals (scientific procedures) Act (1986). All animals were maintained in a C57Bl/6J background (Charles River Laboratories). Mouse line was Lhx6-Cre;Erbb4$^{F/F}$. Animals received food and water *ad libitum*.

Mice underwent surgery at 13-15 weeks of age (~P91-105). Mice were anaesthetized with isoflurane and 5 mg/kg carprofen was delivered via a sub-cutaneous injection for analgesia. Iodine and saline were used to clean the scalp. The skull was cleaned, dried, and scored using a cross hatch pattern with a scalpel blade. A steel headpost was fixed over the frontal suture and skin adhered to skull surface using super glue (ethyl cyanoacrylate). Burr holes were drilled 3.1 mm lateral to lambda (to target binocular V1). Tungsten recording electrodes were implanted 470 µm below surface in both hemispheres. Silver wire reference electrodes were placed bilaterally in prefrontal cortex. All implants and the headpost were fixed in place with Superbond dental cement to form a fully enclosed headcap. Mice were allowed 5 days post-surgery prior to head fixation.

4.3.2 Visual Stimulus presentation

Visual stimuli were generated using software dff Gavornik (https://github.com/jeffgavornik/VEPStimulusSuite). The display was 20 cm in front of the mouse, and mean luminance was 27 cd/m2. Sinusoidal phase reversing gratings were presented full field, reversing at 2 Hz. In most experiments, blocks consisted of 200 phase reversals, each block was presented 5 times interleaved with 30 seconds of grey screen. Gamma-correction was performed to maintain constant luminance between gratings and grey screen. The 5 blocks were repeated until day 6. On the final day, day 7, the familiar orientation (X°) was pseudo-randomly interleaved (such that no more than 2 blocks of the same orientation were shown in sequence) with a novel orientation (X+90°).

PsychoPy was used to generate an oddball paradigm which consisted of 12 blocks of 128 gratings, of which 88% were standard (Y°) and 12% an oddball (Y° + 90°). Stimuli were presented for 500ms and followed by 1000 ms of grey before the next stimulus and each block was separated by 20 s of grey screen.

4.3.3 Data acquisition

As performed in 3.3.5

4.3.4 Analysis and statistics

As performed in 3.3.6

4.4 Results

Multiple lines of evidence point to the importance of SOM+ and PV+ inhibitory neurons in mediating plasticity that takes place over days and seconds in response to sensory experience. These two types of inhibitory neurons derive from the MGE during development. Excitatory synaptic connections onto PV+ inhibitory neurons, as well as PV+ synaptic inputs to excitatory cells are reliant

on ErbB4 during development (Del Pino *et al.*, 2013; Batista-Brito *et al.*, 2023). ErbB4 is a receptor tyrosine kinase expressed in PV+ neurons and a few SOM+ neurons (Fazzari *et al.*, 2010). To produce prenatal deletion of ErbB4, an animal line was developed to make use of the fact that Lhx6 is a transcription factor expressed in neurons that originate in the MGE. Therefore, ErbB4 deletion from MGE derived neurons in neocortex was achieved by crossing an Lhx6-Cre mouse line and a mouse line with loxP-flanked ErbB4 allele (Figure 4.2A). This approach of using Lhx6-Cre to limit ErbB4 knockdown enables a relatively selective prenatal knock-out of ErbB4 from PV+ neurons (Del Pino *et al.*, 2013; Batista-Brito *et al.*, 2023).

4.4.1 Developmental loss of ErbB4 from PV+ neurons alters long and short timescales of plasticity

Erbb4$^{F/F}$ mice produced from the Lhx6-Cre x Erbb4$^{F/F}$ cross were either Cre-positive (Cre), in which case ErbB4 was knocked-out, or Cre-negative (WT) littermate controls in which ErbB4 continued to be expressed as normal. These two groups of littermates underwent repeated visual stimulus presentation in a standard SRP protocol, followed by presentation of familiar and novel stimuli on day 7. Potentiation of VEP magnitude over days also resulted in familiar/novel differences in WT animals (Figure 4.2B; Wilcoxon signed-rank test FDR corrected: WT group – $p = <0.001$). In ErbB4 knockout animals, there was no potentiation of VEP magnitude over days resulting in no differential responses to familiar and novel stimuli (Figure 4.2B; Wilcoxon signed-rank test FDR corrected: Cre group – $p = 0.07$).

As I have shown, short-term adaptation occurs from the 1st to 2nd and 1st to 200th phase reversal in response to novelty but not familiarity (Chaloner & Cooke, 2022). This short-term adaptation of the VEP magnitude was present for

novelty and lost for familiarity in WT littermate controls, as we have shown previously, resulting in an increased adaption ratio for novelty. (Figure 4.2C; Wilcoxon singed-rank FDR corrected: WT group – Day 7 Fam 1 v 2: p = 0.7, Day 7 Nov 1 v 2: p = 0.03. Figure 4.2D; Wilcoxon singed-rank FDR corrected: WT group – AR 1 v 2 p = 0.2. Figure 4.2E; Wilcoxon singed-rank FDR corrected: WT group – Day 7 Fam 1 v 200: p = 0.3, Day 7 Nov 1 v 200: p = 0.2. Figure 4.2F; Wilcoxon singed-rank FDR corrected: WT group – AR 1 v 200 p = 0.4). After deletion of Erbb4, however, there was no short-term adaptation in response to either familiar or novel stimuli (Figure 4.2C; Wilcoxon singed-rank FDR corrected: Cre group – Day 7 Fam 1 v 2: p = 0.3, Day 7 Nov 1 v 2: p = 0.1. Figure 4.2E; Wilcoxon singed-rank FDR corrected: Cre group – Day 7 Fam 1 v 200: p = 0.7, Day 7 Nov 1 v 200: p = 0.7. As a result, the adaptation ratios for both stimuli were equivalent and near to one (Figure 4.2D; Wilcoxon singed-rank FDR corrected: Cre group – AR 1 v 2 p = 0.3. Figure 4.2F; Wilcoxon singed-rank FDR corrected: Cre group – AR 1 v 200 p = 1). Therefore, prenatal expression of ErbB4 in MGE-derived inhibitory neurons is essential for potentiation of the VEP magnitude with long-term familiarity (SRP), as well as short-term adaptation over seconds.

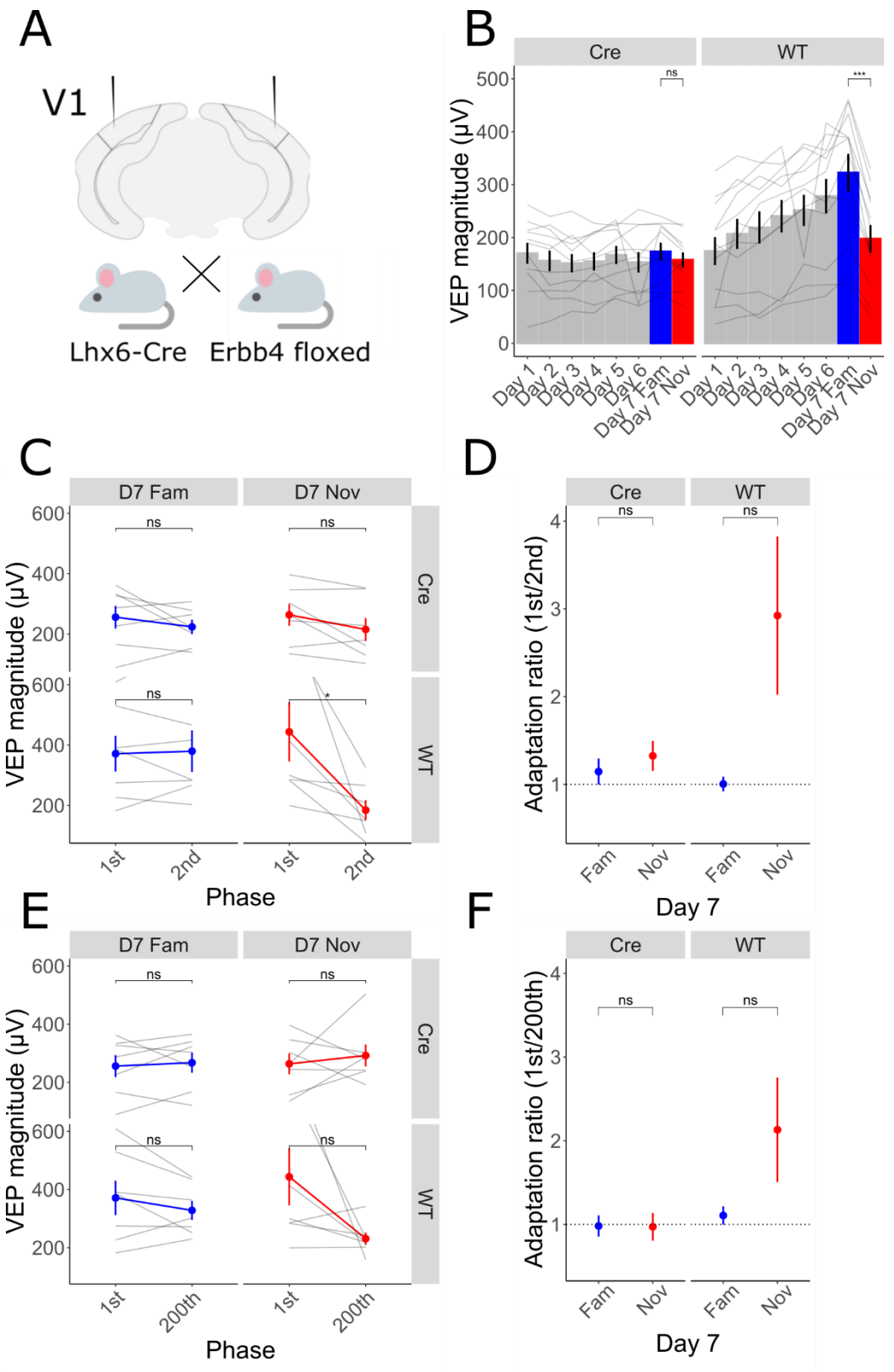

Figure 4.2 Prenatal ErbB4 knock-out alters short- and long-term plasticity: (A) Schematic of animal lines used. (B) VEP magnitude in response to visual stimuli presentation over days and in response to familiar/novel stimuli (Cre: n = 11, WT n = 12). (C) VEP magnitude in response to 1st and 2nd phase reversals during familiar/novel stimuli presentation in knock-out (Cre) and control (WT) groups (Cre: n = 11, WT n = 12). (D) Adaptation ratio (1st/2nd) in response to familiar / novel stimuli in knock-out (Cre) and control (WT) groups (Cre: n = 11, WT n = 12). (E) VEP magnitude in response to 1st and 200th phase reversals during familiar/novel stimuli

presentation in knock-out (Cre) and control (WT) groups (Cre: n = 11, WT n = 12). (F) Adaptation ratio ($1^{st}/200^{th}$) in response to familiar / novel stimuli in knock-out (Cre) and control (WT) groups (Cre: n = 11, WT n = 12).

4.4.2 Developmental loss of ErbB4 from PV+ neurons alters deviance detection

In the oddball paradigm, deviance detection is reflected as increased responses to oddball stimuli and reduced responses to frequent stimuli (Figure 3.17). The VEP magnitude in response to oddball stimuli in WT animals was increased compared to frequent stimuli (Figure 4.3A, Table 4.1). This effect was a result of an increase in both the positive and negative components of the VEP (Figure 4.3B, C, Table 4.1). However, these experiments were performed on a very small number of animals (n = 4) and therefore changes did not reach significance. After prenatal deletion of ErbB4, there was a dramatic loss of altered magnitude produced by oddball stimuli (Figure 4.3A, Table 4.1). The loss of oddball mismatch effect is present in both the negative and positive components of the VEP (Figure 4.3B, C, Table 4.1). Therefore, prenatal expression of ErbB4 in PV+ neurons is likely necessary for expression of deviance detection. However, this must be investigated in a larger number of animals (n = 10) as the current analysis is under powered.

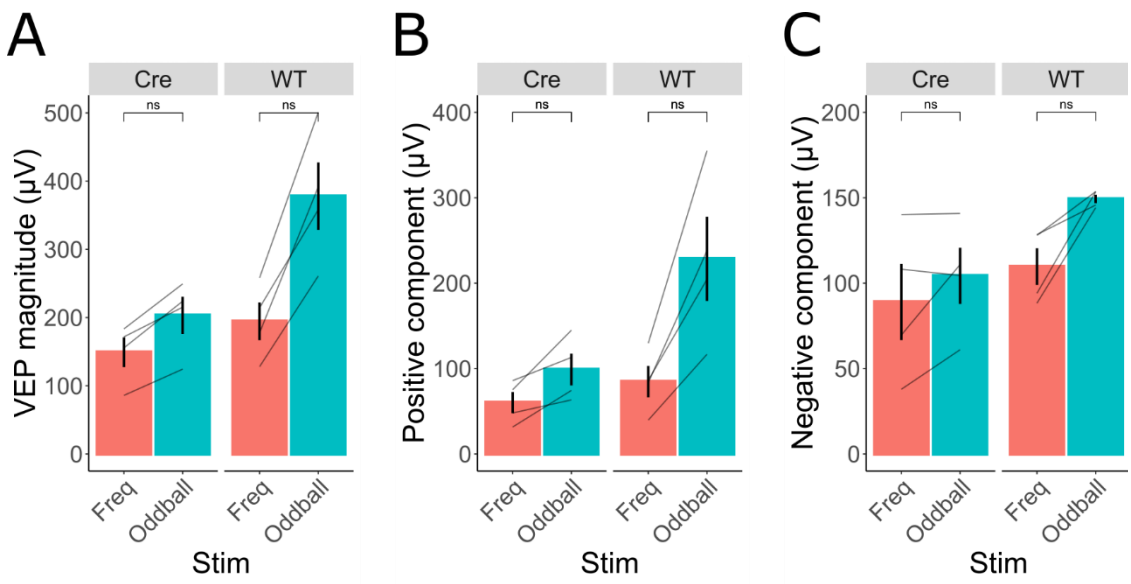

Figure 4.3 Prenatal ErbB4 knock-out alters oddball responses: (A) VEP magnitude in response to frequent, oddball in Lhx6-Cre x ErbB4 and WT animals (n = 4). (B) Positive component magnitude in response to frequent, oddball in Lhx6-Cre x ErbB4 and WT animals (n = 4). (C) Negative component magnitude in response to frequent, oddball in Lhx6-Cre x ErbB4 and WT animals (n = 4).

Table 4.1 Statistics for oddball experiment

Component	Group	group1	group2	p value
Mag	WT	freq	oddball	0.125
Mag	Cre	freq	oddball	0.125
Neg	WT	freq	oddball	0.25
Neg	Cre	freq	oddball	0.375
Pos	WT	freq	oddball	0.125
Pos	Cre	freq	oddball	0.125

4.5 Discussion

In the current chapter, I have described the effect of knock-out of ErbB4 in MGE-derived inhibitory neurons on short- and long-term plasticity. Following relatively selective developmental loss of ErbB4 in MGE-derived neurons, there was no SRP over days resulting in no differential responses to familiar and novel stimuli. Furthermore, there was loss of short-term adaptation across tens of seconds. In addition, oddball responses were impaired following ErbB4 knock-out. Therefore, developmental integration of MGE-derived inhibitory neurons into cortical circuits,

which is disrupted in Lhx6-Erbb4 knockout animals, is essential for expression of long-term plasticity, short-term adaptation, and deviance detection. Given that most ErbB4 expressing inhibitory neurons form the MGE are PV+, this implicates a key role for synaptic connections onto or from PV+ neurons in these forms of plasticity.

4.5.1 Role of normal synaptic connections during development

Knock-out of Erbb4 during development of MGE cells reduces PV+ inhibitory synaptic input onto excitatory cells and reduces excitatory input onto PV+ neurons of cells in the hippocampus (Del Pino *et al.*, 2013; Favuzzi *et al.*, 2017). In addition to changes observed in the hippocampus, knock-out of Erbb4 in developing MGE neurons alters cortical firing of excitatory cells and reduces responses to visual input (Batista-Brito *et al.*, 2023). The dramatic loss of long-term and short-term plasticity observed here may be a result of altered neuronal morphology (Batista-Brito *et al.*, 2023), changes of inhibitory inputs to excitatory cells, or changes in excitatory inputs onto PV+ neurons (Del Pino *et al.*, 2013). Interestingly, loss of SRP and short-term adaptation is not due to impairment in stimulus detection or discrimination of familiar and novel orientations, as orientation selectivity is maintained in prenatal ErbB4 knock-out (Batista-Brito *et al.*, 2023).

To dissect out which inputs are changing following Erbb4 knock-out, it will be important to observe changes at the single cell level. Therefore, *ex vivo* investigation of excitatory and inhibitory inputs (EPSCs/IPSCs) following SRP in ErbB4 mutants, as I have established, would provide insight into the synaptic alterations which leads to disrupted *in vivo* plasticity. Importantly, IPSC recordings from layer 4 excitatory cells (3.4.7.1) would elucidate if inhibitory inputs are disrupted, as they are in the hippocampus (Del Pino *et al.*, 2013). In

addition, EPSC recordings (5.4.1) from PV+ neurons in visual cortex, would elucidate if excitatory inputs are disrupted, again, as they are in the hippocampus (Del Pino *et al.*, 2013). Importantly, not only will EPSC/IPSC recording establish the baseline disruption in cortical connectivity, but it would also test the hypothesis that the reduction in IPSC amplitude following SRP (3.4.7.1) is required for expression of VEP magnitude potentiation. As the ErbB4 mutants lack VEP potentiation, we predict that they lack the shift in IPSC amplitude after SRP.

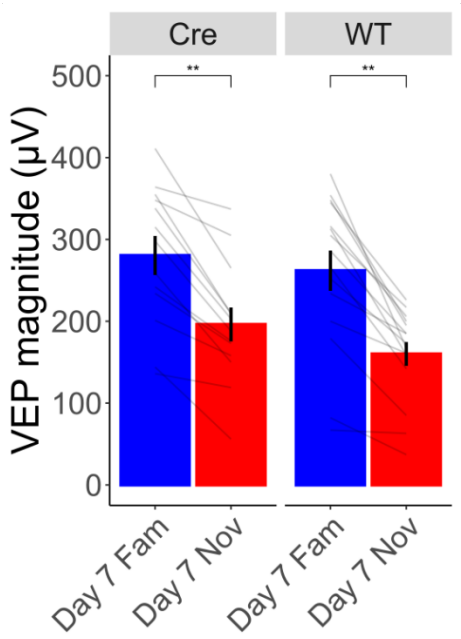

Figure 4.4 Familiar/ novel responses in PV-Cre x ErbB4 and wild-type animals

Conditional knock-out of ErbB4 under the control of PV-Cre generates a late postnatal deletion, as PV is expressed from second post-natal week (P8) (de Lecea *et al.*, 1995). Whereas knock-out of ErbB4 under the control of Lhx6 generates an early prenatal deletion as Lhx6 is expressed from embryonic day 11 (E11.5) (Grigoriou *et al.*, 1998). Late postnatal deletion of ErbB4 has no effect on firing rate and oscillatory state in the cortex (Batista-Brito *et al.*, 2023). Furthermore, there is normal expression of SRP and differential responses to familiar/novel stimuli in late postnatal deletion of ErbB4 (Figure 4.4, Cooke et al. *unpublished*). Therefore, the loss of SRP and deviance detection described in the current chapter is a consequence of disrupted development of cortical circuits, not an acute effect of loss of ErbB4 in adults.

4.5.2 Signals that may be translated across mice and humans

The oddball responses of VEPs recorded from layer 4 in mouse visual cortex have larger positive and negative components compared to VEP responses to frequent stimuli. However, in human EEG, the positive component observed in the mouse layer 4 VEP (~150 ms) exhibits an inverted polarity when recorded from the scalp, resulting in a negative-going component. This negative component in the EEG event related potential (ERP) is larger in response to oddball stimuli. Hence, the oddball phenomenon is often described as mismatch negativity (MMN) in humans (Nagai *et al.*, 2013). Therefore, MMN is a potentially translatable phenomenon which can be observed in humans and rodents (Harms *et al.*, 2016; Tada *et al.*, 2019). Thus, dissection of the mechanisms of the oddball responses and MMN impairments in animal models of circuit disruptions in disease could be done invasively in rodents to provide critical back-translational insight.

Importantly, MMN impairment is associated with disease severity in schizophrenia patients (Light & Braff, 2005). The finding that MMN is disrupted in schizophrenia is robust and may be a reliable biomarker (Nagai *et al.*, 2013). As ErbB4 is a genetic risk factor for schizophrenia (Rico & Marín, 2011; Agim *et al.*, 2013), the mouse knockout model may serve to model MMN deficits in the disorder. We should be cautious in interpreting prenatal deletion of ErbB4 as providing a strong animal model of schizophrenia, given the low penetrance of any known single genetic factor to the condition. However, prenatal deletion of ErbB4 does provide an animal model of a circuit deficit, caused by a loss of a gene implicated in schizophrenia, which replicates some of the biomarkers and behavioural deficits observed in schizophrenia (Karl *et al.*, 2007; Del Pino *et al.*, 2013). Evidence provided in this chapter suggests that prenatal ErbB4 deletion

produces an MMN (oddball) impairment, mimicking the effects observed in schizophrenia (Nagai *et al.*, 2013). However, full validation of this deficit and precisely what causes it in the animal model of prenatal ErbB4 deletion is required. Overall, studying circuit abnormalities that mimic some elements of disease can help us better understand the neurobiological deficits that underpin impaired processing in disease.

Chapter 5 The locus of synaptic modification following experience is not layer 4 and may be in layer 6

5.1 Statement of work

The NMDA receptor knock-out data was collected by Dr. Samuel Cooke while working in the Bear lab (Professor Mark Bear, MIT, http://bearlab.mit.edu/mark-bear). Additional analysis on within-session and short-term adaptation was performed by FC. All other electrophysiological data was collected and analysed by FC. Images of brains were provided by Lucy Menage.

5.2 Introduction

The brain is a modifiable system that possesses the ability to alter connectivity between cells in response to the statistics of the environment, a process termed experience-dependent plasticity. A key mechanism that underlies experience-dependent plasticity is direct strengthening and weaking of existing synaptic connections through Hebbian mechanisms (Cooke & Bear, 2014). Hebbian strengthening and weakening of synapses has been modelled as long-term potentiation (LTP) and long-term depression (LTD), which are laboratory phenomena that nevertheless likely capture the fundamental mechanisms by which experience shapes the brain (Bliss & Lomo, 1973; Lee *et al.*, 1998). Importantly, these Hebbian forms of plasticity, LTP and LTD, both require the NMDA receptor (NMDAR), and this voltage-dependent glutamate receptor is commonly regarded as the canonical Hebbian induction mechanism.

Stimulus-selective response potentiation (SRP) is a well-established form of experience-dependent plasticity. Across multiple days of stimulus presentation there is potentiation of VEP magnitude recorded from thalamo-recipient layer 4. This is a paradoxical effect because it accompanies a reduction

in behavioural response through long-term habituation. This lasting potentiation of VEPs is reliant on the same mechanisms as Hebbian LTP (Cooke & Bear, 2010), notably requiring function and expression of NMDA receptors in visual cortex (Cooke *et al.*, 2015). However, it is unknown which individual populations of synapses in the visual cortex are altered via Hebbian plasticity to produce SRP. Surprisingly, Hebbian plasticity at layer 4 synapses onto glutamatergic excitatory neurons does not contribute to the increased VEP magnitude observed across SRP, as NMDAR knockdown specifically in these neurons produces no deficit in either SRP or accompanying long-term orientation-selective habituation (Fong *et al.*, 2020). Therefore, alterations of other synaptic connections in the cortex must occur to produce SRP, which in turn have an influence over the response measured in layer 4.

A key node within the cortex which can modulate responses of other cell types and layers is layer 6. Layer 6 receives direct input from the thalamus in parallel to layer 4 (Ahmed *et al.*, 1994; Beierlein & Connors, 2002). This input also conveys relatively unprocessed sensory information. Importantly, layer 6 also provides the major feedback to the thalamus, in fact providing far more input to the dLGN than the retina itself (Sillito & Jones, 2002; Spacek *et al.*, 2022). As well as connectivity back to the thalamus, Corticothalamic (CT) cells in layer 6 project to layer 4 within V1. Therefore, layer 6 cells are in a prime location to modulate both thalamic and cortical activity, notably in the other major recipient layer of thalamic input. In the cortex, layer 6 produces inhibition in layer 4 through PV+ neural intermediaries (Olsen *et al.*, 2012; Bortone *et al.*, 2014; Kim *et al.*, 2014; Yetman *et al.*, 2019). It is therefore possible that Hebbian plasticity in layer 6 results in potentiation of the VEP magnitude during SRP by altering the activity of PV+ neurons. In support of this, knock out of NMDA receptors in layer 6

significantly impacts SRP and impairs differential responses to familiar and novel stimuli (Hayden *et al.*, 2023). Critically, engagement of layer 6 cells during NREM sleep is required for potentiation of the VEP magnitude after sleep, which may be due to disrupted corticothalamic coherence (Durkin *et al.*, 2017). This suggests that layer 6 intracortical and thalamic interactions are important in mediating SRP at different stages of this plasticity.

In addition to experience-dependent plasticity that manifests as changes in responses over days, activity of cells and synaptic potentials can alter over the course of seconds (Li *et al.*, 2003; Heintz *et al.*, 2022). In response to repetitive presentation of visual stimuli, there is adaptation of activity across all layers of the cortex (Hamm *et al.*, 2021). Within layer 4, the adaptation of responses may, in part, be due to direct changes in thalamic activity (King *et al.*, 2016). The activity of thalamic cells decreases both during and after the presentation of a visual input (Solomon *et al.*, 2004). Therefore, both the frequency of inputs into layer 4 and the magnitude of the excitatory inputs into layer 4 from the thalamus (Lee & Sherman, 2008) will reduce over several seconds. Synaptic currents recorded within layer 4 reduce in response to both frequent and oddball visual stimuli of different orientations (Gallimore *et al.*, 2023). These currents in layer 4 likely reflect direct thalamic synaptic input, suggesting that adaptation of thalamic inputs is not stimulus specific. One possible contributor to this adaptation of thalamic activity may be cortical feedback. Layer 6 CT cells target both the primary sensory thalamic nucleus and the thalamic reticular nucleus (TRN). The TRN is almost entirely GABAergic and strongly inhibits the primary sensory thalamus (Cruikshank *et al.*, 2010). Therefore, activation of layer 6 has an overall inhibitory influence on the activity of cells in the thalamus (Cruikshank *et al.*, 2010; Olsen *et al.*, 2012). In addition, excitatory inputs from layer 6 to their targets

facilitate over repetitive stimuli (Cruikshank *et al.*, 2010; Jurgens *et al.*, 2012). Therefore, sustained activity of layer 6 may increasingly inhibit the thalamus and cause a progressive reduction in activity.

In the current chapter, I will reveal that after SRP the amplitude of excitatory synaptic currents recorded from layer 4 excitatory cells does not change. Furthermore, I aim to investigate the role of layer 6 alteration of activity across different timescales. I show that knock-out of NMDARs in layer 6 is required for behavioural habituation over several minutes and maintains short-term adaptation of responses, but are not required for long-term habituation. I also discuss attempts to inactivate layer 6 cells with hM4Di and activate layer 6 cells with ChR2.

5.3 Materials and Methods

5.3.1 NMDAR knock-out in layer 6 cells

Data were collected by Dr. Samuel Cooke while working in the Bear Mark Bear, MIT, http://bearlab.mit.edu/mark-bear). Materials and methods outlined in Hayden (2023). Analysis was performed by me (3.3.5, 3.3.6) to investigate the effect of NMDAR knock-out on within-session and within-block adaptation and habituation.

5.3.2 Animals

For new experiments in the Cooke lab, all procedures were performed in accordance with the UK Animals (scientific procedures) Act (1986). All animals were maintained in a C57Bl/6J background (Charles River Laboratories), NTSR1-cre mice were used (B6.129-*Ntsr1*$^{tm1.1(cre)Giml}$/J). Animals received food and water *ad libitum*.

5.3.3 V1 electrode implantation

Mice underwent surgery at ~6 weeks of age. Mice were anaesthetized with isoflurane, 5mg/kg carprofen was delivered via a sub-cutaneous injection for analgesia. Iodine and saline were used to clean the scalp. The skull was cleaned, dried, and scored using a blade. A steel headpost was fixed over the frontal suture and skin adhered to skull surface using super glue (ethyl cyanoacrylate). Burr holes were drilled 3.1 mm lateral to lambda (to target binocular V1). Tungsten recording electrodes were implanted 470 µm bellow surface in both hemispheres. Silver wire reference electrodes were placed in prefrontal cortex bi-laterally.

5.3.4 Viral transfection

All injections were preceded and followed by 3 minutes wait time. Viral injections were performed in both hemispheres at ± 3.1 from lambda and were immediately followed by electrode implantation (outlined above). For all experiments, following surgery, mice were allowed at least 2 weeks before the start of the visual stimulus presentation, and at least 18 days prior to optogenetics stimulation or CNO injection.

5.3.4.1 inactivation of NTSR+ layer 6 cells with hM4Di

In experiments using DREADDs to inactivate layer 6 neurons using NTSR-Cre mice, 100 nl of cre-dependent hM4Di or mCherry virus was injected at ± 3.1 from lambda at 2 nl/s at depths 600 µm, 450 µm, 300 µm, and 150 µm bellow surface (Table 5.1).

5.3.4.2 Activation of NTSR+ layer 6 cells with ChR

In NTSR-Cre animals 100nl of AAV was injected at 2nl/s at depths 600 µm, 450 µm, 300 µm, and 150 µm bellow surface (Table 5.1).

Table 5.1 Table of virus' used

NTSR-Cre	pAAV-hSyn-DIO-hM4D(Gi)-mCherry (AAV8)	DREADDs inhibition
	pAAV-hSyn-DIO-mCherry (AAV8)	Empty vector control
	pAAV-EF1a-double floxed-hChR2(H134R)-EYFP-WPRE-HGHpA (AAV5)	Channel Rhodopsin for excitation (blue 465nm)
	pAAV-Ef1a-DIO EYFP (AAV5)	Empty vector control

5.3.5 Visual Stimuli presentation

The display was 20 cm in front of the mouse and mean luminance was 27 cd/m2. Sinusoidal phase reversing gratings are presented at a spatial frequency of 0.05 cycles/degree and were presented full field, reversing at 2 Hz. Gamma-correction was performed to maintain constant luminance between gratings and grey screen. A piezo-electrical device was placed under the animals against the tube to pick up paw and body movement. Visual stimuli were generated with software from Jeff Gavornik (https://github.com/jeffgavornik/VEPStimulusSuite).

All animals underwent 2 days of habituation prior to visual stimulus presentation. To induce SRP, the same oriented visual stimulus was presented over consecutive days. Within each day, blocks consisted of 200 phase reversals and each of these blocks was presented 5 times interleaved with 30 seconds of grey screen with the first block being preceded by 300s of grey screen (Figure 2.1B).

5.3.5.1 NTSR inactivation during learning

On day 1 through day 3, CNO was administered via I.P injections at 5 mg/kg, then 15 minutes later 5 blocks of stimuli were shown. Then on day 5, 10 blocks of a familiar (X°) and novel stimulus (X° + 90°) were presented in the absence of CNO.

5.3.5.2 NTSR inactivation during presentation of familiar and novel stimuli

On day 7, a familiar (X°) and a novel orientation (X° + 90°) were presented. The next day, CNO was administered via I.P injections at 5 mg/kg. Then, 15 minutes later, 5 blocks of familiar (X°) and a new novel (X° + 120°) were shown with 30 s of grey screen in between each block (20 blocks total).

5.3.5.3 NTSR activation with optogenetics

For experiments involving the genetics, PsychoPy (https://www.psychopy.org/) was used to produce sinusoidal phase reversing grating, because additional software was needed that included digital control of LED driver (PlexBright® Optogenetic Stimulation System) with a DAQ to control digital channel output (National Instruments (NI), USB-6001). On day 7, 5 blocks of the familiar and novel stimuli were shown with or without LED (equal number of blocks per treatment for each stimulus), interleaved with 30 s of grey screen between (20 blocks total). Blue light (465 nm) was presented at an intensity of 1.5 mW and light was initiated 0.5 s prior to onset of block and stopped 0.5 s after end of block. Due to large hang-over effects when interleaved, the protocol was adjusted to show 2 blocks of familiar and novel stimuli, presented with and without LED, interleaved with 210 s of grey screen each time (8 blocks total).

5.3.6 Data acquisition, Analysis, and statistics

Methods are outlined in 3.3.5 and 3.3.6.

5.3.7 *Ex vivo* data acquisition and analysis

Methods are outlined in 3.3.7.

5.4 Results

5.4.1 Excitatory synaptic currents (EPSCs) do not change following SRP

Experience-dependent plasticity (SRP) that occurs over days manifests as increased VEP magnitude recorded from layer 4. Evidence suggests that

Hebbian plasticity at layer 4 excitatory synapses is not responsible for potentiation of VEP magnitude (Fong *et al.*, 2020). To further probe the lack of synaptic alterations in layer 4, I recorded excitatory post synaptic potentials (EPSCs) in layer 4 cells after saturation of SRP. EPSC peak-amplitude is not different between animals that underwent SRP versus those shown a grey screen (Figure 5.1A; Wilcoxon signed-rank test: p = 0.9, n = 9). Quantiles of EPSC peak-amplitudes were calculated for each cell, and then averaged over 9 cells in each group. Average quantile values are plotted, revealing that the curves are not significantly different (Kolmogorov-Smirnov test: p = 1, Figure 5.1B). In addition, histograms of all EPSCs across all cells overlap (Figure 5.1C). This finding suggests that there is no change in excitatory inputs following SRP.

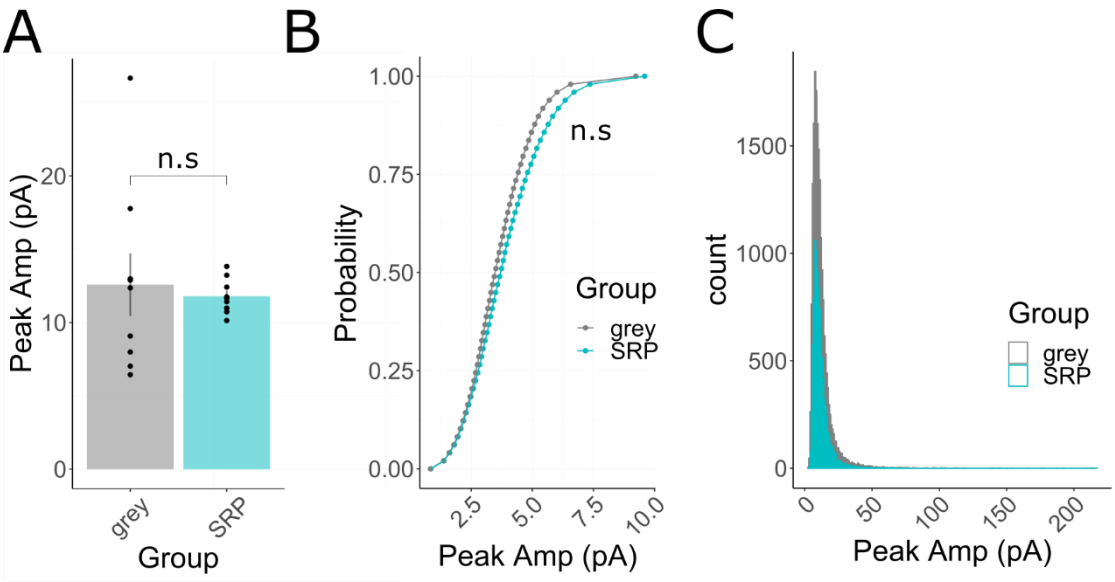

Figure 5.1 EPSCs recorded from layer 4 excitatory cells: (A) Peak amplitude averaged from individual cells in grey and SRP group. (B) Average quantile curve for grey and SRP groups. (C) Histogram of all EPSCs from grey and SRP groups.

5.4.2 Knock-out of NMDA receptors from layer 6 alters shorter timescales of adaptation and habituation

Layer 6 receives input from the thalamus and projects to layer 4 to target PV+ neurons. Therefore, layer 6 is in a prime position to mediate responses of layer 4 cells through PV+ neuronal intermediaries. It has been observed that knock-out

of NMDA receptors in layer 6 impairs potentiation of the VEP across days (SRP) and prevents differential VEP responses to familiar and novel stimuli, phenocopying loss of NMDAR from all cortical excitatory neurons (Hayden *et al.*, 2023). However, in Hayden et al. 2023, there is no investigation of the consequence of knock-out of NMDA receptors in layer 6 on within-session and within-block adaptation and habituation. Here, I sought to investigate any alterations over shorter timescales of adaptation and behavioural habituation following knock-out of NMDARs from layer 6 Ntsr1+ neurons.

5.4.2.1 Knock-out of NMDA receptors from layer 6 impairs behavioural habituation across blocks but not VEP adaptation

We have established that there is a reduction of VEP magnitude from block to block across 5 blocks of visual stimuli presentation, which becomes more substantial as the stimulus is presented each day over 6 days (Chaloner & Cooke, 2022). Knock-out of NMDA receptors from layer 6 had no effect on the adaptation of the VEP magnitude across blocks. This adaptation was equivalent in layer 6 knock-out and wild-type littermate controls (Figure 5.2A, Table 5.2). In addition, behavioural habituation occurred concurrently with VEP dynamics over 5 blocks. This effect manifested as a large reduction in behavioural response from block 1 to block 2, which then plateaued (Chaloner & Cooke, 2022). Wild-type animals showed pronounced habituation from block 1 to block 2 which then remained reduced (Figure 5.2B; Friedman test WT: $p = 0.001$). However, knock-out of NMDA receptors from layer 6 prevented behavioural habituation (Figure 5.2B; Friedman test KO: $p = 0.2$). Therefore, alteration in layer 6 activity impaired behaviourally manifest short-term habituation, but not the VEP correlate of response depression across blocks.

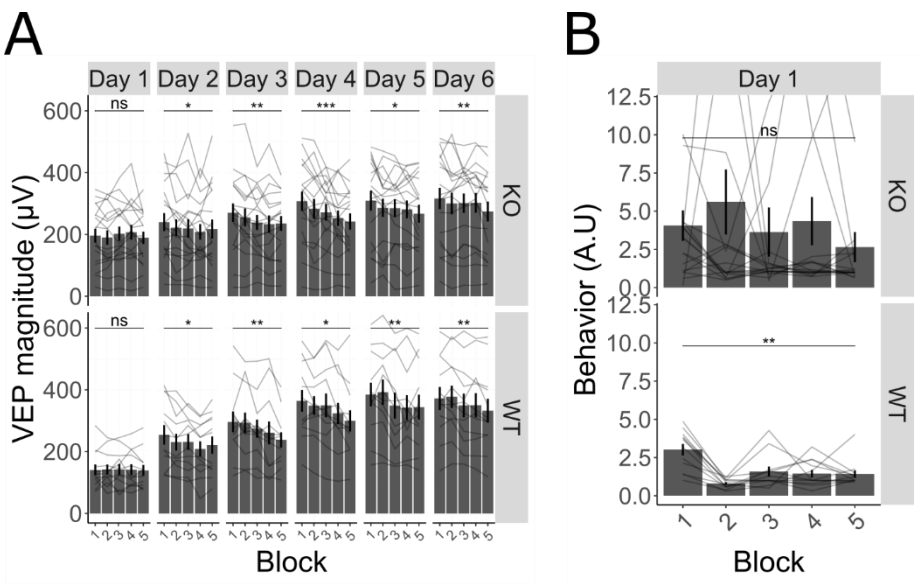

Figure 5.2 NMDA receptor knock-out in layer 6 across blocks: (A) VEP magnitude across 5 blocks in knock-out (KO) and wild-type across day 1 to day 6. (WT) animals. (B) Behavioural responses across 5 blocks in knock-out (KO) and wild-type on day 1.

Table 5.2 Statistics for VEP adaptation across blocks

Group	Day	p-value
WT	D1	0.93
WT	D2	0.03
WT	D3	0.002
WT	D4	0.02
WT	D5	0.002
WT	D6	0.006
KO	D1	0.50
KO	D2	0.05
KO	D3	0.006
KO	D4	0.0006
KO	D5	0.03
KO	D6	0.005

5.4.2.2 Knock-out of NMDAR receptors prevents the loss of adaptation over SRP

In wild-type animals, we have established that there is short-term adaptation of the VEP magnitude from the 1st to 2nd phase reversal only during novel stimuli presentation resulting in a significantly different adaptation ratio (AR) (Figure 5.3A, B; Wilcoxon signed-rank AR WT: p = 0.002, (Chaloner & Cooke, 2022)). In contrast to this observation, adaptation from the 1st to 2nd phase reversal was maintained across days after knock-out of NMDARs from layer 6 (Figure 5.3A,

B). However, there remained a significant difference between the adaptation ratio for familiar and novel stimuli despite the maintained short-term adaptation (Figure 5.3A, B; Wilcoxon signed rank AR KO: $p = 0.002$). In addition, short-term adaptation occurred from the 1st to 200th phase reversal and only manifested in response to novel stimuli in wild-type animals (Figure 5.3C). This effect resulted in a significantly greater AR in response to novel stimuli compared to familiar in wild-type animals (Figure 5.3D; Wilcoxon signed-rank AR WT: $p < 0.001$). Knock-out of NMDARs in layer 6 caused pronounced short-term adaptation from the 1st to 200th phase reversal across all days and stimulus types (Figure 5.3C). The adaptation ratio was large in response to both familiar and novel stimuli and was not significantly different (Figure 5.3D; Wilcoxon signed-rank AR KO: $p = 0.14$). Therefore, loss of NMDA receptors from layer 6 resulted in maintenance of pronounced short-term adaptation after SRP, even for the highly familiar stimulus.

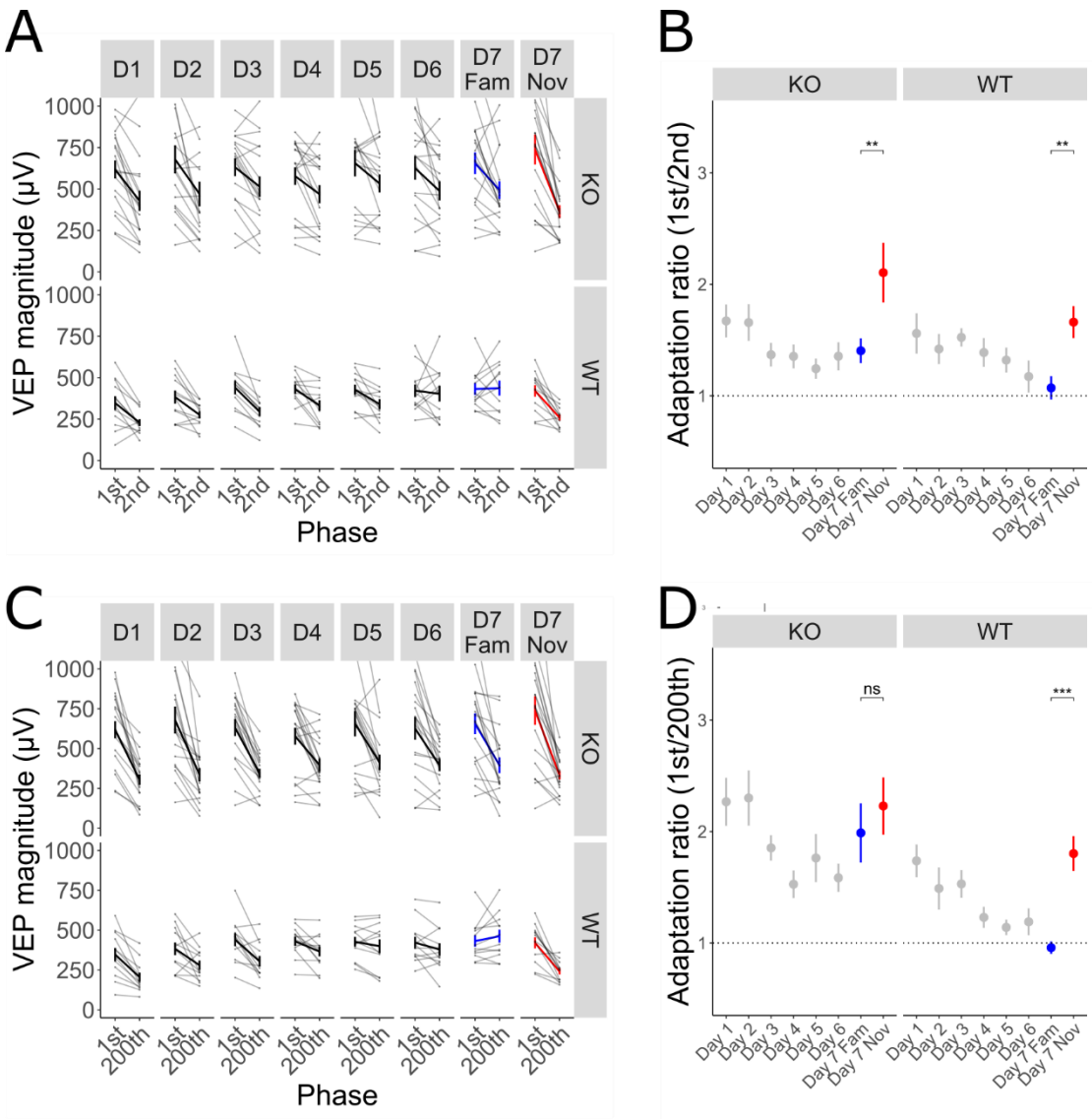

Figure 5.3 Short-term adaptation is altered after NMDA receptor knock-out in layer 6: (A) VEP adaptation from the 1st to 2nd phase reversal across all days for knock-out (KO) and wild-type (WT) animals. (B) Adaptation ratio (1st/2nd) across all days for knock-out (KO) and wild-type (WT) animals. (C) VEP adaptation from the 1st to 200th phase reversal across all days for knock-out (KO) and wild-type (WT) animals. (D) Adaptation ratio (1st/200th) across all days for knock-out (KO) and wild-type (WT) animals.

5.4.3 Inactivation of layer 6 during learning and memory

The use of a floxed-GluN1 mouse crossed with the NTSR1-Cre mouse resulted in a spatially, but not temporally conditional knock-out of NMDA receptors. Altering the activity of these cells during the developmental integration into the cortex may have knock-on effects on sensory processing that are independent of specifically altering layer 6 activity. Therefore, temporally constraining manipulation of these cells will provide further information on their role during

SRP and during familiarity/novelty distinction. Therefore, I sought to inactivate layer 6 cells at different stages of learning and memory. Cell-type specific expression of the Cre-dependent hM4Di virus was achieved in NTSR-Cre animals, a mouse line which labels corticothalamic layer 6 cells (Figure 5.4A).

5.4.3.1 Inactivation of layer 6 cells during presentation of familiar and novel stimuli

To investigate the role of layer 6 cells during presentation of familiar and novel stimuli, animals were shown 6 days of one oriented stimulus, followed by a 7th day where familiar and novel stimuli were shown, pseudorandomly interleaved for blocks as described previously. This protocol was followed by an 8th day of familiar/novel presentation while layer 6 cells were inactivated through application of CNO (Figure 5.4B).

SRP occurred across presentation of visual stimuli for both groups (Figure 5.4C; Friedman test control & DREADDs group: day 1 – day 6: $p = < 0.001$). In control animals the familiar/novel difference held true regardless of CNO application (Figure 5.4C; Wilcoxon signed-rank test FDR corrected: Control D7 Fam v D7 Nov $p = 0.003$, D8 Fam w/CNO v D8 Nov w/CNO $p = 0.003$). There was a very small but significant increase in VEP magnitude in response to the familiar stimulus (Figure 5.4C; Wilcoxon signed-rank test FDR corrected: Control D7 Fam v D8 Fam w/CNO $p = 0.046$). This likely reflects continuation of SRP from day 7 to day 8 as the same oriented familiar stimulus was used in each session. It is unlikely that it is due to off target effects of CNO, as application of CNO has no effect on VEP magnitude in response to different novel stimuli (Figure 5.4C; Wilcoxon signed-rank test FDR corrected: Control D7 Nov v D8 Nov w/CNO $p = 0.16$). In addition, the familiar/novel ratio was equivalent between conditions in control animals (Figure 5.4D; Control $p = 0.62$). Responses to

familiar and novel stimuli were significantly different in animals expressing DREADDs before and after layer 6 inactivation (Figure 5.4C; Wilcoxon signed-rank test FDR corrected: DREADDs D7 Fam v D7 Nov p = 0.003, D8 Fam w/CNO v D8 Nov w/CNO p = 0.003). However, inactivation of layer 6 with CNO caused a small but significant reduction in VEP magnitude responses to familiar stimuli and had no effect on responses to novel stimuli (Wilcoxon signed-rank test FDR corrected: DREADDs D7 Fam v D8 Fam w/CNO p = 0.03, D7 Nov v D8 Nov w/CNO p = 0.12). Furthermore, the familiar/novel ratio after layer 6 inactivation was reduced (Figure 5.4D; DREADDs p = 0.02). Overall, this suggests that inactivation of layer 6 cells somewhat impairs differential responses to familiar and novel stimuli.

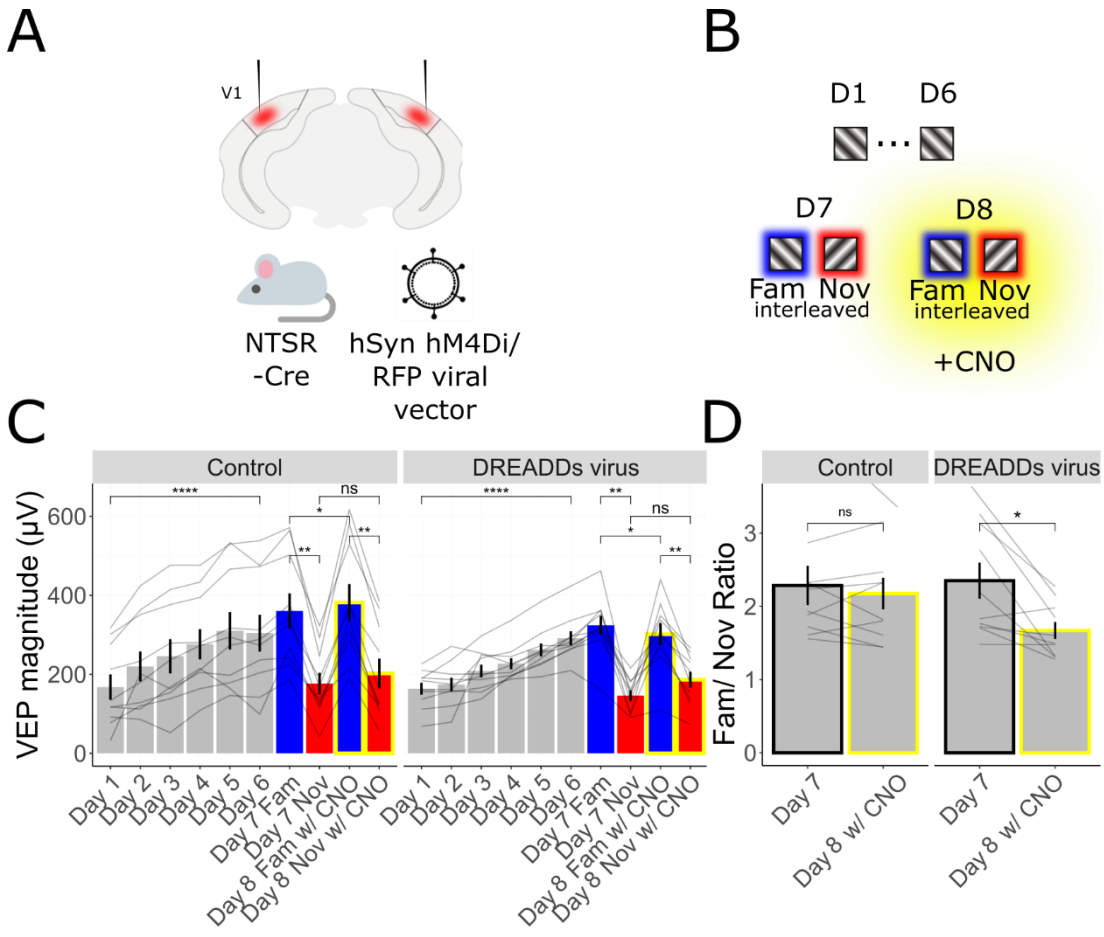

Figure 5.4 Layer 6 inactivation during familiar/novel stimuli: (A) Schematic to show experimental set-up. (B) Schematic to show visual stimuli presentation protocol. (C) VEP magnitude response during visual stimuli presentation across 6 days, and in

response to familiar/novel stimuli with and without CNO application for control and DREADDs groups. (D) Familiar/novel ratio for control and DREADDs groups with and without CNO application.

5.4.3.2 Viral expression in layer 6 cells produces altered short-term effects in control and DREADDs groups but produces normal within-session adaptation

Short-term adaption of the VEP magnitude occurs across 200 phase reversals of visual stimuli. Adaptation from the 1st to 2nd phase reversal and 1st to 200th phase reversal has been observed in wild-type animals across different mouse lines and different acquisition set ups (Chaloner & Cooke, 2022; T. Kim et al., 2020, 3.4.1.2, 3.4.2.3, 0). Assessment of short-term adaptation in control and DREADDs-expressing animals shows no short-term adaptation across day 1 through 6 in both groups. There is a lack of adaptation from the 1st to 2nd and 1st to 200th phase reversal and the adaptation ratio is close to 1 for days 1 through 6 in both control and DREADDs animals (Figure 5.5A, B, C, D), in contrast to almost all other experiments we have conducted ((Kim *et al.*, 2020; Chaloner & Cooke, 2022), 3.4.1.2, 3.4.2.3, 0)

In control animals, the adaptation that occurs from the 1st to the 200th phase reversal in response to familiar and novel stimuli, with and without CNO, did show the normal trend that adaptation ratio is greater in response to novel stimuli (Figure 5.5B; Wilcoxon signed rank FDR corrected: Control day 7 fam v day 7 nov p = 0.002, day 8 fam w/CNO v day 8 nov w/CNO p = 0.002). However, the adaptation ratio (1st/200th) is close to 1 for novel stimuli and below 1 for familiar stimuli, reflecting the very weak adaptation that occurs across all days in all animals within this experiment. During presentation of familiar and novel stimuli in DREADDs animals, the normal relationship held true where the adaptation ratio was greater in response to novel stimuli, but AR was close to 1

for both stimuli (Figure 5.5B; Wilcoxon signed rank FDR corrected: DREADDs day 7 fam v day 7 nov p = 0.01). However, during layer 6 inactivation on day 8, the difference between AR to familiar and novel was reduced (Figure 5.5B; Wilcoxon signed rank FDR corrected: DREADDs day 8 fam w/CNO v day 8 nov w/CNO p = 0.052).

Short-term adaptation that occurred from the 1st to the 2nd phase reversal on day 7 was not present in any condition (with and without CNO) in either group (Figure 5.5D; Wilcoxon signed rank FDR corrected: Control day 7 fam v day 7 nov p = 0.2, day 8 fam w/CNO v day 8 nov w/CNO p = 0.5. DREADDs day 7 fam v day 7 nov p = 0.3, day 8 fam w/CNO v day 8 nov w/CNO p = 0.9). Overall, the effect of inactivating layer 6 cells is uninterpretable, as both control animals expressing mCherry and DREADDs-mCherry animals show a general lack of short-term adaptation. This finding suggests that viral expression of the fluorophore mCherry may have altered the activity of these cells and impaired the normal short-term dynamics of the cortex.

Despite a substantial loss of short-term adaptation in animals expressing mCherry and mCherry-hM4Di there is no effect on within-session adaptation across blocks. In both control and DREADDs animals across the first 6 days of visual stimuli presentation (no CNO) there is a significant reduction in VEP magnitude across blocks (Figure 5.6, Table 5.3). This is equivalent to the normal within-session adaptation observed in wildtype animals (Chaloner & Cooke, 2022).

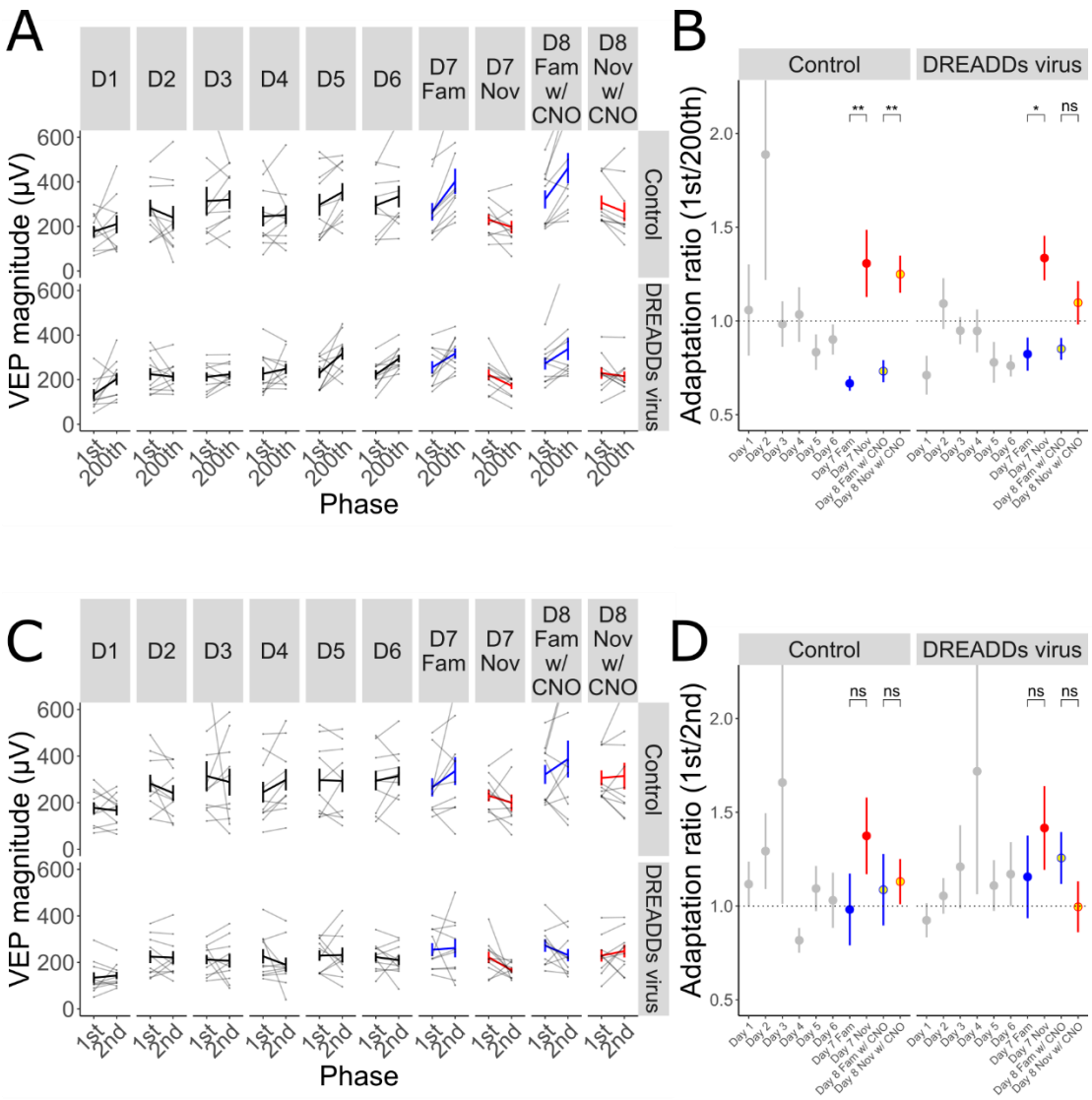

Figure 5.5 Short-term adaptation is altered after viral expression of mCherry and mCherry-hM4Di: (A) VEP adaptation from the 1st to 2nd phase reversal across all days for control and DREADDs animals. (B) Adaptation ratio (1st/2nd) across all days for control and DREADDs animals. (C) VEP adaptation from the 1st to 200th phase reversal across all days for control and DREADDs animals. (D) Adaptation ratio (1st/200th) across all days for control and DREADDs animals.

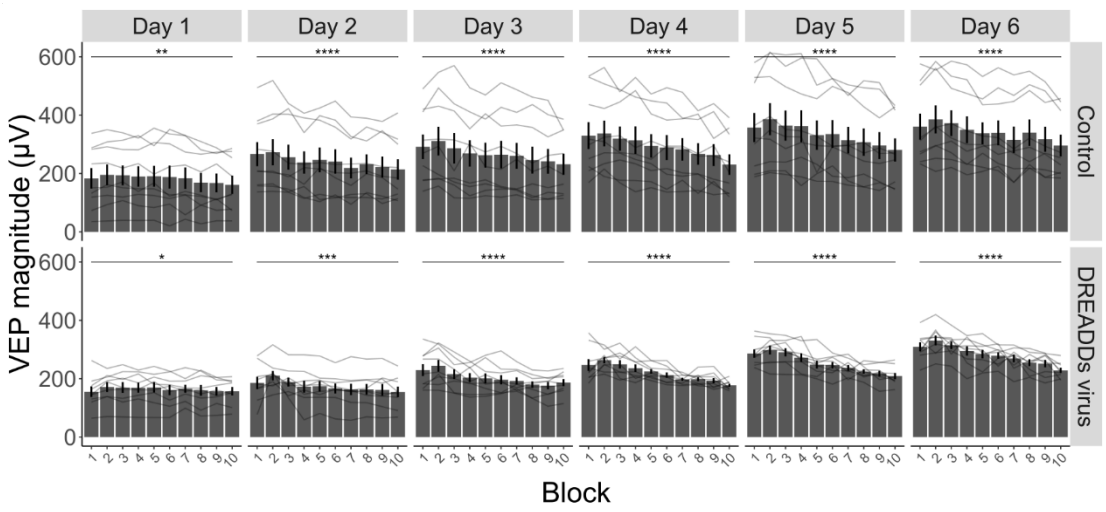

Figure 5.6 Within-session adaptation is normal after viral expression of mCherry and mCherry-hM4Di

Table 5.3 Statistics for Figure 5.6

group	Day	p value
control	D1	0.001
control	D2	< 0.001
control	D3	< 0.001
control	D4	< 0.001
control	D5	< 0.001
control	D6	< 0.001
Dreadds	D1	0.05
Dreadds	D2	0.0004
Dreadds	D3	< 0.001
Dreadds	D4	< 0.001
Dreadds	D5	< 0.001
Dreadds	D6	< 0.001

5.4.3.3 Inactivation of layer 6 cells during learning

To investigate the role of layer 6 cells across learning, the same hM4Di expression strategy was used as described above, but visual stimuli were shown on 3 consecutive days with application of CNO. This approach was followed by 24 hours for washout of CNO and then presentation of familiar and novel stimuli (day 4 visual stimulation) (Figure 5.7A). Control animals showed normal SRP over 3 days of stimulus presentation and differences in VEP magnitude to familiar

and novel stimuli (Figure 5.7B; Control - Friedman test day 1 – day 3 p = 0.03, Wilcoxon signed-rank Day 4 fam v Day 7 Nov p = 0.005). Inactivation of layer 6 cells prevented SRP across days (Figure 5.7B; DREADDs - Friedman test day 1 – day 3 p = 0.3). However, inactivation of layer 6 cells over learning did not abolish differential responses to familiar and novel stimuli after CNO washout (Figure 5.7B; DREADDs - Wilcoxon signed-rank Day 4 fam v Day 7 Nov p = 0.005).

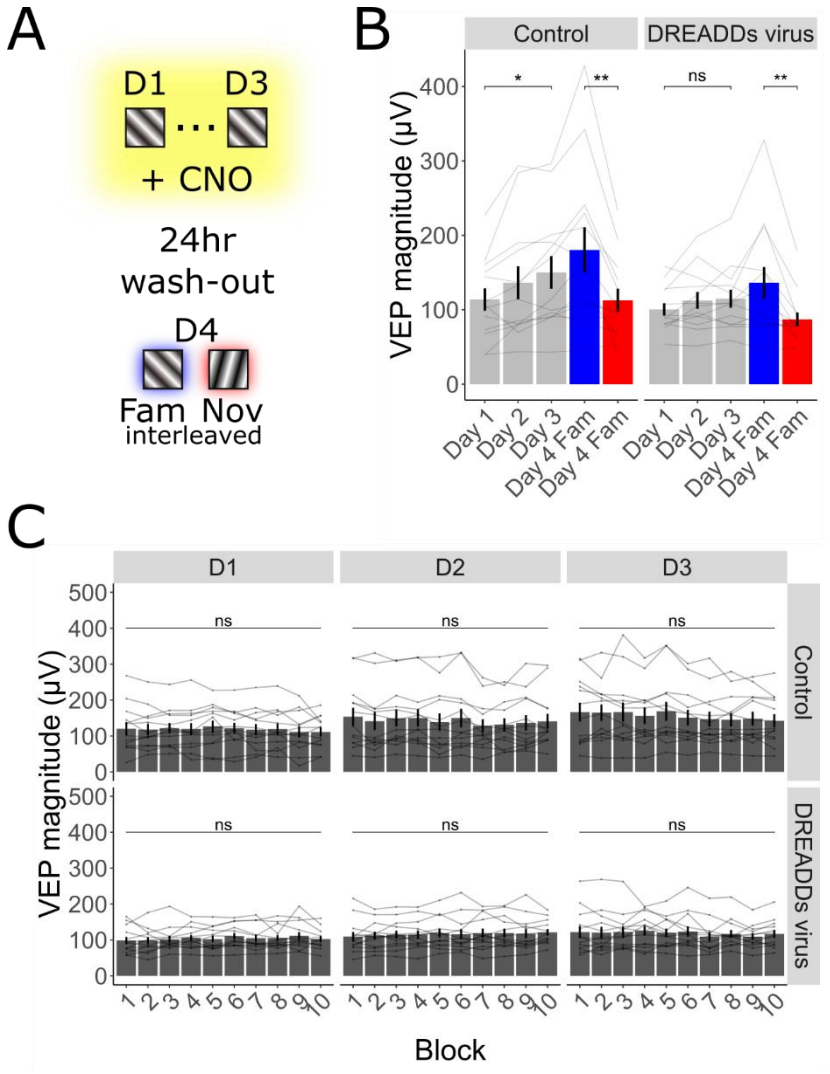

Figure 5.7 Layer 6 inactivation during learning: (A) Schematic to show visual stimuli presentation protocol. (B) VEP magnitude response during visual stimuli presentation across 3 days with CNO application, and in response to familiar/novel stimuli for control and DREADDs groups. (C) Within-session adaptation during visual stimuli presentation across 3 days with CNO application in control and DREADDs groups.

5.4.3.4 Viral expression in layer 6 cells prevents across- and within- block effects in control and DREADDs groups

Within-session adaptation occurs over several blocks of visual stimuli and becomes more pronounced across days (Chaloner & Cooke, 2022). In contrast to the within-session adaptation across blocks observed in both mCherry and DREADDs animals during 6 days of stimulus presentation (Figure 5.6), there was no within-session adaptation in both groups during 3 days of stimuli presentation. In control animals expressing mCherry, there was no adaptation across blocks (Figure 5.7C; Control - Friedman test B1 - B10: D1 $p = 0.5$, D2 $p = 0.5$, D3 $p = 0.4$). In addition, there was no within session adaptation across blocks while inactivating layer 6 cells (Figure 5.7C; DREADDs - Friedman test B1 - B10: D1 $p = 0.2$, D2 $p = 0.5$, D3 $p = 0.5$). The absence of within-session adaptation during layer 6 inactivation, however, cannot be attributed to layer 6 inactivation because control animals also did not exhibit within-session adaptation, implying a potential effect of CNO itself.

There was a complete loss of short-term adaptation from the 1st to 2nd and 1st to 200th phase reversals in animals expressing mCherry and DREADDs across all days (Figure 5.8A, B, C, D). The adaptation ratios were close or equal to 1 across all days and showed no difference in response familiar and novel stimuli in either group (Figure 5.8B; Wilcoxon signed-rank test: Control Day 4 Fam v Day 4 nov $p = 0.17$, DREADDs Day 4 Fam v Day 4 Nov $p = 0.08$. Figure 5.8D; Wilcoxon signed-rank test: Control Day 4 Fam v Day 4 Nov $p = 0.68$, DREADDs Day 4 Fam v Day 4 Nov $p = 0.81$).

Overall, it is not possible to make strong claims about the effects of layer 6 inactivation on within-session and short-term adaptation as control animals did not show the established phenomena.

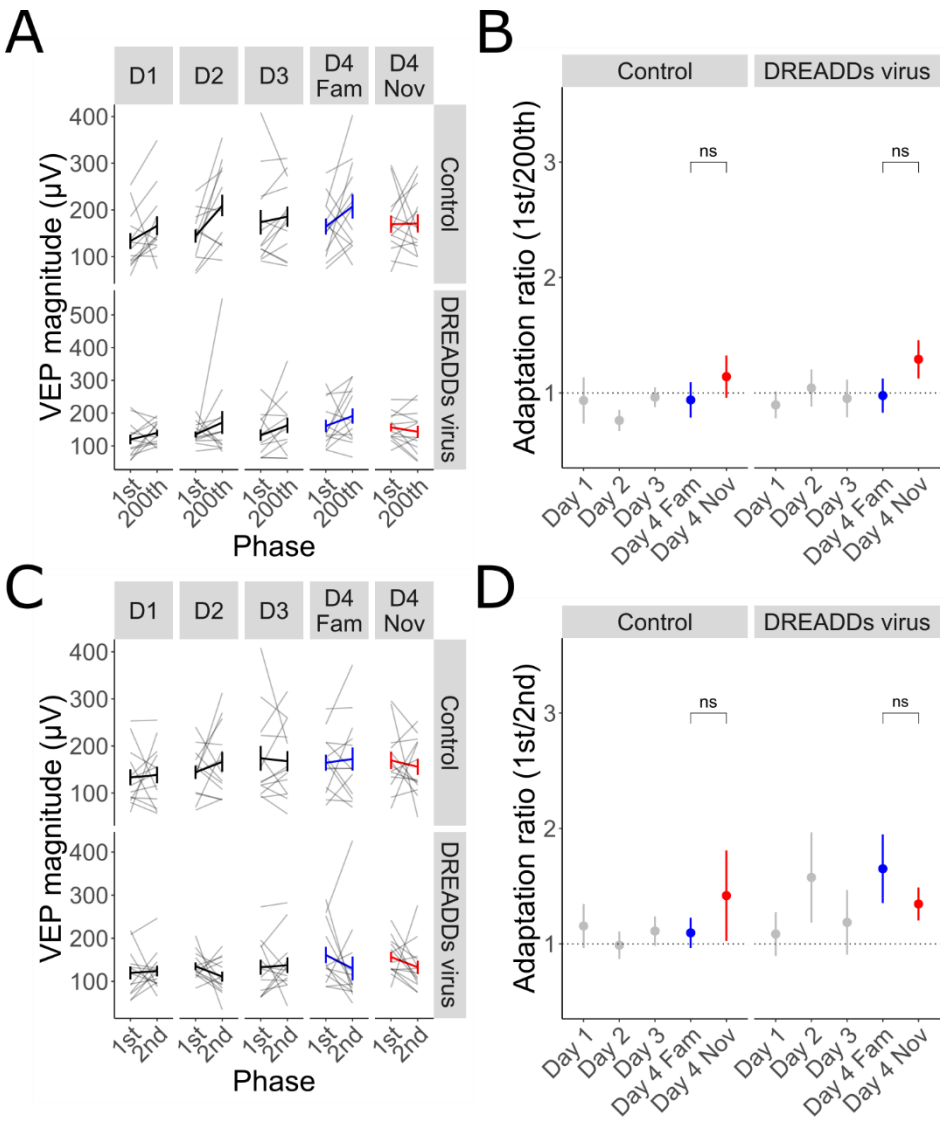

Figure 5.8 Short-term adaptation is altered after viral expression of mCherry and mCherry-hM4Di: (A) VEP adaptation from the 1st to 2nd phase reversal across all days for control and DREADDs animals. (B) Adaptation ratio (1st/2nd) across all days for control and DREADDs animals. (C) VEP adaptation from the 1st to 200th phase reversal across all days for control and DREADDs animals. (D) Adaptation ratio (1st/200th) across all days for control and DREADDs animals.

5.4.4 Layer 6 activation with ChR2 inhibits responses to visual stimuli but maintains familiar/novel difference

Attempts to inactivate layer 6 cells with DREADDs resulted in problematic results in both mCherry empty vector controls and hM4Di-expressing animals. Though not fully investigated, presence of the mCherry fluorophore may disrupt the activity of these cells (elaborated on in discussion). To further probe the

contribution of layer 6 cells, experiments were performed using Channelrhodopsin (ChR) and EYFP empty vector controls.

5.4.4.1 Activating layer 6 cells with ChR causes hang over effects with short inter-block intervals

Initially, a protocol with 5 blocks of familiar and novel stimuli with the LED on and off (pseudorandomly interleaved) was applied. In addition to a substantial reduction in VEP magnitude with LED on, this treatment resulted in a very small familiar/novelty difference with the LED off (Figure 5.9A). Investigation of the VEP magnitude across blocks for familiar and novel stimuli during LED off trials shows large variability (Figure 5.9B). Therefore, hangover effects from LED activation of layer 6 cells disrupts cortical activity in a paradigm using an inter-block internal of 30 seconds.

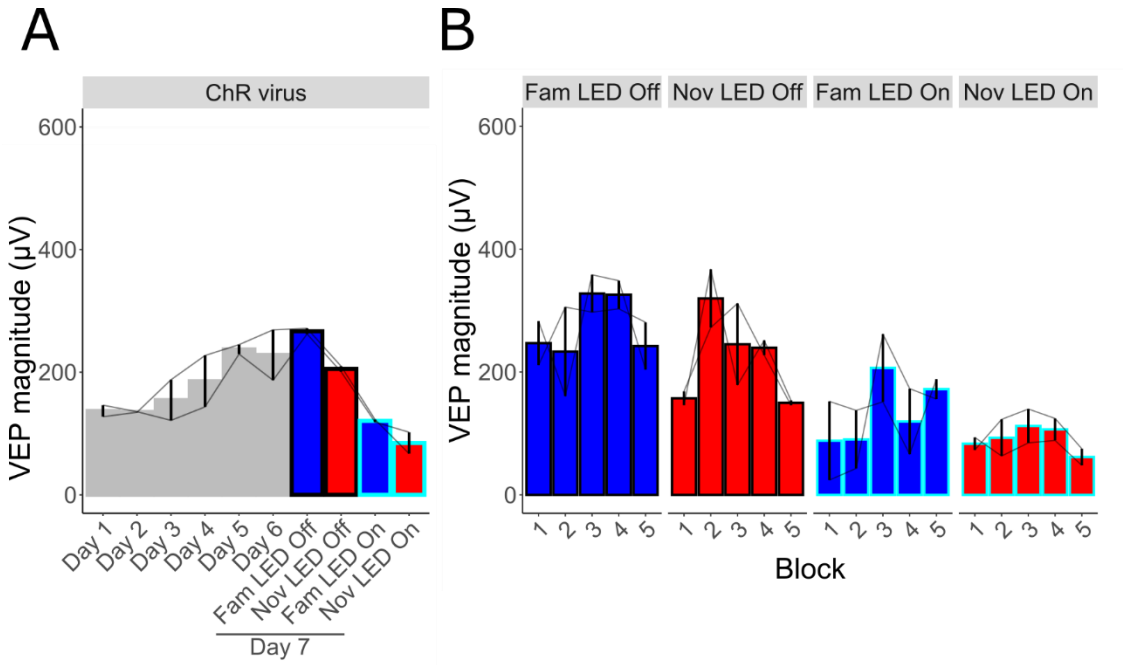

Figure 5.9 Effect of activation of layer 6 cells with ChR using a 5-block paradigm: (A) VEP responses across SRP and during presentation of familiar/novel stimuli with and without LED. (B) VEP responses across 5 blocks during presentation of familiar/novel stimuli with and without LED.

5.4.4.2 Activating layer 6 inhibits VEP responses to familiar and novel stimuli

Due to alterations in cortical activity after optogenetic activation of layer 6 cells with an inter-block interval of 30 seconds, the protocol was modified. On day 7, 2 blocks of familiar and novel stimuli (with and without LED) were presented, interleaved with 210s of grey screen to allow full recovery of cortical activity. To ensure two blocks of LED stimulation never occurred in sequence, the blocks were presented in a specific order: 'novel with LED on', 'novel with LED off', 'familiar with LED on', 'familiar with LED off'. In control animals expressing an empty vector with EYFP, potentiation of the VEP occurred and the familiar/novel difference was present with and without LED (Figure 5.10A). In animals expressing ChR2, the familiar/novel difference with the LED off is present, as expected (Figure 5.10A). After inactivation of layer 6 cells with the LED on, VEP magnitude in response to the familiar stimulus was drastically reduced (Figure 5.10A). Furthermore, responses to novel stimuli were also reduced during activation of layer 6 cells (Figure 5.10A). The reduced responses to both familiar and novel stimuli during layer 6 activation results in a similar familiar/novel ratio pre- and post-inactivation. However, this is variable across the small number of animals recorded from (Figure 5.10B). Hangover effects of layer 6 activation were not present as responses across blocks are equivalent in LED off trials (Figure 5.10D). Furthermore, responses to the familiar stimulus with the LED on were equivalent. However, responses to novel stimuli were massively inhibited during block 1 and then became like novel baseline responses by block 2 (Figure 5.10D). This observation may reflect a physiological effect or may be due to the order of stimulus presentation. 'Novel with LED on' is the first instance of optogenetic activation in the entire session. The first instance of optogenetic activation of layer

6 cells caused a massive inhibition of VEP magnitude, and this effect partially waned by the later blocks of LED delivery. This finding suggests that even ~8 minutes later ('Nov LED On' to 'Fam LED On') the efficacy of layer 6 activation was reduced. Overall, the effect of layer 6 activation was substantial, but careful assessment of the order of blocks and inter-block interval is required.

In control animals expressing mCherry, there was substantial disruption of within-session and within-block adaptation (Figure 5.5, Figure 5.7, Figure 5.8). In animals expressing EYFP (empty vector control and ChR2 fused), within-session adaptation was present, even across a few animals (Figure 5.10C). This control provides some evidence that use of the fluorophore EYFP does not disrupt normal VEP dynamics. Therefore, further experiments using ChR and EYFP will provide information on the effect of activation of layer 6 cells after SRP.

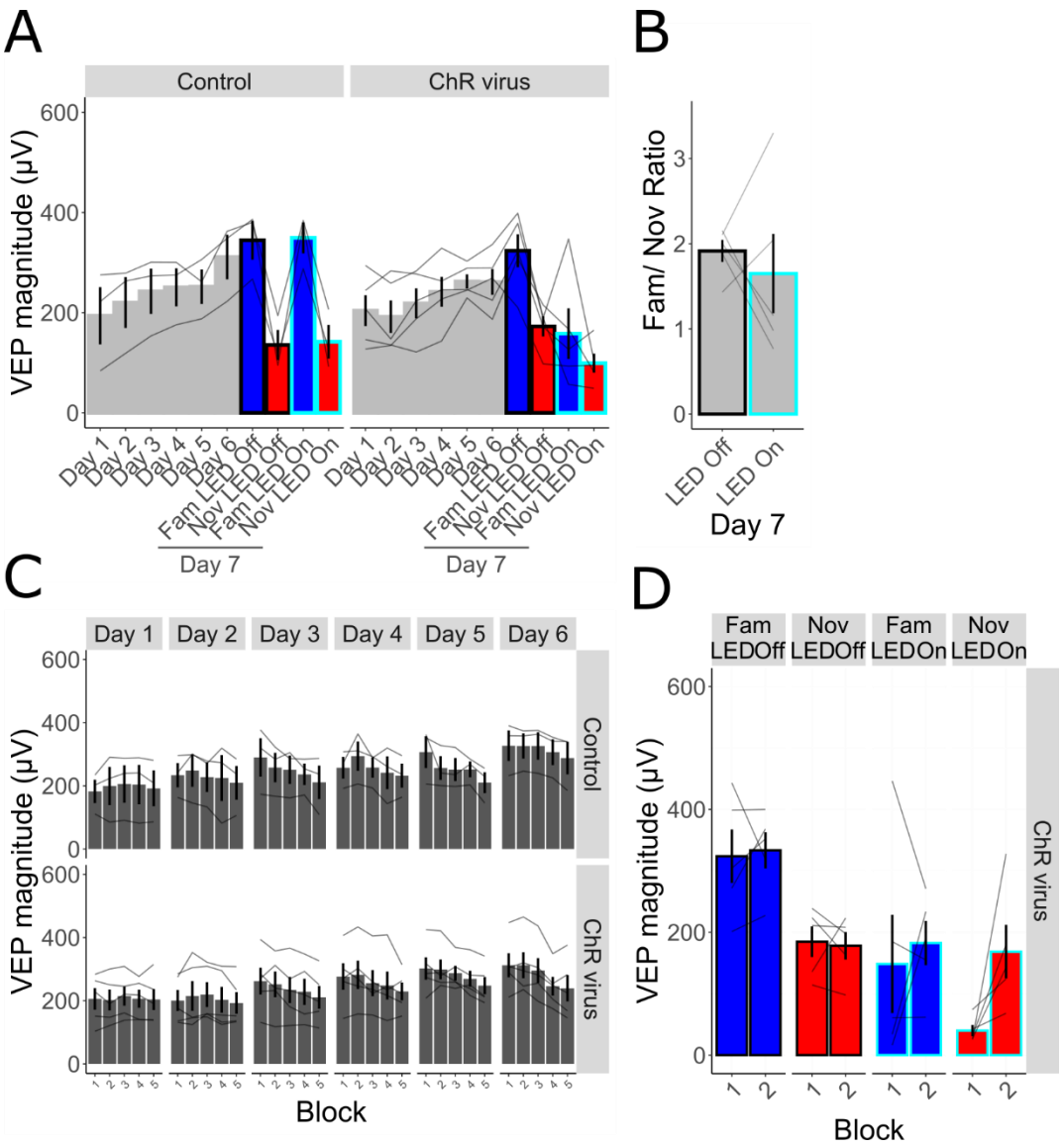

Figure 5.10 Activation of layer 6 cells causes inhibition of VEP responses: (A) VEP responses across SRP and during presentation of familiar/novel stimuli with and without LED on control and ChR animals. (B) Familiar/novel ratio during LED off and LED on trials in ChR animals. (C) VEP responses across 5 blocks during presentation of visual stimuli on day 1 through 6 on control and ChR animals. (D) VEP responses across 2 blocks during presentation of familiar/novel stimuli with and without LED.

5.5 Discussion

In the current chapter, I have discussed the absence of altered excitatory synaptic drive recorded from layer 4 after SRP. Further efforts to probe the role of layer 6 in short- and long-term adaptation and plasticity provided some insight but still lack clarity due to impairments in well-established phenomena in control animals expressing mCherry. Investigation into layer 6 using activating optogenetics did

provide evidence that activation of layer 6 caused inhibition of layer 4 VEPs. In addition, control animals expressing EYFP exhibited normal VEP dynamics, suggesting that EYFP expression in layer 6 cells is less problematic than expression of mCherry.

5.5.1 Potentiation of the VEP magnitude does not occur due to changes in thalamic inputs into layer 4

In response to visual stimuli presented over days, VEPs recorded from layer 4 potentiate, through the phenomenon of SRP. Therefore, it was hypothesised that synaptic input from the thalamus into layer 4 may be the key site of change. It would stand to reason that NMDAR-dependent Hebbian LTP may occur at layer 4 synapses, which become strengthened through insertion of AMPA receptors. This would be expected to increase the peak-amplitude of the synaptic responses and lead to increased VEP magnitude. However, knock-out of NMDA receptors in layer 4 has no effect on potentiation of VEP magnitude over days and responses to familiar and novel stimuli (Fong *et al.*, 2020). In line with this observation, our findings show no difference in the peak amplitude of EPSCs in layer 4. Therefore, Hebbian LTP at layer 4 synapses is not the driver for VEP potentiation.

5.5.2 Role of layer 6 during SRP

The observation that NMDA knock-out in visual cortex (V1) impairs SRP (Cooke *et al.*, 2015) suggests that Hebbian plasticity is occurring at synapses elsewhere within V1 which can influence potentiation of the VEP recorded from layer 4. Thalamic terminals onto corticothalamic (CT) cells in layer 6 are a potential locus of this synaptic plasticity (Beierlein & Connors, 2002; Constantinople & Bruno, 2013). Importantly, these layer 6 cells project to layer 4 and recruit PV+ interneurons to inhibit layer 4 excitatory cells (Olsen *et al.*, 2012; Bortone *et al.*,

2014; Kim *et al.*, 2014). Knock-out of NMDA receptors in layer 6 prevents the potentiation of the VEP over days, resulting in equal responses to familiar and novel stimuli (Hayden *et al.*, 2023). Our preliminary findings suggest that activation of layer 6 cells mimics responses during novelty. Overall, this observation suggests that during presentation of novel stimuli, layer 6 cells are engaged and recruit PV+ neurons, contributing to the increased activity of PV+ cells during novelty (Hayden *et al.*, 2021). During presentation of familiar stimuli, layer 6 cells may not be recruited, removing the driving force onto PV+ neurons. This removal of drive onto PV+ neurons may result in release of excitatory activity that causes potentiation of the VEP magnitude. Our pilot data somewhat agrees with the interpretation that layer 6 activation mimics novelty and recruits PV+ neurons, but the data is variable. After layer 6 inactivation, only 3 out of 5 animals present evidence supporting our hypothesis; they show a reduction in the familiar/novel ratio after activation of layer 6 cells. To fully assess the effect of layer 6 activation, this experiment should be repeated with 10 animals in each group. In addition, it is important to assess the amount of ChR2 expression and therefore the amount of action potential generation in layer 6 cells during ChR2 activation with light. Assessment of the efficacy of optogenetics can be achieved using *ex vivo* electrophysiology. An evaluation of the efficacy of ChR2 is required to resolve the observation of a massive reduction in VEP magnitude during the first ‘LED on’ block. This massive reduction in VEP magnitude suggests pronounced activation of layer 6 and substantial recruitment of PV+ neurons. Current clamp recordings from layer 6 with and without light will elucidate the change in firing rate after ChR2 activation. Furthermore, recording directly from PV+ neurons while stimulating layer 6 will further elucidate the extent to which layer 6 recruit PV+ cells. This will be an important step to take prior to further

experimentation, as adjustment of the viral titre may be needed to reduce the overall efficacy, so as not to completely preclude VEP responses in V1 after layer 6 activation.

5.5.3 Any effects of inactivation of layer 6 are uninterpretable due to confounds in control animals expressing mCherry

The lack of normal VEP dynamics across seconds and minutes in both the experimental and control animals suggests disruption of activity in layer 6 cells by viral expression of mCherry. The fluorophore mCherry is fused with the Gi-coupled hM4Di receptor. Florescent proteins that are fused to a membrane bound receptor are much more likely to form dimers (Costantini *et al.*, 2012). Assessment of the properties of mCherry expressed in cells shows the protein can aggregate (Costantini & Snapp, 2013; Costantini *et al.*, 2015), causing cytotoxicity, and 20% of expressing cells may display abnormalities (Bindels *et al.*, 2017). Investigation into the viral expression in current experiments with animals expressing mCherry and mCherry-hM4Di shows aggregations in layer 6 cells (Figure 5.11). In animals expressing EYFP alone or EYFP fused to ChR2, there is normal within-session adaptation (Figure 5.10C) suggesting that the fluorophore EYFP is less disruptive to these cells than mCherry, even when fused to the membrane protein ChR2. However, assessment of within-block adaptation is required, but can only occur after collection of data from a larger number of animals due to high variability.

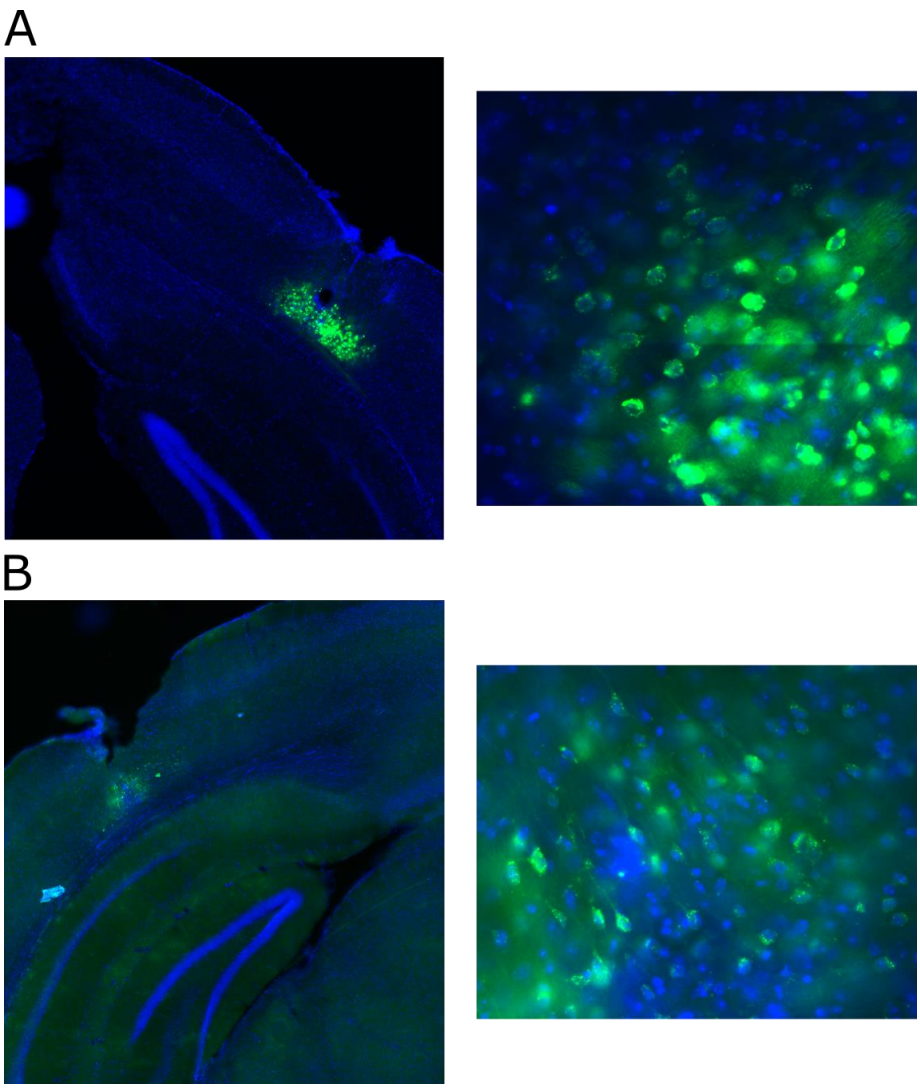

Figure 5.11 Images of layer 6 cells expressing (A) mCherry and (B) mCherry-hM4Di

5.5.4 The role of layer 6 cells at across seconds and minutes

It is unlikely that altering layer 6 activity impairs within-session adaptation across blocks as this phenomenon is present after NMDAR knock-out in layer 6 cells and after viral expression of mCherry and mCherry-hM4Di. However, there is a loss of within-session adaptation in mCherry and mCherry-hM4Di animals during CNO application from day 1 to day 3. There is a possibility the loss of adaptation here is due to off target effects of CNO (Manvich *et al.*, 2018) as within-session adaptation is lost in both groups. Overall, most evidence suggests disruption of layer 6 activity does not impair adaptation of the VEP over minutes. One possible driving force of within-session adaptation may be reduced thalamic drive to layer

4. Averaged currents recorded from layer 4, which likely reflect thalamic inputs, reduce across ~6 minutes (Gallimore *et al.*, 2023). Therefore, adaptation of thalamic inputs into layer 4 across several minutes may result in the reduced VEP magnitude seen across blocks. However, as presented in chapter 3, within-session adaptation following somatostatin activation is altered. Therefore, it is important to test if either or both cell types are the driving force for the reduction in VEP magnitude across blocks. This can be done using laminar probes or calcium imaging to record the activity of thalamic and somatostatin cells across several minutes.

Interestingly, NMDAR knock-out in layer 6 prevents within-session behavioural habituation. This finding suggests that the mechanisms mediating within-session habituation may be different to those mediating within-session VEP adaptation. Layer 6 directly targets layer 5 (Kim *et al.*, 2014) which is the main output layer of the cortex. Altered activation of layer 5 due to loss of normal layer 6 activity may lead to impaired activation of downstream regions (Ramaswamy & Markram, 2015) and therefore impaired behavioural habituation. However, this hypothesis needs to be tested. Temporally precise inactivation of layer 6 and layer 5 cells using inhibiting chemogenetics (Magnus *et al.*, 2019) would provide information on the roles of these cell types during within-session habituation. To provide finer detail of behavioural habituation, video analysis of orofacial movements will be required during inactivation experiments (Mathis *et al.*, 2018; Syeda *et al.*, 2022).

There is a dramatic loss of short-term adaptation after expression of mCherry and mCherry-hM4Di. Furthermore, short-term adaptation is maintained after NMDAR knock-out in layer 6 cells. This observation suggests that normal activity of layer 6 cells and normal integration into the circuit is important in short-

term adaptation. Our current hypothesis is that a reduction in thalamic activity is the driver of short-term adaptation and occurs independently of stimulus type. However, during familiar stimuli, this reduction in thalamic activity occurs concurrently with a matched reduction in PV+ neuronal activity. This reduced PV+ cell activity is mediated through increased inhibition from SOM+ neurons. The loss of PV+ inhibition in parallel with thalamic adaptation is reflected as an unchanged VEP magnitude. The driver of the reduction in thalamic activity across tens of seconds may be layer 6 cells. Layer 6 cells strongly activate the TRN and causes inhibition in the thalamus (Cruikshank *et al.*, 2010; Jurgens *et al.*, 2012; Olsen *et al.*, 2012). Therefore, disrupted layer 6 cellular activity, due to mCherry expression, may prevent the recruitment TRN to inhibit thalamic drive. This effect may result in the loss of short-term adaptation observed after viral expression of mCherry.

As the stimulus becomes familiar, there may be shift in drive from predominantly bottom-up activation of PV+ neurons by layer 6 cells (Olsen *et al.*, 2012; Bortone *et al.*, 2014; Kim *et al.*, 2014; Yetman *et al.*, 2019) to inhibition of PV+ neurons by SOM+ cells (Ma *et al.*, 2012; Xu *et al.*, 2013). The inhibition of PV+ cells by SOM+ neurons may be reliant on a concurrent loss of activation from layer 6 cells. Reduced activation of PV+ neurons may result from lower layer 6 activity because of NMDAR dependent synaptic depression at corticothalamic synapses in layer 6. Therefore, loss of adaptation during SRP never occurs after knock-out of NMDARs in layer 6, as the activity of layer 6 cannot be altered through Hebbian mechanisms.

5.5.5 Future directions

It is likely that the mCherry fusion protein disrupts the activity of layer 6 cells, but EYFP does not. Therefore, to investigate the effect of inactivating layer 6 cells during learning and during familiar/novel stimuli presentation the PSAM system should be used (Magnus *et al.*, 2019). This system allows inactivation of cells by chloride inflow through PSAM-GlyR channels. Importantly, the EGFP protein is not fused to the membrane receptor PSAM-GlyR, reducing the risk of dimerization (Costantini *et al.*, 2012). Therefore, an additional experiment using the non-fusion virus PSAM4 GlyR IRES EGFP (https://www.addgene.org/119741/) should elucidate the role of layer 6 at different timescales of plasticity. It is important to use the PSAM system to inactivate these cells across multiple blocks of stimulation (5 or 10) to assess within-session and within-block adaptation after inactivation of layer 6 cells. This has not yet been possible using optogenetics due to the extended inter-block interval. If, as we expect, inactivation of layer 6 prevents short-term adaptation, it would support the hypothesis that layer 6 feedback to the TRN inhibits the thalamus and results in a reduction in VEP magnitude across seconds.

Chapter 6 Discussion

In this thesis, I have presented the results of experiments investigating plasticity mechanisms supporting adaptation and habituation in response to passive exposure to visual stimuli in mice. I used both *in vivo* and *ex vivo* approaches to elucidate the circuits, cells and synapses which are altered across different timescales. I found that adaptation of visual responses occurs over seconds, resulting in sharply diminished cortical responses, with a more subtle reduction in cortical response manifest across minutes with recurring blocks of phase reversing stimuli. This latter timescale is accompanied by clear behavioural habituation from block to block. In addition, long-term behavioural habituation occurs over days concurrent with a seemingly paradoxical effect of potentiated visual evoked potentials (VEPs) that is in the opposing direction that that observed for shorter timescales. This potentiation is highly selective for the familiar orientation and is therefore described as stimulus-specific potentiation (SRP). Interestingly, as experience-dependent potentiation occurs over days, there is loss of short-term adaptation over tens of seconds as the stimulus becomes increasingly familiar. Presentation of a novel stimulus still produces short-term adaptation of the VEP magnitude even after saturated familiarity to a specific oriented stimulus. Thus, there is a rich array of different forms of plasticity occurring in primary visual cortex simply as a result of passive stimulus viewing.

To gain insight into the mechanisms contributing to these phenomena, I investigated the involvement of SOM+, PV+ and layer 6 excitatory cells across these different timescales. By performing *ex vivo* intracellular measurements of synaptic responses following saturated long-term visual experience I was able to show that there is a reduction in the magnitude of inhibitory inputs into layer 4. Several lines of evidence now indicate that this diminished inhibition is likely a

form of disinhibition, resulting from a reduction of PV+ neuronal inhibition onto layer 4, mediated in turn by an increase of SOM+ inhibitory neuronal activity. Optogenetic activation of SOM+ neurons causes increase in the magnitude of VEPs in layer 4 and occludes short-term adaptation, likely reflecting disinhibition. This result is especially striking in that the increase in VEP magnitude is largely limited to the novel stimulus, consistent with the observation that SOM+ neurons are already highly active in response to familiar stimuli (Hayden *et al.*, 2021). Furthermore, I have shown that manipulation of the activity of PV+ neurons or layer 6 cells during visual experience, when learning first occurs, also impairs experience-dependent potentiation. Inactivation of PV+ neurons and NMDAR knock-out in layer 6 neurons also prevents the loss of short-term adaptation observed that normally occurs with the establishment of long-term familiarity. Overall, the response dynamics across multiple timescales within layer 4 are likely modified by opposing SOM+ inhibitory control and layer 6 excitatory control of PV+ neurons. Therefore PV+ neurons may act as a gating mechanism for adaptation and plasticity within visual cortex. An in-depth discussion of these results are provided in the relevant discussion sections in each chapter. Below, I discuss the proposed hypotheses, general points, ideas, and future directions based on the results collected in this thesis.

6.1 Circuits contributing to visual cortical plasticity and adaptation

Multiple lines of evidence suggest that SRP cannot be explained by long-term Hebbian plasticity at thalamo-cortical synapses into layer 4. LTP manifests immediately after stimulation (Bliss & Lomo, 1973), whereas VEP potentiation only occurs after a day (Frenkel *et al.*, 2006; Cooke & Bear, 2010; Aton *et al.*, 2014). Furthermore, potentiation is specific to the spatial frequency and contrast of the stimulus (Cooke & Bear, 2010) and SRP occurs in response to a

checkerboard stimulus (two overlayed orthogonal orientations) but does not transfer to the component orientations (Frenkel *et al.*, 2006). LTP at feedforward inputs from multiple orientation insensitive dLGN cells (Hubel & Wiesel, 1962; Priebe, 2016) does not explain these results. The discovery that knock-out of NMDARs in layer 4 excitatory cells had no effect on SRP provided conclusive evidence that SRP is not a product of Hebbian plasticity at thalamocortical synapses onto layer 4 excitatory cells (Fong *et al.*, 2020). However, SRP does require NMDAR dependent plasticity in V1 (Cooke *et al.*, 2015) suggesting that synaptic plasticity in the cortex and the onwards effects on the activity of cells must contribute to SRP.

Based on the evidence in this thesis and published literature, SOM+ neurons are likely the key player in mediating VEP potentiation to a familiar stimulus (SRP). Our current hypothesis suggests that as the stimulus becomes familiar, there may be shift in drive from predominantly bottom-up activation of PV+ neurons by layer 6 cells (Olsen *et al.*, 2012; Bortone *et al.*, 2014; Kim *et al.*, 2014; Yetman *et al.*, 2019) to inhibition of PV+ neurons by SOM+ cells (Ma *et al.*, 2012; Xu *et al.*, 2013; Hayden *et al.*, 2021) (Figure 6.1A). This is supported by evidence in this thesis demonstrating that knock-out of NMDARs in layer 6 prevents VEP potentiation. This loss of VEP potentiation suggests that the loss of layer 6 activation of PV+ neurons may be a result of NMDAR dependent synaptic depression (Hebbian LTD) at corticothalamic synapses in layer 6 (Figure 6.1A). The NMDAR dependent plasticity at thalamocortical synapses may require sleep dependent interactions between layer 6 and the thalamus (Aton *et al.*, 2014; Durkin *et al.*, 2017) (Figure 6.1A). In addition, evidence presented here demonstrates that activation of SOM+ neurons with optogenetics (ChR) causes potentiation of the VEP magnitude, suggesting SOM+ neurons are recruited

during familiarity to inhibit PV+ neurons (Figure 6.1A). Importantly, there are a number of alterations that may be mediating the recruitment of SOM+ neurons across days that must be directly tested: (1) NMDAR-dependent plasticity at thalamic to SOM+ synapses, (2) a shift in firing mode from the thalamus from tonic to burst firing causes greater recruitment of SOM+ neurons (Kwan & Dan, 2012), (3) altered top-down control of SOM+ neurons (Makino & Komiyama, 2015) (Figure 6.1A).

The least well understood phenomenon described in this thesis is within-session adaptation of the VEP magnitude across minutes. The adaptation across minutes may reflect NMDAR dependent depression at thalamo-cortical synapses into layer 4 (Figure 6.1B). The increased VEP magnitude across 15 minutes following SOM+ activation suggests these neurons are not recruited during this timescale. However, there is currently no direct evidence that SOM+ neurons may reduce their activity over this timescale. Therefore, adaptation may be a result of increased PV+ neuronal activity over minutes due to decreased SOM+ inhibition or increased thalamic input. Therefore, increasing PV+ mediated shunting inhibition causes the amplitude of any excitatory inputs to be reduced, reflected as VEP adaptation. However, depression at thalamo-cortical synapses is more likely to explain this phenomenon, as thalamic inputs onto layer 4 excitatory cells are depressing (Beierlein *et al.*, 2003). Furthermore, it is unlikely that PV+ neurons are recruited over minutes as thalamic inputs onto PV+ neurons are also depressing (Beierlein *et al.*, 2003). Overall, there is the least experimental support for this hypothesis and must be explored in much greater depth. To understand the driver of these changes, calcium imaging of PV+ neurons, SOM+ neurons and thalamic terminals in layer 4 over several minutes is required.

Our current hypothesis is that short-term adaptation of the VEP magnitude in response to novel stimuli reflects depression of thalamic synaptic drive into V1 (Lee & Sherman, 2008) and/ or a reduced activity of the thalamus due to TRN recruitment by layer 6 feedback (Cruikshank *et al.*, 2010; Jurgens *et al.*, 2012; Olsen *et al.*, 2012). This thalamic adaptation occurs independently of stimulus type (Gallimore *et al.*, 2023), which is supported by evidence that inactivation of PV+ neurons with DREADDs unveils pronounced adaptation to both familiar and novel stimuli, likely reflecting adaptation of thalamic inputs to V1. Importantly, during presentation of novel stimuli, PV+ mediated inhibition is relatively static across tens of seconds (Hayden *et al.*, 2023). It is possible that static PV+ neuronal inhibition is a result of sustained layer 6 activation of PV+ neurons (Figure 6.1C*i*). However, during presentation of familiar stimuli, there is matched reduction in PV+ neuronal activity (Hayden *et al.*, 2021) to the reduction in thalamic drive, this manifests as the VEP magnitude, which is a population-level signal, failing to adapt. The decrease in PV+ neuronal activity may potentially be mediated by increased SOM+ inhibition (Hayden *et al.*, 2021), coupled with the absence of layer 6 activation of PV+ neurons (Figure 6.1C*ii*). Increased SOM+ inhibition of PV+ neurons is supported by evidence presented in this thesis where SOM+ activation during novelty mimics the short-term dynamics during familiarity (Figure 6.1C*ii*). Furthermore, the requirement for a reduction in PV+ cell activity over learning is supported by evidence in this thesis that inactivation of these cells with DREADDs during learning prevents the loss of short-term adaptation over learning (Figure 6.1C*ii*). In addition, the importance that a loss of layer 6 activity is required for loss of adaptation over familiarity is supported by evidence that NMDAR knock-out in layer 6 maintains adaptation over learning (Figure 6.1C*ii*).

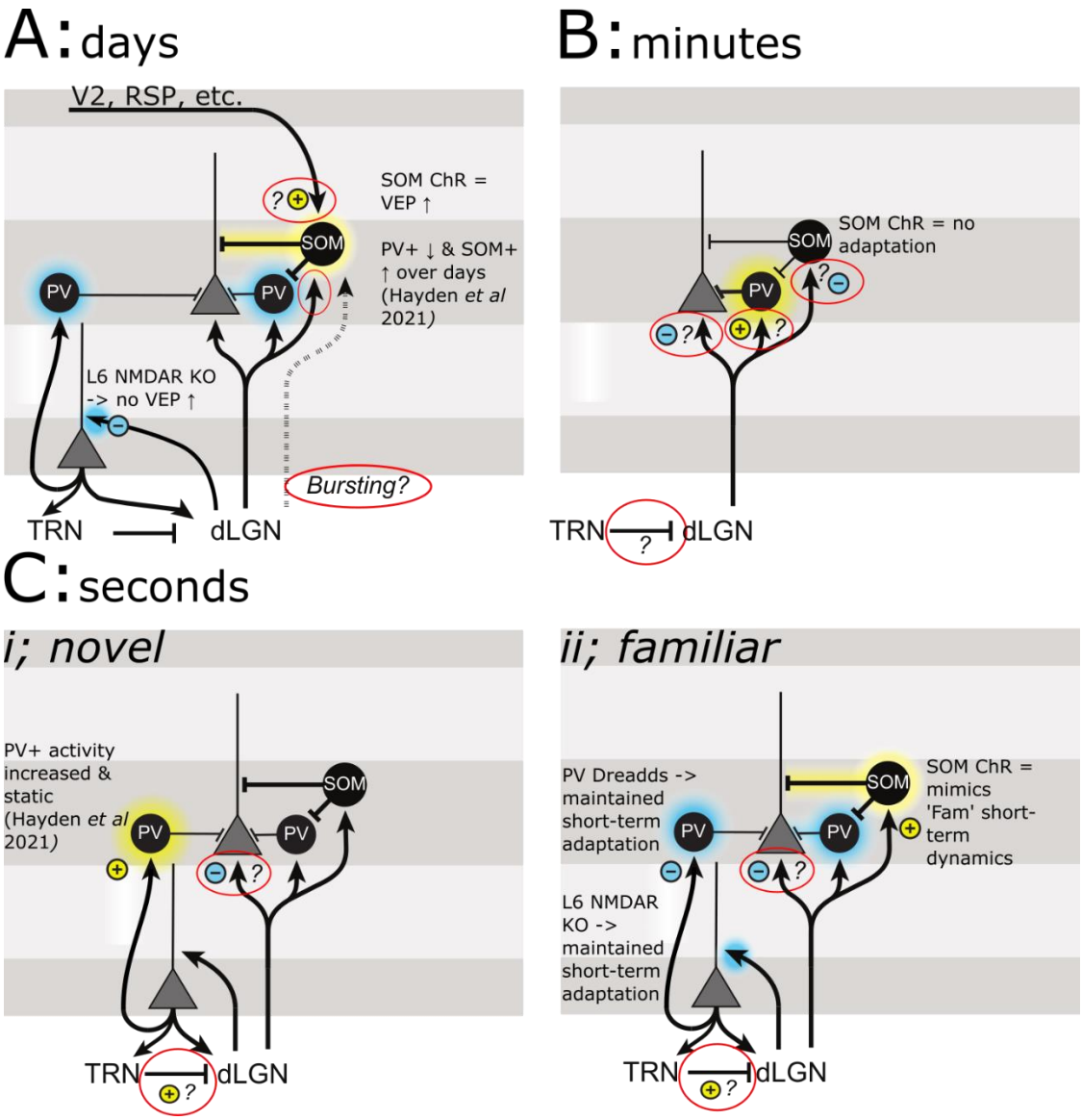

Figure 6.1 Schematic of hypothesised changes across SRP.

6.2 Overarching considerations

An important motif across all timescales is that SOM+ neurons are disinhibitory and activation of SOM+ neurons cause potentiation of the VEP magnitude. This motif is in opposition to predominantly an inhibitory role in superficial layers. This inhibitory role of SOM+ neurons in superficial layers is supported by evidence that activation of SOM+ neurons during oddball stimuli reduces the positive component of the VEP which reflects synaptic activity in superficial layers. The major conclusion of these results is that there is an

interplay between SOM+ inhibition of PV+ cells and layer 6 activation of PV+ cells which is altered over learning. However, a critical missing piece what is driving altered SOM+ activity. The locus of change may be decreased inhibition from VIP cells (Keller *et al.*, 2020), Hebbian LTP of synapses onto SOM+ neurons, or a change in frequency or mode of synaptic activity which drives SOM+ neurons. Thus far we have noted SOM+ neurons as a critical mediator of the changes that occur during learning. However, we must exercise caution as the critical mediator may be another cell type or brain region which feeds onto SOM+ neurons to mediate the changes observed here. Further studies of VIP neurons, thalamic activity, and synaptic inputs onto SOM+ neurons will clarify or alter the models proposed here.

A further important consideration is the interaction effect between SRP and short-term adaptation: can SRP be explained by a loss of within-block adaptation? In wild-type animals, the familiar novel difference only manifests after the 1st phase reversal (Figure 2.2D & H) suggesting that SRP manifests due to the loss of adaptation. In both layer 6 NMDAR KO and PV+ inactivation, maintained adaptation and loss of familiar/ novel differences are concurrent. This supports the idea that loss of adaptation drives the familiar/ novel difference. However, SOM+ neuronal activation prevents within-session adaptation but differential responses to familiar and novel stimuli are maintained, albeit attenuated. This suggests that SRP cannot be wholly described by within-session adaptation and other mechanisms may contribute to expression of differential responses to familiar and novel stimuli.

The LFP reflects, in part, summed synaptic activity. Due to the anatomical organisation in the cortex, substantial evidence suggests that excitatory synapses are considered to contribute more to the LFP than inhibitory

currents (Buzsáki *et al.*, 2012). In this thesis, the potentiation of the VEP magnitude is considered a result of a loss of PV+ mediated shunting inhibition. This loss of PV+ inhibition is mediated through increased SOM+ inhibition of PV+ neurons and results in a relative increase in thalamocortical excitatory synaptic activity in layer 4. However, the LFP may reflect excitatory and inhibitory synaptic currents and the membrane potential of excitatory cells equally (Haider *et al.*, 2016). Current source density analysis reveals that the first negative component of the VEP reflects activity in layer 4 and the positive component reflects activity in layer 2/3 (Cooke *et al.*, 2015; Hayden *et al.*, 2023). Based on these assumptions, we may predict that (1) excitatory inputs form the thalamus are increased, as described previously and/or (2) potentiation of the VEP reflects larger membrane fluctuations of excitatory cells due to altered excitatory and inhibitory inputs. The potentiation of the VEP is unlikely to reflect increases in PV+ mediated inhibition as calcium imaging suggest these cells decrease their activity over days (Hayden *et al.*, 2021). Nonetheless, the increased SOM+ engagement over days (Hayden *et al.*, 2021) may contribute to potentiation of the VEP magnitude if inhibitory currents are captured in the LFP signal.

6.3 Do crude manipulations of cell activity provide useful experimental insight?

In this thesis, I used both chemogenetic and optogenetic methods to inactivate and activate specific genetically defined neuronal types. Despite the fact that the onset of intervention with optogenetics has tight temporal constraint due to the trigger being provided with an LED, one substantial drawback of the technique is the hangover effect that it can produce on cellular activity after the offset of LED output (Lee *et al.*, 2020). In my experiments, use of Halorhodopsin in SOM+ neurons and Channelrhodopsin in layer 6 cells resulted in hangover effects. To

combat these effects, one could ramp the intensity of light at the start and end of LED presentation, use pulsing light across the block, or shorten the block of stimuli (Lee *et al.*, 2020). However, using shorter blocks in the current experiments would limit the ability to investigate short-term adaptation across 100 seconds.

A substantial drawback of the DREADDs chemogenetic system is the use of the ligand CNO, which is metabolised into clozapine, a drug that has well characterized effects on neurons and behaviour (Gomez *et al.*, 2017; Manvich *et al.*, 2018). We have used empty vector controls for all our experiments, and here in particular the utility of having controls that receive CNO is clear. Only over within-session adaptation is there a suggestion in our results that CNO may be affecting the phenomena we are studying but, nevertheless, ideal experiments would use drug triggers that have no potential off-target effects. There is a new ligand which activates DREADDs receptors and isn't metabolised into clozapine and this would be favoured for future experiments (Nagai *et al.*, 2020). Furthermore, there are now other chemogenetic systems that are now commercially available, which can be used to inhibit cell types. For example, the PSAM-GlyR system (Magnus *et al.*, 2019), which has the additional benefit of being an ionotropic receptor. Therefore, the PSAM system is less likely to have chronic effects than DREADDs receptors, which are metabotropic and therefore reliant upon specific intracellular signalling cascades within the targeted cell and subject to resynthesis of receptors. Based on my work presented in this thesis, an important future direction would be to use the PSAM-GlyR system to investigate the role of layer 6 in different timescales of plasticity. It is important to use the PSAM-EGFP system, as expression of mCherry impaired short-term

adaptation in control animals, suggesting there were clearly limitations with the current methodologies.

The methodological approaches of optogenetics and chemogenetics, used extensively in my work presented in this thesis, are incredibly useful for targeting specific cell types and profoundly altering dynamics of the brain across experience-dependent plasticity. However, finer spatial, and temporal control of cell type-specific activity is ultimately required to fully assess experience-dependent adaptation and plasticity. The temporal dynamics of cellular activity across seconds and minutes is an important consideration in these experiments. Both optogenetics (lasting ~100 seconds) and chemogenetics (lasting ~1-2 hours) chronically manipulate neuronal activity. The temporal dynamics of neurons may be critical for the expression of cortical response adaptation across different timescales. Chronic activation and inhibition of cell sub-types, even for a matter of 100 seconds, may not be acute enough to understand the role of different cells in experience-dependent adaptation and plasticity. One solution is to use laminar probs to assess the activity of individual cell types with excellent temporal resolution (Lima *et al.*, 2009; Rossant *et al.*, 2016). Therefore, rather than manipulating cell types and investigating the effects, one can record the direct activity of these cells and how this changes to produce the VEP dynamics observed. In addition, optical and electrophysiological techniques can be combined to both establish the temporal dynamics of cells during normal processing and during optogenetic manipulations (Cardin *et al.*, 2010). Furthermore, after recording with laminar probes to establish an electrophysiological signature of engagement of different cell types, a closed-loop system could be employed. The closed loop system works by manipulating the brain during periods with specific electrophysiological signatures (Paz *et al.*,

2013; Escobar Sanabria *et al.*, 2020; Tafazoli *et al.*, 2020; Kahn *et al.*, 2022). There is evidence that SOM+ neurons mediate beta oscillations (Chen *et al.*, 2017; Veit *et al.*, 2017) and PV+ neurons mediate gamma oscillations (Cardin *et al.*, 2009; Chen *et al.*, 2017). So, for example, a closed-loop system could be used to activate or inhibit SOM+ and PV+ neurons during these oscillatory states. This approach would provide greater temporal control of these cell types while they are active.

In the experiments I have described, optogenetics and chemogenetics have been applied such that neurons of a given type are stimulated or inactivated across all cortical layers at once. However, it is well established that specific spatially-defined groups of the same genetically-defined cell type are critical for response to specific stimuli (Pérez-Ortega *et al.*, 2021). Therefore, the spatial profile of cellular activity is important to replicate during manipulation experiments. Stimulation of groups of cells with optogenetics can be done while simultaneously recording the activity of cells (Packer *et al.*, 2015; Carrillo-Reid *et al.*, 2019). This technique allows spatially precise targeting of cells which share functional responses and can still have profound effects on behaviour through a much more precise intervention (Adesnik & Abdeladim, 2021). Therefore, activation or inhibition of SOM+ or PV+ neurons using targeted optogenetics would provide greater spatial control of these cells. Furthermore, using targeted optogenetics in future experiments may reduce non-specific and hang-over effects observed in some optogenetic experiments performed for this thesis.

It is also important to consider the genetically defined subgroups within the broad classes of PV+ and SOM+ neurons. Activation or inhibition of SOM+ or PV+ neurons will activate diverse subgroups of cells, each likely possessing different connectivity profiles and roles (Harris *et al.*, 2018). In future experiments,

it will be important to assess the transcriptional profile of the cells of interest after recording their activity in response to experience (Condylis *et al.*, 2022). This will elucidate how genetically defined subgroups within the PV+ and SOM+ neuronal classes contribute to information processing and experience-dependent plasticity and may allow for even more nuanced interventional strategies in the future.

6.4 Electrophysiological signals: benefits and drawbacks

The work described in this thesis has largely been reliant on recordings of local field potential (LFP), using visual evoked potentials (VEPs) as the primary readout of cortical activity. The lack of ability to dissociate the specific cells which contribute to the LFP is a major drawback in using the LFP signal to understand core circuit-level mechanisms. However, the current work is complemented by other related studies using single unit electrophysiology (Cooke *et al.*, 2015; Hayden *et al.*, 2023), as well as calcium imaging of individual neuronal activity (Song *et al.*, 2020; Hayden *et al.*, 2021) that, together, can start to provide a clearer picture of circuit-level mechanism. That being said, the major benefits of these alternative techniques could now be used to provide further insight, based on my observations. Calcium imaging provides multiple advantages. Notably, it allows for the same individual neurons to be followed from one day to the next over multiple days and, for the most part, increases the yield of individual neurons over electrophysiology. It also allows for the identification of cell type *post hoc*, meaning that cells with notable response profiles during the experiment can be identified as belonging to a particular class of neuron subsequently (Khan *et al.*, 2018; Poort *et al.*, 2022). Furthermore, GCamp can be expressed under the control of Cre to only be expressed in specific cell types (Zhang *et al.*, 2020). Following on from my results, a key experiment will require GCamp expression in thalamic relay cells projecting to visual cortex. It would be possible to image

terminals originating from these neurons to layer 4 and thereby assess whether thalamic drive is altered over seconds as a major contributing factor in short-term adaptation. The easiest implementation of this technique in our current set-up would be to use fibre photometry. Fibre photometry makes use of optic canula to record the population GCamp signal from the brain, rather than trying to achieve any single cell resolution (Gunaydin *et al.*, 2014). Alternatively, new one-photon endoscopic imaging systems (Jung *et al.*, 2004) could be used to attempt to image individual neurons in the thalamus itself, although this approach has limited capacity for single cell resolution except in sparsely distributed cell types like inhibitory neurons. Nevertheless, adaptation of these techniques may allow single cell resolution without the requirement of 2-photon microscopes (Resendez *et al.*, 2016). That being said, future experiments with single cell resolution will likely benefit from the employment of a two-photon microscope as this provides the necessary capacity to discriminate neurons that spatial overlap in the X and Y planes.

Calcium imaging results using the same paradigm as described in this thesis have been obtained by the Bear lab (Kim *et al.*, 2020; Hayden *et al.*, 2021), providing useful information on the activity of different cell types, both across SRP and shorter timescales. However, a current limitation of calcium imaging is its reduced temporal resolution compared to electrophysiology (Cossart *et al.*, 2005; Higley & Cardin, 2022). Furthermore, imaging calcium transients is an indirect readout of synaptic and action potentials. Thus, recording cell spiking with high temporal resolution can currently only be achieved using electrophysiology. Modern approaches for single unit electrophysiological recordings make use of laminar probes, often with massive numbers of recording sites that can rival the cell yield of calcium imaging (Steinmetz *et al.*, 2021). Spike sorting can be used

to identify unit waveforms that come from individual cells while recording from laminar probes (Rossant *et al.*, 2016). In addition to clustering units that originate from individual cells, the shape of the waveform can be used to identify different cell types. The peak-peak interval and ratio of positive and negative peak can differentiate cells into putative PV+ neurons (fast-spiking) and putative pyramidal cells (regular spiking) (Andermann *et al.*, 2004; Mitchell *et al.*, 2007; Cottam *et al.*, 2013). However, this does not provide a definitive identification of these cell types. Therefore, a more robust method used to identify cell types is photostimulation-assisted identification of neuronal populations (PINP) (Lima *et al.*, 2009). PINP makes use of genetically defined expression of ChR in specific cell types; action potentials can then be evoked in these ChR expressing cells with light during laminar probe recordings to isolate the spikes originating from specific cell classes. An exciting experimental approach that combines the benefits of electrophysiology and calcium imaging, and which is gaining traction, is use of genetically encoded voltage indicators (GEVIs) (Piatkevich *et al.*, 2018; Abdelfattah *et al.*, 2019; Liu *et al.*, 2022). The imaged activity of GEVIs tightly follow electrical dynamics recorded with patch clamping (Villette *et al.*, 2019). Imaging of GEVIs requires fast 2-photon scanning. However, recent advances in 2-photon imaging can provide 15-30 kilohertz 2-photon sampling in awake behaving animals (Kirkby *et al.*, 2010; Villette *et al.*, 2019; Griffiths *et al.*, 2020; Liu *et al.*, 2022). Nonetheless, voltage imaging can be performed using a 1-photon microscope, which may be useful for sparsely distributed populations of neurons such as inhibitory neurons or where single cell resolution is not required (Piatkevich *et al.*, 2019). Therefore, voltage imaging is a technique which makes use of the high spatial resolution of calcium imaging and the high temporal

resolution of electrophysiology and would be an informative approach to understanding the phenomena described in this thesis.

In the current thesis, an extracellular signal, the local field potential (LFP), is recorded from within the cortex of mice using chronically implanted tungsten electrodes. These local field potentials predominantly reflect synchronous synaptic inputs to cells (Buzsáki *et al.*, 2012). In humans, similar electrical potentials and the resultant magnetic fields are recorded through EEG and MEG respectively (Lopes da Silva, 2013), and provide the core readouts of all clinical neurophysiology. Both EEG and MEG are recorded non-invasively from the scalp of humans but reflect activity of the same summated synaptic signal in cortical circuits, albeit attenuated, as the LFP (Buzsáki *et al.*, 2012; Cohen, 2017). Therefore, recording local field potentials and spiking from mouse cortex can contribute to understanding the underlying physiology which contribute to EEG/ MEG recorded in humans. An example of this comes from Sherman and colleagues (2016) who found that model-derived predictions of laminar specific excitatory drive that contribute to beta events recorded using MEG were present in laminar recordings from mice and non-human primates (Sherman *et al.*, 2016). Therefore, Sherman et al. (2016) used animal recordings to confirm their model derived predictions of the electrical currents that contribute to the non-invasive surface signal, serving as an example of the predictive power of depth recordings in animals. Simultaneous depth and surface field potential recordings can be performed in mice (Hayden *et al.*, 2023) and in humans (Barborica *et al.*, 2023). By using depth and surface electrodes in parallel, one could investigate the synaptic currents and spiking activity underlying the event-related potential and oscillatory events recorded from the surface, particularly in conjunction with interventional approaches like optogenetics. Therefore, gaining a deep

understanding of the underlying circuit-level and molecular events that give rise to human EEG/ MEG recordings. In this thesis, for instance, I have discussed the phenomenon of mismatch negativity, which is one of the most widely used plasticity paradigms in human subjects, and our mouse work is contributing an understanding of the contribution of SOM+ neurons to this phenomenon.

6.5 Readouts of behaviour

Behavioural habituation accompanies SRP during visual stimulus presentation (Cooke *et al.*, 2015). However, the behavioural signal recorded during visual stimuli mainly reflects front paw movement and is a relatively crude signal acquired through a piezo-electric device. It is well established that behaviour alters the activity of responses in visual cortex (Niell & Stryker, 2010; Vinck *et al.*, 2015; Pakan *et al.*, 2016). However, the VEP differences observed in response to familiar and novel stimuli discussed here are not due to differences in ongoing behavioural activity or arousal, and persist whether the animal is moving or still (Hayden *et al.*, 2021). Therefore, the resultant VEP difference to familiar and novel stimuli are not influenced by behaviour or arousal. Furthermore, mice exhibit behavioural habituation when allowed to freely explore visual stimuli presented. Following this free exploration of visual stimuli, there is potentiation of the VEP and suppression of head-fixed behavioural responses to the familiar stimulus (Cooke *et al.*, 2015). Therefore, SRP and habituation occur regardless of how much activity the animal is undertaking.

Many previous studies (Niell & Stryker, 2010; Vinck *et al.*, 2015; Pakan *et al.*, 2016) investigated the effect of running on visual responses. In contrast, Cooke et al. (2015) and Hayden et al. (2021) acquire only forepaw movement through a piezoelectric device, as we do in this thesis. Both running and forepaw readouts of behaviour are relatively crude. More recent work has sought to

capture finer behavioural details in mice by videoing orofacial movements and paw digit movement (Mathis *et al.*, 2018; Stringer *et al.*, 2019; Birman *et al.*, 2022; Syeda *et al.*, 2022). The motion in the face of mice is represented in the activity of visual cortex and represents a greater proportion of explainable variance in cortical activity than running, pupil deflections and whisking combined (Stringer *et al.*, 2019). Therefore, use of the analysis pipelines DeepLabCut (Mathis *et al.*, 2018) and FaceMap (Syeda *et al.*, 2022) will be required to asses habituation of face and paw movement in the experiments acquired in this thesis. Fortunately, we have acquired high-definition video recordings of both body and face movements in the mice included in the majority of this thesis, so further analysis of existing data is likely to yield important new insights.

In the current experiments, behaviour must be normalised to pre-stimulus movement from the mouse to ensure an accurate read-out of stimulus evoked behavioural responses. These baseline noise effects will contribute to the variability of the behavioural signal. To prevent baseline noise effects, a closed-loop system can be implemented based on the animal's behaviour (Buccino *et al.*, 2018). Therefore, in future experiments, processing the piezo-electrical signal in real-time will allow presentation of visual stimuli when the animal is not moving to allow a true read-out of stimulus evoked behavioural responses.

6.6 Potential mechanisms of altered neural activity resulting behavioural habituation?

Investigations into the mechanisms that mediate habituation have been ongoing for decades. Some of the original theories as to the mechanisms of habituation postulated that habituation simply results from decrements in the response of the brain through feedforward plasticity, either at the synapse or intrinsically within receptive neurons (Horn, 1967). However, this theory failed to account for the

phenomenon of dishabituation, by which presentation of novelty can restore response to a repeated familiar stimulus. An alternative theory, known as the dual-process model, suggests that in response to stimuli there is both response decrement in stimulus-specific pathways and concomitant sensitisation of overall 'state', which additively can account for the dishabituation effect. These two phenomena interact to produce an output curve which has an initial increase followed by depression (Groves & Thompson, 1970). Both these ideas predict that depression of responses to sensory input are the key driver for habituation. However, there are alternative theories that suggest that behavioural habituation results from inhibition gating behavioural output. The comparator model theory states that this inhibitory output may stem from a top-down system that has a true 'memory' of the familiar stimuli and the inhibitory output matches the excitatory input from the stimulus itself (Sokolov, 1963). An alternative explanation, the negative model theory suggests that reduced behavioural output results from increased local inhibitory drive which matches the excitatory output (Ramaswami, 2014).

The theories implicating inhibition align somewhat with the ideas discussed in this thesis. However, our findings add another layer of complexity in the sense that inhibition of inhibition seems to play a critical role in long-term habituation. We find that increased SOM+ mediated inhibition of PV+ neurons result in potentiation of the VEP magnitude. As SOM+ mediated inhibition increases and PV+ mediated inhibition decreases the peak firing in layer 4 cells is increased. This tightly controlled increased firing of layer 4 and layer 2/3 may recruit local inhibitory drive resulting in inhibition of layer 5 (Pluta *et al.*, 2015, 2019). This local inhibition in V1 which results in decreased output from layer 5

may act as a 'negative image' (Ramaswami, 2014) of the increased excitatory activity originating from layer 4.

Thus, following SRP it is likely that the net output of the visual cortex is reduced. This reduced output from the visual cortex may decrease drive of the neuron in the pulvinar nucleus (Blot *et al.*, 2021) and therefore reduce visually guided behaviour (Kaas & Lyon, 2007) manifesting as habituation observed in the current thesis. The pulvinar nucleus may be acting as a comparator-like system (Sokolov, 1963) and rather than receiving inhibition from a top-down source (the visual cortex), it computes the relative activity level of V1 and uses this signal for visually guided behaviour. However, we currently have no direct evidence of how altered engagement of inhibition in V1 ultimately leads changes in downstream brain regions and results in behavioural habituation.

6.7 Why are habituation, adaptation and the mechanisms underlying these phenomena important?

Despite theoretical models and experimental studies suggesting that synaptic/cellular response decrements and recruitment of inhibitory systems underlie adaptation and habituation, the question remains as to why the brain adapts and gates behavioural output. One theory is that adaptation serves to create efficiency in the system by reducing redundancy. Barlow (1961) states that:

> 'The hypothesis says that, for a given class of input message, it will choose the code that requires the smallest average expenditure of impulses in the output. Or putting it briefly, it economizes impulses; but it is important to realize that it can only do this on the average; the commonly occurring inputs are allotted outputs with few impulses, but there may be infrequent inputs that require more impulses in the output than in the input.' (Barlow, 1961)

Therefore, the temporal dynamics of sensory inputs produces adaptation of neuronal activity to result in efficient processing. Importantly, adaptation can serve to shift the input-output responses to represent the probability distribution

of the stimulus (Louie & Glimcher, 2012). Therefore, the system may be acting in the most efficient way as the neuronal response distribution matches the stimulus distribution, and therefore reduces energy expenditure.

Habituation of the system may promote appropriate dedication of attention to only the most salient aspects of the environment. Novelty may focus attention, but this may prevent detection of change elsewhere. A habituated state may be better set up for detection of change. The habituated state likely reflects an inattentive state, as there is a loss of high gamma and increased in lower frequency oscillations (Fries *et al.*, 2001; Hayden *et al.*, 2021). There is increased bursting of thalamic neurons following a shift from an attentive to inattentive state (Bezdudnaya *et al.*, 2006) and bursting is negatively corrected with attention (Weyand *et al.*, 2001). This shift in bursting may ready the system for information breakthrough by circumventing feedforward inhibition (Swadlow & Gusev, 2001) and allow dedication of attention to this salient stimulus.

An additional theory is that the brain is acting to reduce the difference between its internal representation of inputs (i.e. a prediction based on a prior model) and the direct sensory input (Friston, 2010). Predictive coding states that there is balancing of top-down inputs (the prediction signal) and sensory input such that only information which was not predicted (the error signal) can pass up the processing stream (Keller & Mrsic-Flogel, 2018). This theory is cohesive with the finding in this thesis that inhibitory systems may mediate top-down control over bottom up-sensory input. The average increase in firing among layer 4 cells in response to novel stimuli compared to familiar (Kim *et al.*, 2020; Hayden *et al.*, 2023) may reflect an error signal, which is the result of modified inhibition. However, the finding that there is modified inhibition of inhibition which results in potentiation of the VEP and increased peak firing at 50 ms in response to a

familiar stimulus (Cooke *et al.*, 2015; Hayden *et al.*, 2023) is not cohesive with the predictive coding theory.

In humans, deficits in habituation occur across a range of psychiatric disorders (McDiarmid *et al.*, 2017). Investigating the underlying cell types and circuits which contribute to adaptation and behavioural habituation will provide mechanistic insight into habituation and therefore the systems that may be disrupted in disease. Impairments in inhibition are common in neurological disorders (Heinze *et al.*, 2021) and likely contribute to habituation deficits (Barron *et al.*, 2017). Furthermore, use of animal models of disorders, such as genetically defined forms of autism and intellectual disability, have found disruption in sleep, adaptation, and habituation (Kissinger *et al.*, 2020). Interventional methodologies and animal models of disease could be used in concert to identify the origins of circuit dysfunction as a result of these genetic conditions. However, when using these experimental techniques, care must be taken in the methodology used as different mechanisms may mediate different forms of habituation (McDiarmid *et al.*, 2019).

Behavioural habituation, experience-dependent plasticity and sensory adaptation are fundamental forms of learning and sensory processing which are easily measurable in mice, primates, and humans. Investigation into these phenomena has provided further understanding of the cells and circuits which mediate these changes. In addition, plasticity and adaptation are disrupted in an animal model of disease. The underlying physiology contributing to simple forms of learning and sensory processing in animals may provide insight into comparable recordings from humans and the disruptions observed in disease.

Bibliography

Abdelfattah, A.S., Kawashima, T., Singh, A., Novak, O., Liu, H., Shuai, Y., Huang, Y.-C., Campagnola, L., Seeman, S.C., Yu, J., Zheng, J., Grimm, J.B., Patel, R., Friedrich, J., Mensh, B.D., Paninski, L., Macklin, J.J., Murphy, G.J., Podgorski, K., Lin, B.-J., Chen, T.-W., Turner, G.C., Liu, Z., Koyama, M., Svoboda, K., Ahrens, M.B., Lavis, L.D., & Schreiter, E.R. (2019) Bright and photostable chemigenetic indicators for extended in vivo voltage imaging. *Science*, **365**, 699–704.

Adesnik, H. & Abdeladim, L. (2021) Probing neural codes with two-photon holographic optogenetics. *Nat. Neurosci.*, **24**, 1356–1366.

Adesnik, H., Bruns, W., Taniguchi, H., Huang, Z.J., & Scanziani, M. (2012) A neural circuit for spatial summation in visual cortex. *Nature*, **490**, 226–231.

Agim, Z.S., Esendal, M., Briollais, L., Uyan, O., Meschian, M., Martinez, L.A.M., Ding, Y., Basak, A.N., & Ozcelik, H. (2013) Discovery, validation and characterization of Erbb4 and Nrg1 haplotypes using data from three genome-wide association studies of schizophrenia. *PLoS ONE*, **8**, e53042.

Ahmed, B., Anderson, J.C., Douglas, R.J., Martin, K.A., & Nelson, J.C. (1994) Polyneuronal innervation of spiny stellate neurons in cat visual cortex. *J. Comp. Neurol.*, **341**, 39–49.

Alitto, H.J. & Dan, Y. (2010) Function of inhibition in visual cortical processing. *Curr. Opin. Neurobiol.*, **20**, 340–346.

Andermann, M.L., Ritt, J., Neimark, M.A., & Moore, C.I. (2004) Neural correlates of vibrissa resonance; band-pass and somatotopic representation of high-frequency stimuli. *Neuron*, **42**, 451–463.

Armbruster, B.N., Li, X., Pausch, M.H., Herlitze, S., & Roth, B.L. (2007) Evolving the lock to fit the key to create a family of G protein-coupled receptors potently activated by an inert ligand. *Proc Natl Acad Sci USA*, **104**, 5163–5168.

Atallah, B.V., Bruns, W., Carandini, M., & Scanziani, M. (2012) Parvalbumin-expressing interneurons linearly transform cortical responses to visual stimuli. *Neuron*, **73**, 159–170.

Aton, S.J., Suresh, A., Broussard, C., & Frank, M.G. (2014) Sleep promotes cortical response potentiation following visual experience. *Sleep*, **37**, 1163–1170.

Barborica, A., Mindruta, I., López-Madrona, V.J., Alario, F.-X., Trébuchon, A., Donos, C., Oane, I., Pistol, C., Mihai, F., & Bénar, C.G. (2023) Studying memory processes at different levels with simultaneous depth and surface EEG recordings. *Front. Hum. Neurosci.*, **17**, 1154038.

Barlow, H.B. (1961) Possible principles underlying the transformations of sensory messages. In Rosenblith, W.A. (ed), *Sensory Communication*. The MIT Press, pp. 216–234.

Barron, H.C., Vogels, T.P., Behrens, T.E., & Ramaswami, M. (2017) Inhibitory engrams in perception and memory. *Proc Natl Acad Sci USA*, **114**, 6666–6674.

Batista-Brito, R., Majumdar, A., Nuño, A., Ward, C., Barnes, C., Nikouei, K., Vinck, M., & Cardin, J.A. (2023) Developmental loss of ErbB4 in PV interneurons disrupts state-dependent cortical circuit dynamics. *Mol. Psychiatry*,.

Beattie, E.C., Carroll, R.C., Yu, X., Morishita, W., Yasuda, H., von Zastrow, M., & Malenka, R.C. (2000) Regulation of AMPA receptor endocytosis by a signaling mechanism shared with LTD. *Nat. Neurosci.*, **3**, 1291–1300.

Beierlein, M. & Connors, B.W. (2002) Short-term dynamics of thalamocortical and intracortical synapses onto layer 6 neurons in neocortex. *J. Neurophysiol.*, **88**, 1924–1932.

Beierlein, M., Gibson, J.R., & Connors, B.W. (2003) Two dynamically distinct inhibitory networks in layer 4 of the neocortex. *J. Neurophysiol.*, **90**, 2987–3000.

Benucci, A., Saleem, A.B., & Carandini, M. (2013) Adaptation maintains population homeostasis in primary visual cortex. *Nat. Neurosci.*, **16**, 724–729.

Bezdudnaya, T., Cano, M., Bereshpolova, Y., Stoelzel, C.R., Alonso, J.-M., & Swadlow, H.A. (2006) Thalamic burst mode and inattention in the awake LGNd. *Neuron*, **49**, 421–432.

Bindels, D.S., Haarbosch, L., van Weeren, L., Postma, M., Wiese, K.E., Mastop, M., Aumonier, S., Gotthard, G., Royant, A., Hink, M.A., & Gadella, T.W.J. (2017) mScarlet: a bright monomeric red fluorescent protein for cellular imaging. *Nat. Methods*, **14**, 53–56.

Binzegger, T., Douglas, R.J., & Martin, K.A.C. (2004) A quantitative map of the circuit of cat primary visual cortex. *J. Neurosci.*, **24**, 8441–8453.

Birman, D., Bonacchi, N., Buchanan, K., Chapuis, G., Hutenburg, J.M., Meijer, G., Paninski, L., Schartner, M., Svoboda, K., Wells, M., Whiteway, M.R., Winter, O., & The International Brain Laboratory (2022) Video hardware and software for the International Brain Laboratory. *Figshare*,.

Blatt, G.J. & Fatemi, S.H. (2011) Alterations in GABAergic biomarkers in the autism brain: research findings and clinical implications. *Anat Rec (Hoboken)*, **294**, 1646–1652.

Bliss, T.V. & Collingridge, G.L. (1993) A synaptic model of memory: long-term potentiation in the hippocampus. *Nature*, **361**, 31–39.

Bliss, T.V. & Lomo, T. (1973) Long-lasting potentiation of synaptic transmission in the dentate area of the anaesthetized rabbit following stimulation of the perforant path. *J Physiol (Lond)*, **232**, 331–356.

Blot, A., Roth, M.M., Gasler, I., Javadzadeh, M., Imhof, F., & Hofer, S.B. (2021) Visual intracortical and transthalamic pathways carry distinct information to cortical areas. *Neuron*, **109**, 1996-2008.e6.

Bonds, A.B. (1984) Spatial adaptation of the cortical visual evoked potential of the cat. *Invest. Ophthalmol. Vis. Sci.*, **25**, 640–646.

Borden, P.Y., Wright, N.C., Morrissette, A.E., Jaeger, D., Haider, B., & Stanley, G.B. (2022) Thalamic bursting and the role of timing and synchrony in thalamocortical signaling in the awake mouse. *Neuron*, **110**, 2836-2853.e8.

Borg-Graham, L.J., Monier, C., & Frégnac, Y. (1998) Visual input evokes transient and strong shunting inhibition in visual cortical neurons. *Nature*, **393**, 369–373.

Bortone, D.S., Olsen, S.R., & Scanziani, M. (2014) Translaminar inhibitory cells recruited by layer 6 corticothalamic neurons suppress visual cortex. *Neuron*, **82**, 474–485.

Buccino, A.P., Lepperød, M.E., Dragly, S.-A., Häfliger, P., Fyhn, M., & Hafting, T. (2018) Open source modules for tracking animal behavior and closed-loop stimulation based on Open Ephys and Bonsai. *J. Neural Eng.*, **15**, 055002.

Buzsáki, G., Anastassiou, C.A., & Koch, C. (2012) The origin of extracellular fields and currents--EEG, ECoG, LFP and spikes. *Nat. Rev. Neurosci.*, **13**, 407–420.

Calebiro, D. & Godbole, A. (2018) Internalization of G-protein-coupled receptors: Implication in receptor function, physiology and diseases. *Best Pract. Res. Clin. Endocrinol. Metab.*, **32**, 83–91.

Campagnola, L., Seeman, S.C., Chartrand, T., Kim, L., Hoggarth, A., Gamlin, C., Ito, S., Trinh, J., Davoudian, P., Radaelli, C., Kim, M.-H., Hage, T., Braun, T., Alfiler, L., Andrade, J., Bohn, P., Dalley, R., Henry, A., Kebede, S., Alice, M., Sandman, D., Williams, G., Larsen, R., Teeter, C., Daigle, T.L., Berry, K., Dotson, N., Enstrom, R., Gorham, M., Hupp, M., Dingman Lee, S., Ngo, K., Nicovich, P.R., Potekhina, L., Ransford, S., Gary, A., Goldy, J., McMillen, D., Pham, T., Tieu, M., Siverts, L., Walker, M., Farrell, C., Schroedter, M., Slaughterbeck, C., Cobb, C., Ellenbogen, R., Gwinn, R.P., Keene, C.D., Ko, A.L., Ojemann, J.G., Silbergeld, D.L., Carey, D., Casper, T., Crichton, K., Clark, M., Dee, N., Ellingwood, L., Gloe, J., Kroll, M., Sulc, J., Tung, H., Wadhwani, K., Brouner, K., Egdorf, T., Maxwell, M., McGraw, M., Pom, C.A., Ruiz, A., Bomben, J., Feng, D., Hejazinia, N., Shi, S., Szafer, A., Wakeman, W., Phillips, J., Bernard, A., Esposito, L., D'Orazi, F.D., Sunkin, S., Smith, K., Tasic, B., Arkhipov, A., Sorensen, S., Lein, E., Koch, C., Murphy, G., Zeng, H., & Jarsky, T. (2022) Local connectivity and synaptic dynamics in mouse and human neocortex. *Science*, **375**, eabj5861.

Capogna, M. & Pearce, R.A. (2011) GABA A,slow: causes and consequences. *Trends Neurosci.*, **34**, 101–112.

Cardin, J.A., Carlén, M., Meletis, K., Knoblich, U., Zhang, F., Deisseroth, K., Tsai, L.-H., & Moore, C.I. (2009) Driving fast-spiking cells induces gamma rhythm and controls sensory responses. *Nature*, **459**, 663–667.

Cardin, J.A., Carlén, M., Meletis, K., Knoblich, U., Zhang, F., Deisseroth, K., Tsai, L.-H., & Moore, C.I. (2010) Targeted optogenetic stimulation and recording of neurons in vivo using cell-type-specific expression of Channelrhodopsin-2. *Nat. Protoc.*, **5**, 247–254.

Carrillo-Reid, L., Han, S., Yang, W., Akrouh, A., & Yuste, R. (2019) Controlling visually guided behavior by holographic recalling of cortical ensembles. *Cell*, **178**, 447-457.e5.

Carrillo-Reid, L., Miller, J.-E.K., Hamm, J.P., Jackson, J., & Yuste, R. (2015) Endogenous sequential cortical activity evoked by visual stimuli. *J. Neurosci.*, **35**, 8813–8828.

Chaloner, F.A. & Cooke, S.F. (2022) Multiple mechanistically distinct timescales of neocortical plasticity occur during habituation. *Front. Cell. Neurosci.*, **16**, 840057.

Chamberland, S., Nebet, E.R., Valero, M., Hanani, M., Egger, R., Larsen, S.B., Eyring, K.W., Buzsáki, G., & Tsien, R.W. (2023) Brief synaptic inhibition persistently interrupts firing of fast-spiking interneurons. *Neuron*, **111**, 1264-1281.e5.

Chance, F.S., Abbott, L.F., & Reyes, A.D. (2002) Gain modulation from background synaptic input. *Neuron*, **35**, 773–782.

Chen, G., Zhang, Y., Li, X., Zhao, X., Ye, Q., Lin, Y., Tao, H.W., Rasch, M.J., & Zhang, X. (2017) Distinct Inhibitory Circuits Orchestrate Cortical beta and gamma Band Oscillations. *Neuron*, **96**, 1403-1418.e6.

Chen, I.-W., Helmchen, F., & Lütcke, H. (2015) Specific Early and Late Oddball-Evoked Responses in Excitatory and Inhibitory Neurons of Mouse Auditory Cortex. *J. Neurosci.*, **35**, 12560–12573.

Chung, S., Li, X., & Nelson, S.B. (2002) Short-term depression at thalamocortical synapses contributes to rapid adaptation of cortical sensory responses in vivo. *Neuron*, **34**, 437–446.

Clawson, B.C., Durkin, J., Suresh, A.K., Pickup, E.J., Broussard, C.G., & Aton, S.J. (2018) Sleep promotes, and sleep loss inhibits, selective changes in firing rate, response properties and functional connectivity of primary visual cortex neurons. *Front. Syst. Neurosci.*, **12**, 40.

Cohen, M.X. (2017) Where does EEG come from and what does it mean? *Trends Neurosci.*, **40**, 208–218.

Collingridge, G.L., Kehl, S.J., & McLennan, H. (1983) Excitatory amino acids in synaptic transmission in the Schaffer collateral-commissural pathway of the rat hippocampus. *J Physiol (Lond)*, **334**, 33–46.

Collingridge, G.L., Peineau, S., Howland, J.G., & Wang, Y.T. (2010) Long-term depression in the CNS. *Nat. Rev. Neurosci.*, **11**, 459–473.

Condylis, C., Ghanbari, A., Manjrekar, N., Bistrong, K., Yao, S., Yao, Z., Nguyen, T.N., Zeng, H., Tasic, B., & Chen, J.L. (2022) Dense functional and molecular readout of a circuit hub in sensory cortex. *Science*, **375**, eabl5981.

Connors, B.W., Malenka, R.C., & Silva, L.R. (1988) Two inhibitory postsynaptic potentials, and GABAA and GABAB receptor-mediated responses in neocortex of rat and cat. *J Physiol (Lond)*, **406**, 443–468.

Constantinople, C.M. & Bruno, R.M. (2013) Deep cortical layers are activated directly by thalamus. *Science*, **340**, 1591–1594.

Cooke, S.F. & Bear, M.F. (2010) Visual experience induces long-term potentiation in the primary visual cortex. *J. Neurosci.*, **30**, 16304–16313.

Cooke, S.F. & Bear, M.F. (2014) How the mechanisms of long-term synaptic potentiation and depression serve experience-dependent plasticity in primary visual cortex. *Philos. Trans. R. Soc. Lond. B Biol. Sci.*, **369**, 20130284.

Cooke, S.F., Komorowski, R.W., Kaplan, E.S., Gavornik, J.P., & Bear, M.F. (2015) Visual recognition memory, manifested as long-term habituation, requires synaptic plasticity in V1. *Nat. Neurosci.*, **18**, 262–271.

Cooke, S.F. & Ramaswami, M. (2020) Ignoring the Innocuous: The Neural Mechanisms of Habituation. In Poeppel, D., Mangun, G., & Gazzaniga, M. (eds), *The Cognitive Neurosciences: 6th Edition*, 6th edn. MIT Press, Cambridge, Massachusetts, USA, p. 197.

Cossart, R., Ikegaya, Y., & Yuste, R. (2005) Calcium imaging of cortical networks dynamics. *Cell Calcium*, **37**, 451–457.

Costantini, L.M., Baloban, M., Markwardt, M.L., Rizzo, M.A., Guo, F., Verkhusha, V.V., & Snapp, E.L. (2015) A palette of fluorescent proteins optimized for diverse cellular environments. *Nat. Commun.*, **6**, 7670.

Costantini, L.M., Fossati, M., Francolini, M., & Snapp, E.L. (2012) Assessing the tendency of fluorescent proteins to oligomerize under physiologic conditions. *Traffic*, **13**, 643–649.

Costantini, L.M. & Snapp, E.L. (2013) Fluorescent proteins in cellular organelles: serious pitfalls and some solutions. *DNA Cell Biol.*, **32**, 622–627.

Cottam, J.C.H., Smith, S.L., & Häusser, M. (2013) Target-specific effects of somatostatin-expressing interneurons on neocortical visual processing. *J. Neurosci.*, **33**, 19567–19578.

Cruikshank, S.J., Lewis, T.J., & Connors, B.W. (2007) Synaptic basis for intense thalamocortical activation of feedforward inhibitory cells in neocortex. *Nat. Neurosci.*, **10**, 462–468.

Cruikshank, S.J., Urabe, H., Nurmikko, A.V., & Connors, B.W. (2010) Pathway-specific feedforward circuits between thalamus and neocortex revealed by selective optical stimulation of axons. *Neuron*, **65**, 230–245.

de Lecea, L., del Río, J.A., & Soriano, E. (1995) Developmental expression of parvalbumin mRNA in the cerebral cortex and hippocampus of the rat. *Brain Res. Mol. Brain Res.*, **32**, 1–13.

Deitch, D., Rubin, A., & Ziv, Y. (2021) Representational drift in the mouse visual cortex. *Curr. Biol.*, **31**, 4327-4339.e6.

Del Pino, I., García-Frigola, C., Dehorter, N., Brotons-Mas, J.R., Alvarez-Salvado, E., Martínez de Lagrán, M., Ciceri, G., Gabaldón, M.V., Moratal, D., Dierssen, M., Canals, S., Marín, O., & Rico, B. (2013) Erbb4 deletion from fast-spiking interneurons causes schizophrenia-like phenotypes. *Neuron*, **79**, 1152–1168.

Dorsett, C., Philpot, B.D., Smith, S.L., & Smith, I.T. (2021) The impact of SST and PV interneurons on nonlinear synaptic integration in the neocortex. *eNeuro*, **8**.

Dudek, S.M. & Bear, M.F. (1992) Homosynaptic long-term depression in area CA1 of hippocampus and effects of N-methyl-D-aspartate receptor blockade. *Proc Natl Acad Sci USA*, **89**, 4363–4367.

Durkin, J., Suresh, A.K., Colbath, J., Broussard, C., Wu, J., Zochowski, M., & Aton, S.J. (2017) Cortically coordinated NREM thalamocortical oscillations play an essential, instructive role in visual system plasticity. *Proc Natl Acad Sci USA*, **114**, 10485–10490.

Durkin, J.M. & Aton, S.J. (2019) How sleep shapes thalamocortical circuit function in the visual system. *Annu. Rev. Vis. Sci.*, **5**, 295–315.

El-Boustani, S. & Sur, M. (2014) Response-dependent dynamics of cell-specific inhibition in cortical networks in vivo. *Nat. Commun.*, **5**, 5689.

Escobar Sanabria, D., Johnson, L.A., Yu, Y., Busby, Z., Nebeck, S., Zhang, J., Harel, N., Johnson, M.D., Molnar, G.F., & Vitek, J.L. (2020) Real-time suppression and amplification of frequency-specific neural activity using stimulation evoked oscillations. *Brain Stimulat.*, **13**, 1732–1742.

Farel, P.B. & Thompson, R.F. (1976) Habituation of a monosynaptic response in frog spinal cord: evidence for a presynaptic mechanism. *J. Neurophysiol.*, **39**, 661–666.

Favuzzi, E., Marques-Smith, A., Deogracias, R., Winterflood, C.M., Sánchez-Aguilera, A., Mantoan, L., Maeso, P., Fernandes, C., Ewers, H., & Rico, B. (2017) Activity-Dependent Gating of Parvalbumin Interneuron Function by the Perineuronal Net Protein Brevican. *Neuron*, **95**, 639-655.e10.

Fazzari, P., Paternain, A.V., Valiente, M., Pla, R., Luján, R., Lloyd, K., Lerma, J., Marín, O., & Rico, B. (2010) Control of cortical GABA circuitry development by Nrg1 and ErbB4 signalling. *Nature*, **464**, 1376–1380.

Feldmeyer, D. (2012) Excitatory neuronal connectivity in the barrel cortex. *Front. Neuroanat.*, **6**, 24.

Ferguson, K.A. & Cardin, J.A. (2020) Mechanisms underlying gain modulation in the cortex. *Nat. Rev. Neurosci.*, **21**, 80–92.

Finnie, P.S.B., Komorowski, R.W., & Bear, M.F. (2021) The spatiotemporal organization of experience dictates hippocampal involvement in primary visual cortical plasticity. *BioRxiv*,.

Fino, E. & Yuste, R. (2011) Dense inhibitory connectivity in neocortex. *Neuron*, **69**, 1188–1203.

Fong, M.-F., Finnie, P.S., Kim, T., Thomazeau, A., Kaplan, E.S., Cooke, S.F., & Bear, M.F. (2020) Distinct Laminar Requirements for NMDA Receptors in Experience-Dependent Visual Cortical Plasticity. *Cereb. Cortex*, **30**, 2555–2572.

Foster, K.A. & Regehr, W.G. (2004) Variance-mean analysis in the presence of a rapid antagonist indicates vesicle depletion underlies depression at the climbing fiber synapse. *Neuron*, **43**, 119–131.

Frenkel, M.Y., Sawtell, N.B., Diogo, A.C.M., Yoon, B., Neve, R.L., & Bear, M.F. (2006) Instructive effect of visual experience in mouse visual cortex. *Neuron*, **51**, 339–349.

Fries, P., Reynolds, J.H., Rorie, A.E., & Desimone, R. (2001) Modulation of oscillatory neuronal synchronization by selective visual attention. *Science*, **291**, 1560–1563.

Friston, K. (2010) The free-energy principle: a unified brain theory? *Nat. Rev. Neurosci.*, **11**, 127–138.

Gabbott, P.L. & Bacon, S.J. (1994) Two types of interneuron in the dorsal lateral geniculate nucleus of the rat: a combined NADPH diaphorase histochemical and GABA immunocytochemical study. *J. Comp. Neurol.*, **350**, 281–301.

Gabernet, L., Jadhav, S.P., Feldman, D.E., Carandini, M., & Scanziani, M. (2005) Somatosensory integration controlled by dynamic thalamocortical feed-forward inhibition. *Neuron*, **48**, 315–327.

Gallimore, C.G., Ricci, D., & Hamm, J.P. (2023) Spatiotemporal dynamics across visual cortical laminae support a predictive coding framework for interpreting mismatch responses. *BioRxiv*,.

Garrett, M., Groblewski, P., Piet, A., Ollerenshaw, D., Yavorska, I., Najafi, F., Amster, A., Bennett, C., Buice, M., Caldejon, S., Casal, L., D'Orazi, F., Daniel, S., de Vries, S.E., Kapner, D., Kiggins, J., Lecoq, J., Ledochowitsch, P., Manavi, S., Mei, N., Morrison, C.B., Naylor, S., Orlova, N., Perkins, J., Ponvert, N., Roll, C., Seid, S., Williams, D., Williford, A., Ahmed, R., Amine, D., Billeh, Y., Bowman, C., Cain, N., Cho, A., Dawe, T., Departee, M., Desoto, M., Feng, D., Gale, S., Gelfand, E., Gradis, N., Grasso, C., Hancock, N., Hu, B., Hytnen, R., Jia, X., Johnson, T., Kato, I., Kivikas, S., Kuan, L., L'Heureux, Q., Lambert, S., Leon, A., Liang, E., Long, F., Mace, K., de Abril, I.M., Mochizuki, C., Nayan, C., North, K., Ng, L., Ocker, G.K., Oliver, M., Rhoads, P., Ronellenfitch, K., Schelonka, K., Sevigny, J., Sullivan, D., Sutton, B., Swapp, J., Nguyen, T.K., Waughman, X., Wilkes, J., Wang, M., Farrell, C., Wakeman, W., Zeng, H., Phillips, J., Mihalas, S., Arkhipov, A., Koch, C., & Olsen, S.R. (2023) Stimulus novelty uncovers coding diversity in visual cortical circuits. *BioRxiv*,.

Garrido, M.I., Kilner, J.M., Stephan, K.E., & Friston, K.J. (2009) The mismatch negativity: a review of underlying mechanisms. *Clin. Neurophysiol.*, **120**, 453–463.

George, W. & Peckham, E.G. (1887) Some observations on the mental powers of spiders. *J. Morphol.*, **1**, 383–419.

Gomez, J.L., Bonaventura, J., Lesniak, W., Mathews, W.B., Sysa-Shah, P., Rodriguez, L.A., Ellis, R.J., Richie, C.T., Harvey, B.K., Dannals, R.F., Pomper, M.G., Bonci, A., & Michaelides, M. (2017) Chemogenetics revealed: DREADD occupancy and activation via converted clozapine. *Science*, **357**, 503–507.

Griffiths, V.A., Valera, A.M., Lau, J.Y., Roš, H., Younts, T.J., Marin, B., Baragli, C., Coyle, D., Evans, G.J., Konstantinou, G., Koimtzis, T., Nadella, K.M.N.S., Punde, S.A., Kirkby, P.A., Bianco, I.H., & Silver, R.A. (2020) Real-time 3D movement correction for two-photon imaging in behaving animals. *Nat. Methods*, **17**, 741–748.

Grigoriou, M., Tucker, A.S., Sharpe, P.T., & Pachnis, V. (1998) Expression and regulation of Lhx6 and Lhx7, a novel subfamily of LIM homeodomain encoding genes, suggests a role in mammalian head development. *Development*, **125**, 2063–2074.

Groves, P.M. & Thompson, R.F. (1970) Habituation: a dual-process theory. *Psychol. Rev.*, **77**, 419–450.

Guillery, R.W. & Sherman, S.M. (2002) Thalamic relay functions and their role in corticocortical communication. *Neuron*, **33**, 163–175.

Gunaydin, L.A., Grosenick, L., Finkelstein, J.C., Kauvar, I.V., Fenno, L.E., Adhikari, A., Lammel, S., Mirzabekov, J.J., Airan, R.D., Zalocusky, K.A., Tye, K.M., Anikeeva, P., Malenka, R.C., & Deisseroth, K. (2014) Natural neural projection dynamics underlying social behavior. *Cell*, **157**, 1535–1551.

Haider, B., Häusser, M., & Carandini, M. (2013) Inhibition dominates sensory responses in the awake cortex. *Nature*, **493**, 97–100.

Haider, B., Schulz, D.P.A., Häusser, M., & Carandini, M. (2016) Millisecond coupling of local field potentials to synaptic currents in the awake visual cortex. *Neuron*, **90**, 35–42.

Hamm, J.P., Shymkiv, Y., Han, S., Yang, W., & Yuste, R. (2021) Cortical ensembles selective for context. *Proc Natl Acad Sci USA*, **118**.

Hamm, J.P. & Yuste, R. (2016) Somatostatin interneurons control a key component of mismatch negativity in mouse visual cortex. *Cell Rep.*, **16**, 597–604.

Harms, L., Michie, P.T., & Näätänen, R. (2016) Criteria for determining whether mismatch responses exist in animal models: Focus on rodents. *Biol. Psychol.*, **116**, 28–35.

Harris, K.D., Hochgerner, H., Skene, N.G., Magno, L., Katona, L., Bengtsson Gonzales, C., Somogyi, P., Kessaris, N., Linnarsson, S., & Hjerling-Leffler, J. (2018) Classes and continua of hippocampal CA1 inhibitory neurons revealed by single-cell transcriptomics. *PLoS Biol.*, **16**, e2006387.

Harris, K.D. & Mrsic-Flogel, T.D. (2013) Cortical connectivity and sensory coding. *Nature*, **503**, 51–58.

Hasenstaub, A., Shu, Y., Haider, B., Kraushaar, U., Duque, A., & McCormick, D.A. (2005) Inhibitory postsynaptic potentials carry synchronized frequency information in active cortical networks. *Neuron*, **47**, 423–435.

Hayden, D.J., Finnie, P.S.B., Thomazeau, A., Li, A.Y., Cooke, S.F., & Bear, M.F. (2023) Electrophysiological signatures of visual recognition memory across all layers of mouse V1. *BioRxiv*,.

Hayden, D.J., Montgomery, D.P., Cooke, S.F., & Bear, M.F. (2021) Visual recognition is heralded by shifts in local field potential oscillations and inhibitory networks in primary visual cortex. *J. Neurosci.*,.

Hebb, D.O. (1949) *The Organization of Behavior*. Routledge, London.

Heintz, T.G., Hinojosa, A.J., Dominiak, S.E., & Lagnado, L. (2022) Opposite forms of adaptation in mouse visual cortex are controlled by distinct inhibitory microcircuits. *Nat. Commun.*, **13**, 1031.

Heinze, K., Barron, H.C., Howes, E.K., Ramaswami, M., & Broome, M.R. (2021) Impaired inhibitory processing: a new therapeutic target for autism and psychosis? *Br. J. Psychiatry*, **218**, 295–298.

Hendry, S.H., Jones, E.G., Emson, P.C., Lawson, D.E., Heizmann, C.W., & Streit, P. (1989) Two classes of cortical GABA neurons defined by differential calcium binding protein immunoreactivities. *Exp. Brain Res.*, **76**, 467–472.

Henschke, J.U., Dylda, E., Katsanevaki, D., Dupuy, N., Currie, S.P., Amvrosiadis, T., Pakan, J.M.P., & Rochefort, N.L. (2020) Reward Association Enhances Stimulus-Specific Representations in Primary Visual Cortex. *Curr. Biol.*, **30**, 1866-1880.e5.

Heynen, A.J., Yoon, B.-J., Liu, C.-H., Chung, H.J., Huganir, R.L., & Bear, M.F. (2003) Molecular mechanism for loss of visual cortical responsiveness following brief monocular deprivation. *Nat. Neurosci.*, **6**, 854–862.

Higley, M.J. & Cardin, J.A. (2022) Spatiotemporal dynamics in large-scale cortical networks. *Curr. Opin. Neurobiol.*, **77**, 102627.

Higley, M.J. & Contreras, D. (2006) Balanced excitation and inhibition determine spike timing during frequency adaptation. *J. Neurosci.*, **26**, 448–457.

Hodgkin, A.L. & Huxley, A.F. (1952) A quantitative description of membrane current and its application to conduction and excitation in nerve. *J Physiol (Lond)*, **117**, 500–544.

Hofer, S.B., Ko, H., Pichler, B., Vogelstein, J., Ros, H., Zeng, H., Lein, E., Lesica, N.A., & Mrsic-Flogel, T.D. (2011) Differential connectivity and response dynamics of excitatory and inhibitory neurons in visual cortex. *Nat. Neurosci.*, **14**, 1045–1052.

Holt, G.R. & Koch, C. (1997) Shunting inhibition does not have a divisive effect on firing rates. *Neural Comput.*, **9**, 1001–1013.

Homann, J., Koay, S.A., Chen, K.S., Tank, D.W., & Berry, M.J. (2022) Novel stimuli evoke excess activity in the mouse primary visual cortex. *Proc Natl Acad Sci USA*, **119**.

Hong, Y.K., Lacefield, C.O., Rodgers, C.C., & Bruno, R.M. (2018) Sensation, movement and learning in the absence of barrel cortex. *Nature*, **561**, 542–546.

Hooks, B.M. & Chen, C. (2020) Circuitry Underlying Experience-Dependent Plasticity in the Mouse Visual System. *Neuron*, **106**, 21–36.

Horn, G. (1967) Neuronal mechanisms of habituation. *Nature*, **215**, 707–711.

Hubel, D.H., Wiesel, T.N., & LeVay, S. (1977) Plasticity of ocular dominance columns in monkey striate cortex. *Philos. Trans. R. Soc. Lond. B Biol. Sci.*, **278**, 377–409.

Hubel, D.H. & Wiesel, T.N. (1962) Receptive fields, binocular interaction and functional architecture in the cat's visual cortex. *J Physiol (Lond)*, **160**, 106–154.

Huberman, A.D. & Niell, C.M. (2011) What can mice tell us about how vision works? *Trends Neurosci.*, **34**, 464–473.

Jiang, X., Shen, S., Cadwell, C.R., Berens, P., Sinz, F., Ecker, A.S., Patel, S., & Tolias, A.S. (2015) Principles of connectivity among morphologically defined cell types in adult neocortex. *Science*, **350**, aac9462.

Jin, M. & Glickfeld, L.L. (2020) Magnitude, time course, and specificity of rapid adaptation across mouse visual areas. *J. Neurophysiol.*, **124**, 245–258.

Jung, J.C., Mehta, A.D., Aksay, E., Stepnoski, R., & Schnitzer, M.J. (2004) In vivo mammalian brain imaging using one- and two-photon fluorescence microendoscopy. *J. Neurophysiol.*, **92**, 3121–3133.

Jurgens, C.W.D., Bell, K.A., McQuiston, A.R., & Guido, W. (2012) Optogenetic stimulation of the corticothalamic pathway affects relay cells and GABAergic neurons differently in the mouse visual thalamus. *PLoS ONE*, **7**, e45717.

Kaas, J.H. & Lyon, D.C. (2007) Pulvinar contributions to the dorsal and ventral streams of visual processing in primates. *Brain Res. Rev.*, **55**, 285–296.

Kahn, M., Krone, L.B., Blanco-Duque, C., Guillaumin, M.C.C., Mann, E.O., & Vyazovskiy, V.V. (2022) Neuronal-spiking-based closed-loop stimulation during cortical ON- and OFF-states in freely moving mice. *J. Sleep Res.*, **31**, e13603.

Kapfer, C., Glickfeld, L.L., Atallah, B.V., & Scanziani, M. (2007) Supralinear increase of recurrent inhibition during sparse activity in the somatosensory cortex. *Nat. Neurosci.*, **10**, 743–753.

Kaplan, E.S., Cooke, S.F., Komorowski, R.W., Chubykin, A.A., Thomazeau, A., Khibnik, L.A., Gavornik, J.P., & Bear, M.F. (2016) Contrasting roles for parvalbumin-expressing inhibitory neurons in two forms of adult visual cortical plasticity. *eLife*, **5**.

Karl, T., Duffy, L., Scimone, A., Harvey, R.P., & Schofield, P.R. (2007) Altered motor activity, exploration and anxiety in heterozygous neuregulin 1 mutant mice: implications for understanding schizophrenia. *Genes Brain Behav.*, **6**, 677–687.

Kato, H.K., Gillet, S.N., & Isaacson, J.S. (2015) Flexible sensory representations in auditory cortex driven by behavioral relevance. *Neuron*, **88**, 1027–1039.

Katzner, S., Nauhaus, I., Benucci, A., Bonin, V., Ringach, D.L., & Carandini, M. (2009) Local origin of field potentials in visual cortex. *Neuron*, **61**, 35–41.

Kawaguchi, Y. & Kubota, Y. (1997) GABAergic cell subtypes and their synaptic connections in rat frontal cortex. *Cereb. Cortex*, **7**, 476–486.

Kawaguchi, Y., Otsuka, T., Morishima, M., Ushimaru, M., & Kubota, Y. (2019) Control of excitatory hierarchical circuits by parvalbumin-FS basket cells in layer 5 of the frontal cortex: insights for cortical oscillations. *J. Neurophysiol.*, **121**, 2222–2236.

Keller, A.J., Dipoppa, M., Roth, M.M., Caudill, M.S., Ingrosso, A., Miller, K.D., & Scanziani, M. (2020) A disinhibitory circuit for contextual modulation in primary visual cortex. *Neuron*, **108**, 1181-1193.e8.

Keller, G.B. & Mrsic-Flogel, T.D. (2018) Predictive processing: A canonical cortical computation. *Neuron*, **100**, 424–435.

Kerlin, A.M., Andermann, M.L., Berezovskii, V.K., & Reid, R.C. (2010) Broadly tuned response properties of diverse inhibitory neuron subtypes in mouse visual cortex. *Neuron*, **67**, 858–871.

Khan, A.G., Poort, J., Chadwick, A., Blot, A., Sahani, M., Mrsic-Flogel, T.D., & Hofer, S.B. (2018) Distinct learning-induced changes in stimulus selectivity and interactions of GABAergic interneuron classes in visual cortex. *Nat. Neurosci.*, **21**, 851–859.

Kim, J., Matney, C.J., Blankenship, A., Hestrin, S., & Brown, S.P. (2014) Layer 6 corticothalamic neurons activate a cortical output layer, layer 5a. *J. Neurosci.*, **34**, 9656–9664.

Kim, T., Chaloner, F.A., Cooke, S.F., Harnett, M.T., & Bear, M.F. (2020) Opposing Somatic and Dendritic Expression of Stimulus-Selective Response Plasticity in Mouse Primary Visual Cortex. *Front. Cell. Neurosci.*, **13**, 555.

Kim, U., Sanchez-Vives, M.V., & McCormick, D.A. (1997) Functional dynamics of GABAergic inhibition in the thalamus. *Science*, **278**, 130–134.

King, J.L., Lowe, M.P., Stover, K.R., Wong, A.A., & Crowder, N.A. (2016) Adaptive Processes in Thalamus and Cortex Revealed by Silencing of Primary Visual Cortex during Contrast Adaptation. *Curr. Biol.*, **26**, 1295–1300.

Kirkby, P.A., Srinivas Nadella, K.M.N., & Silver, R.A. (2010) A compact Acousto-Optic Lens for 2D and 3D femtosecond based 2-photon microscopy. *Opt. Express*, **18**, 13721–13745.

Kirmse, K. & Zhang, C. (2022) Principles of GABAergic signaling in developing cortical network dynamics. *Cell Rep.*, **38**, 110568.

Kissinger, S.T., Wu, Q., Quinn, C.J., Anderson, A.K., Pak, A., & Chubykin, A.A. (2020) Visual Experience-Dependent Oscillations and Underlying Circuit Connectivity Changes Are Impaired in Fmr1 KO Mice. *Cell Rep.*, **31**, 107486.

Kloc, M. & Maffei, A. (2014) Target-specific properties of thalamocortical synapses onto layer 4 of mouse primary visual cortex. *J. Neurosci.*, **34**, 15455–15465.

Kohn, A. (2007) Visual adaptation: physiology, mechanisms, and functional benefits. *J. Neurophysiol.*, **97**, 3155–3164.

Konorski, J. (1967) *Integrative Activity of the Brain.*, Integrative activity of the brain. Chicago, University of Chicago Press.

Kwan, A.C. & Dan, Y. (2012) Dissection of cortical microcircuits by single-neuron stimulation in vivo. *Curr. Biol.*, **22**, 1459–1467.

Latimer, K.W., Barbera, D., Sokoletsky, M., Awwad, B., Katz, Y., Nelken, I., Lampl, I., Fairhall, A.L., & Priebe, N.J. (2019) Multiple Timescales Account for Adaptive Responses across Sensory Cortices. *J. Neurosci.*, **39**, 10019–10033.

Lee, C., Lavoie, A., Liu, J., Chen, S.X., & Liu, B.-H. (2020) Light Up the Brain: The Application of Optogenetics in Cell-Type Specific Dissection of Mouse Brain Circuits. *Front. Neural Circuits*, **14**, 18.

Lee, C.C. & Sherman, S.M. (2008) Synaptic properties of thalamic and intracortical inputs to layer 4 of the first- and higher-order cortical areas in the auditory and somatosensory systems. *J. Neurophysiol.*, **100**, 317–326.

Lee, H.K., Kameyama, K., Huganir, R.L., & Bear, M.F. (1998) NMDA induces long-term synaptic depression and dephosphorylation of the GluR1 subunit of AMPA receptors in hippocampus. *Neuron*, **21**, 1151–1162.

Lee, S.-H., Kwan, A.C., Zhang, S., Phoumthipphavong, V., Flannery, J.G., Masmanidis, S.C., Taniguchi, H., Huang, Z.J., Zhang, F., Boyden, E.S., Deisseroth, K., & Dan, Y. (2012) Activation of specific interneurons improves V1 feature selectivity and visual perception. *Nature*, **488**, 379–383.

Lewis, D.A., Hashimoto, T., & Volk, D.W. (2005) Cortical inhibitory neurons and schizophrenia. *Nat. Rev. Neurosci.*, **6**, 312–324.

Lien, A.D. & Scanziani, M. (2013) Tuned thalamic excitation is amplified by visual cortical circuits. *Nat. Neurosci.*, **16**, 1315–1323.

Light, G.A. & Braff, D.L. (2005) Mismatch negativity deficits are associated with poor functioning in schizophrenia patients. *Arch. Gen. Psychiatry*, **62**, 127–136.

Li, J., Guido, W., & Bickford, M.E. (2003) Two distinct types of corticothalamic EPSPs and their contribution to short-term synaptic plasticity. *J. Neurophysiol.*, **90**, 3429–3440.

Li, J.Y. & Glickfeld, L.L. (2023) Input-specific synaptic depression shapes temporal integration in mouse visual cortex. *BioRxiv*,.

Li, N., Chen, S., Guo, Z.V., Chen, H., Huo, Y., Inagaki, H.K., Chen, G., Davis, C., Hansel, D., Guo, C., & Svoboda, K. (2019) Spatiotemporal constraints on optogenetic inactivation in cortical circuits. *eLife*, **8**.

Lima, S.Q., Hromádka, T., Znamenskiy, P., & Zador, A.M. (2009) PINP: a new method of tagging neuronal populations for identification during in vivo electrophysiological recording. *PLoS ONE*, **4**, e6099.

Liu, Z., Lu, X., Villette, V., Gou, Y., Colbert, K.L., Lai, S., Guan, S., Land, M.A., Lee, J., Assefa, T., Zollinger, D.R., Korympidou, M.M., Vlasits, A.L., Pang, M.M., Su, S., Cai, C., Froudarakis, E., Zhou, N., Patel, S.S., Smith, C.L., Ayon, A., Bizouard, P., Bradley, J., Franke, K., Clandinin, T.R., Giovannucci, A., Tolias, A.S., Reimer, J., Dieudonné, S., & St-Pierre, F. (2022) Sustained deep-tissue voltage recording using a fast indicator evolved for two-photon microscopy. *Cell*, **185**, 3408-3425.e29.

Lopes da Silva, F. (2013) EEG and MEG: relevance to neuroscience. *Neuron*, **80**, 1112–1128.

Louie, K. & Glimcher, P.W. (2012) Efficient coding and the neural representation of value. *Ann. N. Y. Acad. Sci.*, **1251**, 13–32.

MacLaren, D.A.A., Browne, R.W., Shaw, J.K., Krishnan Radhakrishnan, S., Khare, P., España, R.A., & Clark, S.D. (2016) Clozapine N-Oxide Administration Produces Behavioral Effects in Long-Evans Rats: Implications for Designing DREADD Experiments. *eNeuro*, **3**.

Maffei, A., Nataraj, K., Nelson, S.B., & Turrigiano, G.G. (2006) Potentiation of cortical inhibition by visual deprivation. *Nature*, **443**, 81–84.

Magnus, C.J., Lee, P.H., Bonaventura, J., Zemla, R., Gomez, J.L., Ramirez, M.H., Hu, X., Galvan, A., Basu, J., Michaelides, M., & Sternson, S.M. (2019) Ultrapotent chemogenetics for research and potential clinical applications. *Science*, **364**.

Makino, H. & Komiyama, T. (2015) Learning enhances the relative impact of top-down processing in the visual cortex. *Nat. Neurosci.*, **18**, 1116–1122.

Manvich, D.F., Webster, K.A., Foster, S.L., Farrell, M.S., Ritchie, J.C., Porter, J.H., & Weinshenker, D. (2018) The DREADD agonist clozapine N-oxide (CNO) is reverse-metabolized to clozapine and produces clozapine-like interoceptive stimulus effects in rats and mice. *Sci. Rep.*, **8**, 3840.

Mathis, A., Mamidanna, P., Cury, K.M., Abe, T., Murthy, V.N., Mathis, M.W., & Bethge, M. (2018) DeepLabCut: markerless pose estimation of user-defined body parts with deep learning. *Nat. Neurosci.*, **21**, 1281–1289.

Ma, W., Liu, B., Li, Y., Huang, Z.J., Zhang, L.I., & Tao, H.W. (2010) Visual representations by cortical somatostatin inhibitory neurons--selective but with weak and delayed responses. *J. Neurosci.*, **30**, 14371–14379.

Ma, Y., Hu, H., & Agmon, A. (2012) Short-term plasticity of unitary inhibitory-to-inhibitory synapses depends on the presynaptic interneuron subtype. *J. Neurosci.*, **32**, 983–988.

Ma, Y., Hu, H., Berrebi, A.S., Mathers, P.H., & Agmon, A. (2006) Distinct subtypes of somatostatin-containing neocortical interneurons revealed in transgenic mice. *J. Neurosci.*, **26**, 5069–5082.

McDiarmid, T.A., Bernardos, A.C., & Rankin, C.H. (2017) Habituation is altered in neuropsychiatric disorders-A comprehensive review with recommendations for experimental design and analysis. *Neurosci. Biobehav. Rev.*, **80**, 286–305.

McDiarmid, T.A., Yu, A.J., & Rankin, C.H. (2019) Habituation is more than learning to ignore: multiple mechanisms serve to facilitate shifts in behavioral strategy. *Bioessays*, **41**, e1900077.

McGarry, L.M., Packer, A.M., Fino, E., Nikolenko, V., Sippy, T., & Yuste, R. (2010) Quantitative classification of somatostatin-positive neocortical interneurons identifies three interneuron subtypes. *Front. Neural Circuits*, **4**, 12.

McGaugh, J.L. (2000) Memory--a century of consolidation. *Science*, **287**, 248–251.

Mele, M., Leal, G., & Duarte, C.B. (2016) Role of GABAA R trafficking in the plasticity of inhibitory synapses. *J. Neurochem.*, **139**, 997–1018.

Meyer, H.S., Schwarz, D., Wimmer, V.C., Schmitt, A.C., Kerr, J.N.D., Sakmann, B., & Helmstaedter, M. (2011) Inhibitory interneurons in a cortical column form hot zones of inhibition in layers 2 and 5A. *Proc Natl Acad Sci USA*, **108**, 16807–16812.

Miller, J.-E.K., Miller, B.R., O'Neil, D.A., & Yuste, R. (2022) An increase in spontaneous activity mediates visual habituation. *Cell Rep.*, **39**, 110751.

Mitchell, J.F., Sundberg, K.A., & Reynolds, J.H. (2007) Differential attention-dependent response modulation across cell classes in macaque visual area V4. *Neuron*, **55**, 131–141.

Mitchell, S.J. & Silver, R.A. (2003) Shunting inhibition modulates neuronal gain during synaptic excitation. *Neuron*, **38**, 433–445.

Mitzdorf, U. (1987) Properties of the evoked potential generators: current source-density analysis of visually evoked potentials in the cat cortex. *Int. J. Neurosci.*, **33**, 33–59.

Mody, I. & Pearce, R.A. (2004) Diversity of inhibitory neurotransmission through GABA(A) receptors. *Trends Neurosci.*, **27**, 569–575.

Moghaddam, B. & Krystal, J.H. (2012) Capturing the angel in “angel dust”: twenty years of translational neuroscience studies of NMDA receptor antagonists in animals and humans. *Schizophr. Bull.*, **38**, 942–949.

Montgomery, D.P., Hayden, D.J., Chaloner, F.A., Cooke, S.F., & Bear, M.F. (2021) Stimulus-Selective Response Plasticity in Primary Visual Cortex: Progress and Puzzles. *Front. Neural Circuits*, **15**, 815554.

Moulder, K.L. & Mennerick, S. (2006) Synaptic vesicles: turning reluctance into action. *Neuroscientist*, **12**, 11–15.

Mukherjee, A., Carvalho, F., Eliez, S., & Caroni, P. (2019) Long-Lasting Rescue of Network and Cognitive Dysfunction in a Genetic Schizophrenia Model. *Cell*, **178**, 1387-1402.e14.

Muller, D., Joly, M., & Lynch, G. (1988) Contributions of quisqualate and NMDA receptors to the induction and expression of LTP. *Science*, **242**, 1694–1697.

Murphy, B.K. & Miller, K.D. (2003) Multiplicative gain changes are induced by excitation or inhibition alone. *J. Neurosci.*, **23**, 10040–10051.

Näätänen, R., Paavilainen, P., Rinne, T., & Alho, K. (2007) The mismatch negativity (MMN) in basic research of central auditory processing: a review. *Clin. Neurophysiol.*, **118**, 2544–2590.

Nagai, T., Tada, M., Kirihara, K., Araki, T., Jinde, S., & Kasai, K. (2013) Mismatch negativity as a “translatable” brain marker toward early intervention for psychosis: a review. *Front. Psychiatry*, **4**, 115.

Nagai, Y., Miyakawa, N., Takuwa, H., Hori, Y., Oyama, K., Ji, B., Takahashi, M., Huang, X.-P., Slocum, S.T., DiBerto, J.F., Xiong, Y., Urushihata, T., Hirabayashi, T., Fujimoto, A., Mimura, K., English, J.G., Liu, J., Inoue, K.-I., Kumata, K., Seki, C., Ono, M., Shimojo, M., Zhang, M.-R., Tomita, Y., Nakahara, J., Suhara, T., Takada, M., Higuchi, M., Jin, J., Roth, B.L., & Minamimoto, T. (2020) Deschloroclozapine, a potent and selective chemogenetic actuator enables rapid neuronal and behavioral modulations in mice and monkeys. *Nat. Neurosci.*, **23**, 1157–1167.

Natan, R.G., Briguglio, J.J., Mwilambwe-Tshilobo, L., Jones, S.I., Aizenberg, M., Goldberg, E.M., & Geffen, M.N. (2015) Complementary control of sensory adaptation by two types of cortical interneurons. *eLife*, **4**.

Natan, R.G., Rao, W., & Geffen, M.N. (2017) Cortical Interneurons Differentially Shape Frequency Tuning following Adaptation. *Cell Rep.*, **21**, 878–890.

Neves, G., Cooke, S.F., & Bliss, T.V.P. (2008) Synaptic plasticity, memory and the hippocampus: a neural network approach to causality. *Nat. Rev. Neurosci.*, **9**, 65–75.

Niell, C.M. & Scanziani, M. (2021) How cortical circuits implement cortical computations: mouse visual cortex as a model. *Annu. Rev. Neurosci.*, **44**, 517–546.

Niell, C.M. & Stryker, M.P. (2008) Highly selective receptive fields in mouse visual cortex. *J. Neurosci.*, **28**, 7520–7536.

Niell, C.M. & Stryker, M.P. (2010) Modulation of visual responses by behavioral state in mouse visual cortex. *Neuron*, **65**, 472–479.

Ohki, K., Chung, S., Ch'ng, Y.H., Kara, P., & Reid, R.C. (2005) Functional imaging with cellular resolution reveals precise micro-architecture in visual cortex. *Nature*, **433**, 597–603.

Olsen, S.R., Bortone, D.S., Adesnik, H., & Scanziani, M. (2012) Gain control by layer six in cortical circuits of vision. *Nature*, **483**, 47–52.

Packer, A.M., Russell, L.E., Dalgleish, H.W.P., & Häusser, M. (2015) Simultaneous all-optical manipulation and recording of neural circuit activity with cellular resolution in vivo. *Nat. Methods*, **12**, 140–146.

Pakan, J.M., Lowe, S.C., Dylda, E., Keemink, S.W., Currie, S.P., Coutts, C.A., & Rochefort, N.L. (2016) Behavioral-state modulation of inhibition is context-dependent and cell type specific in mouse visual cortex. *eLife*, **5**.

Pan-Vazquez, A., Wefelmeyer, W., Gonzalez Sabater, V., Neves, G., & Burrone, J. (2020) Activity-Dependent Plasticity of Axo-axonic Synapses at the Axon Initial Segment. *Neuron*, **106**, 265-276.e6.

Paz, J.T., Davidson, T.J., Frechette, E.S., Delord, B., Parada, I., Peng, K., Deisseroth, K., & Huguenard, J.R. (2013) Closed-loop optogenetic control of thalamus as a tool for interrupting seizures after cortical injury. *Nat. Neurosci.*, **16**, 64–70.

Pérez-Ortega, J., Alejandre-García, T., & Yuste, R. (2021) Long-term stability of cortical ensembles. *eLife*, **10**.

Pfeffer, C.K., Xue, M., He, M., Huang, Z.J., & Scanziani, M. (2013) Inhibition of inhibition in visual cortex: the logic of connections between molecularly distinct interneurons. *Nat. Neurosci.*, **16**, 1068–1076.

Phillips, E.A. & Hasenstaub, A.R. (2016) Asymmetric effects of activating and inactivating cortical interneurons. *eLife*, **5**.

Piatkevich, K.D., Bensussen, S., Tseng, H.-A., Shroff, S.N., Lopez-Huerta, V.G., Park, D., Jung, E.E., Shemesh, O.A., Straub, C., Gritton, H.J., Romano, M.F., Costa, E., Sabatini, B.L., Fu, Z., Boyden, E.S., & Han, X. (2019) Population imaging of neural activity in awake behaving mice. *Nature*, **574**, 413–417.

Piatkevich, K.D., Jung, E.E., Straub, C., Linghu, C., Park, D., Suk, H.-J., Hochbaum, D.R., Goodwin, D., Pnevmatikakis, E., Pak, N., Kawashima, T., Yang, C.-T., Rhoades, J.L., Shemesh, O., Asano, S., Yoon, Y.-G., Freifeld, L., Saulnier, J.L., Riegler, C., Engert, F., Hughes, T., Drobizhev, M., Szabo, B., Ahrens, M.B., Flavell, S.W., Sabatini, B.L., & Boyden, E.S. (2018) A robotic multidimensional directed evolution approach applied to fluorescent voltage reporters. *Nat. Chem. Biol.*, **14**, 352–360.

Pluta, S., Naka, A., Veit, J., Telian, G., Yao, L., Hakim, R., Taylor, D., & Adesnik, H. (2015) A direct translaminar inhibitory circuit tunes cortical output. *Nat. Neurosci.*, **18**, 1631–1640.

Pluta, S.R., Telian, G.I., Naka, A., & Adesnik, H. (2019) Superficial Layers Suppress the Deep Layers to Fine-tune Cortical Coding. *J. Neurosci.*, **39**, 2052–2064.

Poort, J., Wilmes, K.A., Blot, A., Chadwick, A., Sahani, M., Clopath, C., Mrsic-Flogel, T.D., Hofer, S.B., & Khan, A.G. (2022) Learning and attention increase visual response selectivity through distinct mechanisms. *Neuron*, **110**, 686-697.e6.

Porter, J.T., Johnson, C.K., & Agmon, A. (2001) Diverse types of interneurons generate thalamus-evoked feedforward inhibition in the mouse barrel cortex. *J. Neurosci.*, **21**, 2699–2710.

Priebe, N.J. (2016) Mechanisms of orientation selectivity in the primary visual cortex. *Annu. Rev. Vis. Sci.*, **2**, 85–107.

Raimondo, J.V., Kay, L., Ellender, T.J., & Akerman, C.J. (2012) Optogenetic silencing strategies differ in their effects on inhibitory synaptic transmission. *Nat. Neurosci.*, **15**, 1102–1104.

Ramaswami, M. (2014) Network plasticity in adaptive filtering and behavioral habituation. *Neuron*, **82**, 1216–1229.

Ramaswamy, S. & Markram, H. (2015) Anatomy and physiology of the thick-tufted layer 5 pyramidal neuron. *Front. Cell. Neurosci.*, **9**, 233.

Rankin, C.H., Abrams, T., Barry, R.J., Bhatnagar, S., Clayton, D.F., Colombo, J., Coppola, G., Geyer, M.A., Glanzman, D.L., Marsland, S., McSweeney, F.K., Wilson, D.A., Wu, C.-F., & Thompson, R.F. (2009) Habituation revisited: an updated and revised description of the behavioral characteristics of habituation. *Neurobiol. Learn. Mem.*, **92**, 135–138.

Resendez, S.L., Jennings, J.H., Ung, R.L., Namboodiri, V.M.K., Zhou, Z.C., Otis, J.M., Nomura, H., McHenry, J.A., Kosyk, O., & Stuber, G.D. (2016) Visualization of cortical, subcortical and deep brain neural circuit dynamics during naturalistic mammalian behavior with head-mounted microscopes and chronically implanted lenses. *Nat. Protoc.*, **11**, 566–597.

Reyes, A., Lujan, R., Rozov, A., Burnashev, N., Somogyi, P., & Sakmann, B. (1998) Target-cell-specific facilitation and depression in neocortical circuits. *Nat. Neurosci.*, **1**, 279–285.

Rico, B. & Marín, O. (2011) Neuregulin signaling, cortical circuitry development and schizophrenia. *Curr. Opin. Genet. Dev.*, **21**, 262–270.

Rikhye, R.V., Yildirim, M., Hu, M., Breton-Provencher, V., & Sur, M. (2021) Reliable Sensory Processing in Mouse Visual Cortex through Cooperative Interactions between Somatostatin and Parvalbumin Interneurons. *J. Neurosci.*, **41**, 8761–8778.

Rittenhouse, C.D., Shouval, H.Z., Paradiso, M.A., & Bear, M.F. (1999) Monocular deprivation induces homosynaptic long-term depression in visual cortex. *Nature*, **397**, 347–350.

Rossant, C., Kadir, S.N., Goodman, D.F.M., Schulman, J., Hunter, M.L.D., Saleem, A.B., Grosmark, A., Belluscio, M., Denfield, G.H., Ecker, A.S., Tolias, A.S., Solomon, S., Buzsaki, G., Carandini, M., & Harris, K.D. (2016) Spike sorting for large, dense electrode arrays. *Nat. Neurosci.*, **19**, 634–641.

Ross, J.M. & Hamm, J.P. (2020) Cortical microcircuit mechanisms of mismatch negativity and its underlying subcomponents. *Front. Neural Circuits*, **14**, 13.

Rudy, B., Fishell, G., Lee, S., & Hjerling-Leffler, J. (2011) Three groups of interneurons account for nearly 100% of neocortical GABAergic neurons. *Dev. Neurobiol.*, **71**, 45–61.

Sanderson, D.J. & Bannerman, D.M. (2011) Competitive short-term and long-term memory processes in spatial habituation. *J. Exp. Psychol. Anim. Behav. Process.*, **37**, 189–199.

Sawtell, N.B., Frenkel, M.Y., Philpot, B.D., Nakazawa, K., Tonegawa, S., & Bear, M.F. (2003) NMDA receptor-dependent ocular dominance plasticity in adult visual cortex. *Neuron*, **38**, 977–985.

Sceniak, M.P. & Maciver, M.B. (2008) Slow GABA(A) mediated synaptic transmission in rat visual cortex. *BMC Neurosci.*, **9**, 8.

Schmid, S., Wilson, D.A., & Rankin, C.H. (2014) Habituation mechanisms and their importance for cognitive function. *Front. Integr. Neurosci.*, **8**, 97.

Scholl, B., Tan, A.Y.Y., Corey, J., & Priebe, N.J. (2013) Emergence of orientation selectivity in the Mammalian visual pathway. *J. Neurosci.*, **33**, 10616–10624.

Sermet, B.S., Truschow, P., Feyerabend, M., Mayrhofer, J.M., Oram, T.B., Yizhar, O., Staiger, J.F., & Petersen, C.C. (2019) Pathway-, layer- and cell-type-specific thalamic input to mouse barrel cortex. *eLife*, **8**.

Shapiro, J.T., Gosselin, E.A.R., Michaud, N.M., & Crowder, N.A. (2022) Activating parvalbumin-expressing interneurons produces iceberg effects in mouse primary visual cortex neurons. *Neurosci. Lett.*, **786**, 136804.

Shatz, C.J. & Stryker, M.P. (1978) Ocular dominance in layer IV of the cat's visual cortex and the effects of monocular deprivation. *J Physiol (Lond)*, **281**, 267–283.

Sherman, M.A., Lee, S., Law, R., Haegens, S., Thorn, C.A., Hämäläinen, M.S., Moore, C.I., & Jones, S.R. (2016) Neural mechanisms of transient neocortical beta rhythms: Converging evidence from humans, computational modeling, monkeys, and mice. *Proc Natl Acad Sci USA*, **113**, E4885-94.

Sherman, S.M. & Guillery, R.W. (2002) The role of the thalamus in the flow of information to the cortex. *Philos. Trans. R. Soc. Lond. B Biol. Sci.*, **357**, 1695–1708.

Silberberg, G. & Markram, H. (2007) Disynaptic inhibition between neocortical pyramidal cells mediated by Martinotti cells. *Neuron*, **53**, 735–746.

Sillito, A.M., Cudeiro, J., & Jones, H.E. (2006) Always returning: feedback and sensory processing in visual cortex and thalamus. *Trends Neurosci.*, **29**, 307–316.

Sillito, A.M. & Jones, H.E. (2002) Corticothalamic interactions in the transfer of visual information. *Philos. Trans. R. Soc. Lond. B Biol. Sci.*, **357**, 1739–1752.

Silver, R.A. (2010) Neuronal arithmetic. *Nat. Rev. Neurosci.*, **11**, 474–489.

Sokolov, E.N. (1963) Higher nervous functions; the orienting reflex. *Annu. Rev. Physiol.*, **25**, 545–580.

Solomon, S.G., Peirce, J.W., Dhruv, N.T., & Lennie, P. (2004) Profound contrast adaptation early in the visual pathway. *Neuron*, **42**, 155–162.

Song, Y.-H., Hwang, Y.-S., Kim, K., Lee, H.-R., Kim, J.-H., Maclachlan, C., Dubois, A., Jung, M.W., Petersen, C.C.H., Knott, G., Lee, S.-H., & Lee, S.-H. (2020) Somatostatin enhances visual processing and perception by suppressing excitatory inputs to parvalbumin-positive interneurons in V1. *Sci. Adv.*, **6**, eaaz0517.

Spacek, M.A., Crombie, D., Bauer, Y., Born, G., Liu, X., Katzner, S., & Busse, L. (2022) Robust effects of corticothalamic feedback and behavioral state on movie responses in mouse dLGN. *eLife*, **11**.

Steinmetz, N.A., Aydin, C., Lebedeva, A., Okun, M., Pachitariu, M., Bauza, M., Beau, M., Bhagat, J., Böhm, C., Broux, M., Chen, S., Colonell, J., Gardner, R.J., Karsh, B., Kloosterman, F., Kostadinov, D., Mora-Lopez, C., O'Callaghan, J., Park, J., Putzeys, J., Sauerbrei, B., van Daal, R.J.J., Vollan, A.Z., Wang, S., Welkenhuysen, M., Ye, Z., Dudman, J.T., Dutta, B., Hantman, A.W., Harris, K.D., Lee, A.K., Moser, E.I., O'Keefe, J., Renart, A., Svoboda, K., Häusser, M., Haesler, S., Carandini, M., & Harris, T.D. (2021) Neuropixels 2.0: A miniaturized high-density probe for stable, long-term brain recordings. *Science*, **372**.

Stringer, C., Pachitariu, M., Steinmetz, N., Reddy, C.B., Carandini, M., & Harris, K.D. (2019) Spontaneous behaviors drive multidimensional, brainwide activity. *Science*, **364**, 255.

Sun, W., Tan, Z., Mensh, B.D., & Ji, N. (2016) Thalamus provides layer 4 of primary visual cortex with orientation- and direction-tuned inputs. *Nat. Neurosci.*, **19**, 308–315.

Suter, K.J., Smith, B.N., & Dudek, F.E. (1999) Electrophysiological recording from brain slices. *Methods*, **18**, 86–90.

Swadlow, H.A. & Gusev, A.G. (2001) The impact of "bursting" thalamic impulses at a neocortical synapse. *Nat. Neurosci.*, **4**, 402–408.

Syeda, A., Zhong, L., Tung, R., Long, W., Pachitariu, M., & Stringer, C. (2022) Facemap: a framework for modeling neural activity based on orofacial tracking. *BioRxiv*,.

Tada, M., Kirihara, K., Mizutani, S., Uka, T., Kunii, N., Koshiyama, D., Fujioka, M., Usui, K., Nagai, T., Araki, T., & Kasai, K. (2019) Mismatch negativity (MMN) as a tool

for translational investigations into early psychosis: A review. *Int. J. Psychophysiol.*, **145**, 5–14.

Tafazoli, S., MacDowell, C.J., Che, Z., Letai, K.C., Steinhardt, C.R., & Buschman, T.J. (2020) Learning to control the brain through adaptive closed-loop patterned stimulation. *J. Neural Eng.*, **17**, 056007.

Teyler, T.J., Hamm, J.P., Clapp, W.C., Johnson, B.W., Corballis, M.C., & Kirk, I.J. (2005) Long-term potentiation of human visual evoked responses. *Eur. J. Neurosci.*, **21**, 2045–2050.

Tremblay, R., Lee, S., & Rudy, B. (2016) Gabaergic interneurons in the neocortex: from cellular properties to circuits. *Neuron*, **91**, 260–292.

Ulanovsky, N., Las, L., Farkas, D., & Nelken, I. (2004) Multiple time scales of adaptation in auditory cortex neurons. *J. Neurosci.*, **24**, 10440–10453.

Urban-Ciecko, J. & Barth, A.L. (2016) Somatostatin-expressing neurons in cortical networks. *Nat. Rev. Neurosci.*, **17**, 401–409.

Urban, D.J. & Roth, B.L. (2015) DREADDs (designer receptors exclusively activated by designer drugs): chemogenetic tools with therapeutic utility. *Annu. Rev. Pharmacol. Toxicol.*, **55**, 399–417.

Veit, J., Hakim, R., Jadi, M.P., Sejnowski, T.J., & Adesnik, H. (2017) Cortical gamma band synchronization through somatostatin interneurons. *Nat. Neurosci.*, **20**, 951–959.

Vélez-Fort, M., Rousseau, C.V., Niedworok, C.J., Wickersham, I.R., Rancz, E.A., Brown, A.P.Y., Strom, M., & Margrie, T.W. (2014) The stimulus selectivity and connectivity of layer six principal cells reveals cortical microcircuits underlying visual processing. *Neuron*, **83**, 1431–1443.

Villette, V., Chavarha, M., Dimov, I.K., Bradley, J., Pradhan, L., Mathieu, B., Evans, S.W., Chamberland, S., Shi, D., Yang, R., Kim, B.B., Ayon, A., Jalil, A., St-Pierre, F., Schnitzer, M.J., Bi, G., Toth, K., Ding, J., Dieudonné, S., & Lin, M.Z. (2019) Ultrafast Two-Photon Imaging of a High-Gain Voltage Indicator in Awake Behaving Mice. *Cell*, **179**, 1590-1608.e23.

Vinck, M., Batista-Brito, R., Knoblich, U., & Cardin, J.A. (2015) Arousal and locomotion make distinct contributions to cortical activity patterns and visual encoding. *Neuron*, **86**, 740–754.

Voigts, J., Deister, C.A., & Moore, C.I. (2020) Layer 6 ensembles can selectively regulate the behavioral impact and layer-specific representation of sensory deviants. *eLife*, **9**.

von der Behrens, W., Bäuerle, P., Kössl, M., & Gaese, B.H. (2009) Correlating stimulus-specific adaptation of cortical neurons and local field potentials in the awake rat. *J. Neurosci.*, **29**, 13837–13849.

Vu, E.T. & Krasne, F.B. (1992) Evidence for a computational distinction between proximal and distal neuronal inhibition. *Science*, **255**, 1710–1712.

Wagner, A.R. (1981) SOP: A Model of Automatic Memory Processing in Animal Behavior. In *Information Processing in Animals*, 1st edn. Psychology Press.

Wang, Q., Webber, R.M., & Stanley, G.B. (2010) Thalamic synchrony and the adaptive gating of information flow to cortex. *Nat. Neurosci.*, **13**, 1534–1541.

Wang, Y., Toledo-Rodriguez, M., Gupta, A., Wu, C., Silberberg, G., Luo, J., & Markram, H. (2004) Anatomical, physiological and molecular properties of Martinotti cells in the somatosensory cortex of the juvenile rat. *J Physiol (Lond)*, **561**, 65–90.

Weyand, T.G., Boudreaux, M., & Guido, W. (2001) Burst and tonic response modes in thalamic neurons during sleep and wakefulness. *J. Neurophysiol.*, **85**, 1107–1118.

Whitmire, C.J. & Stanley, G.B. (2016) Rapid sensory adaptation redux: A circuit perspective. *Neuron*, **92**, 298–315.

Wiesel, T.N. & Hubel, D.H. (1963) Single-cell responses in striate cortex of kittens deprived of vision in one eye. *J. Neurophysiol.*, **26**, 1003–1017.

Wilent, W.B. & Contreras, D. (2004) Synaptic responses to whisker deflections in rat barrel cortex as a function of cortical layer and stimulus intensity. *J. Neurosci.*, **24**, 3985–3998.

Wilson, N.R., Runyan, C.A., Wang, F.L., & Sur, M. (2012) Division and subtraction by distinct cortical inhibitory networks in vivo. *Nature*, **488**, 343–348.

Wonders, C.P. & Anderson, S.A. (2006) The origin and specification of cortical interneurons. *Nat. Rev. Neurosci.*, **7**, 687–696.

Wong, A.Y.C., Graham, B.P., Billups, B., & Forsythe, I.D. (2003) Distinguishing between presynaptic and postsynaptic mechanisms of short-term depression during action potential trains. *J. Neurosci.*, **23**, 4868–4877.

Xue, M., Atallah, B.V., & Scanziani, M. (2014) Equalizing excitation-inhibition ratios across visual cortical neurons. *Nature*, **511**, 596–600.

Xu, H., Jeong, H.-Y., Tremblay, R., & Rudy, B. (2013) Neocortical somatostatin-expressing GABAergic interneurons disinhibit the thalamorecipient layer 4. *Neuron*, **77**, 155–167.

Xu, X., Roby, K.D., & Callaway, E.M. (2010) Immunochemical characterization of inhibitory mouse cortical neurons: three chemically distinct classes of inhibitory cells. *J. Comp. Neurol.*, **518**, 389–404.

Yau, H.-J., Wang, H.-F., Lai, C., & Liu, F.-C. (2003) Neural development of the neuregulin receptor ErbB4 in the cerebral cortex and the hippocampus: preferential expression by interneurons tangentially migrating from the ganglionic eminences. *Cereb. Cortex*, **13**, 252–264.

Yetman, M.J., Washburn, E., Hyun, J.H., Osakada, F., Hayano, Y., Zeng, H., Callaway, E.M., Kwon, H.-B., & Taniguchi, H. (2019) Intersectional monosynaptic tracing for dissecting subtype-specific organization of GABAergic interneuron inputs. *Nat. Neurosci.*, **22**, 492–502.

Zhang, Y., Rózsa, M., Bushey, D., Zheng, J., Reep, D., Broussard, G.J., Tsang, A., Tsegaye, G., Patel, R., Narayan, S., Lim, J.X., Zhang, R., Ahrens, M.B., Turner, G.C., Wang, S.S.-H., Svoboda, K., Korff, W., Schreiter, E.R., Hasseman, J.P., Kolb, I., & Looger, L.L. (2020) jGCaMP8 Fast Genetically Encoded Calcium Indicators. *Janelia Research Campus*,.

Zhang, Z.W. & Deschênes, M. (1997) Intracortical axonal projections of lamina VI cells of the primary somatosensory cortex in the rat: a single-cell labeling study. *J. Neurosci.*, **17**, 6365–6379.

Appendix A

frontiers | Frontiers in Cellular Neuroscience

ORIGINAL RESEARCH
published: 08 April 2022
doi: 10.3389/fncel.2022.840057

Multiple Mechanistically Distinct Timescales of Neocortical Plasticity Occur During Habituation

*Francesca A. Chaloner[1,2] and Sam F. Cooke[1,2]**

[1] MRC Centre for Neurodevelopmental Disorders (CNDD), King's College London, London, United Kingdom, [2] Department of Basic and Clinical Neuroscience, King's College London, London, United Kingdom

Recognizing familiar but innocuous stimuli and suppressing behavioral response to those stimuli are critical steps in dedicating cognitive resources to significant elements of the environment. Recent work in the visual system has uncovered key neocortical mechanisms of this familiarity that emerges over days. Specifically, exposure to phase-reversing gratings of a specific orientation causes long-lasting stimulus-selective response potentiation (SRP) in layer 4 of mouse primary visual cortex (V1) as the animal's behavioral responses are reduced through habituation. This plasticity and concomitant learning require the NMDA receptor and the activity of parvalbumin-expressing (PV+) inhibitory neurons. Changes over the course of seconds and minutes have been less well studied in this paradigm, so we have here characterized cortical plasticity occurring over seconds and minutes, as well as days, to identify separable forms of plasticity accompanying familiarity. In addition, we show evidence of interactions between plasticity over these different timescales and reveal key mechanistic differences. Layer 4 visual-evoked potentials (VEPs) are potentiated over days, and they are depressed over minutes, even though both forms of plasticity coincide with significant reductions in behavioral response. Adaptation, classically described as a progressive reduction in synaptic or neural activity, also occurs over the course of seconds, but appears mechanistically separable over a second as compared to tens of seconds. Interestingly, these short-term forms of adaptation are modulated by long-term familiarity, such that they occur for novel but not highly familiar stimuli. Genetic knock-down of NMDA receptors within V1 prevents all forms of plasticity while, importantly, the modulation of short-term adaptation by long-term familiarity is gated by PV+ interneurons. Our findings demonstrate that different timescales of adaptation/habituation have divergent but overlapping mechanisms, providing new insight into how the brain is modified by experience to encode familiarity.

Keywords: primary visual cortex, learning, adaptation, habituation, inhibition, novelty, stimulus-selective response potentiation, NMDA receptors

OPEN ACCESS

Edited by:
Ricardo M. Leao, University of São Paulo, Brazil

Reviewed by:
Dennis Kätzel, University of Ulm, Germany
Rodrigo N. Romcy-Pereira, Federal University of Rio Grande do Norte, Brazil

***Correspondence:**
Sam F. Cooke
samuel.cooke@kcl.ac.uk

Specialty section:
This article was submitted to Cellular Neurophysiology, a section of the journal Frontiers in Cellular Neuroscience

Received: *20 December 2021*
Accepted: *03 March 2022*
Published: *08 April 2022*

Citation:
Chaloner FA and Cooke SF (2022) Multiple Mechanistically Distinct Timescales of Neocortical Plasticity Occur During Habituation. Front. Cell. Neurosci. 16:840057. doi: 10.3389/fncel.2022.840057

SIGNIFICANCE STATEMENT

Habituation is a foundational cognitive process that reduces the requirement for neural resources to be allocated to innocuous stimuli, thereby freeing up attention and energy to detect and explore salience. Memories of innocuous familiar stimuli must be formed so that they can be selectively ignored while novel stimuli, which have the potential for significance, are detected. Within the visual system, we have previously shown that increases in neural activity in cerebral cortex occur

during habituation that emerges over days, but many forms of habituation must occur over shorter timescales to allow allocation of resources to appropriate stimuli within a single session. Here we characterize cortical plasticity and habituation over seconds, minutes, and days within the same subjects, revealing short-term plasticity that diminishes neural activity, an opposing effect to the better characterized long-term plasticity. In addition, we have revealed overlapping but distinct molecular and cellular mechanisms mediating these different timescales of plasticity. Elucidating the mechanisms that underlie habituation will inform us how the brain can learn to recognize familiar stimuli and thereby detect novelty. This work also provides unique insight into core processes of learning that are affected in the disordered brain, where habituation and novelty detection are commonly dysfunctional.

INTRODUCTION

Learning and memory enable organisms to adapt to altered pressures in the environment to produce appropriate responses to stimulus and context over a variety of timescales (McGaugh, 2000). Substantial gaps remain in our understanding of the neural underpinnings of these processes, in part due to difficulties in observing and intervening in underlying plasticity as learning and memory occur (Neves et al., 2008). Habituation is one relatively robust, easy to observe and apparently simple form of learning, in which organisms acquire familiarity with innocuous stimuli and selectively reduce behavioral responses to those stimuli over seconds, minutes, and days (Cooke and Ramaswami, 2020). Habituation forms a foundation for further learning by enabling energy and attention to be devoted to stimuli of already established salience, or novel stimuli that may have future significance (Rankin et al., 2009; Schmid et al., 2014) and disruptions in this process likely contribute to a range of psychiatric and neurological disorders (Ramaswami, 2014; McDiarmid et al., 2017). This form of learning has commonly been ascribed to a neural process known as adaptation, which reduces feedforward synaptic activity in response to repeated non-associative stimulation (Groves and Thompson, 1970), especially over shorter timescales (Chung et al., 2002). However, a competing theory, known as the comparator model (Sokolov, 1963), suggests the formation of long-lasting memory of familiar stimuli through Hebbian synaptic potentiation, which in turn suppresses behavioral output by recruiting inhibitory systems. It remains possible that both models apply but over different timescales (Cooke and Ramaswami, 2020). In this study, we have assessed plasticity in primary visual cortex (V1) of mice in response to repeated presentations of oriented, phase reversing visual stimuli to assess whether different directions of plasticity can be observed across different timescales.

It is now well established that the magnitude of visual-evoked potentials (VEPs) recorded in layer 4 of mouse binocular V1 increases dramatically over days of repeated stimulation through an orientation-specific form of plasticity known as stimulus-selective response potentiation (SRP) (Frenkel et al., 2006; Cooke and Bear, 2010). This form of plasticity is also manifest as an increase in the peak firing rate of V1 neurons (Aton et al., 2014; Cooke et al., 2015) and many of the known molecular mechanisms are consistent with the involvement of Hebbian synaptic potentiation, notably including a requirement for the NMDA receptor during induction and AMPA receptor insertion during expression (Frenkel et al., 2006; Cooke and Bear, 2010). Importantly, mice produce behavioral responses to the onset of these visual stimuli that exhibit significant orientation-selective habituation over days (Cooke et al., 2015; Kaplan et al., 2016; Fong et al., 2020; Finnie et al., 2021), and this process also requires the presence of NMDA receptors in V1. In addition, a cortical cell-type that exerts exquisite inhibitory control over excitatory cell activity, the parvalbumin-expressing (PV+) inhibitory interneurons (Atallah et al., 2012), are critical for differential cortical and behavioral responses to familiar and novel stimuli after SRP and accompanying habituation (Kaplan et al., 2016). Thus, SRP comprises a robust and relatively well understood form of plasticity that occurs concomitantly with and shares mechanism with long-term memory.

One fascinating feature of SRP is that it does not manifest within a ~30-min recording session but starts to emerge the following day (Frenkel et al., 2006) and recent work has demonstrated that SRP is dependent on consolidation processes that occur during sleep (Aton et al., 2014; Durkin et al., 2017). Activity in the primary visual relay nucleus of the thalamus, the dorsal lateral geniculate nucleus (dLGN), does increase over the course of 30 min prior to the emergence of SRP in the cortex (Durkin et al., 2017), but there has so far been no description of what happens over this time-course in V1. Although we have previously described evidence for a faster adaptation that is apparent when comparing the beginning of a 200-phase reversal block with the end (Kim et al., 2020), we have not described the time-course of this adaptation during this 100-s block. In neither case is there any understanding of the underlying mechanism. In the current study, we show that cortical plasticity accompanying behavioral habituation occurs across seconds, minutes, and days of repeated stimulus experience. Notably, these forms of plasticity diverge in direction and mechanism, and there is evidence of an interaction in which long-term familiarity suppresses adaptation. In striking opposition to our observations of SRP during long-term habituation (Cooke et al., 2015), layer 4 response magnitude decreases over seconds and minutes in V1. Loss of expression of NMDA receptors from neurons in V1 impairs plasticity and adaptation across all timescales. However, inactivation of PV+ neurons has a more nuanced effect, revealing the existence of two separable forms of fast adaptation within a stimulus block. Moreover, we show that the interaction between long-lasting familiarity and adaptation requires the activity of PV+ neurons. Thus, a range of mechanistically separable forms of plasticity can be assayed across different timescales in the same learning mouse.

MATERIALS AND METHODS

Animals

All procedures were carried out in accordance with the guidelines of the National Institutes of Health

and protocols approved by the Committee on Animal Care at the Massachusetts Institute of Technology. **Figures 1, 2** are composed of data from male C57B6/J mice (Charles River laboratory international, Wilmington, MA). NMDA knock-down experiments (**Figures 3, 4**) make use of $GRIN^{fl/fl}$ mice (B6.129S4-*Grin1*^{tm2Stl}/J—Jackson laboratory). PV+ interneuron inactivation (**Figure 5**) uses PV-Cre mice (B6;129P2-*Pvalb*$^{TM1(cre)Arbr}$/J—Jackson laboratory). All animals had food and water available *ad libitum* and were maintained on a 12-h light-dark cycle.

Viral Transfection

In the NMDAR knock-down and PV+ inactivation experiments viral vectors were administered *via* stereotaxic injections into the mice. For the NMDA knock-down, $GRIN^{fl/fl}$ mice (B6.129S4-*Grin1*^{tm2Stl}/J—Jackson laboratory) underwent surgery at ∼ 1 month. AAV8-hSyn-GFP-Cre (knockdown; UNC viral core) or AAV8-hSyn-GFP (control; UNC viral core; generated by Dr. Bryan Roth's laboratory) were injected in quantities of 13.5 nl 10 times at depths 600, 450, 300, and 150 μm bellow surface. Each injection was separated by 15 s and after repositioning 5 min was allowed. For the PV+ inactivation experiment, AAV9-hSyn-DIO-HA-hM4D(Gi)-IRES-mCitrine virus (UNC viral core—generated by B. Roth's laboratory) was injected into PV-Cre or WT-littermates in quantities of 81 nl at depths 600, 450, and 300 μm below surface, including a 5-min delay after repositioning. Viral transfections were performed in both hemispheres and were immediately followed by V1 electrode implantation, outlined below. Following surgery, mice were allowed 3 weeks for full viral expression.

V1 Electrode Implantation

Mice were anesthetized with an intraperitoneal (i.p) injection of 50 mg/kg ketamine and 10 mg/kg xylazine for surgery. 1% lidocaine hydrochloride anesthetic was injected locally under the scalp and 0.1 mg/kg Buprenex was delivered sub-cutaneously for analgesia. Iodine and 70% ethanol were used to clean the scalp. The skull was cleaned, dried, and scored using a blade. A steel headpost was fixed over the frontal suture using super glue (ethyl cyanoacrylate). Burr holes were drilled 3.1 mm lateral to lambda (to target binocular V1). Tungsten recording electrodes (FHC, Bowdoinham, ME, United States) were implanted 450 μm below surface in both hemispheres. Silver wire reference electrodes were placed in prefrontal cortex bilaterally.

Visual Stimuli

Visual stimuli were generated using software developed by Jeff Gavornik.[1] The display was 20 cm in front of the mouse, and mean luminance was 27 cd/m^2. Sinusoidal phase reversing gratings were presented full field, reversing at 2 Hz. In most experiments, blocks consisted of 200 phase reversals, each block was presented 5 times interleaved with 30 s of gray screen. Gamma-correction was performed to maintain constant luminance between gratings and gray screen. The 5 blocks were repeated until day 6. On the final day, day 7, the familiar orientation (X°) was pseudo-randomly interleaved (such that no more than 2 blocks of the same orientation were shown in sequence) with a novel orientation (X+90°). Orientations were never within 25° of horizontal. In the PV+ inactivation experiment (**Figure 5**) 10 blocks were shown. On day 7 familiar (X°) and novel (X°-60°) stimuli were shown. Then CNO was administered at 5 mg/kg *via* intraperitoneal (i.p) injection. After a 15-min wait, the familiar stimulus (X°) was presented with a new novel stimulus (X°+60°).

[1]https://github.com/jeffgavornik/VEPStimulusSuite

In vivo Data Acquisition and Analysis

Mice recovered from electrode implantation then underwent 2 days of habituation, followed by the 7-day protocol outlined above. All data was acquired using the Plexon data acquisition system (Plexon Inc., Dallas, TX, United States). Local field potentials (LFP) were collected from V1 in both hemispheres, and piezoelectrical signal was reduced in amplitude and digitized into a third recording channel. Animals were head fixed at the opening of a metal cylinder tube and positioned on a piezoelectric transducer placed under the front paws but touching the metal cylinder. This piezoelectric signal therefore consists mainly of front paw movement but hind paw/whole body movements also contribute to the signal due to vibrations *via* the metal tube. All digital channels were recorded at 1 kHz sampling and run through a 500 Hz low-pass filter. Data was extracted into Matlab using custom software. For the analysis over days, 450 ms traces following stimulus onset were averaged over 1,000 phase reversals (5 blocks × 200 phase reversals). For the across block analysis, traces were averaged over 200 phase reversals. For the within-block analysis (1v2, 1v200), each individual phase reversal was averaged over 5 blocks. VEP magnitude was taken as the minimum microvolt value from 1 to 100 ms following onset subtracted from the maximum microvolt value taken from 75 to 250 ms following onset.

Statistics

All data is expressed as mean ± SEM and number of animals is represented by n. All statistical analysis is non-parametric due to small n numbers negating true testing of normality. For comparisons between two groups or time points, a paired Wilcoxon signed rank test is used, for adaptation ratio analysis a one-sample Wilcoxon signed rank test is used with a μ of 1. Repeated measures Friedman test is used for analysis across multiple time points within one group. Where multiple tests have been performed, all p-values are adjusted using false discovery rate (FDR) correction.

Data Collection and Use

Data was originally collected by Sam Cooke in Mark Bear's lab (MIT). Raw data used in **Figures 1, 2** was previously published by Kim et al. (2020). Raw data used in **Figures 3, 4** was previously published by Cooke et al. (2015), and **Figure 5** was published by Kaplan et al. (2016). Extended data analysis was performed

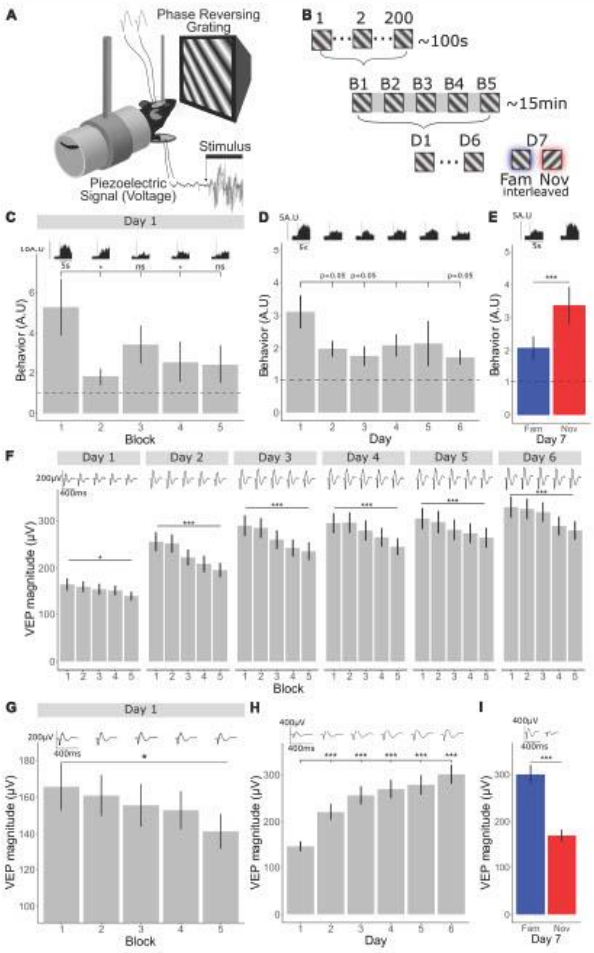

FIGURE 1 | V1 plasticity accompanying long- and short-term habituation occurs in opposing directions. **(A)** Schematic of recording set-up. Mice viewed phase reversing gratings while layer 4 local-field potentials were recorded through implanted tungsten electrodes and movement was recorded through a piezo-electrical device. **(B)** 1 through 200 individual phase reversals were shown lasting approximately 100 s (1 block). Five blocks were shown lasting approximately 15 min within one session. One session of 5 blocks was shown for 6 days. On the 7th day, the familiar orientation (previously viewed) and a novel orientation were shown pseudo-randomly interleaved. **(C)** Comparison of behavior across blocks ($n = 30$). Friedman test $\chi^2(4) = 13.8$, $p = 0.008$. *Post-hoc* analysis of individual comparisons of blocks 1–2: $p = 0.02$, blocks 1–3: $p = 0.7$, blocks 1–4: $p = 0.04$, blocks 1–5: $p = 0.5$. FDR correction for multiple comparisons. **(D)** Behavioral change over days 1–6 ($n = 30$). Freidman test $\chi^2(5) = 6.55$, $p = 0.3$. *Post-hoc* analysis of individual comparisons of days 1–2: $p = 0.05$, days 1–3: $p = 0.05$, days 1–4: $p = 0.2$, days 1–5: $p = 0.09$, days 1–6: $p = 0.05$. FDR correction for multiple comparisons. **(E)** Behavioral response to familiar and novel ($n = 30$). Wilcoxon signed-rank test fam vs. nov: $p < 0.001$. **(F)** VEP magnitude from block 1 to 5 over 6 days ($n = 33$). Comparison across blocks, Friedman test, day 1: $\chi^2(4) = 12.8$, $p = 0.01$, day 2: $\chi^2(4) = 69.8$, $p < 0.001$, day 3: $\chi^2(4) = 55.1$, $p < 0.001$, day 4: $\chi^2(4) = 43.8$, $p < 0.001$, day 5: $\chi^2(4) = 32.5$, $p < 0.001$, day 6: $\chi^2(4) = 38.6$, $p < 0.001$. FDR correction for multiple comparisons. **(G)** VEP magnitude from block 1 to 5 on day 1 ($n = 33$). Friedman test across blocks on day 1; $p = 0.01$. **(H)** VEP magnitude potentiation over days 1–6 ($n = 33$). Freidman test $\chi^2(5) = 95.9$, $p < 0.001$. *Post-hoc* analysis of individual comparisons of days 1, 2, 3, 4, 5, day 6: all $p < 0.001$, FDR correction for multiple comparisons. **(I)** VEP magnitude response to familiar and novel ($n = 33$). Wilcoxon signed-rank test fam vs. nov: $p < 0.001$. Asterisks throughout denote significance (*$p < 0.05$, ***$p < 0.001$) while ns denotes non-significant. Where $p = 0.05$, this is explicitly stated.

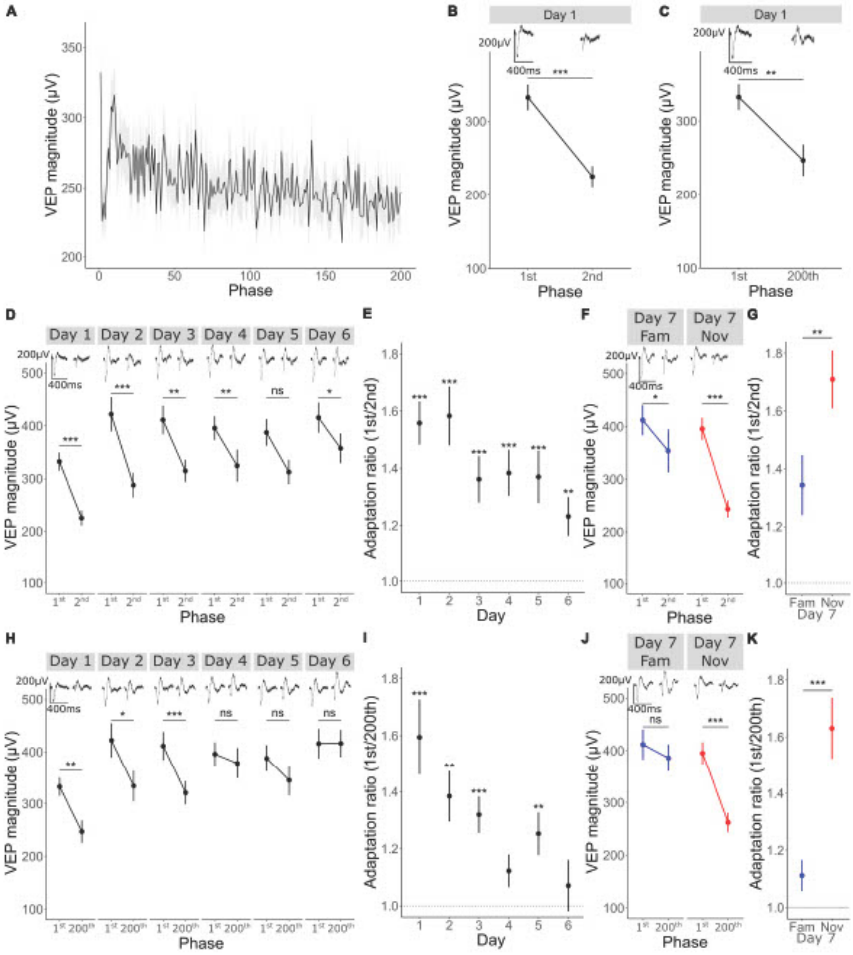

FIGURE 2 | Short-term adaptation occurs within a stimulus block and is modulated by familiarity. **(A)** Mean ± SEM VEP magnitude for phase reversal 1–200 ($n = 33$). **(B)** VEP magnitude in response to the first phase reversal and the 2nd, Wilcoxon signed rank 1st vs. 2nd: $p < 0.001$ ($n = 33$). **(C)** VEP magnitude in response to the first phase reversal and the 200th, Wilcoxon signed rank 1st vs. 200th: $p = 0.001$ ($n = 33$). **(D)** VEP potential magnitude in response to the 1st vs. 2nd phase reversal over 6 days ($n = 33$). Wilcoxon signed rank 1st vs. 2nd day 1: $p < 0.001$, day 2: $p < 0.001$, day 3: $p = 0.002$, day 4: $p = 0.008$, day 5: $p = 0.05$, day 6: $p = 0.04$. FDR correction for multiple comparisons. **(E)** Adaptation ratio (1st/2nd) over 6 days. Wilcoxon signed-rank test on AR ($\mu = 1$) day 1: $p < 0.001$, day 2: $p < 0.001$, day 3: $p < 0.001$, day 4: $p < 0.001$, day 5: $p < 0.001$, day 6: $p = 0.002$. FDR correction for multiple comparisons. **(F)** VEP potential magnitude in response to the 1st vs. 2nd phase reversal on day 7 ($n = 33$). Wilcoxon signed rank 1st vs. 2nd day 7 fam: $p = 0.02$, day 7 nov: $p < 0.001$. FDR correction for multiple comparisons. **(G)** Adaptation ratio (1st/2nd) on day 7. Wilcoxon signed-rank test fam vs. nov: $p = 0.009$. **(H)** VEP potential magnitude in response to the 1st vs. 200th phase reversal over 6 days ($n = 33$). Wilcoxon signed rank 1st vs. 200th day 1: $p = 0.008$, day 2: $p = 0.04$, day 3: $p < 0.001$, day 4: $p = 1$, day 5: $p = 0.4$, day 6: $p = 1$. **(I)** Adaptation ratio (1st/200th) over 6 days. Wilcoxon signed-rank test on AR ($\mu = 1$) day 1: $p < 0.001$, day 2: $p = 0.001$, day 3: $p < 0.001$, day 4: $p = 0.1$, day 5: $p = 0.006$, day 6: $p = 1$. FDR correction for multiple comparisons. **(J)** VEP potential magnitude in response to the 1st vs. 2nd phase reversal on day 7 ($n = 33$). Wilcoxon signed rank 1st vs. 200th day 7 fam: $p = 1$, day 7 nov: $p < 0.001$. **(K)** Adaptation ratio (1st/200th) on day 7. Wilcoxon signed-rank test fam vs. nov: $p < 0.001$. Asterisks throughout denote significance (*$p < 0.05$, **$p < 0.01$, ***$p < 0.001$) while ns denotes non-significant.

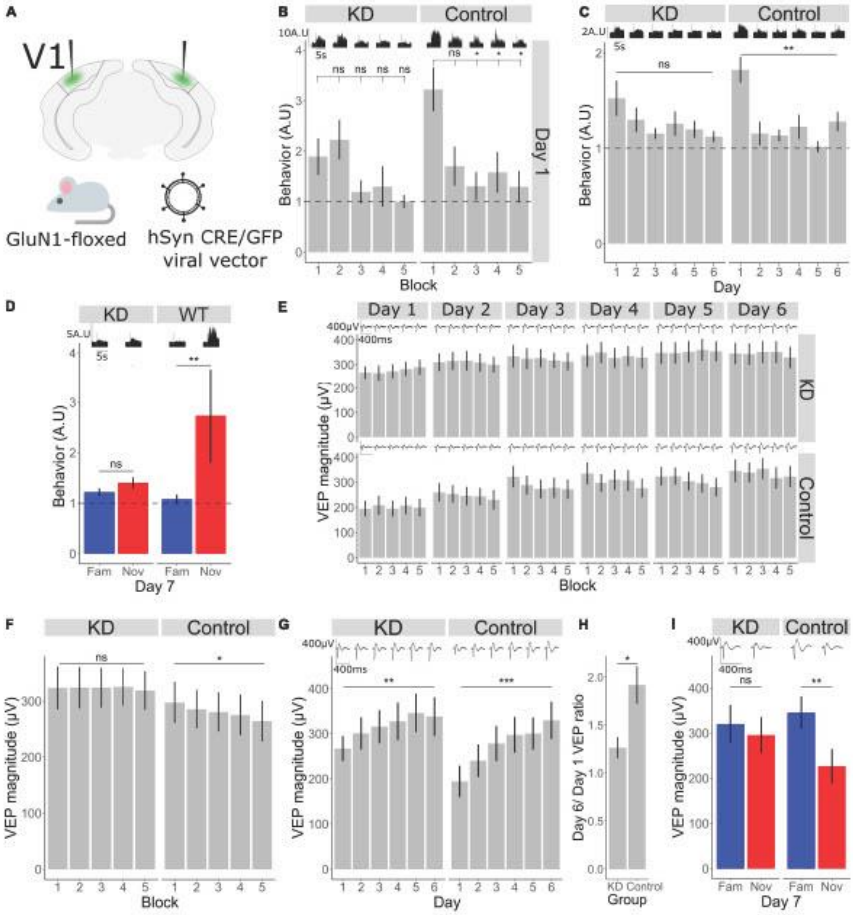

FIGURE 3 | Bidirectional plasticity occurring in V1 during short- and long-term habituation require NMDA receptors in V1. **(A)** Schematic of the experimental set-up in which a Cre recombinase was locally expressed bilaterally in binocular V1 using an AAV viral vector to knockdown the mandatory GluN1 subunit of the NMDA receptor in GluN1-floxed mice. **(B)** Comparison of behavior across blocks for KD group ($n = 11$). Friedman test $\chi^2(4) = 4.7$, $p = 0.3$. *Post-hoc* analysis of individual comparisons of blocks 1–2: $p = 0.8$, blocks 1–3: $p = 0.5$, blocks 1–4: $p = 0.3$, blocks 1–5: $p = 0.1$. Comparison of behavior across blocks for WT group ($n = 11$). Friedman test $\chi^2(4) = 10.8$, $p = 0.03$. *Post-hoc* analysis of individual comparisons of blocks 1–2: $p = 0.1$, blocks 1–3: $p = 0.02$, blocks 1–4: $p = 0.02$, blocks 1–5: $p = 0.02$. FDR correction for multiple comparisons. **(C)** Behavioral change over days 1–6 in KD group ($n = 11$), Freidman test $\chi^2(5) = 5.9$, $p = 0.3$. In WT group ($n = 11$), Freidman test $\chi^2(5) = 21.6$, $p = 0.001$. FDR correction for multiple comparisons. **(D)** Behavioral response to familiar and novel. Wilcoxon signed-rank test fam vs. nov in KD group: $p = 0.2$, in WT group: $p = 0.009$. FDR correction for multiple comparisons. **(E)** VEP magnitude change from block 1 to block 5 for day 1 to day 6 ($n = 11$ for each group). **(F)** VEP potential magnitude averaged over day 1–6. Comparison over blocks for KD group, Friedman test $\chi^2(4) = 0.7$, $p = 0.9$ ($n = 11$). Comparison over blocks for WT group, Friedman test $\chi^2(4) = 12.1$, $p = 0.03$ ($n = 11$). FDR correction for multiple comparisons. **(G)** VEP magnitude across days 1–6 in knock-down (KD) and wild-type (WT groups). Friedman test for KD group: $\chi^2(5) = 15.4$, $p = 0.008$ ($n = 11$). Friedman test for WT group: $\chi^2(5) = 36.5$, $p < 0.001$ ($n = 11$). FDR correction for multiple comparisons. **(H)** Ratio of day 6 VEP magnitude to day 1 VEP magnitude in KD and control group. Wilcoxon signed rank between groups: $p = 0.04$. **(I)** VEP magnitude response to familiar and novel, Wilcoxon signed-rank test fam vs. nov for KD group: $p = 0.2$, for WT group: $p = 0.003$ ($n = 11$). FDR correction for multiple comparisons. Asterisks throughout denote significance (*$p < 0.05$, **$p < 0.01$, ***$p < 0.001$) while ns denotes non-significant.

on this data which elucidated further phenotypes which are discussed below.

RESULTS

Habituation Can Be Observed Within and Across Days in the Same Animal

Visual stimuli were presented over multiple timescales to awake head-fixed mice within a longitudinal experimental design. This approach allowed for investigation into the change in neocortical activity across these different timescales as visual-evoked behavior was concomitantly monitored. Awake mice were head-fixed and viewed full field, oriented, 0.05 cycles/degree, 100% contrast, phase-reversing, sinusoidal grating stimuli while concurrently recording layer 4 local fields potentials (LFPs) with chronically implanted tungsten microelectrodes and behavior using a piezoelectric sensor (**Figure 1A**). After a 5-min period of gray screen (equivalent luminance to the grating stimuli to follow) to settle the animal into head-fixation, a stimulus of one fixed orientation (X°) was presented at a temporal frequency of 2 Hz for 200 phase reversals, resulting in ∼100 s of continuous stimulus presentation (we describe this as a stimulus block throughout). This block was repeated 5 times with 30-s-long gray screen intervals separating them. Overall, this session lasted approximately 15 min (5 min of gray followed by ∼10 min of stimulus blocks and intervening gray). These sessions, each containing 5 separated blocks, were then repeated once each over 6 days. On the 7th day, 5 blocks of the original orientation (X°) were presented pseudo-randomly interleaved with a novel orientation (X+90°), such that no more than 2 blocks of one orientation were presented in sequence (**Figure 1B**). This experimental design allowed for analysis of habituation and cortical plasticity across days and within a day.

We found that behavioral habituation occurred both within a day and across days. After the onset of a block of visual stimuli, animals produce a pronounced behavioral response, which we measured using a piezoelectric device and previously termed a vidget (Cooke et al., 2015). Using the vidget, we were able to observe behavioral habituation within a single recording session on day 1 (n = 30), when the X° stimulus was novel. The vidget magnitude dropped considerably by the second block and remained low (**Figure 1C**; Friedman test: p = 0.008, Wilcoxon signed-rank on B1–B2: p = 0.02, B1–B3: p = 0.7, B1–B4: p = 0.04, B1–B5: p = 0.5; FDR correction for multiple comparisons), indicating the occurrence of short-term habituation on day 1. When averaged over all 5 blocks, the overall magnitude of vidgets was greater on day 1 than on the following days (**Figure 1D**; Friedman test: p = 0.3; Wilcoxon signed-rank on days 1–2: p = 0.05, days 1–3: p = 0.05, days 1–4: p = 0.2, days 1–5: p = 0.09, days 1–6: p = 0.05; FDR correction for multiple comparisons), indicating the occurrence of long-term habituation. During presentation of blocks of a novel stimulus (X+90°), interleaved with the familiar X° stimulus on the final day, vidgets were increased in magnitude for the novel compared to the familiar stimulus (**Figure 1E**; Wilcoxon signed-rank test: p <0.001), just as we have described previously (Cooke et al., 2015; Kaplan et al., 2016; Fong et al., 2020).

V1 Plasticity Accompanying Long- and Short-Term Habituation Occurs in Opposing Directions

Phase-locked LFP responses from layer 4 were averaged together to assess changes in visual-evoked potential (VEP) magnitude within a day and across days (n = 33). We found that the changes in VEP magnitude occurred in differing directions dependent upon the timescale. A very clear decrement in VEP magnitude was apparent over the course of 5 blocks of stimulus presentation (∼10 min) within day 1 (**Figures 1F,G**; Friedman test across blocks on day 1; p = 0.01), following the trend of behavioral habituation. This effect became more pronounced after the first day of stimulus presentation (**Figure 1F**; Friedman test: day 1; p = 0.01, day 2–6 p < 0.001; FDR multiple comparisons corrected). In contrast, across days there was significant potentiation of VEP magnitude (**Figure 1H**; Friedman test: p < 0.001) and this potentiation was orientation specific, because VEP magnitude was reduced to baseline in response to the novel orientation (**Figure 1I**; Wilcoxon signed-rank test: p < 0.001). Thus, SRP is also present in these animals, just as described previously (Frenkel et al., 2006; Cooke and Bear, 2010). Importantly, a response decrement accompanies short-term habituation, while response potentiation accompanies long-term habituation in the same animals.

Short-Term Adaptation Occurs Within a Stimulus Block

Next, we wanted to determine whether even shorter timescales of plasticity could be identified within the same experiments, this time focusing on plasticity across a single stimulus block. We averaged VEP magnitude for each of the 200 phase reversals within a block across all 5 blocks on day 1 and across animals (n = 33). Over the course of 200 phase reversals (∼100 s) we observed a reduction in the VEP magnitude (**Figure 2A**). Most notably, there was an immediate reduction from phase 1 to phase 2 (**Figures 2A,B**; Wilcoxon signed-rank on phase 1–2: p < 0.001), followed by a striking rebound over the next few phase reversals. A steadier reduction in VEP magnitude was observed across all 200 phase reversals, culminating in a significant difference between phase reversal 1 and phase reversal 200 (**Figures 2A,C**; Wilcoxon signed-rank on phase 1–200: p = 0.001). Thus, clear evidence is apparent of adaptation within a stimulus block, indicating at least one, and perhaps two additional potential timescales of plasticity to be investigated.

Short-Term Adaptation Is Modulated by Stimulus Familiarity

Short-term adaptation occurred from both the first to the second and the first to the last phase reversal in a stimulus block when a stimulus was relatively novel on day 1, but did that plasticity persist for highly familiar stimuli? By assessing averaged within-block adaptation over the course of 6 days of long-term observation, we found that adaptation from the first to the second

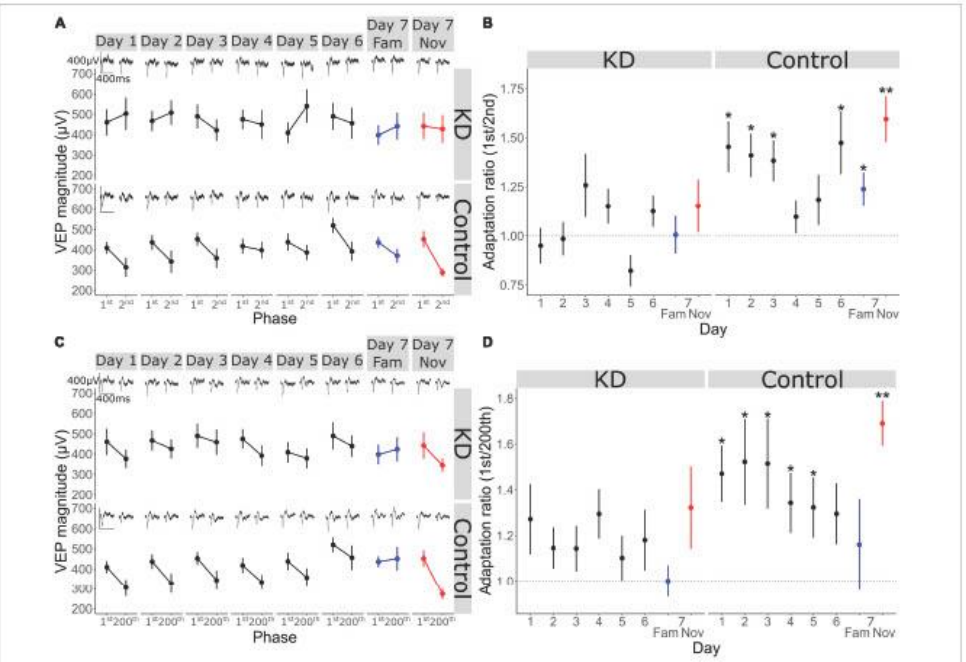

FIGURE 4 | V1 adaptation requires NMDA receptors in V1 across short timescales. **(A)** VEP magnitude in response to the 1st and 2nd phase reversal in GluN1 KD and WT group across all days ($n = 11$) **(B)** adaptation ratio (1st/2nd) across days. Wilcoxon signed-rank test on AR ($\mu = 1$) in KD group on day 1: $p = 0.6$, day 2: $p = 0.9$, day 3: $p = 0.5$, day 4: $p = 0.4$, day 5: $p = 0.4$, day 6: $p = 0.4$, day 7 fam: $p = 1$, day 7 nov: $p = 0.6$. Wilcoxon signed-rank test on AR ($\mu = 1$) in WT group on day 1: $p = 0.02$, day 2: $p = 0.01$, day 3: $p = 0.02$, day 4: $p = 0.2$, day 5: $p = 0.3$, day 6: $p = 0.03$, day 7 fam: $p = 0.03$, day 7 nov: $p = 0.008$. FDR correction for multiple comparisons. **(C)** VEP magnitude in response to the 1st and 200th phase reversal in KD and WT group across all days. **(D)** Adaptation ratio (1st/200th) across days. Wilcoxon signed-rank test on AR ($\mu = 1$) in KD group on day 1: $p = 0.3$, day 2: $p = 0.3$, day 3: $p = 0.3$, day 4: $p = 0.3$, day 5: $p = 0.5$, day 6: $p = 0.5$, day 7 fam: $p = 0.5$, day 7 nov: $p = 0.4$. Wilcoxon signed-rank test on AR ($\mu = 1$) in WT group on day 1: $p = 0.02$, day 2: $p = 0.02$, day 3: $p = 0.02$, day 4: $p = 0.02$, day 5: $p = 0.05$, day 6: $p = 0.08$, day 7 fam: $p = 0.8$, day 7 nov: $p = 0.008$. FDR correction for multiple comparisons. Asterisks throughout denote significance ($^*p < 0.05$, $^{**}p < 0.01$).

phase reversal was gradually reduced over days (**Figure 2D**; Wilcoxon signed-rank test on phase 1 vs. 2 on day 1: $p < 0.001$, day 2: $p < 0.001$, day 3: $p = 0.002$, day 4: $p = 0.008$, day 5: $p = 0.05$, day 6: $p = 0.04$; FDR correction for multiple comparisons). Although this adaptation from the first to the second phase reversal lessened as the stimulus became familiar over days, significant adaptation remained and the adaptation ratio (AR) (1st/2nd) was always significantly above 1 (**Figure 2E**; one sample Wilcoxon signed-rank test on AR ($\mu = 1$) on day 1: $p < 0.001$, day 2: $p < 0.001$, day 3: $p < 0.001$, day 4: $p < 0.001$, day 5: $p < 0.001$, day 6: $p = 0.002$; FDR correction for multiple comparisons). On day 7, there was greater adaptation for the novel stimulus than for the familiar orientation in pseudo-randomly interleaved blocks (**Figure 2F**; Wilcoxon signed-rank test on phase 1 vs. 2 on day 7 fam: $p = 0.02$, day 7 nov: $p < 0.001$; FDR correction for multiple comparisons) and the AR (1st/2nd) for the familiar stimulus was significantly reduced compared to that in response to the novel stimulus (**Figure 2G**; Wilcoxon signed rank day 7 fam AR vs. day 7 nov AR: $p = 0.009$) suggesting modulation of adaptation from the 1st to 2nd phase reversal by long-term familiarity.

A more pronounced modulation of adaptation by long-term familiarity was observed for adaptation from the first to the last phase reversal. Adaptation from phase reversal 1 to 200 was no longer significant by day 4 and thereafter (**Figure 2H**; Wilcoxon signed-rank phase 1 vs. 200 on day 1: $p = 0.008$, day 2: $p = 0.04$, day 3: $p < 0.001$, day 4: $p = 1$, day 5: $p = 0.4$, day 6: $p = 1$; FDR correction for multiple comparisons). In this case, the adaptation ratio (1st/200th) became statistically indistinguishable from 1 by day 4 for the familiar orientation [**Figure 2I**; one sample Wilcoxon signed-rank test on AR ($\mu = 1$) on day 1: $p < 0.001$, day 2: $p = 0.001$, day 3: $p < 0.001$, day 4: $p = 0.1$, day 5: $p = 0.006$, day 6: $p = 1$; FDR correction for multiple comparisons]. The adaptation

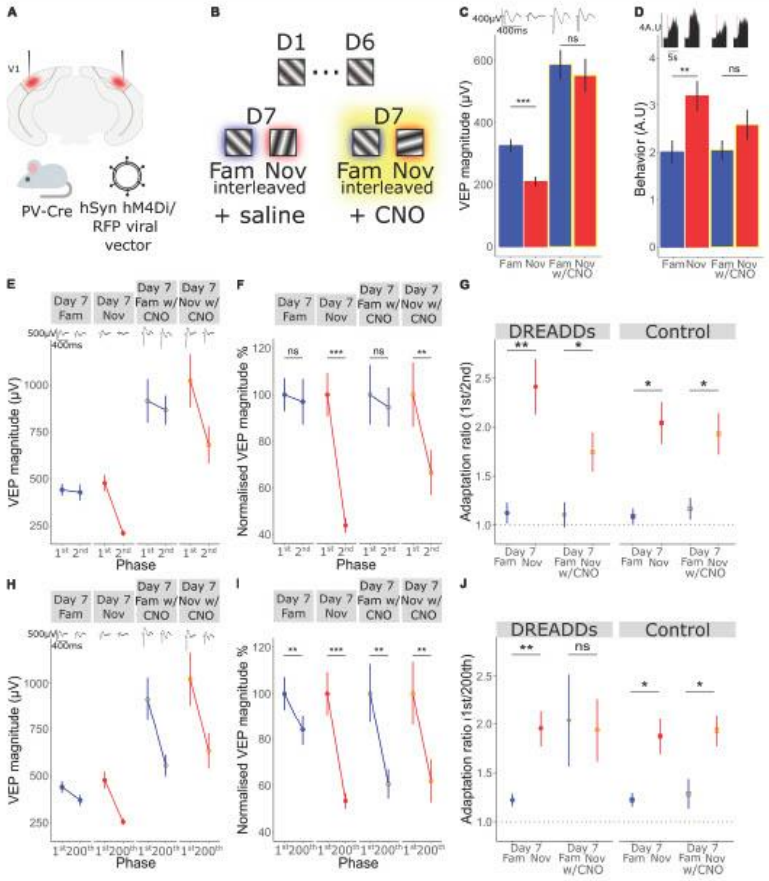

FIGURE 5 | A key role for the activity of Parvalbumin-expressing inhibitory interneurons in long-term familarity exposes a mechanistic difference between timescales of adaptation. **(A)** Schematic of the experimental set-up in which hM4Di was selectively expressed in parvalbumin-expressing (PV) inhibitory neurons of V1 using an AAV viral vector in PV-Cre mice. **(B)** Schematic of visual presentation protocol in which all mice underwent a standard 6-day SRP protocol before testing response to familiar and novel stimuli during systemic saline injection or CNO application, which were administered prior to presentation of familiar and novel stimuli. **(C)** VEP magnitude in response to familiar and novel stimuli with and without CNO-induced PV+ neuronal inactivation. Wilcoxon signed rank day 7 fam vs. nov: $p < 0.001$. Wilcoxon signed rank day 7 fam vs. nov with CNO: $p = 0.09$. **(D)** Behavioral change in response to familiar and novel stimuli with and without CNO. Wilcoxon signed rank day 7 fam vs. nov: $p = 0.02$. Wilcoxon signed rank day 7 fam vs. nov with CNO: $p = 0.2$. **(E)** VEP magnitude in response to the 1st and the 2nd phase reversal for familiar and novel stimuli with and without CNO. **(F)** VEP magnitude to the 1st and the 2nd phase reversal normalized to the 1st phase reversal in response to familiar and novel stimuli with and without CNO. Wilcoxon signed rank phase 1 vs. 2 on day 7 fam ($n = 14$): $p = 0.5$, day 7 nov: $p < 0.001$, day 7 fam w/CNO: $p = 0.9$, day 7 nov w/CNO: $p = 0.004$. **(G)** Adaptation ratio (1st/2nd) in response to familiar and novel stimuli with and without CNO. Wilcoxon signed rank ($n = 14$): day 7 fam AR vs. day 7 nov AR in DREAADs group: $p = 0.007$; day 7 fam w/CNO AR vs. day 7 nov AR w/CNO in DREAADs group: $p = 0.02$. Wilcoxon signed rank ($n = 7$): day 7 fam AR vs. day 7 nov AR in WT group: $p = 0.03$; day 7 fam w/CNO AR vs. day 7 nov AR w/CNO in WT group: $p = 0.02$. FDR correction for multiple comparisons. **(H)** VEP magnitude in response to the 1st and the 200th phase reversal in response to familiar and novel stimuli with and without CNO. **(I)** VEP magnitude to the 1st and the 200th phase reversal normalized to the 1st phase reversal in response to familiar and novel stimuli with and without CNO. Wilcoxon signed rank phase 1 vs. 200 on day 7 fam: $p = 0.005$, day 7 nov ($n = 14$): $p < 0.001$, day 7 fam w/CNO: $p = 0.005$, day 7 nov w/CNO: $p = 0.003$. **(J)** Adaptation ratio (1st/200th) in response to familiar and novel stimuli with and without CNO. Wilcoxon signed rank day 7 fam AR vs. day 7 nov AR in DREAADs group ($n = 14$): $p = 0.007$; day 7 fam w/CNO AR vs. day 7 nov AR w/CNO in DREAADs group: $p = 0.8$. Wilcoxon signed rank ($n = 7$); day 7 fam AR vs. day 7 nov AR in WT group: $p = 0.03$; day 7 fam w/CNO AR vs. day 7 nov AR w/CNO in WT group: $p = 0.04$. FDR correction for multiple comparisons. Asterisks throughout denote significance (*$p < 0.05$, **$p < 0.01$, ***$p < 0.001$) while ns denotes non-significant.

from reversal 1 to 200 only returned when a novel orientation was presented on the final day (**Figure 2J**; Wilcoxon signed-rank phase 1 vs. 200 on day 7 fam: $p = 1$, day 7 nov: $p < 0.001$; FDR correction for multiple comparisons). The AR (1st/200th) for the familiar stimulus was significantly different to that in response to the novel stimulus (**Figure 2K**; Wilcoxon signed rank day 7 fam AR vs. day 7 nov AR: $p < 0.001$) showing that adaptation from the 1st to 200th phase reversal is strongly modulated by long-term familiarity.

Both Short-Term and Long-Term Habituation Require NMDA Receptors in V1

Given the critical role of NMDA receptors (NMDAR) in a wide range of plasticity, and a known requirement in SRP and long-term habituation (Frenkel et al., 2006; Cooke et al., 2015), we sought to investigate habituation and accompanying plasticity over shorter timescales after local NMDAR knock-down in V1. Knock-down of NMDAR was achieved by expressing CRE recombinase *via* AAV viral vector injection bilaterally into V1 in a GluN1-floxed (GRIN1 fl/fl) mouse line (**Figure 3A**), thus knocking down expression of this mandatory subunit for NMDAR only within V1 ($n = 11$ mice). In the control condition, GRIN1 fl/fl littermates were injected with a comparable vector, sharing serotype, promoter and fluorophore, that lacked CRE recombinase ($n = 11$). As we have shown (**Figure 1**), behavioral habituation occurs both across days and within a day from block 1 to block 5. We found that loss of NMDARs from V1 affects both timescales. Behavioral activity usually drops from the first block to the second and remains low (**Figure 1**), and we found that to also be true in the WT littermate control mice (**Figure 3B**; Friedman test for block 1–5: $p = 0.003$, Wilcoxon signed-rank test in WT group B1–B2: $p = 0.1$, B1–B3: $p = 0.02$, B1–B4: $p = 0.02$, B1–B5: $p = 0.02$; FDR correction for multiple comparisons). However, knock-down of NMDARs in V1 prevents the reduction in behavior across blocks (**Figure 3B**; Friedman test for block 1–5: $p = 0.3$, Wilcoxon signed-rank in KD group B1–B2: $p = 0.8$, B1–B3: $p = 0.5$, B1–B4: $p = 0.2$, B1–B5: $p = 0.1$; FDR correction for multiple comparisons). As we reported previously (Cooke et al., 2015), behavioral habituation from day 1 to day 6 is absent in the KD group (**Figure 3C**; Friedman test in KD group: $p = 0.3$, in WT group: $p = 0.001$; FDR correction for multiple comparisons). On day 7 there was no difference in the behavioral response between the novel and familiar stimulus in the KD group, whereas in the WT group behavioral activity was higher in response to the novel stimulus (**Figure 3D**; Wilcoxon signed-rank fam vs. nov in KD: $p = 0.2$, in WT: $p = 0.009$).

Bidirectional Plasticity Occurring in V1 During Short- and Long-Term Habituation Require NMDA Receptors in V1

Within the same dataset, we now assessed the within-day VEP magnitude reduction that accompanies within-day habituation. The reduction in VEP magnitude across 5 blocks was modest in this dataset and was less apparent in these subjects than in the subjects described in **Figure 1** (**Figure 3E**). Nevertheless, by averaging the block-to-block VEP magnitudes observed during short-term habituation across days, a significant within-day VEP suppression was observed in the GRIN fl/fl littermate control animals (**Figure 3F**; $n = 11$; Friedman test in control group: $p = 0.03$; FDR correction for multiple comparisons). In contrast, this significant VEP decrement was not observed in the NMDAR KD mice (**Figure 3F**; $n = 11$; Friedman test in KD group: $p = 0.9$, FDR correction for multiple comparisons), indicating that the within-day reduction in VEP magnitude accompanying short-term habituation requires NMDAR, just as with the habituation itself. As previously reported (Cooke et al., 2015), VEP magnitude potentiation from day 1 to 6, or SRP, is reduced in the knock-down (KD) group compared to control (**Figure 3G**; $n = 11$; Friedman test in KD group: $p = 0.008$, WT group: $p < 0.001$; FDR correction for multiple comparisons). Comparing the ratio of day 6–1 in the control and KD group shows a significant reduction in this plasticity over days after NMDAR KD (**Figure 3H**; Wilcoxon signed rank between control and KD day 6/day 1 ratio: $p = 0.04$). On day 7, there was no difference in VEP magnitude between the familiar and novel orientation in the KD group, whereas the VEP magnitude to the novel stimulus in the control group was significantly different (**Figure 3I**; $n = 11$; Wilcoxon signed-rank fam vs. nov in KD: $p = 0.2$, control: $p = 0.003$; FDR correction for multiple comparisons).

V1 Adaptation Requires NMDA Receptors in V1 Across Short and Longer Timescales

As we have shown above, short-term adaptation within our paradigm ordinarily occurs from both the 1st to the 2nd phase reversal and the 1st to the 200th phase reversal but disappears as the stimulus becomes familiar (**Figure 2**). Within the GRIN1 fl/fl dataset, this adaptation was similarly present in the GRIN1 fl/fl controls on day 1 and the subsequent 2 days, eventually becoming non-significant by day 4 and thereafter for highly familiar stimuli [**Figures 4A,B**; one sample Wilcoxon signed-rank test on AR (1st/2nd) ($\mu = 1$) control group on day 1: $p = 0.02$, day 2: $p = 0.01$, day 3: $p = 0.02$, day 4: $p = 0.2$, day 5: $p = 0.3$, day 6: $p = 0.03$; FDR correction for multiple comparisons]. However, after knock-down of NMDAR in V1, adaptation from the 1st to the 2nd phase reversal was absent on day 1 and all subsequent days [**Figures 4A,B**; one sample Wilcoxon signed-rank test on AR (1st/2nd) ($\mu = 1$) KD group on day 1: $p = 0.6$, day 2: $p = 0.9$, day 3: $p = 0.5$, day 4: $p = 0.4$, day 5: $p = 0.4$, day 6: $p = 0.4$]. When blocks of stimuli for familiar and novel orientations were presented pseudo-randomly interleaved on day 7, this 1st/2nd reversal adaptation was reduced for familiar but not novel stimuli in the control mice [**Figures 4A,B**; one sample Wilcoxon signed-rank test on AR (1st/2nd) ($\mu = 1$) on day 7 fam: $p = 0.03$, day 7 nov: $p = 0.008$; FDR correction for multiple comparisons], but not present for either stimulus in the NMDAR KD mice [**Figures 4A,B**; one sample Wilcoxon signed-rank test on AR (1st/2nd) ($\mu = 1$) KD group on day 7 fam: $p = 1$, day 7 nov: $p = 0.6$]. The same phenotype was present when investigating adaptation from the 1st to the 200th phase reversal. Loss of

NMDARs prevented any short-term adaptation expression across all days and stimulus type [**Figures 4C,D**; one sample Wilcoxon signed-rank test on AR (1st/200th) (μ = 1) KD group on day 1: p = 0.3, day 2: p = 0.3, day 3: p = 0.3, day 4: p = 0.3, day 5: p = 0.5, day 6: p = 0.5, day 7 fam: p = 0.5, day 7 nov: p = 0.4; FDR correction for multiple comparisons], while it remained present in the control mice over the first 5 days of stimulus presentation, and re-emerged to a novel stimulus on day 7 [**Figures 4C,D**; one sample Wilcoxon signed-rank test on AR (1st/200th) (μ = 1) control group on day 1: p = 0.02, day 2: p = 0.02, day 3: p = 0.02, day 4: p = 0.02, day 5: p = 0.04, day 6: p = 0.08, day 7 fam: p = 0.8, day 7 nov: p = 0.008; FDR correction for multiple comparisons]. Thus, short-term adaptation of VEP magnitude in V1 requires the presence of functional NMDAR.

A Key Role for the Activity of Parvalbumin-Expressing Interneurons in Long-Term Familiarity Exposes a Mechanistic Difference Between Timescales of Adaptation

Previously, we have shown that parvalbumin-expressing (PV+) inhibitory neurons in V1 are critical for the expression of long-term familiarity. We inactivated these neurons using a cell type-specific chemo-genetic approach in which the hM4Di DREADDS receptor was expressed in PV+ neurons of V1, disrupting SRP expression (Kaplan et al., 2016). Therefore, we decided to assess whether these PV+ neurons in V1 are required for the modulation of adaptation by long-term familiarity that we have described in the current study (**Figure 2**). Bilateral injection of an AAV viral vector into V1 of a PV-Cre mouse to express hM4Di in these cells (**Figure 5A**) enabled subsequent inactivation of V1 PV+ interneurons after SRP and long-term habituation had been established over 6 days. Specifically, on day 7, familiar (X°) and novel (X+60°) orientations were pseudo-randomly interleaved in a standard design to test for selective SRP/habituation to the familiar orientation. After this, mice were systemically injected (i.p.) with clozapine-n-oxide (CNO), which binds to hM4Di to inactivate expressing neurons, before re-testing response to blocks of the familiar and a new novel stimulus (X-60°) to assess modulation of adaptation by long-term familiarity (**Figure 5B**). Prior to inactivation of PV+ neurons, VEP magnitude was significantly potentiated in response to the familiar stimulus and therefore significantly greater in magnitude than response to the novel stimulus (**Figure 5C**; Wilcoxon signed-rank day 7 fam vs. nov: $p < 0.001$; FDR correction for multiple comparisons). However, as we have reported previously (Kaplan et al., 2016), after inactivation of PV+ interneurons, there was no significant difference in VEP magnitude in response to familiar and novel stimuli (**Figure 5C**; Wilcoxon signed-rank day 7 fam vs. nov w/CNO: p = 0.09; FDR correction for multiple comparisons). It is important to note that after inactivation of PV+ interneurons, the general VEP magnitude was higher due to the loss of inhibition in the cortex. The inactivation of V1 PV+ inhibitory neurons also impaired behaviorally manifest novelty detection as the behavioral response to a novel stimulus was significantly greater than the response to the familiar stimulus before inactivation of

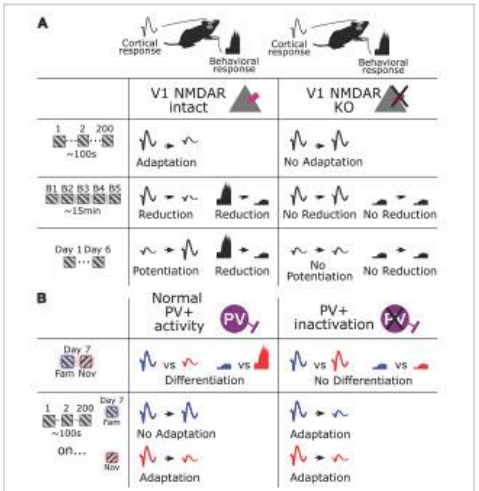

FIGURE 6 | Schematic summarizing fundamental cortical and behavioral changes across multiple timescales. **(A)** Cortical and behavioral changes over seconds, minutes, and days (left), and the result of V1 NMDAR KO on these changes. **(B)** Cortical and behavioral changes in response to a familiar and novel stimulus and the associated adaptation (left), and the result of PV+ interneuron inactivation on these changes.

PV+ neurons (**Figure 5D**; Wilcoxon signed-rank day 7 fam vs. nov: p = 0.02; FDR correction for multiple comparisons), but was suppressed after inactivation of these neurons and no longer different during PV+ inactivation (**Figure 5D**; Wilcoxon signed-rank day 7 fam vs. nov w/CNO: p = 0.2; FDR correction for multiple comparisons).

As we have shown in the current study, short-term adaptation from the first to the second phase reversal progressively reduces as the stimulus becomes familiar and is selectively suppressed on day 7 to highly familiar stimuli, but not novel stimuli (**Figure 2**). Here we show that, although VEP magnitude generally increases, inactivation of PV+ interneurons had no effect on the modulation of 1st/2nd phase reversal short-term adaptation (**Figures 5E–G**). Strong adaptation from the first to the second phase reversal was absent when the stimulus was familiar and present when the stimulus was novel, regardless of whether PV+ neurons were inactivated. This observation is most clear when we normalize to the magnitude of the first phase reversal in order to remove the confound of increased overall response after PV+ inactivation [**Figure 5F**; normalized to the first phase reversal; Wilcoxon signed rank phase 1 vs. 2 on day 7 fam: p = 0.5, day 7 nov: $p < 0.001$, day 7 fam w/CNO: p = 0.9, day 7 nov w/CNO: p = 0.004 (n = 14)]. The adaptation ratio (1st/2nd) was significantly different between the familiar and the novel stimulus both before and after PV+ neuronal inactivation [**Figure 5G**; Wilcoxon signed rank on day 7 fam AR vs. day 7 nov AR: p = 0.007, Wilcoxon signed rank on day 7 fam w/CNO AR vs.

day 7 nov w/CNO AR: $p = 0.02$ ($n = 14$)]. Thus, inactivation of PV+ interneurons does not affect the short-term adaptation from the 1st to the 2nd phase reversal, nor its suppression by long-term familiarity.

Strikingly, the adaptation from the first to the last phase reversal of a stimulus block follows a different pattern. While adaptation is suppressed by familiarity on day 7 but present for the novel stimulus before PV+ neuronal inactivation (**Figures 5H–J**), it is strongly apparent for both familiar and novel stimuli during PV+ neuronal inactivation [**Figure 5I**; normalized to the first phase reversal; Wilcoxon signed rank phase 1 vs. 200 on day 7 fam: $p = 0.005$, day 7 nov: $p < 0.001$, day 7 fam w/CNO: $p = 0.005$, day 7 nov w/CNO: $p = 0.003$ ($n = 14$)]. The adaptation ratio (1st/200th) is significantly different for familiar and novel stimuli before PV+ inactivation [**Figure 5J**; Wilcoxon signed rank on day 7 fam AR vs. day 7 nov AR: $p = 0.007$ ($n = 14$)]. After application of CNO the AR is equivalent for both the familiar and novel stimuli (**Figure 5J**; Wilcoxon signed rank on day 7 fam w/CNO AR vs. day 7 nov w/CNO AR: $p = 0.8$). Therefore, the modulation of the short-term adaptation from the 1st/200th phase reversal by familiarity is not present after inactivation of PV+ interneurons, which differs from the effect on adaptation from the 1st/2nd phase reversal, indicating two mechanistically distinct processes.

DISCUSSION

In the current study we have identified multiple timescales of visual response adaptation that occur during habituation in mice. We have expanded on our previous characterization of stimulus-selective response potentiation (SRP), a form of long-term cortical response potentiation that occurs concomitantly with long-term habituation, to reveal that the reverse effect of response decrement coincides with short-term habituation. Moreover, we have identified shorter-term forms of adaptation that occur over seconds. We also reveal that the NMDA receptor serves as a key molecular mechanism shared by all these forms of plasticity (**Figure 6A**). In addition, we show that these various forms of plasticity are not isolated phenomena, because short-term adaptation and SRP over days clearly interact, such that adaptation no longer occurs for highly familiar stimuli. We also demonstrate that this suppression of adaptation across hundreds of stimuli by long-term familiarity is gated by the activity of PV+ inhibitory interneurons in V1 because inactivating these neurons causes short-term adaptation to re-emerge to highly familiar stimuli (**Figure 6B**). Finally, we make the important observation that the fastest form of adaptation that we have measured, occurring within a second of stimulus presentation, remains suppressed for familiar stimuli even after inactivation of PV+ interneurons, indicating that there may be at least two mechanistically separable timescales of adaptation present within our paradigm. Thus, we have revealed a multitude of forms of cortical plasticity that can be assessed in passively viewing mice to gain a deeper understanding of the processes of habituation.

The longest-term form of plasticity we have described here is already well characterized: potentiation of the VEP in layer 4 over days is described as SRP due to its high degree of stimulus-selectivity (Frenkel et al., 2006; Cooke and Bear, 2010) and it occurs concurrently with long-term behavioral habituation (Cooke et al., 2015; Kaplan et al., 2016; Fong et al., 2020; Finnie et al., 2021), just as we further confirm here. Despite the clear reliance of SRP and accompanying habituation on V1 NMDA receptors, selective knock-down of NMDARs in excitatory neurons of layer 4, the locus where SRP is manifest, does not impair SRP or accompanying habituation (Fong et al., 2020). This observation indicates that the potentiation is an echo of plasticity occurring elsewhere in V1, or in a different cell type within layer 4. Therefore, the direct strengthening of synapses at thalamocortical inputs to layer 4 now seems an unlikely explanation for SRP. Although local field potentials are thought to primarily report synaptic activity rather than action potentials (Katzner et al., 2009; Buzsáki et al., 2012), potentiation of VEP magnitude may reflect a loss of shunting inhibition that allows an increased synaptic response to thalamic input, rather than a potentiation of the synaptic input itself. We have previously shown that parvalbumin-expressing (PV+) inhibitory interneurons, which provide this powerful shunting inhibition, show reduced activity over days as the stimulus becomes familiar during SRP (Hayden et al., 2021). In addition, cell-specific interventional approaches reveal that a normal range of activity in PV+ neurons is required for differential response to familiar or novel stimuli after SRP, either cortically or behaviorally (Kaplan et al., 2016). Thus, it seems likely that SRP reflects a loss of PV+ inhibition. How this contributes to a decrement in behavior, as is observed in the concomitant long-term habituation, remains unclear (Montgomery et al., 2021). One possible arrangement is that increased cortical output recruits another form of inhibition to suppress behavioral output. This arrangement would accord with the comparator model of habituation, in which long-lasting memory is formed in the cortex through elevated synaptic activity that enables recognition of familiarity and suppresses output through feedforward inhibition, as suggested by Sokolov (1963) and others (Konorski, 1967; Wagner, 1981). To confirm that SRP conforms to this model will require measurement of V1 output from the deeper layers of neocortex, with the prediction that this activity is suppressed by superficial layers as they exhibit potentiation. It will also be critical to identify the inhibitory intermediary that leads to this cortical output. One strong candidate for this inhibitory suppression has recently emerged (Pluta et al., 2019).

The behavioral response decrement over the course of minutes, reflecting habituation over an intermediate time-scale, has been investigated by others (Sanderson and Bannerman, 2011). The reduction in VEP magnitude that coincides with this within session habituation has not formally been described by us previously. Our observations of a decrement in VEP magnitude are notable because of the striking contrast with SRP, which coincides with a similar reduction in behavior in the same animals, but in that case over days (**Figure 1**). Visual cortical activity decreases during repetitive presentation of natural movies (Deitch et al., 2021), suggesting that this reduced activity can occur in response to multiple different types of visual stimuli, and the well-documented phenomenon

of mis-match negativity, in which novel oddball stimuli evoke increased magnitudes of event-related potentials (ERP) relative to repetitions of increasingly familiar stimuli, occurs across similar timescales (Näätänen et al., 2007; Garrido et al., 2009). In a similar paradigm to ours, thalamic activity has been observed to increase over ∼30 min (Durkin and Aton, 2019), and it remains possible that the plasticity they have observed is, through some unidentified inversion, the origin of cortical decrement and behavioral habituation. However, the reliance of both VEP decrement and concomitant habituation on NMDARs within V1 strongly suggests that this is not the case (**Figure 3**). Dual recordings of thalamic and cortical neurons may be required to resolve the origins of these effects, and targeted interventions in the thalamus may also prove informative. Investigation of changes over the course of minutes in response to both a familiar and novel grating (currently not possible due to the interleaving of these stimuli) would elucidate if this reduction of cortical activity is indiscriminate to the type of visual stimulus being shown or is also orientation specific, indicating cortical plasticity that is potentially very similar to the familiarity effect observed leading up to mismatch negativity. Recent work has shown that mismatch negativity depends upon activity of the somatostatin-expressing (SST+) inhibitory interneurons (Hamm and Yuste, 2016), suggesting that modification of SST+ inhibition may account for our observations. This class of interneurons primarily target dendrites of excitatory cells and PV+ interneurons (Cottam et al., 2013; Pfeffer et al., 2013; Xu et al., 2013; Rikhye et al., 2021) and they have been shown to be strongly influenced by stimulus familiarity (Kato et al., 2015; Makino and Komiyama, 2015; Hayden et al., 2021). Inhibition on the dendrites of excitatory neurons, where the majority of synaptic contacts are made, may contribute to reduced synaptic activity during habituation (Natan et al., 2015), or these cells may influence the activity of PV+ neurons to mediate the reduction in V1 response, as they are known to do in layer 4 (Xu et al., 2013). It would be informative to measure the activity of these inhibitory neurons in layer 4 of V1 across this timescale and more informative still to monitor inhibitory responses in principle excitatory neurons during this within-session habituation. Given the dependency of the phenomenon that we have described on NMDARs, one intriguing hypothesis is that excitatory synapses onto SST+ neurons are potentiated during repeated stimulus presentation. Knocking down the NMDAR expression within these cells would test this hypothesis. It also remains possible that other types of inhibition are increasingly engaged to produce habituation, as has recently been hypothesized (Ramaswami, 2014). In line with the NMDAR dependence of the reduced behavioral responses, again, this process may involve synaptic depression of excitatory synapses within V1. Much further work is required to investigate the underlying mechanisms of this intermediate form of behavioral and cortical response adaptation.

Over even shorter timescales of seconds, the VEP adaptation that we observe here within continuous blocks of stimulation is a commonly reported phenomenon (Chung et al., 2002; Beierlein et al., 2003; von der Behrens et al., 2009; Cruikshank et al., 2010). The most parsimonious explanation for response decrement is that it reflects a depression of excitatory synapses within the canonical excitatory pathway of V1 through a process of adaptive filtration, which is perhaps the dominant theory of habituation (Horn, 1967; Groves and Thompson, 1970). This depression could potentially occur through Hebbian depression mechanisms (Lee et al., 1998) at excitatory synapses within the cortex (Chen et al., 2015), or the thalamus (Li et al., 2003), or through short-term effects on synaptic release (Moulder and Mennerick, 2006). That the origin of response depression is cortical is supported by its reliance on V1 NMDARs. Specifically, we show that both the adaptation from the 1st to the 2nd phase reversal (0.5 s), and the adaptation from the 1st to 200th phase reversal (100 s) is impaired by a loss of NMDAR expression in V1 (**Figure 3**). This somewhat surprising finding implicates the occurrence of a Hebbian form of plasticity that is at least induced post-synaptically at short timescales (Bliss and Collingridge, 1993). Additionally, we have made the intriguing additional observation that a loss of activity in PV+ neurons after chemo-genetic inactivation re-instates short-term adaptation even to highly familiar stimuli (**Figure 4**). The immediate conclusion from this observation is that short-term adaptation does not rely in any way on inhibition mediated by PV+ neuronal activity, in striking contrast to long-term familiarity. The reinstated short-term adaptation may therefore arise from the cortex responding to a familiar stimulus as if it were novel. Alternatively, it remains possible that the loss of adaptation with long-term familiarity arises from a gradual reduction in PV+ mediated inhibition through the course of a stimulus block that perfectly matches excitatory synaptic depression. Inactivation of PV+ neurons would remove this gradual effect and expose the depression occurring at those excitatory inputs. Using calcium imaging, we have previously observed the gradual loss of PV+ neuronal engagement across phase reversals for familiar but not novel stimuli, so this remains a plausible arrangement (Hayden et al., 2021). Interestingly, using a similar method in excitatory neurons we have also previously reported a perplexing mismatch with the electrophysiological measurements of SRP: when measuring VEP magnitude or peak unit firing rate, a pronounced potentiation is observed (Cooke et al., 2015), while a reduction of signal is observed with calcium imaging (Kim et al., 2020). In the current study we have added to that conundrum, as we reveal short-term adaptation across seconds that is limited to novel stimuli (**Figure 2**), while we previously revealed a similar effect with calcium imaging but limited to familiar stimuli (Kim et al., 2020). The only likely explanation for these curiously mismatched observations is that our electrophysiological methods have detected a fast phasic effect which is potentiated by familiarity over days and diminished to novel stimuli over seconds, while the calcium sensors detect a more sustained diminishment of calcium flux as a result of familiarity over either time-course. Further experiments comparing phasic and drifting gratings or using intracellular electrophysiology may be informative in this regard. It will also be interesting to use calcium imaging to assess the intermediate timescale that we have reported here which occurs from block to block over minutes within a session (**Figure 1**), to determine if the mismatch between the two methods persists even across this timescale. Our prior study indicates that for this timescale,

at least, findings with electrophysiology and calcium imaging will align (Kim et al., 2020).

The storage and retrieval of familiarity plays a major role in reserving energy and attention for only those stimuli that are most pertinent to a task or context and is therefore critical for survival and wellbeing. Understanding how these apparently simple forms of learning and memory are implemented is a greater challenge than expected and there appear to be multiple solutions to the same problem, some of which engage feedforward plasticity, others which engage inhibitory systems and more complicated circuitry. These various mechanisms may all play out within one structure but across different timescales. In this study, we have revealed the measurement of multiple mechanistically distinct forms of plasticity occurring in the same animals across seconds, minutes, and days of repeated stimulus presentation, providing great potential to gain a deep understanding of a foundational set of learning and memory processes. We have monitored these changes using LFP recordings, suggesting that much of the observed phenomenology is likely to translate to non-invasive electroencephalogram (EEG) recordings, providing future potential for translation into human subjects, where forms of plasticity such as mismatch negativity have already been described (Näätänen et al., 2007).

DATA AVAILABILITY STATEMENT

The original contributions presented in the study are included in the article/supplementary material. Further inquiries can be directed to the corresponding author/s.

ETHICS STATEMENT

The animal study was reviewed and approved by the Committee on Animal Care at the Massachusetts Institute of Technology.

AUTHOR CONTRIBUTIONS

SC acquired all the data and participated in experimental design. FC analyzed the data. FC and SC interpreted the data and wrote the manuscript. Both authors contributed to the article and approved the submitted version.

FUNDING

FC is currently funded by the MRC Centre for Neurodevelopmental Disorders (MRC CNDD) and SC is currently funded by the Wellcome Trust (207727/Z/17/Z) and the Biotechnology and Biological Sciences Research Council (BBSRC) (BB/S008276/1).

ACKNOWLEDGMENTS

We thank Mark Bear, the former and current Bear lab members at MIT, where this data was collected, and the generosity of Mark Bear for the release of data to us. We thank Jeff Gavornik for the development and distribution of the stimulus generation software and his support during implementation.

REFERENCES

Atallah, B. V., Bruns, W., Carandini, M., and Scanziani, M. (2012). Parvalbumin-expressing interneurons linearly transform cortical responses to visual stimuli. *Neuron* 73, 159–170. doi: 10.1016/j.neuron.2011.12.013

Aton, S. J., Suresh, A., Broussard, C., and Frank, M. G. (2014). Sleep promotes cortical response potentiation following visual experience. *Sleep* 37, 1163–1170. doi: 10.5665/sleep.3830

Beierlein, M., Gibson, J. R., and Connors, B. W. (2003). Two dynamically distinct inhibitory networks in layer 4 of the neocortex. *J. Neurophysiol.* 90, 2987–3000. doi: 10.1152/jn.00283.2003

Bliss, T. V., and Collingridge, G. L. (1993). A synaptic model of memory: long-term potentiation in the hippocampus. *Nature* 361, 31–39. doi: 10.1038/361031a0

Buzsáki, G., Anastassiou, C. A., and Koch, C. (2012). The origin of extracellular fields and currents–EEG, ECoG, LFP and spikes. *Nat. Rev. Neurosci.* 13, 407–420. doi: 10.1038/nrn3241

Chen, I.-W., Helmchen, F., and Lütcke, H. (2015). Specific Early and Late Oddball-Evoked Responses in Excitatory and Inhibitory Neurons of Mouse Auditory Cortex. *J. Neurosci.* 35, 12560–12573. doi: 10.1523/JNEUROSCI.2240-15.2015

Chung, S., Li, X., and Nelson, S. B. (2002). Short-term depression at thalamocortical synapses contributes to rapid adaptation of cortical sensory responses *in vivo*. *Neuron* 34, 437–446. doi: 10.1016/s0896-6273(02)00659-1

Cooke, S. F., and Bear, M. F. (2010). Visual experience induces long-term potentiation in the primary visual cortex. *J. Neurosci.* 30, 16304–16313. doi: 10.1523/JNEUROSCI.4333-10.2010

Cooke, S. F., Komorowski, R. W., Kaplan, E. S., Gavornik, J. P., and Bear, M. F. (2015). Visual recognition memory, manifested as long-term habituation, requires synaptic plasticity in V1. *Nat. Neurosci.* 18, 262–271. doi: 10.1038/nn.3920

Cooke, S. F., and Ramaswami, M. (2020). "Ignoring the Innocuous: the Neural Mechanisms of Habituation," in *The Cognitive Neurosciences*, 6th Edn, eds D. Poeppel, G. Mangun, and M. Gazzaniga (Cambridge: MIT Press), 197.

Cottam, J. C. H., Smith, S. L., and Häusser, M. (2013). Target-specific effects of somatostatin-expressing interneurons on neocortical visual processing. *J. Neurosci.* 33, 19567–19578. doi: 10.1523/JNEUROSCI.2624-13.2013

Cruikshank, S. J., Urabe, H., Nurmikko, A. V., and Connors, B. W. (2010). Pathway-specific feedforward circuits between thalamus and neocortex revealed by selective optical stimulation of axons. *Neuron* 65, 230–245. doi: 10.1016/j.neuron.2009.12.025

Deitch, D., Rubin, A., and Ziv, Y. (2021). Representational drift in the mouse visual. cortex. *Curr. Biol.* 31, 4327–4339.e6. doi: 10.1016/j.cub.2021.07.062

Durkin, J., Suresh, A. K., Colbath, J., Broussard, C., Wu, J., Zochowski, M., et al. (2017). Cortically coordinated NREM thalamocortical oscillations play an essential, instructive role in visual system plasticity. *Proc. Natl. Acad. Sci. U.S.A.* 114, 10485–10490. doi: 10.1073/pnas.1710613114

Durkin, J. M., and Aton, S. J. (2019). How sleep shapes thalamocortical circuit function in the visual system. *Annu. Rev. Vis. Sci.* 5, 295–315. doi: 10.1146/annurev-vision-091718-014715

Finnie, P. S. B., Komorowski, R. W., and Bear, M. F. (2021). The spatiotemporal organization of experience dictates hippocampal involvement in primary visual cortical plasticity. *BioRxiv*. [preprint] doi: 10.1101/2021.03.01.433430

Fong, M.-F., Finnie, P. S., Kim, T., Thomazeau, A., Kaplan, E. S., Cooke, S. F., et al. (2020). Distinct Laminar Requirements for NMDA Receptors in Experience-Dependent Visual Cortical Plasticity. *Cereb. Cortex* 30, 2555–2572. doi: 10.1093/cercor/bhz260

Frenkel, M. Y., Sawtell, N. B., Diogo, A. C. M., Yoon, B., Neve, R. L., and Bear, M. F. (2006). Instructive effect of visual experience in mouse visual cortex. *Neuron* 51, 339–349. doi: 10.1016/j.neuron.2006.06.026

Garrido, M. I., Kilner, J. M., Stephan, K. E., and Friston, K. J. (2009). The mismatch negativity: a review of underlying mechanisms. *Clin. Neurophysiol.* 120, 453–463. doi: 10.1016/j.clinph.2008.11.029

Groves, P. M., and Thompson, R. F. (1970). Habituation: a dual-process theory. *Psychol. Rev.* 77, 419–450. doi: 10.1037/h0029810

Hamm, J. P., and Yuste, R. (2016). Somatostatin interneurons control a key component of mismatch negativity in mouse visual cortex. *Cell Rep.* 16, 597–604. doi: 10.1016/j.celrep.2016.06.037

Hayden, D. J., Montgomery, D. P., Cooke, S. F., and Bear, M. F. (2021). Visual recognition is heralded by shifts in local field potential oscillations and inhibitory networks in primary visual cortex. *J. Neurosci.* 41, 6257-6272. doi: 10.1523/JNEUROSCI.0391-21.2021

Horn, G. (1967). Neuronal mechanisms of habituation. *Nature* 215, 707–711. doi: 10.1038/215707a0

Kaplan, E. S., Cooke, S. F., Komorowski, R. W., Chubykin, A. A., Thomazeau, A., Khibnik, L. A., et al. (2016). Contrasting roles for parvalbumin-expressing inhibitory neurons in two forms of adult visual cortical plasticity.*eLife* 15:e11450. doi: 10.7554/eLife.11450

Kato, H. K., Gillet, S. N., and Isaacson, J. S. (2015). Flexible sensory representations in auditory cortex driven by behavioral relevance. *Neuron* 88, 1027–1039. doi: 10.1016/j.neuron.2015.10.024

Katzner, S., Nauhaus, I., Benucci, A., Bonin, V., Ringach, D. L., and Carandini, M. (2009). Local origin of field potentials in visual cortex. *Neuron* 61, 35–41. doi: 10.1016/j.neuron.2008.11.016

Kim, T., Chaloner, F. A., Cooke, S. F., Harnett, M. T., and Bear, M. F. (2020). Opposing Somatic and Dendritic Expression of Stimulus-Selective Response Plasticity in Mouse Primary Visual Cortex. *Front. Cell. Neurosci.* 13:555. doi: 10.3389/fncel.2019.00555

Konorski, J. (1967). *Integrative Activity of the Brain.* Chicago: University of Chicago Press.

Lee, H. K., Kameyama, K., Huganir, R. L., and Bear, M. F. (1998). NMDA induces long-term synaptic depression and dephosphorylation of the GluR1 subunit of AMPA receptors in hippocampus. *Neuron* 21, 1151–1162. doi: 10.1016/s0896-6273(00)80632-7

Li, J., Guido, W., and Bickford, M. E. (2003). Two distinct types of corticothalamic EPSPs and their contribution to short-term synaptic plasticity. *J. Neurophysiol.* 90, 3429–3440. doi: 10.1152/jn.00456.2003

Makino, H., and Komiyama, T. (2015). Learning enhances the relative impact of top-down processing in the visual cortex. *Nat. Neurosci.* 18, 1116–1122. doi: 10.1038/nn.4061

McDiarmid, T. A., Bernardos, A. C., and Rankin, C. H. (2017). Habituation is altered in neuropsychiatric disorders-A comprehensive review with recommendations for experimental design and analysis. *Neurosci. Biobehav. Rev.* 80, 286–305. doi: 10.1016/j.neubiorev.2017.05.028

McGaugh, J. L. (2000). Memory–a century of consolidation. *Science* 287, 248–251. doi: 10.1126/science.287.5451.248

Montgomery, D. P., Hayden, D. J., Chaloner, F. A., Cooke, S. F., and Bear, M. F. (2021). Stimulus-Selective Response Plasticity in Primary Visual Cortex: progress and Puzzles. *Front. Neural Circuits* 15:815554. doi: 10.3389/fncir.2021.815554

Moulder, K. L., and Mennerick, S. (2006). Synaptic vesicles: turning reluctance into action. *Neuroscientist* 12, 11–15. doi: 10.1177/1073858405282431

Näättänen, R., Paavilainen, P., Rinne, T., and Alho, K. (2007). The mismatch negativity (MMN) in basic research of central auditory processing: a review. *Clin. Neurophysiol.* 118, 2544–2590. doi: 10.1016/j.clinph.2007.04.026

Natan, R. G., Briguglio, J. J., Mwilambwe-Tshilobo, L., Jones, S. I., Aizenberg, M., Goldberg, E. M., et al. (2015). Complementary control of sensory adaptation by two types of cortical interneurons. *eLife* 4:e09868. doi: 10.7554/eLife.09868

Neves, G., Cooke, S. F., and Bliss, T. V. P. (2008). Synaptic plasticity, memory and the hippocampus: a neural network approach to causality. *Nat. Rev. Neurosci.* 9, 65–75. doi: 10.1038/nrn2303

Pfeffer, C. K., Xue, M., He, M., Huang, Z. J., and Scanziani, M. (2013). Inhibition of inhibition in visual cortex: the logic of connections between molecularly distinct interneurons. *Nat. Neurosci.* 16, 1068–1076. doi: 10.1038/nn.3446

Pluta, S. R., Telian, G. I., Naka, A., and Adesnik, H. (2019). Superficial layers suppress the deep layers to fine-tune cortical coding. *J. Neurosci.* 39, 2052–2064. doi: 10.1523/JNEUROSCI.1459-18.2018

Ramaswami, M. (2014). Network plasticity in adaptive filtering and behavioral habituation. *Neuron* 82, 1216–1229. doi: 10.1016/j.neuron.2014.04.035

Rankin, C. H., Abrams, T., Barry, R. J., Bhatnagar, S., Clayton, D. F., Colombo, J., et al. (2009). Habituation revisited: an updated and revised description of the behavioral characteristics of habituation. *Neurobiol. Learn. Mem.* 92, 135–138. doi: 10.1016/j.nlm.2008.09.012

Rikhye, R. V., Yildirim, M., Hu, M., Breton-Provencher, V., and Sur, M. (2021). Reliable sensory processing in mouse visual cortex through cooperative interactions between somatostatin and parvalbumin interneurons. *J. Neurosci.* 41, 8761-8778. doi: 10.1523/JNEUROSCI.3176-20.2021

Sanderson, D. J., and Bannerman, D. M. (2011). Competitive short-term and long-term memory processes in spatial habituation. *J. Exp. Psychol. Anim. Behav. Process.* 37, 189–199. doi: 10.1037/a0021461

Schmid, S., Wilson, D. A., and Rankin, C. H. (2014). Habituation mechanisms and their importance for cognitive function. *Front. Integr. Neurosci.* 8:97. doi: 10.3389/fnint.2014.00097

Sokolov, E. N. (1963). Higher nervous functions; the orienting reflex. *Annu. Rev. Physiol.* 25, 545–580. doi: 10.1146/annurev.ph.25.030163.002553

von der Behrens, W., Bäuerle, P., Kössl, M., and Gaese, B. H. (2009). Correlating stimulus-specific adaptation of cortical neurons and local field potentials in the awake rat. *J. Neurosci.* 29, 13837–13849. doi: 10.1523/JNEUROSCI.3475-09.2009

Wagner, A. R. (1981). "SOP: A model of automatic memory processing in animal behavior," in *Information Processing in Animals* (Psychology Press).

Xu, H., Jeong, H.-Y., Tremblay, R., and Rudy, B. (2013). Neocortical somatostatin-expressing GABAergic interneurons disinhibit the thalamorecipient layer 4. *Neuron* 77, 155–167. doi: 10.1016/j.neuron.2012.11.004

Conflict of Interest: The authors declare that the research was conducted in the absence of any commercial or financial relationships that could be construed as a potential conflict of interest.